Patterns in the sky

Natural Visualization of Aircraft Flow Fields

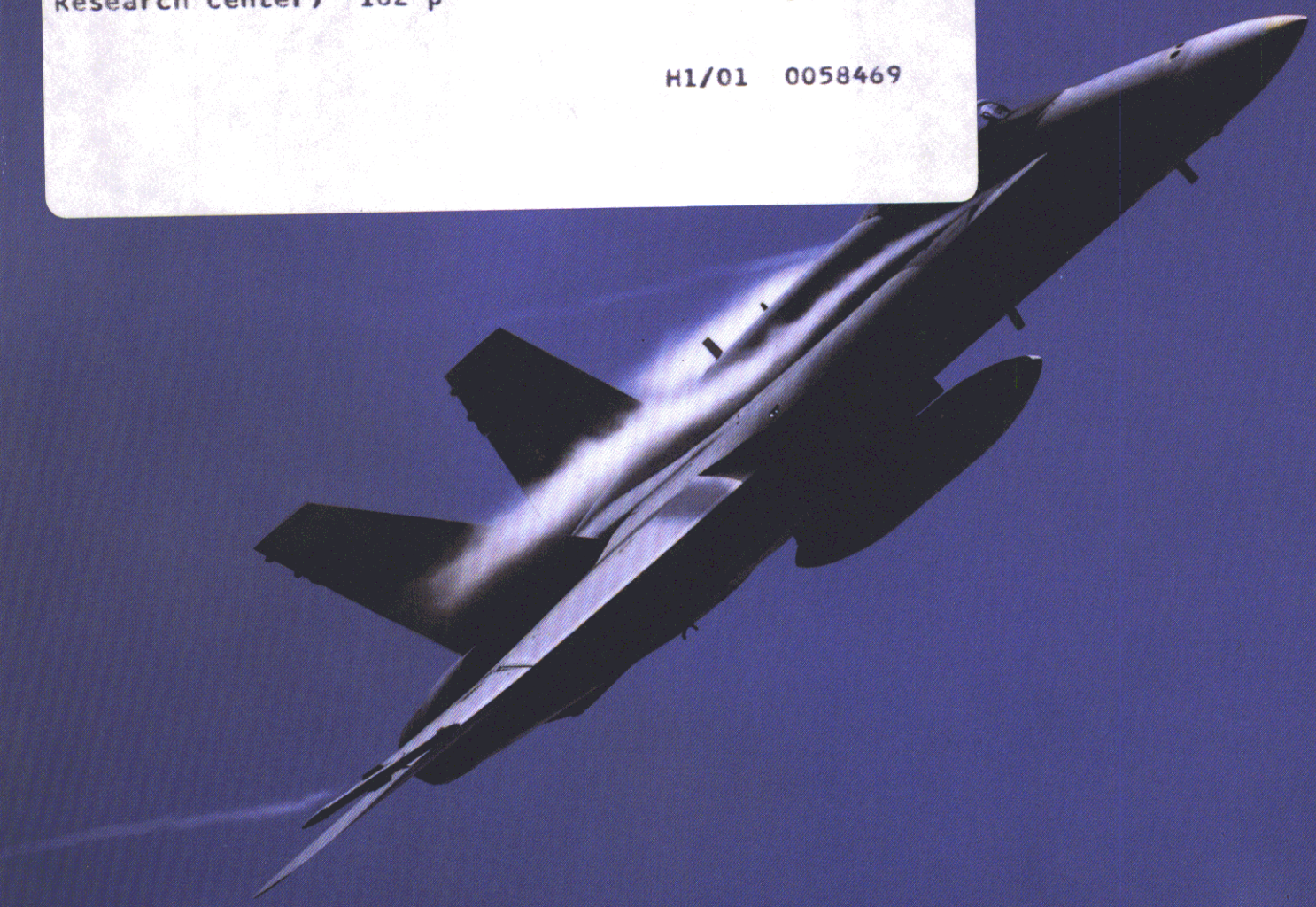

James F. Campbell and Joseph R. Chambers

NASA SP-514

Patterns in the sky

Natural Visualization of Aircraft Flow Fields

Langley Research Center
Hampton, Virginia 23681-0001

1994

James F. Campbell and Joseph R. Chambers

NASA SP-514

CONTENTS

Vortex flows generated by wing and chine leading edges for SR-71 during knife-edge turn. Balls of flame in wake resulted from flame-out that occurred during high-g maneuver.

FOREWORD

For many years, NASA has been involved with aerodynamics research to determine the effects of separated flows on airplane performance. This is a very difficult problem particularly for high performance military vehicles which encounter shock-induced flow separation and separation-induced vortex flow during routine flight operations. Some vortex flows, like those from wings with highly swept leading edges, are designed into an airplane because they induce favorable effects. Many other separated and vortex flows occur inadvertently and can adversely affect the performance, controllability, and stability of an aircraft; this results in undesirable aeroelastic effects, critical structural design loads, and unsteady flows that affect adjacent and downstream surfaces. Historically, airplane designs are first tested with scale models in wind tunnels at considerably lower Reynolds numbers than occur in flight, which can result in significant differences between the flow fields obtained on these models compared with the actual airplane. Scaling techniques have been successfully developed for attached flows but are not yet mature for separated flows from aircraft. The flow may separate from an airplane surface for a number of reasons, which include the geometry, angle of attack, Mach number, and Reynolds number. Compounding the situation, airplanes usually experience different flow combinations simultaneously, including attached and vortex flow, separated and vortex flow, multiple vortices, and vortex-shock interactions.

Currently, the National Aeronautics and Space Administration is developing improved wind tunnel and flight testing techniques and computational methods to evaluate these complex airplane flow fields during the design stages. These include studies to validate advanced computational theories which predict separated flow fields and aerodynamic characteristics of an airplane at wind tunnel and flight conditions and scaling laws which extrapolate separated and vortex flows from wind tunnel to flight results. In wind tunnel experiments, visualization techniques are available to obtain a qualitative description of the flow and determine when and where the flow separates from the airplane model to form the resulting flow fields; this is generally not known for an airplane in flight because it is very difficult to acquire flow visualization data. Significant flight research efforts are underway on specific airplanes, such as the NASA F/A-18 High Alpha Research Vehicle (HARV) which is yielding important flow-field data. However, a need exists for more information, even qualitative, on a variety of airplanes and flows that is not currently available. One way a portion of the flow field of the airplane is revealed is when it flies in moist air and condensation occurs.

Because condensed flows have not been evaluated previously for this use, NASA undertook this initial effort to collect photographs, describe the flow patterns, and document the visual evidence of which flows can be visualized because of condensation.

The results of this study showed that many flight condensation patterns were obtained for a variety of airplane flow fields, which represent a unique source of in-flight flow visualization not previously utilized. The flight patterns suggested that expansions in leading-edge and separation-induced vortex flows and in supersonic flows at transonic speeds can cause flows to condense, and that shock waves, wing trailing-edge pressure recovery, and vortex burst can cause condensed flows to vaporize. Water vapor relationships were postprocessed with solution fields of standard computational codes to calculate relative humidity, which provided a qualitative indicator of flight condensation patterns. Analysis revealed that relative humidity is more sensitive to temperature changes than to the changes in pressure and that vortex cores have low relative humidity; this helps explain voids in the condensed vortex flows. Some flow features were found that had not been seen in flight previously or were not known to exist, which provide information at full-scale Reynolds numbers for researchers conducting experiments in subscale wind and water tunnels or using computational codes. To help interpret the flight condensation patterns, similar flow fields were shown that were made visible by in-flight smoke flow, from wind and water tunnel results, and by computer code calculations. The document was written for the aerodynamicist, although it is of interest to and readable by a wide range of individuals including other aviation specialists, airplane manufacturers, pilots, and university students.

The authors of Patterns in the Sky are uniquely qualified to collaborate on this effort. They are both aeronautical engineers at NASA Langley Research Center where they have been involved with research of aerodynamic technologies for high performance military vehicles, including research of separation-induced vortex flows involving experiments in subsonic and transonic wind tunnels and airplane designs impacted by vortex flows. James F. Campbell is currently a Senior Aerospace Engineer in the Transonic Aerodynamics Branch, Applied Aerodynamics Division, and has been employed at Langley since 1963. As an expert in the aerodynamics of leading-edge vortices, he was responsible for conferences on Vortex Flow Aerodynamics sponsored in 1985 by NASA and the U.S. Air Force and in 1990 by AGARD, where he served on the Fluid Dynamics Panel (1986–90). Among his honors have been the NASA Award to the Advanced Fighter Technology Team and to the Vortex Flap Development Team (1982).

Joseph R. Chambers, employed at Langley since 1962, served as the Head of the research branch that uses the Langley 30- by 60-Foot and the Langley 20-Foot Vertical Spin Tunnels and as Chief of the Flight Applications Division. The division conducted fundamental and applied research on the aerodynamics and flight dynamics of advanced military and civil aircraft. He is an international authority in the field of high-angle-of-attack flight and has recently established a High Alpha Technology Program to research existing and new military technologies for that demanding flight environment. He has received a number of awards for this work, including the AIAA Mechanics and Control of Flight Award, the NASA Exceptional Service Medal, and the NASA Outstanding Leadership Medal. He is currently Chief of the Aeronautics Systems Analysis Division.

Wesley L. Harris
Associate Administrator of Aeronautics

National Aeronautics
and Space Administration
Washington, D.C.

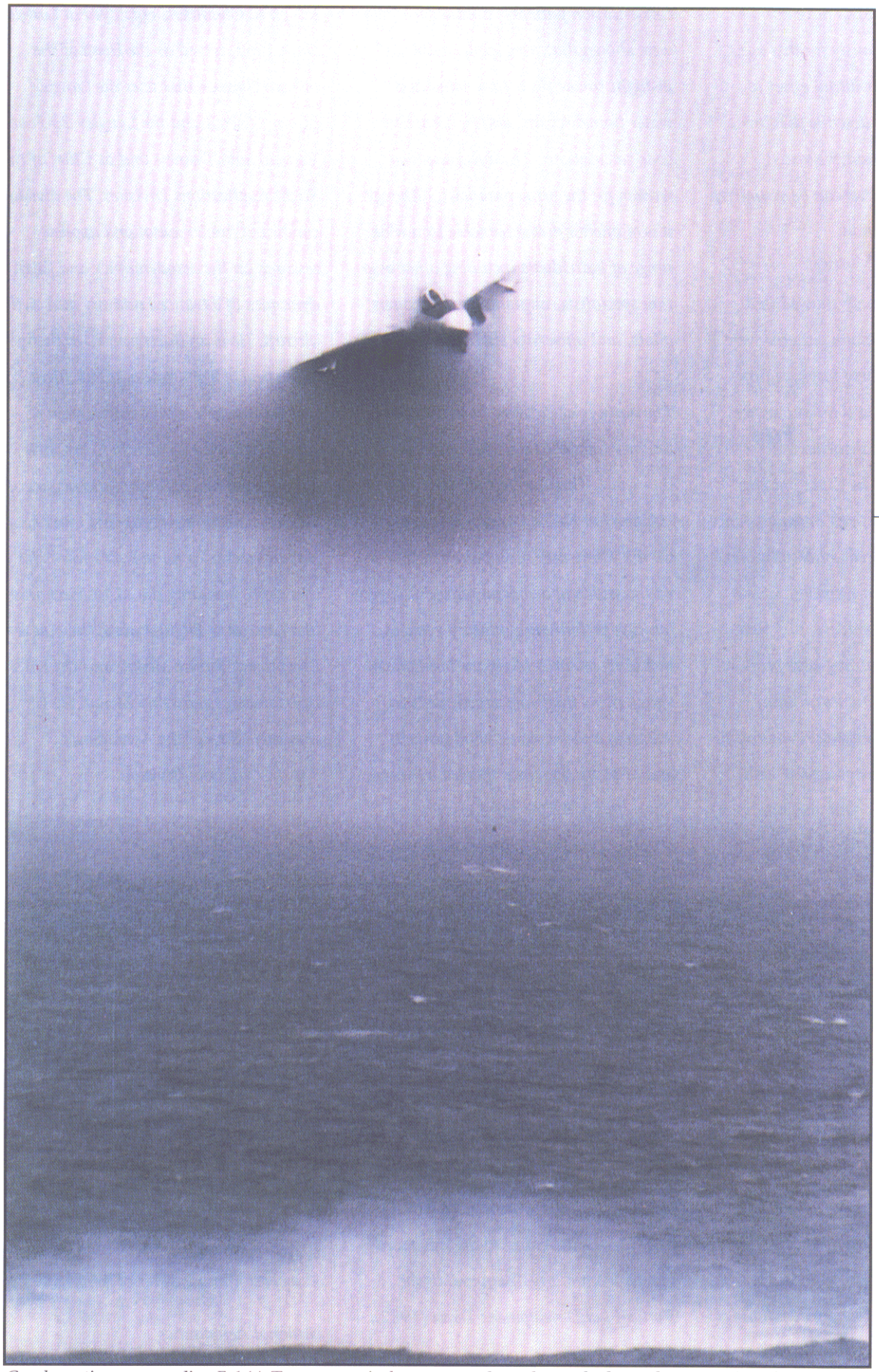

Condensation surrounding F-14A Tomcat as airplane passes through speed of sound near carrier. Shock wave is seen on water surface.

PREFACE

Like most aeronautical engineers, we were always interested in seeing flows that became naturally visible during flights, which meant in or around commercial transports and at air shows for the military airplanes. Many times that you could see a condensing flow, it was difficult to get quality pictures; the few pictures that existed for our engineering peers usually were hanging in frames on the wall. We kept collecting photographs, especially those that illustrated leading-edge and strake vortices, until several years ago when we saw a photograph of an F-18 that showed a condensation pattern streamwise from the wing leading edge, appearing to be a separated type of flow where we thought the flow should be attached. Since the pattern was not artificially induced and was a real flow field, we began collecting aircraft photographs from a variety of sources to determine what expected and unexpected flow fields would be disclosed by condensation.

Although we provide an explanation for the cause of most of the flow patterns, much of this is speculative because this is the first opportunity for the aeronautical research community to see and examine condensed airplane flow fields. There are a number of questions and uncertainties about how to interpret the patterns. The flight and atmospheric conditions and configuration variables are provided for the photographs if they are known. As might be expected, most of the photographs do not have these conditions available; however, at this time it is more important to show that these flows exist than to have the detailed flight conditions.

To help interpret the flight condensation patterns, similar flow fields were shown that were made visible by in-flight smoke flow, from wind and water tunnel results, and by computer code calculations. If the reader is interested in more detail than is provided in this current publication, part of this investigation was published in a Review Paper entitled "Observation of Airplane Flowfields by Natural Condensation Effects" by James F. Campbell, Joseph R. Chambers, and Christopher L. Rumsey, Journal of Aircraft, Vol. 26, No. 7, July 1989, pages 593–604. The paper includes the derivation of the relative humidity equations and an extensive reference list.

1 Introduction

In-flight separated flows, including shock flows, separation-induced vortex flows, and general flow separation, are of crucial importance because they can degrade flying abilities of the aircraft, especially for high performance military vehicles. The airplane designer needs to understand the consequences of these flows early in the development of an aircraft in order to make design changes to improve the aerodynamics, stability, and control characteristics. An additional importance of separated flows is that experimental data are needed to validate advanced computational methods which predict model and airplane flow fields. Traditionally, the surface and off-surface flow fields of airplanes have been observed and diagnosed in wind tunnels with special instrumentation and flow visualization equipment. NASA is making significant progress to develop more sophisticated experimental and computational methods to visualize, measure, and compute flow fields in flight as evidenced by results generated by the NASA F/A-18 High Alpha Research Vehicle (HARV). In order to extrapolate from wind tunnel to flight conditions, airplane designers, wind tunnel and flight experimentalists, and computational specialists need additional information about flight flow fields, even qualitative, for a broad range of aircraft types and flight regimes. This technology area represents a formidable challenge which currently limits our ability to correlate between wind tunnel and flight results.

When clear humid air expands around an airplane, portions of its flow field can condense and become visible and illustrate certain flow patterns, such as the leading-edge vortices on the SR-71 (p. ii) and the supersonic expansions and shock waves on the F-14A (p. vi). These condensation patterns are often observed in flight on transports, bombers, and fighters but often occur without warning because they are affected by atmospheric weather, lighting conditions, and airplane flight conditions. This unpredictability compounds the problem of obtaining quality photographs of condensation patterns, which are usually obtained by photographers or pilots who are not aware of their potential engineering value. On the other hand, aeronautical engineers design the airplane from ground-based laboratories and rarely get to see these in-flight visualizations.

Currently, no studies have been conducted to document these condensation patterns nor to examine its potential as a test technique to visualize flight flow fields. Hence, there is a need to determine what types of condensation patterns can be seen in flight and to provide an interpretation of what the patterns mean. To help meet this need, the NASA Langley Research Center conducted an extensive

solicitation of visual material showing condensation effects on airplanes from professional aircraft photographers, military squadrons, industry peers, and aviation enthusiasts. Over 400 photographs were obtained from domestic sources as well as European, Canadian, Japanese, and Australian sources.

The objective of the current publication is to present the collection of flight photographs to illustrate the types of flow patterns that were visualized and to present qualitative correlations with computational and wind tunnel results. Initially in section 2, the condensation process is discussed, including a review of relative humidity, vapor pressure, and factors which determine the presence of visible condensate. Next, outputs from computer code calculations are postprocessed by using water-vapor relationships to determine if computed values of relative humidity in the local flow field correlate with the qualitative features of the in-flight condensation patterns. The photographs are then presented in section 3 by flow type and subsequently in section 4 by aircraft type to demonstrate the variety of condensed flow fields that was visualized for a wide range of aircraft and flight maneuvers. The photographs are presented only once unless otherwise noted. To help interpret the flight condensation patterns, similar flow fields are shown that are made visible by in-flight smoke flow, from wind and water tunnel results, and by computer code calculations.

2 HUMID AIRFLOW

This section presents some of the properties of humid airflow to make it easier to interpret the condensed flow patterns presented in sections 3 and 4. It is not intended to be a complete treatment of condensing flows, but enough information is provided to understand how airplane flows condense and evaporate to form a pattern.

Research studies of moist and condensing flows have been conducted for many years to understand the effects of condensation in high-speed wind tunnel flows and on wind tunnel models. These studies have provided valuable information about condensation effects on tunnel calibration, data accuracy, and on the tunnel operational envelope where condensation first occurs locally around a model. An example of the expansion of moist air in a supersonic wind tunnel is shown in figure 2.1, which presents the variation of stream temperature and dew point along the tunnel axis. The flow expands from low speed at tunnel station 0 to a Mach number M of 2.56 at tunnel station 160. Before the flow expands, the stream temperature is 110°F, which is much higher than the dew point. The expansion to supersonic speeds results in a slight decrease in the dew point and a very large decrease in stream temperature, which drops to about –200°F. Condensation is possible in the moist expanding tunnel flow once the stream temperature drops below the dew point.

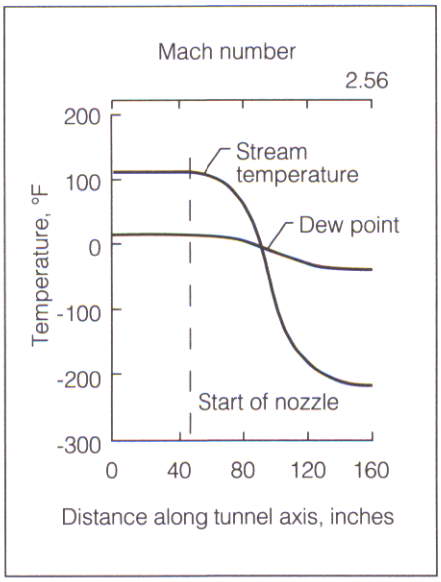

Expansion of moist air in supersonic wind tunnel. 2 • 1

A similar process occurs when airplanes fly through clear humid air as depicted in the sketch in figure 2.2. The flow around the airplane can experience rapid flow expansions, where the velocity increases and the pressure and temperature decrease. When the local flow temperature decreases to the dew point, the flow has reached the saturated condition and the water vapor can begin to condense and become visible. When the flow experiences a contraction or deceleration, the velocity decreases and the pressure and temperature

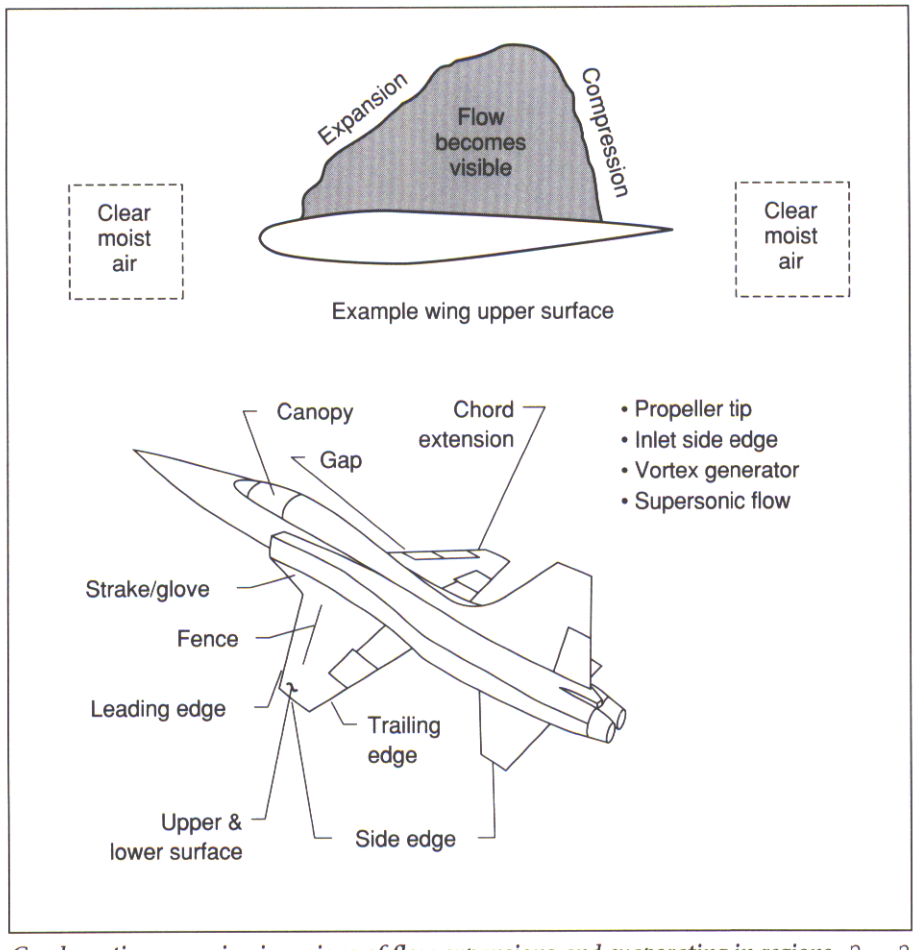

Condensation occurring in regions of flow expansions and evaporating in regions of flow compressions to create pattern with airplanes flying through moist air. 2 • 2

increase. If the flow is already condensed and the temperature rises above dew point, the condensed particles evaporate, or vaporize, and are no longer visible. The flow around an airplane combines expansions and compressions to yield a condensation pattern like that found in the SR-71 and the F-14A photographs shown previously. Most rapid expansions for an airplane are near edges, such as the leading edges of the wings, wingtips, pylons, fences, side edges of deflected trailing-edge flaps, and propeller tips. In addition, maximum velocities, and hence minimum pressures and temperatures, can occur near regions of maximum wing thickness.

One property of the atmosphere is that it contains a certain amount of water vapor. Humidity is a measure of the water vapor or moisture in the atmosphere. To understand how humid airflow condenses and evaporates is a very complicated flow process, which in flight involves small particulates in the air, such as dust and pollution, to provide the seed particles for condensation to commence. Detailed modeling of the exact condensation process is beyond the scope of the current publication. However, relative humidity RH is used as a qualitative indicator of where the flow is likely to begin to condense or where already existing condensate is likely to begin to evaporate. Some existing computational methods were used to compute flow fields, which were postprocessed to determine relative humidity in the local flow. Thus, it was possible to examine the sensitivity of relative humidity to changes in flow pressure and temperature during expansions and compressions and to generate visual patterns of airplane flows.

An expression is desirable for local relative humidity as a function of free-stream relative humidity and local and free-stream values of static pressures and temperatures. In this way, relative humidity is given as a function of local variables which are computed by the computational methods. The flow properties of Mach number M, static pressure p, static temperature T, and relative humidity RH are used with subscripts l and ∞ for the local and free-stream values, respectively. The equations used in this analysis can be derived by taking moist air as a mixture of two gases, dry air and water vapor. For moist air, the ratio of specific heat is a constant and approximately 1.4 for the ranges of pressure and temperature of this study. In addition, the perfect gas law can be used for the mixture as well as the individual components of the mixture. Because each component of the gas mixture has a partial pressure, the static pressure in the flow p is given by the sum of the partial pressures of dry air and water vapor.

Relative humidity is defined as the ratio of the partial pressure of water vapor in air to the pressure of saturated water vapor at the local temperature of the air, which is applied at local and free-stream flow conditions to get RH_l and RH_∞ at T_l and T_∞, respectively. The mole fraction for water vapor is given as the ratio of the partial pressure of water vapor to the sum of the partial pressures, which is the static pressure p. This pressure allows expressions for the partial pressure of the water vapor at free-stream and local conditions to be substituted in the respective equations for RH. Taking the mole fraction to be constant throughout the flow leads to an expression for RH_l which is proportional to the pressures of saturated water vapor p_s at free-stream and local conditions.

The vapor-pressure curve for water, presented in figure 2.3, defines the conditions of static pressure and static temperature where a vapor and liquid can coexist; that is, where RH = 1. Dew point is the temperature at which water vapor may begin to condense, and it occurs when RH reaches a value of 1. To the left of the curve, condensation begins where RH > 1, and to the right of the curve, already existing condensation would evaporate where RH < 1. The curve is given by the expression,

$$\log_{10} p_s = 6.064 - \frac{2263}{T}$$

where p_s is in atmospheres and T is in Kelvins.

This equation defines a functional relationship to use with values of free-stream and local temperatures to obtain values for saturated vapor pressure. This results in the following expression for the local relative humidity as a function of the free-stream relative humidity and the local and free-stream values of static pressures and temperatures:

$$RH_l = RH_\infty \frac{p_l}{p_\infty} 10^{\left\{ -\frac{2263}{T_\infty} \left[\frac{(T_l/T_\infty)-1}{T_l/T_\infty} \right] \right\}}$$

Thus, RH_l is a linear function of RH_∞, local and free-stream static pressures, and an exponential function of the local and free-stream static temperatures.

This relationship is important because it helps explain the influence of atmospheric and local properties on the possibility of flow condensing around an airplane. An increase in the atmospheric relative humidity level results in a comparable increase in the local relative humidity levels and, thus, a better chance of condensation occurring. A lower free-stream static pressure corresponds to a higher speed or Mach number, which also increases the local relative humidity levels. In addition, increasing p_l and decreasing T_l increase RH_l, whereas decreasing p_l and increasing T_l decrease RH_l.

A viscous, compressible computational method was used to provide a sample calculation of the flow properties, including relative humidity, over the upper surface of an RAE 2822 airfoil. The results shown in figure 2.4 were obtained at $\alpha = 2.8°$, $M_\infty = 0.75$, and $RH_\infty = 0.85$. The angle of attack is the angle between a longitudinal reference line on the airplane and the velocity vector.

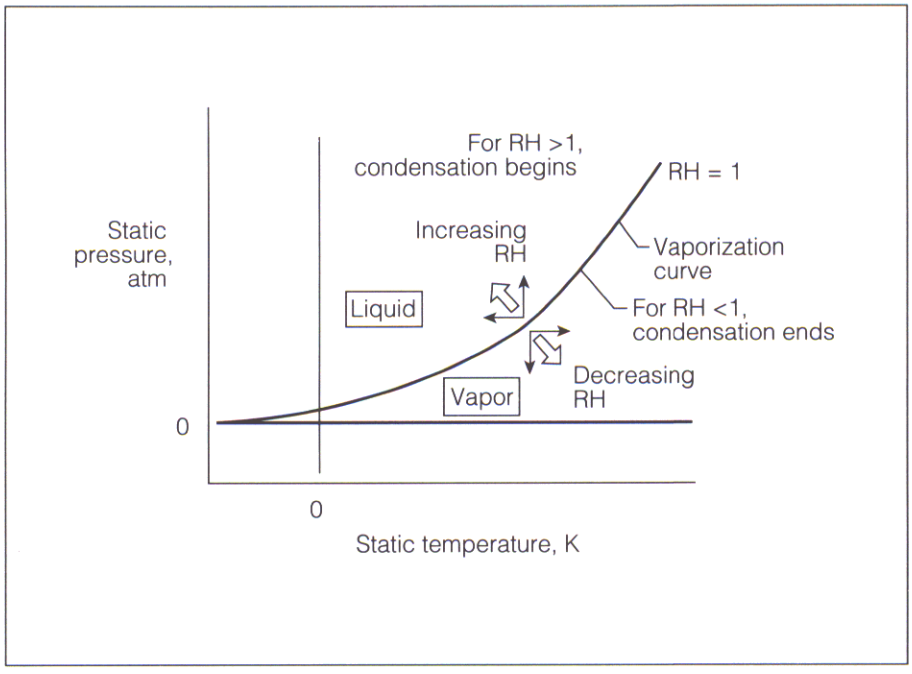

Pressure of saturated water vapor as function of temperature. 2 • 3

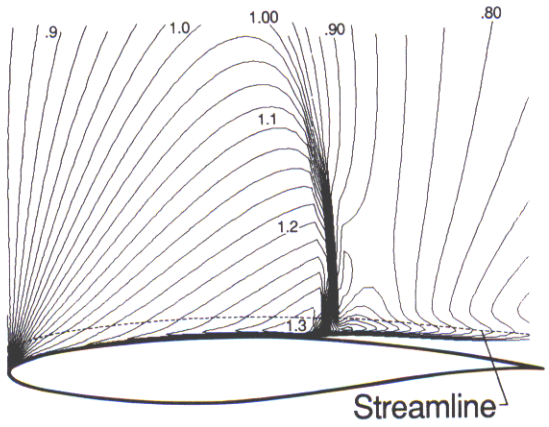

(a) Mach number contours.

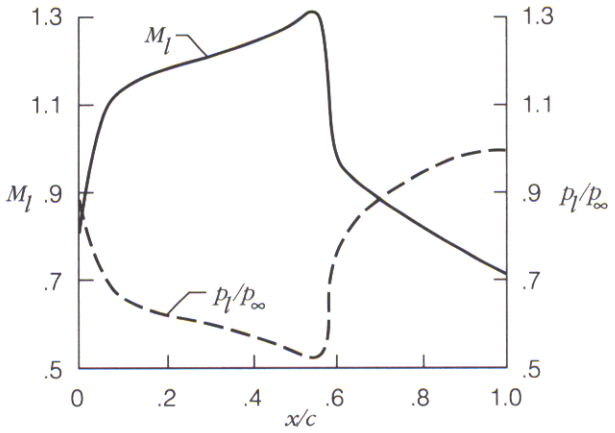

(c) p_l and M_l along streamline.

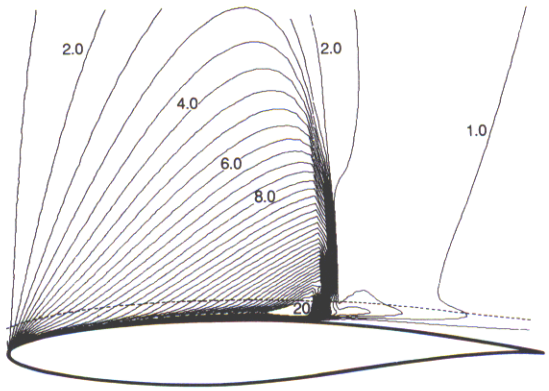

(b) Relative humidity contours.

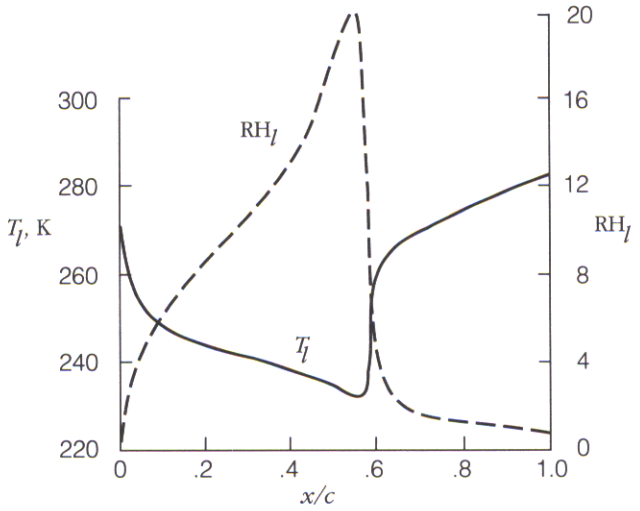

(d) T_l and RH_l along streamline.

Calculated flow properties and relative humidity for RAE 2822 airfoil at $\alpha = 2.8°$, $M_\infty = 0.75$, and $RH_\infty = 0.85$. 2 • 4

The Mach number contours (fig. 2.4(a)) show that the flow expands from the subsonic free-stream to supersonic speeds over the airfoil, then compresses through a shock wave to subsonic flow at the trailing edge. Correspondingly, the relative humidity (fig. 2.4(b)) increases rapidly in the expansion portion of the airfoil flow, then decreases rapidly through the shock wave to a value less than 1.0 at the trailing edge. The relative humidity contours are very similar to the Mach number contours because relative humidity is a function of Mach number. Although it is difficult to see in the contour plot, the calculations showed that the boundary-layer flow adjacent to the airfoil surface had higher temperatures, and this resulted in low values of RH_l. A shear flow is one of the ways to evaporate condensed flow back into a vapor.

The flow properties of Mach number, static pressure and temperature, and relative humidity along the indicated streamline through the airfoil flow are plotted in figures 2.4(c) and (d). The properties along the streamline show that the flow expands quickly from the nose region; this results in rapid increases in Mach number, decreases in pressure and temperature, and increases in relative humidity. Rapid flow compressions through the shock wave result in large increases in static pressure and temperature and a corresponding significant decrease in the relative humidity.

The functional expression for RH_l has shown that decreasing temperature results in higher values of relative humidity through an exponential function, whereas decreasing pressure results in lower values through a linear function. The temperature decrease along the streamline in front of the shock results in a strong rise in relative humidity in spite of the pressure decrease. Through the shock, the sharp temperature rise causes the decrease in relative humidity in spite of the rising pressures. Therefore, a given change in temperature has a much greater effect on the value of relative humidity than a proportional change in pressure. The extremely high local values of relative humidity are not realistic because the flow can begin condensing at $RH_l = 1$ and will condense even without seed particles when RH_l is about 4, when homogeneous nucleation occurs. Once condensation occurs, the resulting heat released keeps the value of RH_l between roughly 1 and 4.

Additional computational results of visual patterns of calculated relative humidity for different types of airplane flows are presented in sections 3.1, 3.2, and 3.3.1. The condensation patterns are presented by flow type in figures 3.1 to 3.71 and by airplane type in figures 4.1 to 4.104.

3

Condensation Patterns by Flow Type

Three flight condensation patterns were found to be common for a variety of airplanes: the so-called gull pattern for swept wing-bodies, expansion and shock patterns for configurations with transonic flow, and leading-edge separation-induced vortex flow for slender wings. Calculations of relative humidity were obtained for these three types of flow fields to compare qualitatively with the condensation patterns in flight. These relative humidity calculations were made by postprocessing existing solutions that were calculated with a standard computer code that does not take into account the possibility of condensation. The existing solutions were not calculated with the specific geometries of the flight examples, but they are believed to be generally representative of the classes of flow. Values of $RH_\infty = 0.85$ and $T_\infty = 280$ K used for these calculations were arbitrarily chosen to represent a typical atmospheric condition.

All color graphics are shown with a light blue background. Values for RH_l ranged from black for the minimum values shown to white for the maximum values shown. Geometries are shown as gray for the wing-body and delta-wing configurations and as brown for the airfoil.

3 • 1

Wing-Body Flows/Gull Pattern

A flow pattern observed on a number of swept-wing airplanes during maneuvering flight is the so-called gull shape shown in figure 3.1. This example is for the Transonic Aircraft Technology (TACT) airplane, which was a modified F/B-111, at a Mach number of about 0.8 during a 3.3*g* turn and an angle of attack of 6.9°. During the turn, the airplane creates a normal force 3.3 times larger than its weight. At this flight condition, the flow is not condensed over the fuselage but builds up progressively from the wing root to a maximum about mid-span, then diminishes as the wingtip is approached. There is no apparent condensation on the lower wing surface, and the wingtip vortices trail rearward from the tips. The fact that you can see the trailing-edge region of the wing suggests that vaporization of the water has taken place in that area. Examination of flight data showed that there is supercritical flow and a shock wave over the wing. As noted in the prior discussion, a shock wave would increase temperature, decrease relative humidity, and induce evaporation. Separated flow at the wing trailing edge could cause a similar result.

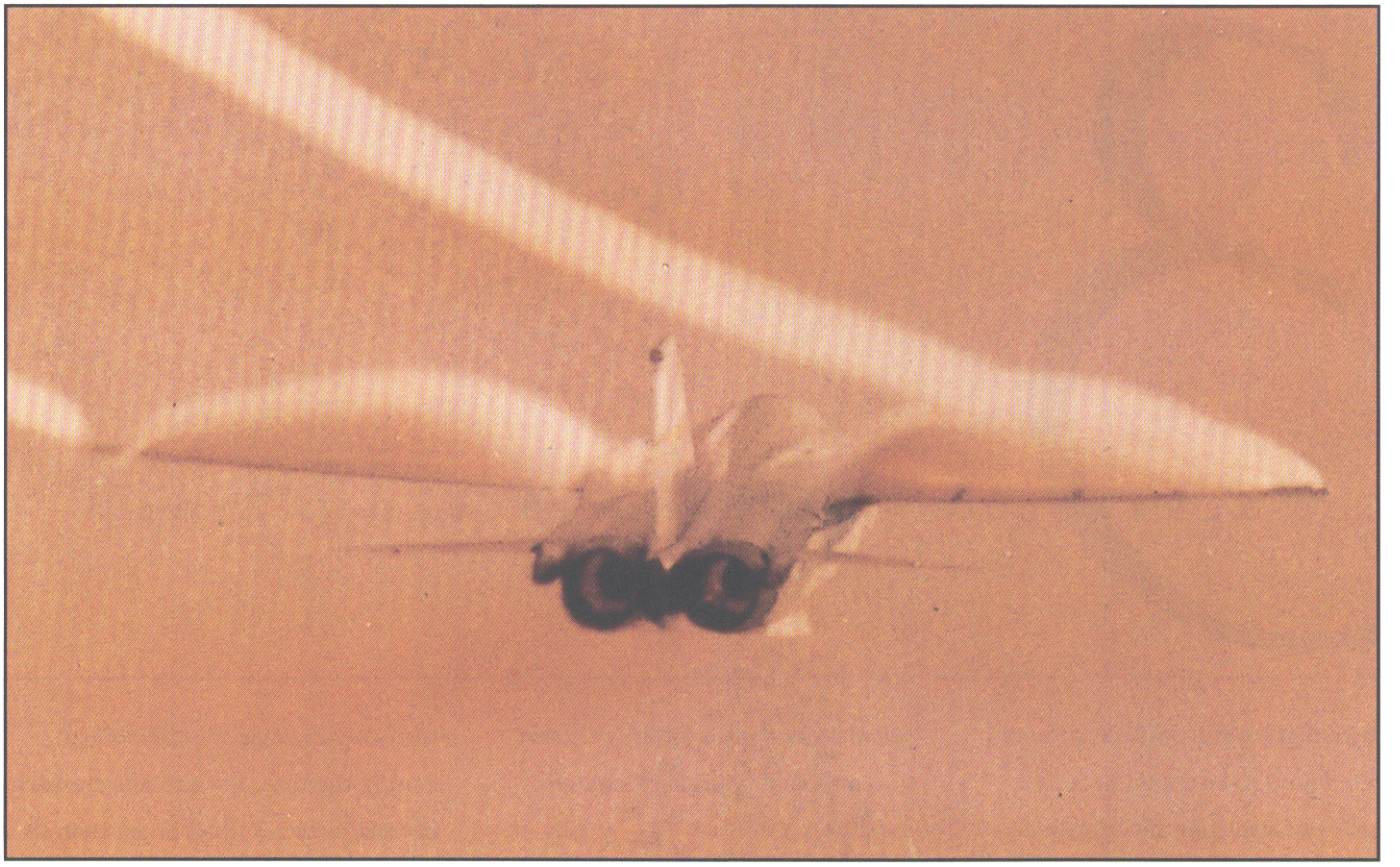

Gull pattern and wingtip vortices created on TACT airplane during 3.3g maneuver. M = 0.82; α = 6.9°; wing sweep, 26°. 3 • 1

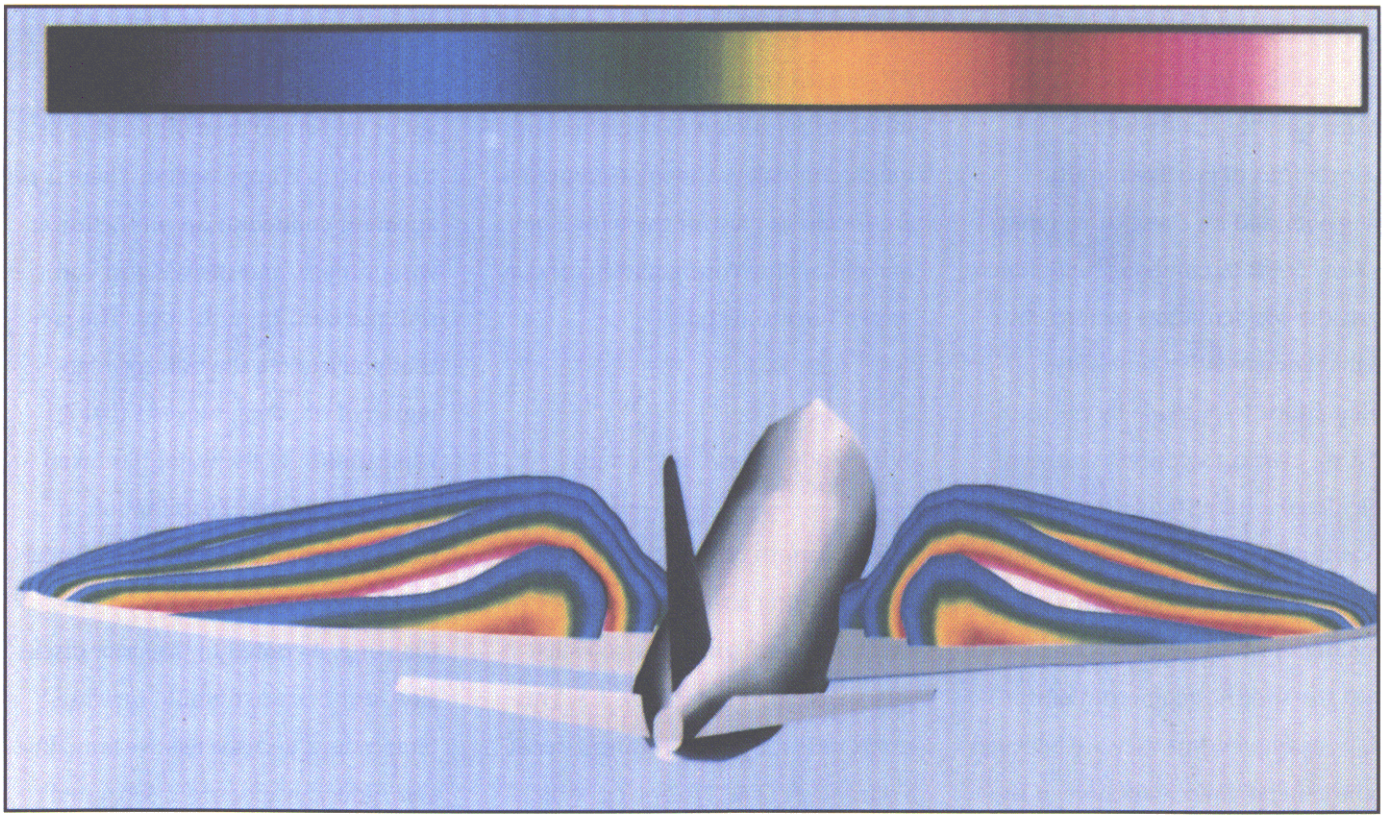

Gull pattern of calculated relative humidity for Boeing 747. M = 0.84; α = 2.4°. 3 • 2

A calculated relative humidity pattern shown in figure 3.2 was obtained with a computer code that calculates complex, three-dimensional, compressible flow fields for swept wing-body configurations. The flow calculation is obtained for a transport airplane, the Boeing 747-200, at a comparable Mach number to the TACT airplane with angle of attack of 2.4° and an atmospheric relative humidity RH_∞ of 0.85. The pattern was generated for spanwise planes of relative humidity ranging from 1.6 to 12.0. For clarity, values of $RH_l < 1.6$ are not shown. These are plotted at varying chordwise locations and result in a similar spanwise pattern on the wing and body as was observed for the flight condensation on the TACT airplane. Maximum velocities, and hence minimum temperatures and pressures, occur over the mid-section of the wing and result in the largest values of RH_l (shown as white). Similar to the results for the RAE 2822 airfoil described previously in figure 2.4, the temperature change has a greater effect on RH_l than the pressure change. The values of RH_l decrease at the wing root, wingtip, and trailing edge because of temperature recovery and in spite of pressure increases. As before, the temperature effect dominates RH_l because it is the stronger function.

Front view of gull pattern on F-14A during maneuver with wings at low sweep. 3 • 3

Rear view of gull pattern on F-14A during maneuver with wings at low sweep. 3 • 4

The gull type of condensation pattern can occur on any airplane if the lift conditions are right. Figures 3.3 and 3.4 show an F-14A Tomcat during a maneuver where the wings are at a low sweep position for both front and rear views. The front view (fig. 3.3) shows the gull pattern and wingtip vortices similar to the TACT photograph. Wing condensation disappears over the fuselage, and the aft vertical tails are visible. The whiter, rounded areas near the wing upper surfaces may be caused by vorticity from the glove-wing junctions, or from the missile pylons, which pass over the wings during maneuvering flight. Note also the lighter patches in the top of the gull pattern.

In the rear view (fig. 3.4), the condensation has progressed to include the region over the fuselage, which is indicative of a higher lifting condition. In addition to the tip vortices, the clearer areas near the wing upper surfaces are evidence of the vortical flow features. Also some small dark spots are noted at the wing upper surface. The last example (fig. 3.5) shows a U.S. Marine Corps A-4M making a high-speed pull-up. The gull pattern on the wing panel is beginning to form as is the condensation in the engine housing flow field.

3 • 2

High-Speed Flows

Some of the most dramatic condensation patterns occur at transonic conditions, where the supersonic flow around an airplane extends large vertical distances from the airplane and terminates in a shock wave. The F-14A airplane (fig. 3.6) provides an excellent example of this class of condensed flow. The airplane is flying with full-aft wing sweep during level flight at a subsonic speed of $M = 0.9$. The free-stream flow accelerates to supersonic speeds above and below the wing; this causes the flow to condense in an almost straight line in the expansion waves in the front portion of the condensation pattern. The aft end of the pattern is created by a shock wave through which the flow is decelerated to subsonic speeds aft of the airplane. The previous discussion for the effect of supersonic conditions on moist airflow suggests

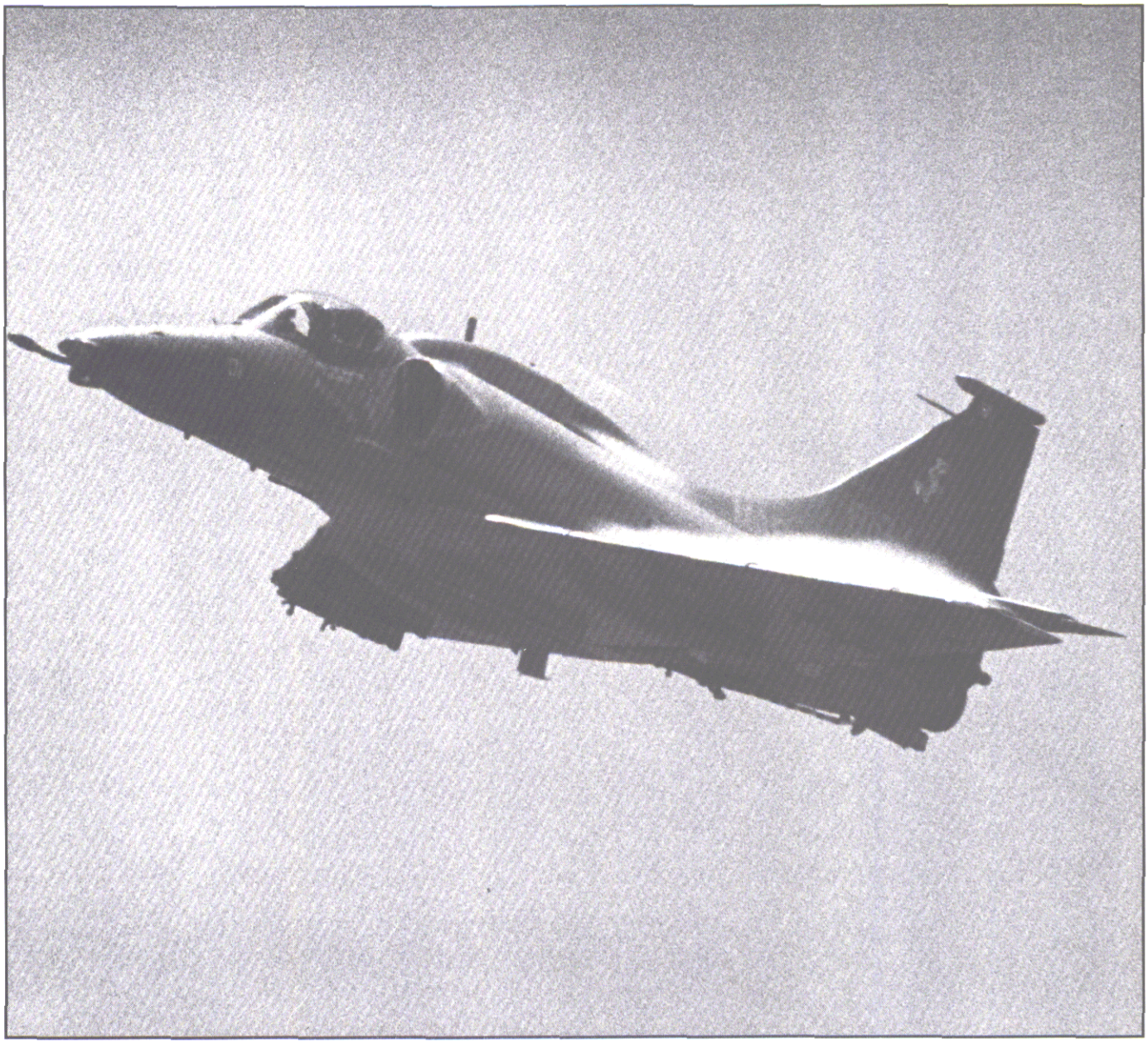

Gull pattern on A-4M airplane making high-speed pull-up. 3 • 5

that the rapid temperature rise through the shock wave of the F-14A causes the condensed flow to evaporate. Note also there is an expansion on the canopy.

A viscous, compressible computational method was used to calculate the relative humidity pattern for transonic flow over an NACA 0012 airfoil at $\alpha = 2°$ and $M = 0.9$. (See fig. 3.7.) Relative humidity values are shown from 2.0 to 44.0; RH_l values less than 2.0 are shown as light blue. The light blue at the airfoil surface represents the low values of relative humidity in the boundary layer. The calculated pattern is qualitatively similar to the condensed pattern on the F-14A in showing expansion regions of supercritical flow and shock waves. Of course, the intent here is not to compare the two-dimensional airfoil solution directly with patterns created by the three-dimensional F-14A geometry but just to illustrate the effects of relative humidity in supercritical flows.

Transonic flows around fighter airplanes occur for a wide range of speed and maneuver conditions. Two examples include an F-4J in a

Expansions and shock patterns on F-14A in level flight at M = 0.9 with full-aft wing sweep.

3 • 6

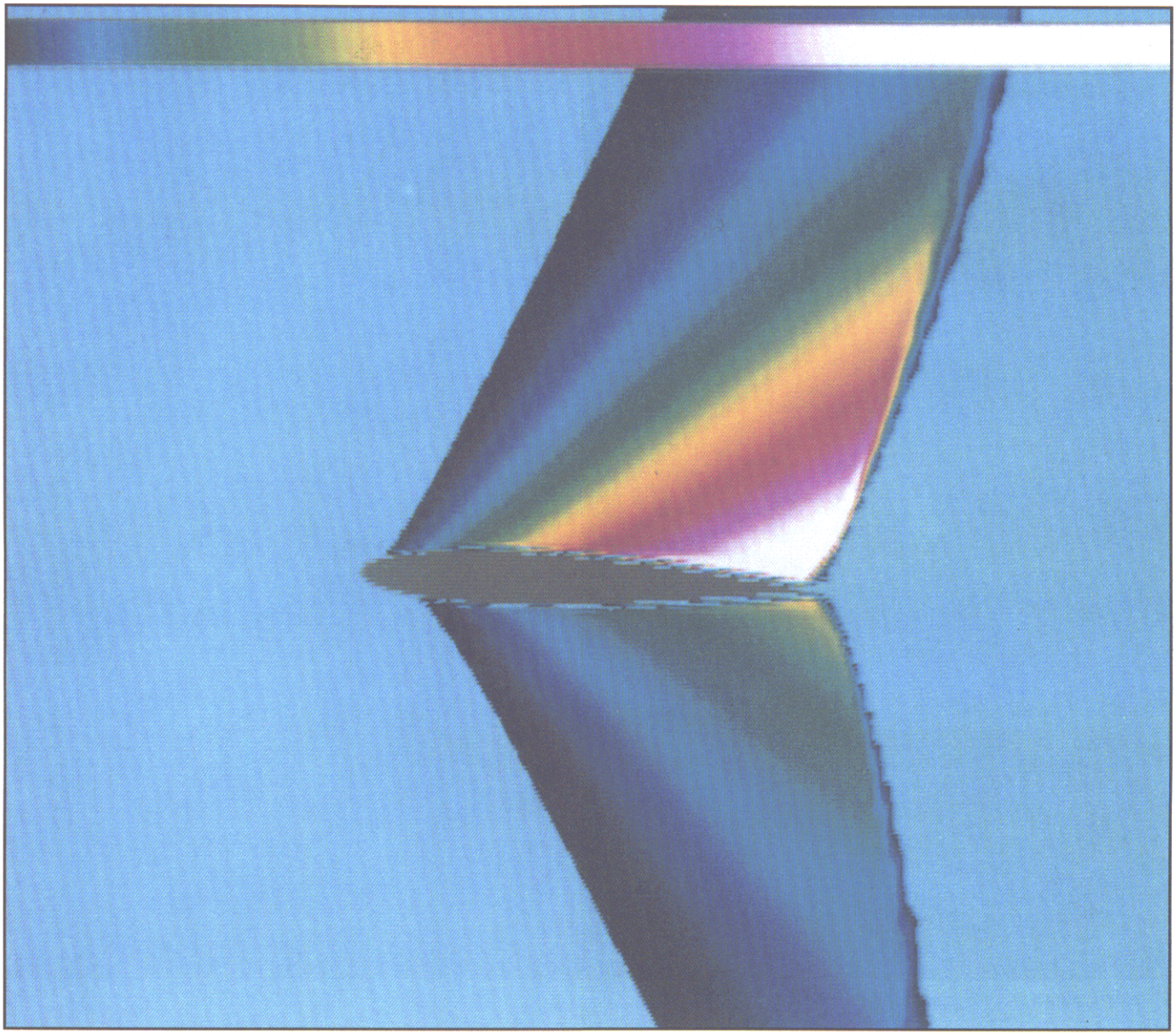

Expansions and shock patterns of calculated relative humidity for NACA 0012 airfoil at $\alpha = 2°$ and $M = 0.9$. 3 • 7

high-speed pass over a runway (fig. 3.8) and an F/A-18 in a high-speed pull-up (fig. 3.9). The condensed patterns are similar to the patterns obtained for the F-14A, where the flow condenses in the expansion region and evaporates as the flow goes through the shock wave. The resulting pattern is often referred to as a Mach diamond.

Comparing the condensed flow patterns for the F-4 and F/A-18 leads to several observations. At low angles of attack and high subsonic speed, the F-4 has supercritical flow above and below the airplane and the shock wave appears to be essentially perpendicular and appears to reach to the runway surface. Unlike the F-4, the F/A-18 has condensation only over the upper part of the airplane, which is due to having much less expansion or more compression on the lower surface, which inhibits condensation. In addition, the shock wave for the F/A-18 slopes forward, which is indicative of a lower subsonic Mach number than the F-4 with its shock essentially normal to the fuselage. Both airplanes have condensation over their canopies because of flow expansion in that area.

Transonic flows on F-4J making high-speed pass over runway. 3 • 8

Condensation patterns, even vortex flows, can occur during supersonic flight as evidenced by the photograph of the XB-70 bomber (fig. 3.10) at supersonic cruise. As you can see, vortex flows originate from the canard tip and from the outer wing panel dihedral break, deflected downward from the wing plane about 25°. Additionally, there is condensation over the forward fuselage and canard themselves because of flow expansions. The trailing-edge flaps are deflected downward together with the canard deflected upward to trim the pitching moment. The expansion over the trailing-edge flaps results in flow condensation. In addition, the canard vortices appear to thin out as they pass over the aft end of the vehicle. This thinning is probably due to its passing through the trailing shock wave, which is comparable with the essentially perpendicular shock waves observed earlier for transonic flow, but at this higher supersonic speed has shifted to the trailing edge of the wings and slopes rearward.

3 • 3
Vortical Flows

3 . 3 . 1
Leading-edge vortex

Leading-edge vortex flows often occur during takeoff, landing, and maneuvering of airplanes with slender highly swept wings. The airflow

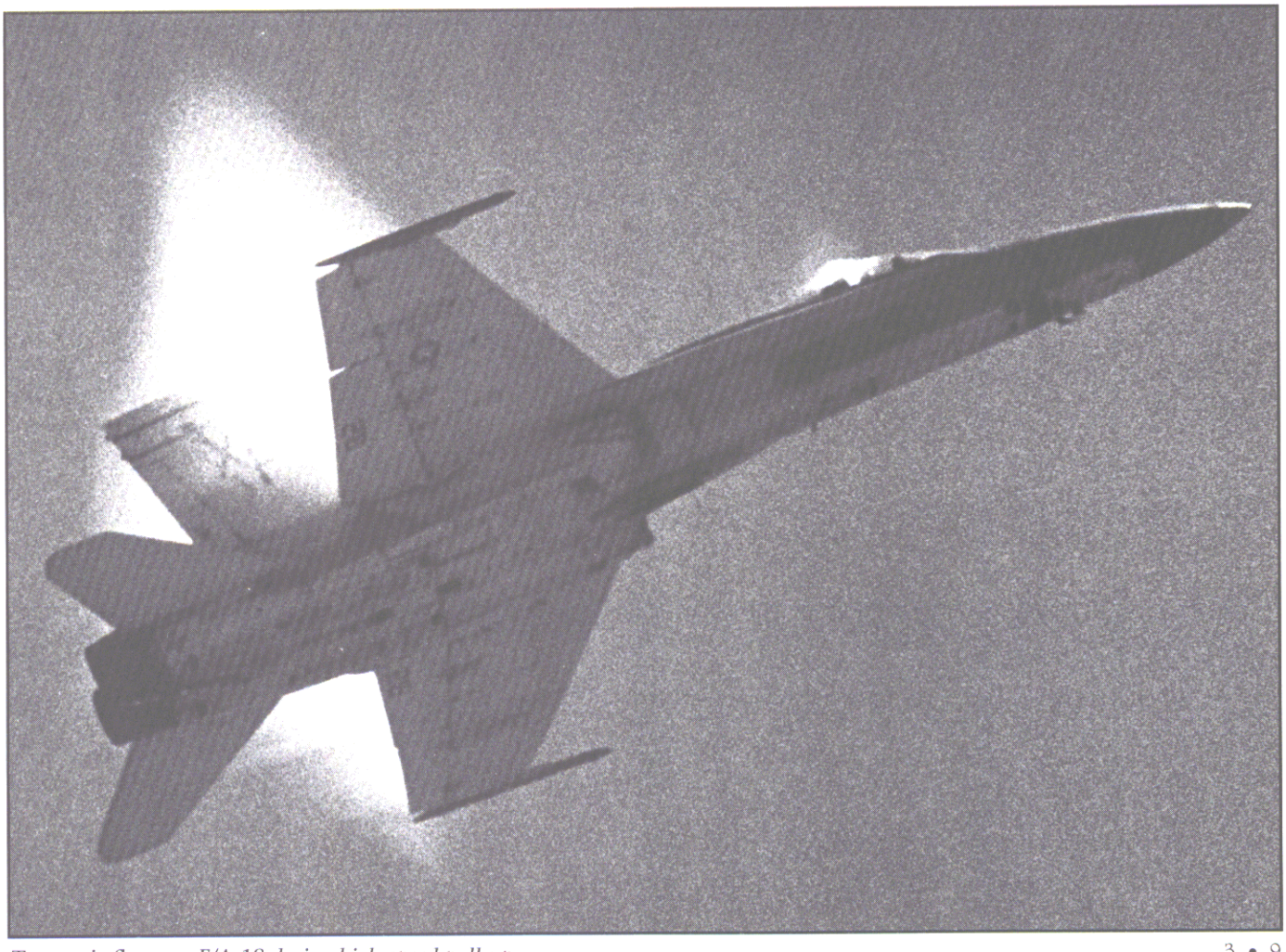

Transonic flows on F/A-18 during high-speed pull-up. 3 • 9

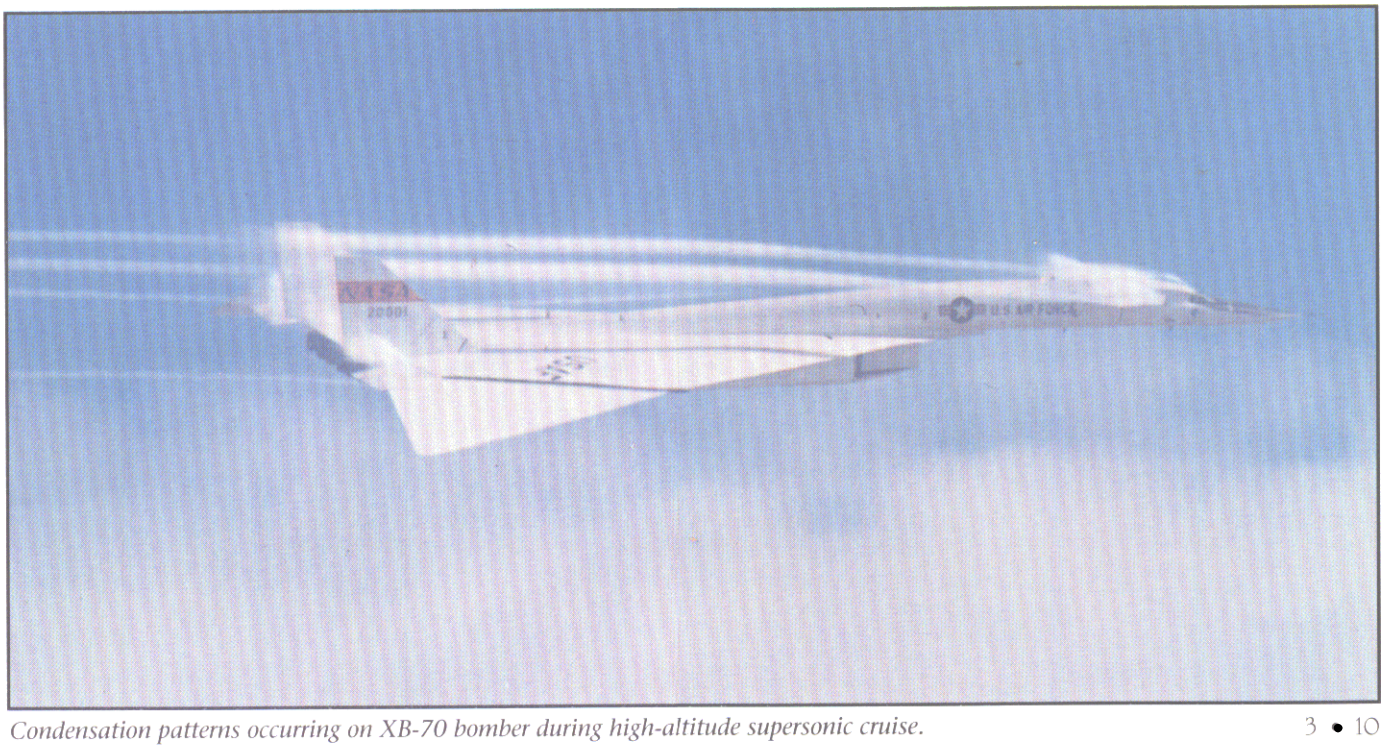

Condensation patterns occurring on XB-70 bomber during high-altitude supersonic cruise. 3 • 10

separates at the wing leading edges and forms organized vortices over the wing planform, which induce high suction pressures and increase lift. The leading-edge vortex flows appear as condensed patterns on top of the wings of the XB-70 bomber during takeoff in figure 3.11 and the Concorde civil transport during landing in figure 3.12. The wings for both these airplanes are slender and highly swept, are designed for supersonic cruise, and generate leading-edge vortices to produce high lifts for takeoff and landing operations. Using vortex lift on fixed-geometry, slender highly swept wings was a dramatic departure from the usual high-lift systems for moderately swept wings that featured deflected flaps at the leading and trailing edges of the wing.

A comparable pattern of calculated relative humidity was obtained for a slender delta wing by using a three-dimensional viscous computational method (fig. 3.13). The calculations were made for a subsonic Mach number of 0.3 at an angle of attack of 21° and are plotted for RH_I values from 1.0 to 1.25; values less than 1.0 are not shown for clarity. The calculated relative humidity pattern shows the leading-edge separation-induced vortex system over a 76° delta wing. Flow expansion occurs around the

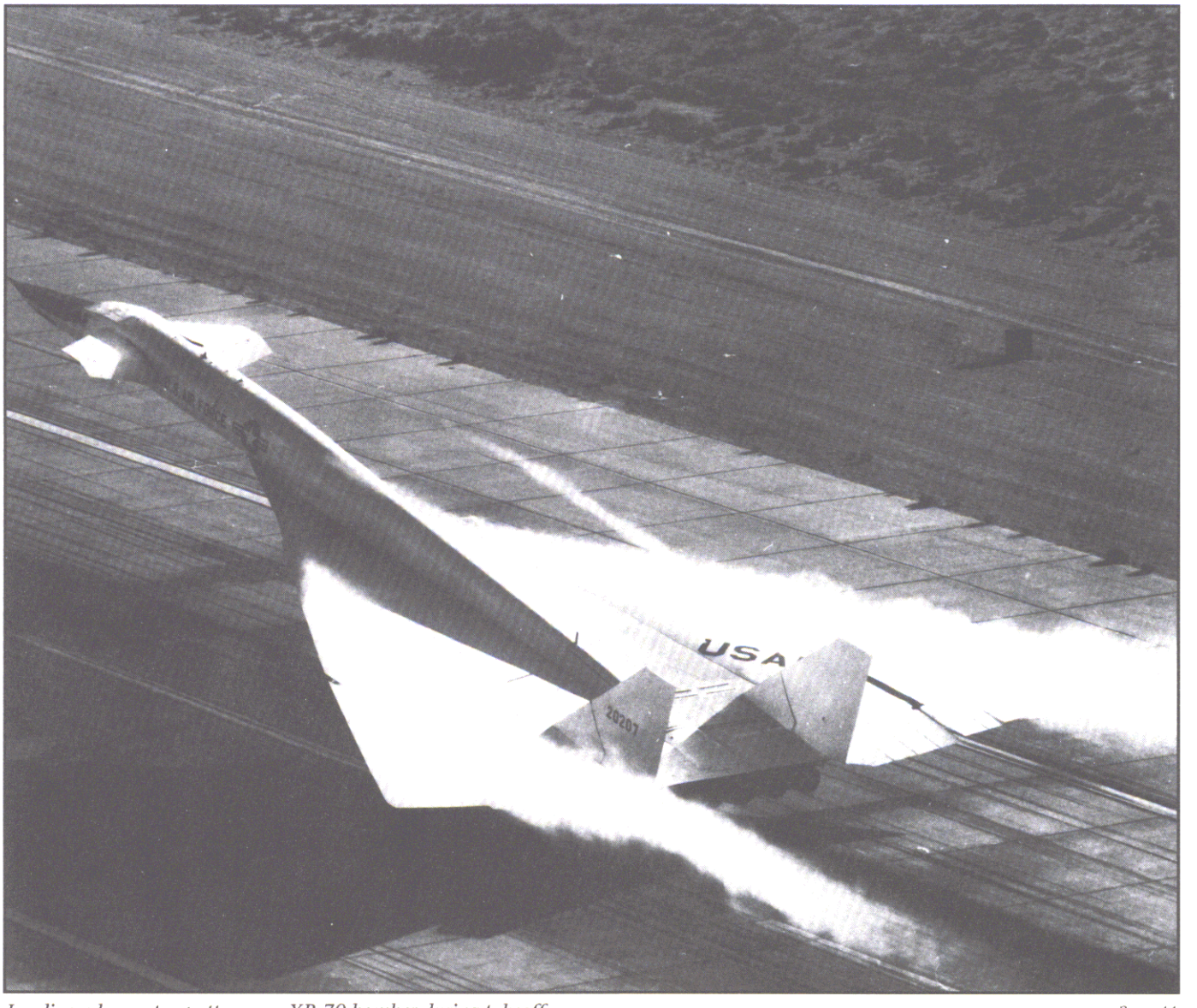

Leading-edge vortex patterns on XB-70 bomber during takeoff.

3 • 11

Leading-edge vortex patterns on Concorde transport during landing. 3 • 12

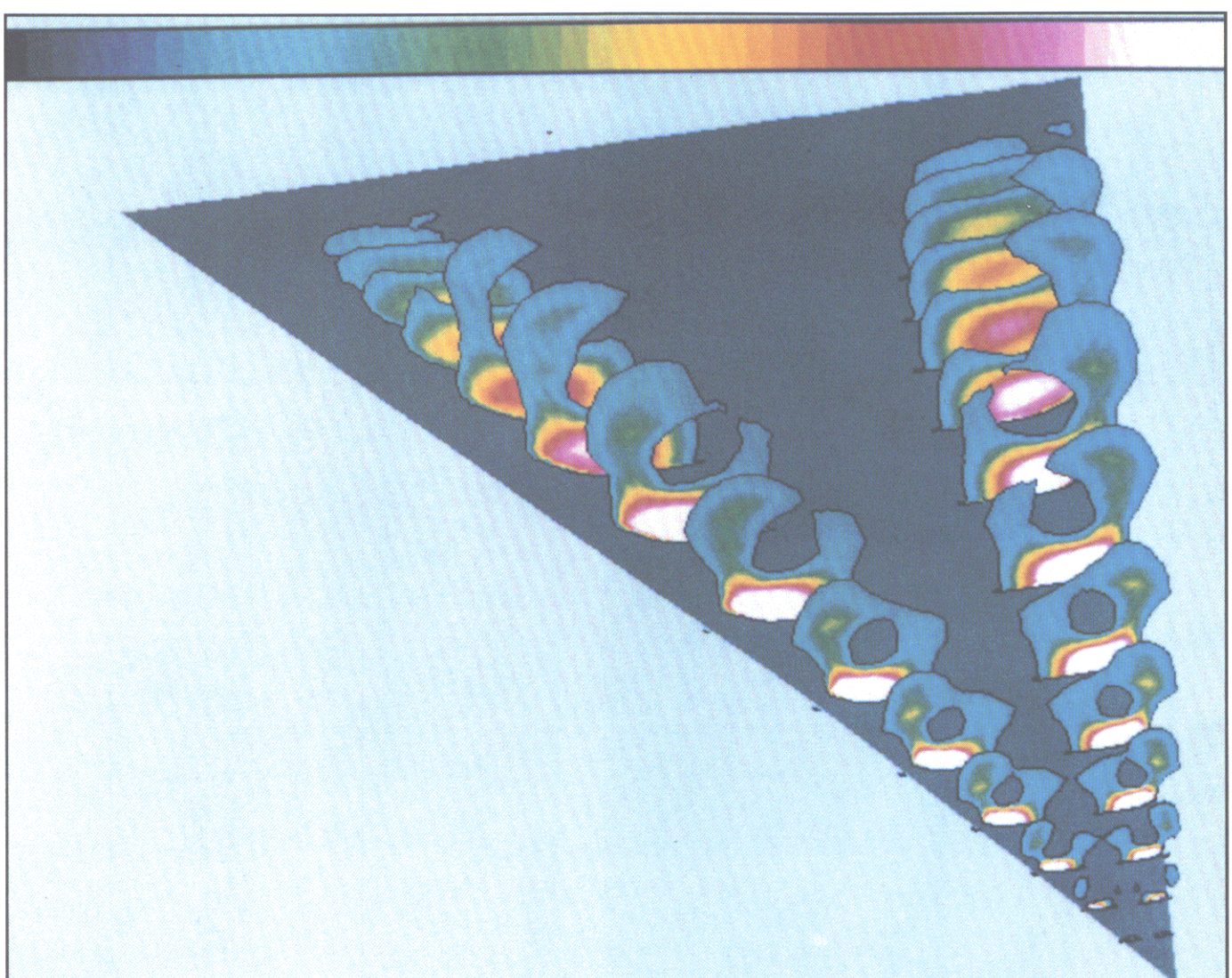

Leading-edge vortex patterns of calculated relative humidity for 76° delta wing at $\alpha = 21°$ and $M = 0.3$. 3 • 13

vortex with the highest relative humidity values in white being under the vortex core. The size of the pattern grows from the apex rearward to about 60 percent of the distance to the trailing edge, where it reaches a maximum and then diminishes as the trailing edge is approached because of the trailing-edge recovery, which causes a rise in temperature and pressure, and not because of a vortex breakdown. For this 76° swept delta wing, vortex burst occurs at the trailing edge at an angle of attack of about 33°.

An interesting outcome of the calculated RH_I pattern is that the core region of the vortex appears as a hole, where relative humidity values were less than 1.0 and thus were not plotted. Examination of the flow-field calculations showed that the core experiences an increase in temperature and a decrease in pressure compared with just outside the core, which results in a core value for relative humidity less than 1.0. This may be an additional explanation of why vortex cores sometimes appear to be hollow or clear, as noted in other photographs shown later, in addition to the classical explanation of centrifugal effects on core fluid particles.

An additional example of a leading-edge vortex flight pattern that develops along the wing of an RAF Lightning airplane during a turn is

Leading-edge vortices on RAF Lightning during maneuver. 3 • 14

Leading-edge vortex patterns on Rafale fighter with canard and cropped delta wing in a maneuver. 3 • 15

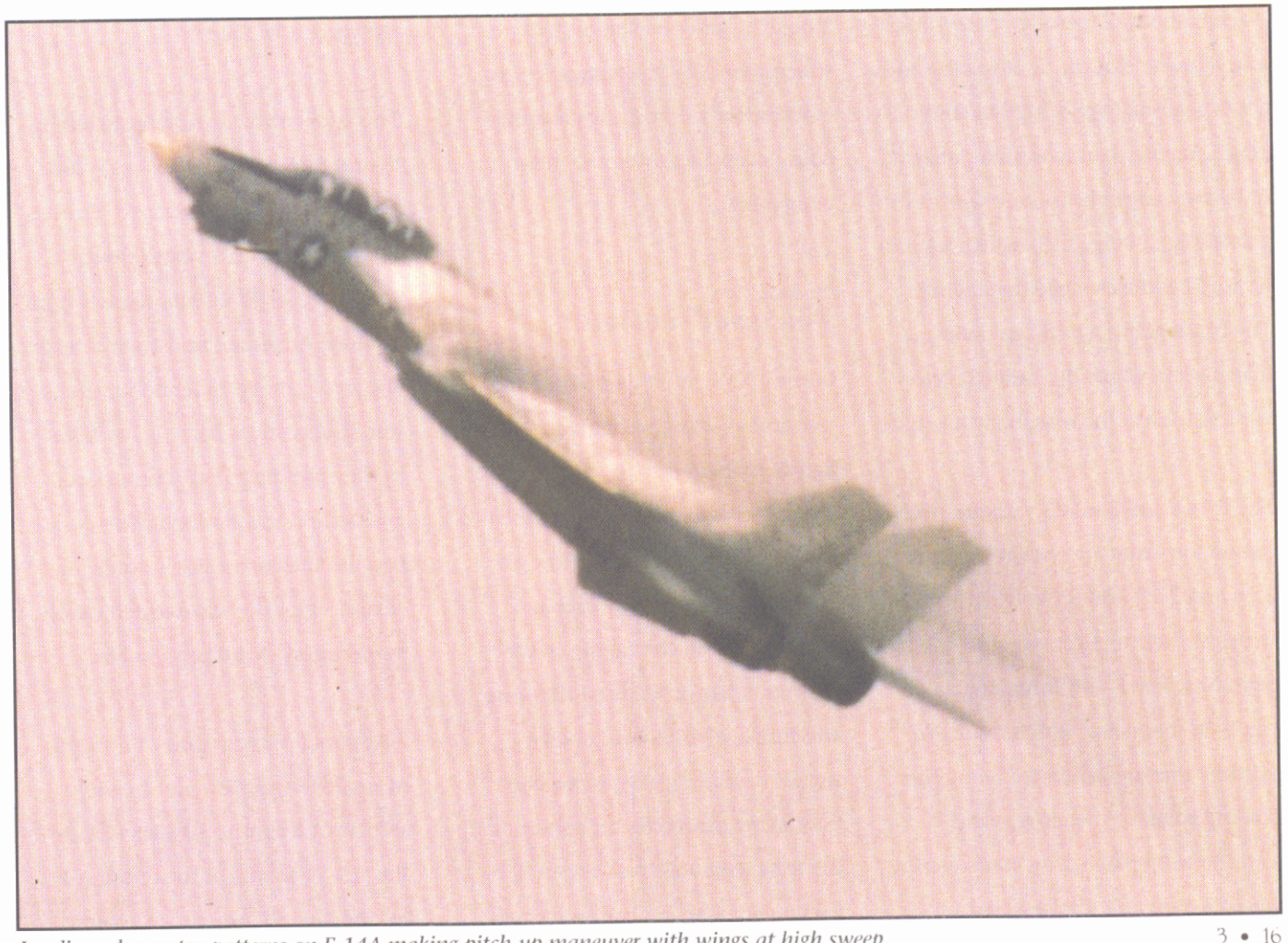

Leading-edge vortex patterns on F-14A making pitch-up maneuver with wings at high sweep. 3 • 16

Leading-edge vortex patterns on MiG-23 during maneuver with wings at high sweep.

shown in figure 3.14. The vortex grows along the leading edge until it reaches about 66 percent span, where a streamwise slot causes it to stop and a new leading-edge vortex to start outboard. Further condensation patterns of leading-edge vortices are shown for a Rafale fighter (fig. 3.15), which features a canard and a cropped delta wing. The photograph was taken during a maneuver in which the leading-edge vortices form at the wing-body juncture.

The F-14A and MiG-23 variable-sweep fighter airplanes are shown in figures 3.16 and 3.17, respectively, with their wings at their highest swept-back positions. The F-14A is making a pitch-up maneuver which results in vortices that are generated along the leading edges of the glove, vane, and the wing panel. The maneuvering MiG-23 has variable-sweep wing panels which are separated from the inner glove panel by a notch or break. Leading-edge vortices are generated along the glove and then shed streamwise over the wing when it reaches the notch. A new leading-edge vortex begins on the outer wing panel.

3.3.2 Wing-body strake/LEX

In the 1970's, a new aerodynamic technology was developed to improve fighter maneuverability at subsonic and transonic speeds. Two flow fields were combined: attached flow on the moderately swept wings and vortex flows on the highly swept fairings at the junction of the wing and fuselage, called wing-body strakes or leading-edge extensions (LEX's). At maneuver lift conditions, the flow separates from the strake leading edges to generate a pair of strong vortices, which generate vortex lift on the strake surfaces and interact favorably to energize the wing flow field.

This type of vortex flow is shown in figures 3.18 and 3.19 for the F-16B and F/A-18, respectively, two fighters which employ this vortex flow concept. The F/A-18 airplane is from the Blue Angels demonstration team and has a smoke generator at the rear. The vortices become invisible as they pass by the aft tail surfaces and behind the airplanes; this is because the vortex flows decelerate as they enter the wake which causes evaporation of the condensate.

Additional photographs of this type of strake vortex flow are shown in sections 4.8 for the F-16 and 4.9 for the F/A-18 as well as in section 4.17 for the MiG-29, which is a recent variant of this design philosophy.

Strake vortex flows on F-16B during maneuver. 3 • 18

In addition, there are many similarities between the vortex flows generated by strakes described here and those generated by chines on the SR-71, shown in section 4.19.

At some angle of attack, strake vortices begin to breakdown or burst, which is a common aerodynamic phenomenon that occurs for all separation-induced leading-edge vortex flows. At low levels of lift the strake vortex bursts at some point behind the airplane. As the airplane angle of attack increases, the burst point moves upstream until it is over the wing and strake surfaces as illustrated in figure 3.20, where the condensation pattern for the LEX vortices on the F/A-18 evaporates near the vortex burst point, probably because the vortex core experiences an adverse pressure gradient and deceleration which cause a rise in pressure and temperature that is great enough to cause evaporation to occur. A similar process occurs for condensed flow that vaporizes at a shock wave, discussed previously. The vortex burst flow field can have strong interactions with the structure and control of twin vertical tails, which must be understood for operation at high angles of attack.

The vortex burst flow field is visualized in figure 3.21 by dye ejected from a scale model of the F/A-18 in a water tunnel. The vortex core suddenly increases in diameter at the burst point, and this larger vortical flow continues over the wing and passes the vertical tails. This suggests that condensation may be a good way of visualizing the

LEX vortices, wing condensations, and wingtip vortices on F/A-18 during Blue Angels air show. 3 • 19

LEX vortices appearing to end in midair on F/A-18 during pitch-up to high angles of attack. 3 • 20

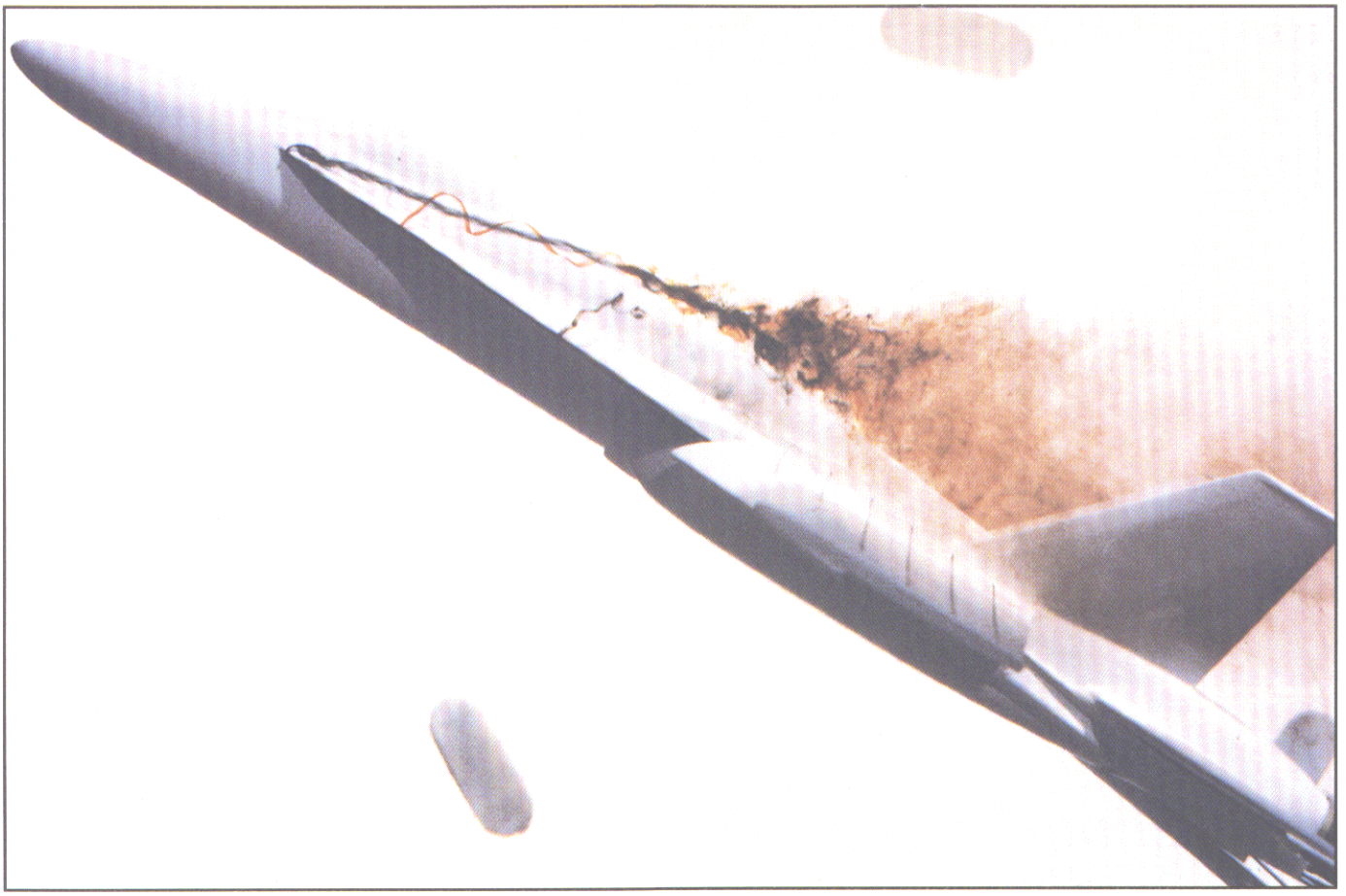

Vortex burst on F/A-18 model at α = 32° visualized with dyes in water tunnel. 3 • 21

location of vortex burst but care should be exercised when comparing flows visualized by condensation with those by seeding, like dyes or smoke.

When flows separate from highly swept leading edges, the resulting vortex flow is often depicted as a vortex sheet, noted in the sketch on the left of figure 3.22. Recent wind tunnel studies have found that the vortex sheet, which is a shear layer, becomes unstable and forms small filaments of vorticity as noted on the right side of figure 3.22. This fascinating flow phenomenon is illustrated in the photograph of figure 3.23 taken during a low-speed

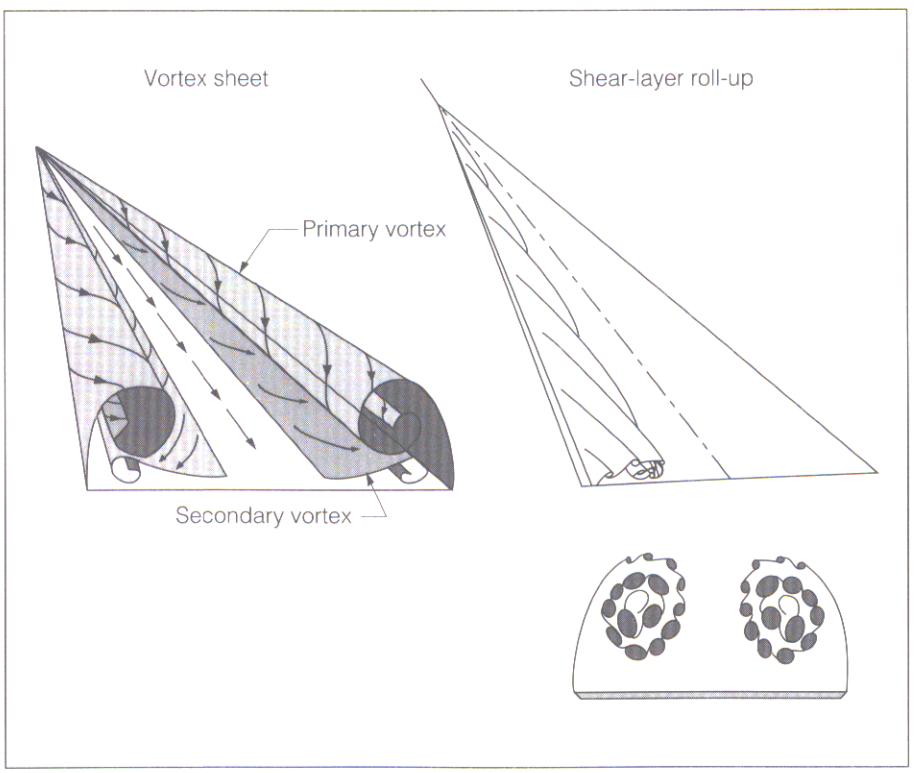

Sketches of leading-edge vortex flow above wing represented as vortex sheet or instability vortices in separated shear layer. 3 • 22

ORIGINAL PAGE
COLOR PHOTOGRAPH

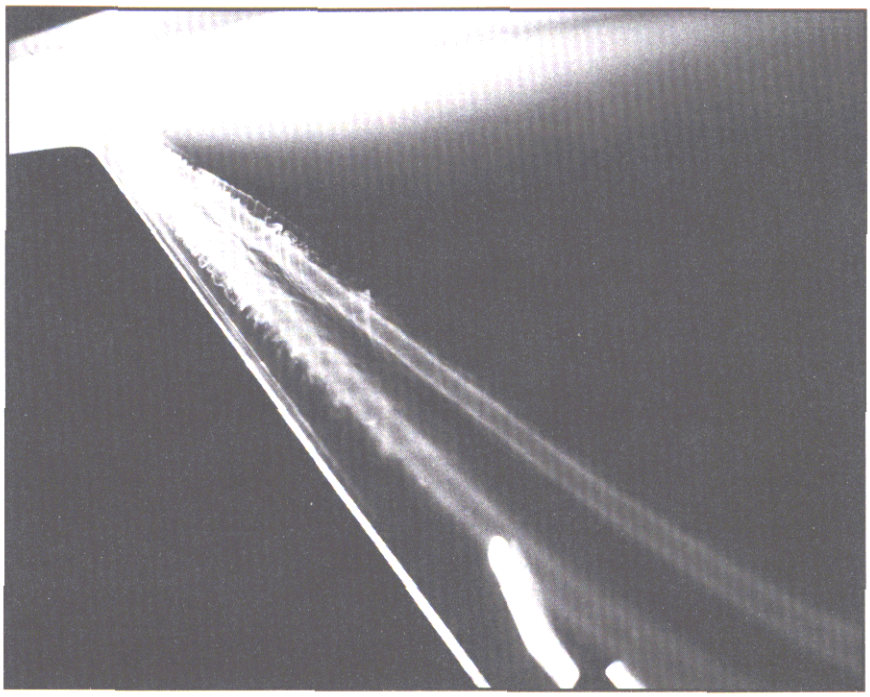

(a) Regular smoke flow visualization; α = 30°.

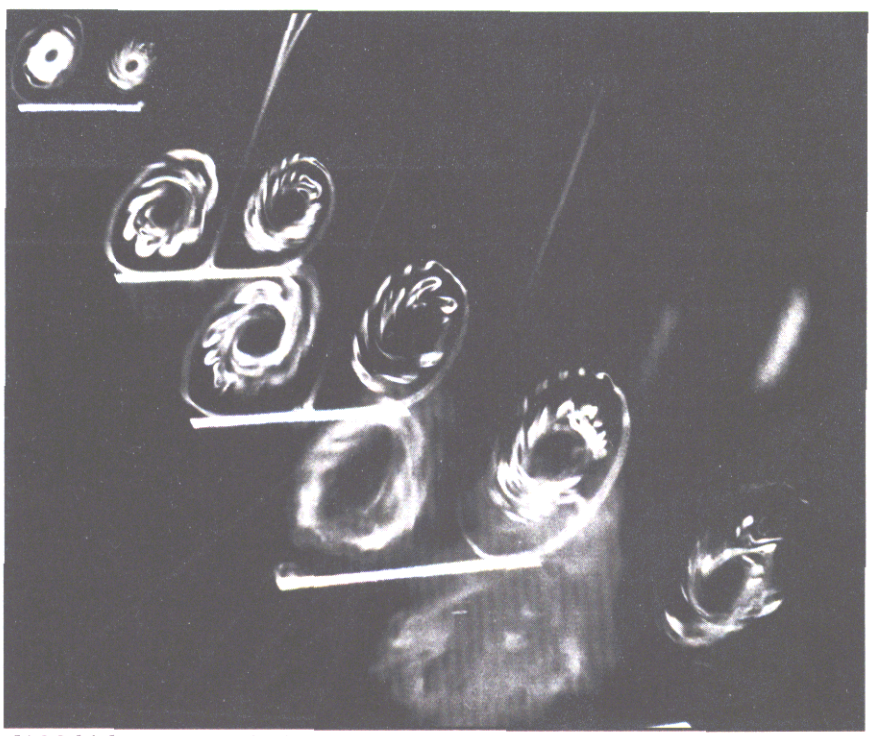

(b) Multiple exposures of different longitudinal cross sections; α = 40°.

Shear-layer instability vortices in leading-edge vortex flows for 85° delta wing visualized with smoke in low-speed wind tunnel.

3 • 23

wind tunnel experiment, where smoke was introduced at the apex of an 85° delta wing to visualize the flow. The tunnel air is blowing from left to right. A regular type of smoke flow visualization is shown in figure 3.23(a) for α = 30°. With the wing at α = 40° in figure 3.23(b), the photograph was made with multiple exposures at different longitudinal cross sections with a laser light sheet. As noted in both photographs, small vortex filaments begin at the outer edge of the sheet and follow a spiraling path until, at some distance downstream, they coalesce along the outer edge of the vortex core.

A similar type of condensed flow pattern was observed for a number of airplanes which had leading-edge strake, LEX, or chine vortex flows and gives visual evidence for the first time that this flow mechanism exists in flight. The F-16 and F/A-18 airplanes had very distinctive features in the strake and LEX vortex flows. Two maneuver conditions are shown for an F-16, one at moderate lift (fig. 3.18) and the other at high lift (fig. 3.24), where the strake vortex has burst and evaporated over the wing. At moderate lift, the condensation pattern for the left strake vortex begins as a straight line at the apex, begins to undulate about halfway down, and continues to have larger undulations over the wing. At first

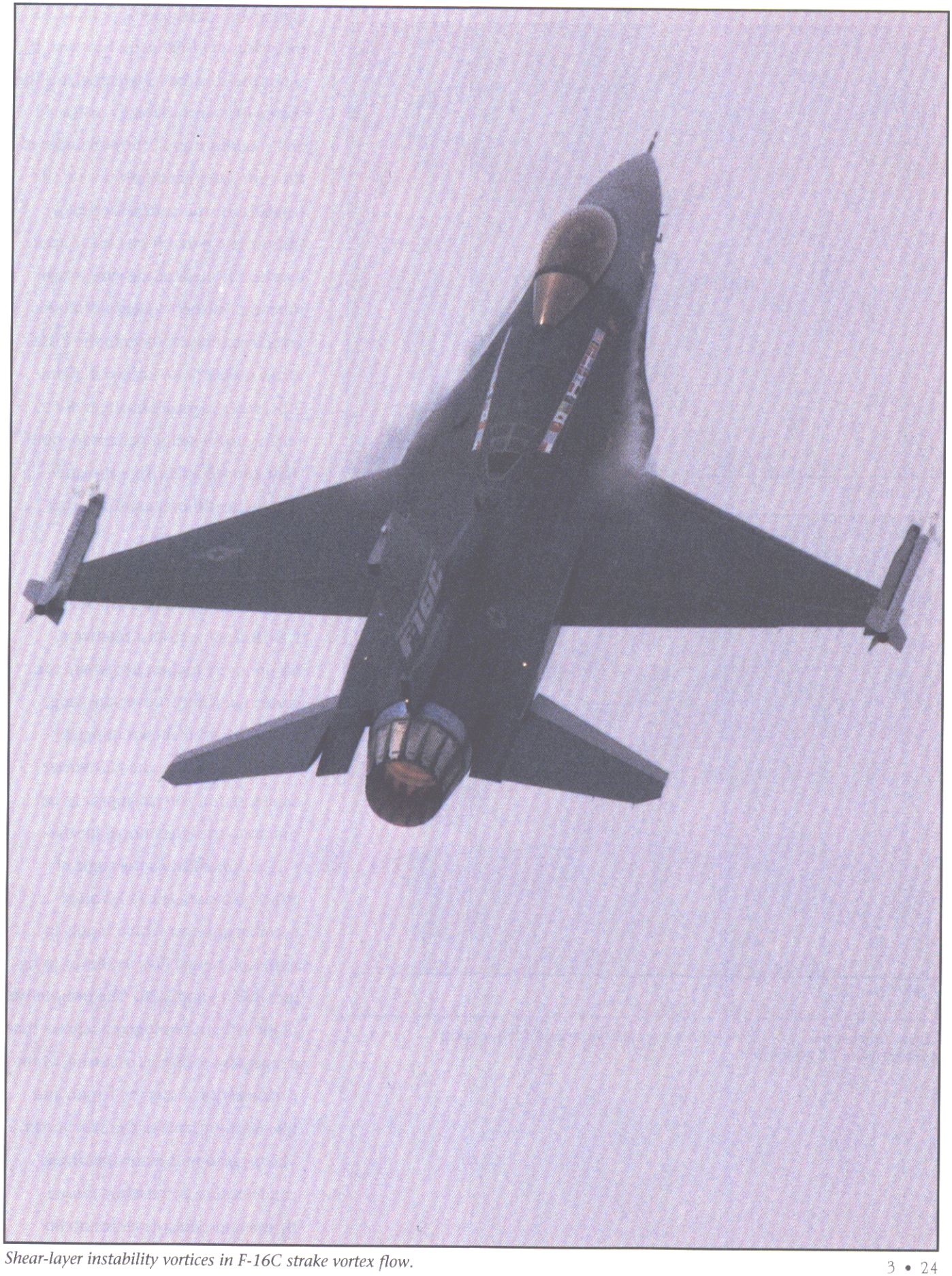

Shear-layer instability vortices in F-16C strake vortex flow.

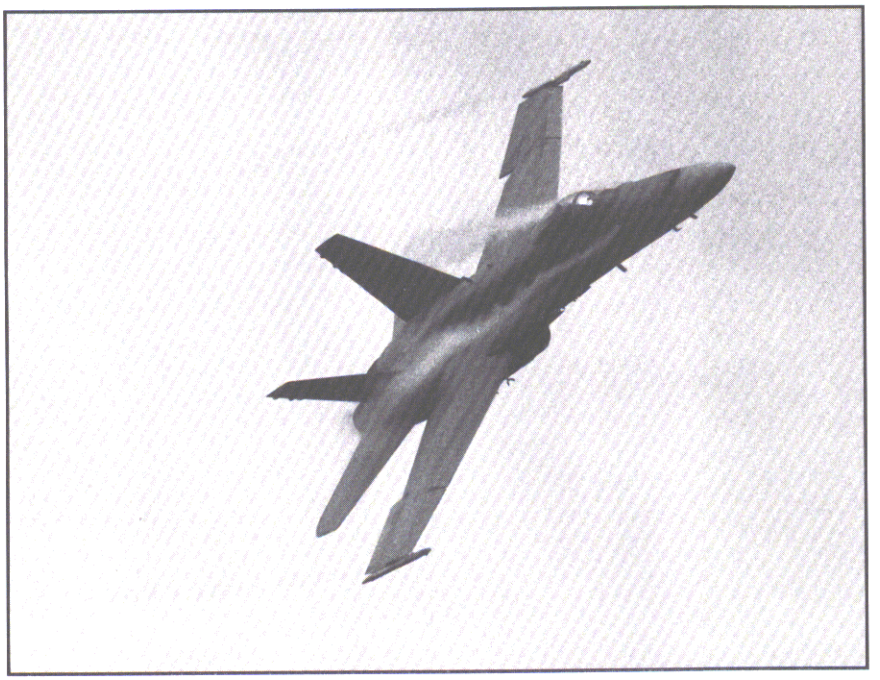

(a) Lower lift.

(b) Higher lift.

Maneuvering sequence of CF/A-18 showing shear-layer instability vortices developing in LEX vortex flow. 3 • 25

glance the vortex core appears to be following a twisted path; however, it is not the core that is twisting, it is the vortex filaments that are condensed and rotating around the outer edge of the core. They get bigger toward the rear because the vortex sheet grows from where it first forms at the apex to where it sheds at the wing-strake juncture. Further evidence of shear-layer instability vortices in the F-16C strake vortex flow is noted in figure 3.24, where periodic changes occur in the condensation pattern for both right and left sides. This airplane is at higher lift because the vortex is burst over the wing.

Figures 3.25 and 3.26 show the F/A-18 ranging from a moderate lift up to the highest lift, where the vortex burst occurs over the wing. At the lower lift shown in figure 3.25(a), changes in the LEX vortex condensation pattern appear to be similar to the effect noted for the F-16 at lower lift. As the angle of attack increases, the LEX vortex becomes stronger which results in more condensed flow as shown in figures 3.25(b) and 3.26. The perspective of these flight photographs shows that a repeating pattern is occurring in the condensation along the length and the outer portions of the LEX vortex. The suggestion is made that these condensation patterns are caused by the same shear-layer instability vortices as those just described for

Shear-layer instability vortices in F/A-18 LEX vortex flow.

the wind tunnel experiment. Additional examples were found where this flow pattern occurred, including the wing and chine vortex for the SR-71 in the Foreword and figure 4.96 and the leading-edge vortex of the RAF Lightning (fig. 4.73).

3.3.3 Glove/Fairing

Gloves and fairings are used in the designs of many bomber and fighter airplanes. Highly swept gloves located at the wing-fuselage juncture of variable-sweep airplanes enable these airplanes to perform a variety of missions. Lowering the wing sweep increases the wingspan to provide high lift for takeoff and landing and to yield the optimum cruise and best maneuver at subsonic speeds. Increasing the wing sweep lowers the wingspan to provide the lowest drag for supersonic cruise and low gust response for high-speed on-the-deck runs at high dynamic pressures. The gloves cover the wing-pivot mechanism

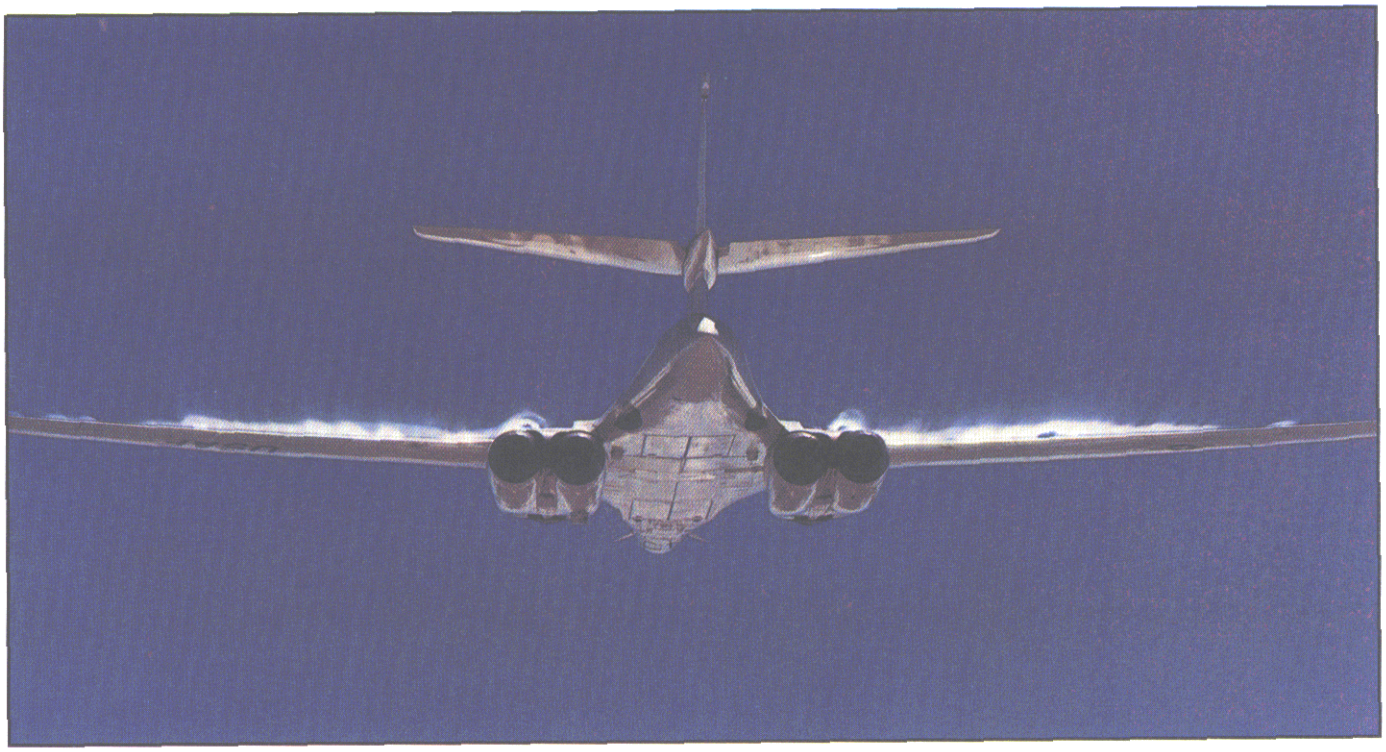

Vortices generated by gloves on B-1A in high-lift condition at M = 0.7 with wings swept to 25°. 3 • 27

Vortices generated by gloves on MiG-23 during pitch-up. 3 • 28

and reduce the shift of the aerodynamic center when flying from subsonic to supersonic speeds.

The B-1A bomber with variable-sweep wings has gloves with thick, rounded leading edges designed to delay leading-edge separation; however, because of the high sweep angle of the glove, the flow does separate at some conditions to form a vortex. The photograph in figure 3.27 shows glove vortices over the inboard portion of the B-1A wing just above the engines. The B-1A is in a high-lift condition with the wings swept to 25° and at a Mach number of 0.7. There are some similarities between the glove vortex and the wing-body strake and the LEX vortices described in section 3.3.2. Typically, however, glove vortices for bombers are a form

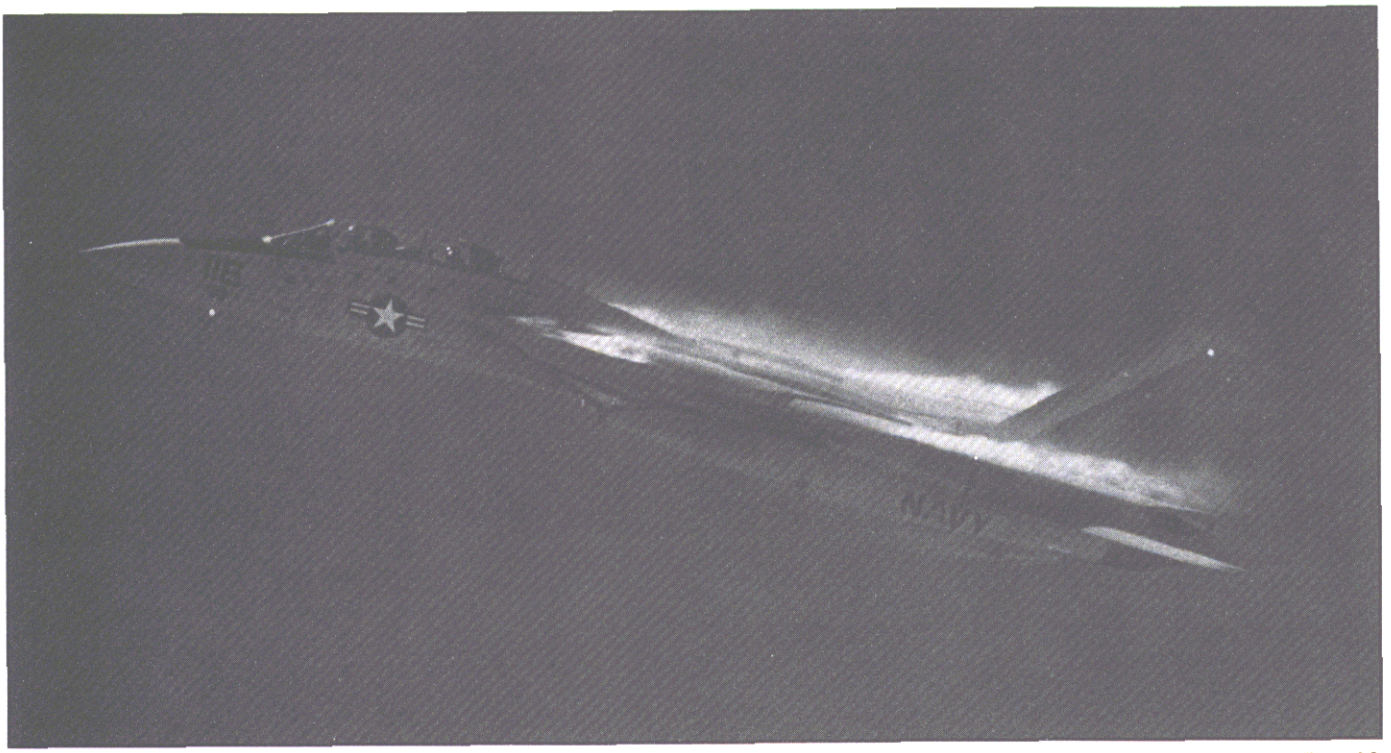

Vortices generated by highly swept glove and wing surfaces on F-14A. 3 • 29

Vortices generated by fairings at wing root of SEPECAT Jaguar. 3 • 30

of separated flow and are not designed to enhance performance like strake or LEX vortices.

Variable-sweep fighter airplanes are designed with thinner gloves that generate leading-edge vortices to augment their performance to higher angles of attack. The condensation patterns for the MiG-23 airplane are shown in figure 3.28. At the wing-glove juncture, the wing panel has a sizable chord extension that creates a notch between the two surfaces which interrupts the flow at the end of the glove and starts a new flow on the wing panel. The evaporation of the glove vortices over the inboard part of the wing may be due to bursting. The wing sweep of 45° is high enough to create leading-edge vortices which cause the condensation on the wing panels. Higher wing sweeps generate stronger leading-edge vortices as

Vortices on engine chine and wing outer panel rotating around each other during landing of SR-71. 3 • 31

illustrated for the F-14A (fig. 3.29), where vortex flows occur on the gloves and the 68° swept wings. Figure 3.30 is an example of separation-induced leading-edge vortex flows created by fairings during a maneuver of the SEPECAT Jaguar. The fairings that begin at the upper part of the engine housing are small, highly swept surfaces located at the wing root. They curve around to match the wing leading-edge sweep angle of about 44° to fill in the junction between these surfaces. These fairings have a much smaller surface area compared with that of the gloves or strakes or LEX's. The vortices have probably burst over the wing.

3.3.4 Multiple Interacting

As was discussed previously, configurations that have strakes and LEX's, like the F-16 and F/A-18, have trapezoidal wing planforms with moderate leading-edge sweep angles to maintain attached flow during maneuvering flight. Supersonic cruise designs like the SR-71 require thinner wings with higher sweep to minimize cruise drag, and they feature a double-delta type of wing planforms with a leading-edge sweep break. Inboard the wing is highly swept and changes to a lower sweep outboard. Leading-edge vortices can be generated by both planforms and can interact with each other as they flow over the wing. A rough rule of thumb is that a leading-edge vortex forms when the wing leading-edge sweep angle is ≥50°. Also, if the leading-edge sweep angles are within 10° of each other, there is little evidence of dual vortices.

The SR-71 airplane (fig. 3.31) provides an excellent example of the condensation pattern that occurs because of multiple vortex interactions. The vortex flows are generated from the leading edge of the chine, located on the outboard side of the engine housing, and from the leading edge of the outboard wing panel. Because the two vortices are corotating, that is, rotate in the same direction, the vortex flows rotate about each other. The outer-panel vortex is displaced upward and inboard, whereas the

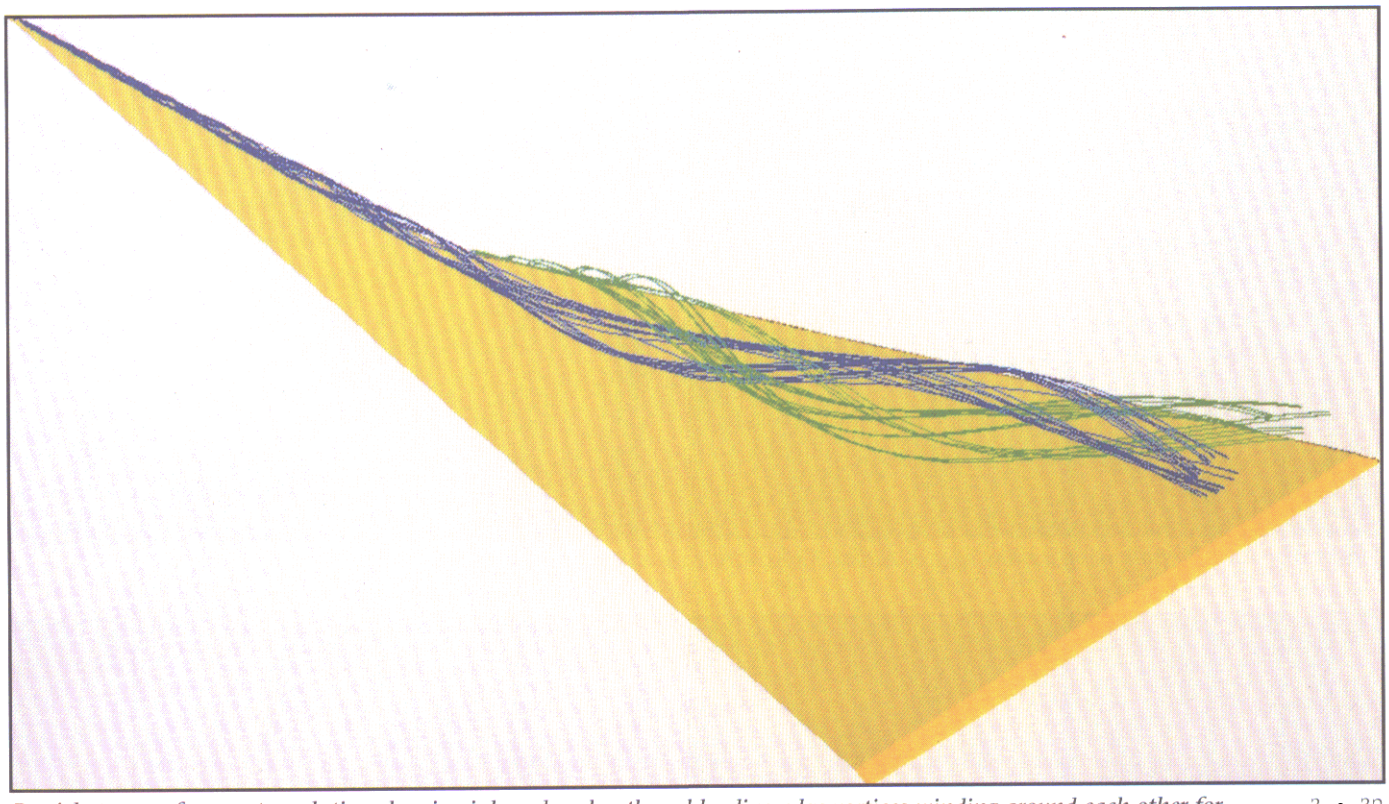

Particle traces of computer solution showing inboard and outboard leading-edge vortices winding around each other for 76°/60° double-delta wing geometry at α = 20°. 3 • 32

chine vortex is displaced downward and outboard to form the spiraling pattern in the photograph.

Computational techniques can be employed to predict this complicated vortex interaction. Figure 3.32 shows an example for a calculation of two leading-edge vortices over a double-delta planform at an angle of attack of 20° and shows only the right side. The spiraling interaction of the two leading-edge vortices is illustrated with particle tracing techniques to track the flow; purple particles are emitted along the inboard leading edge and green particles along part of the outboard leading edge.

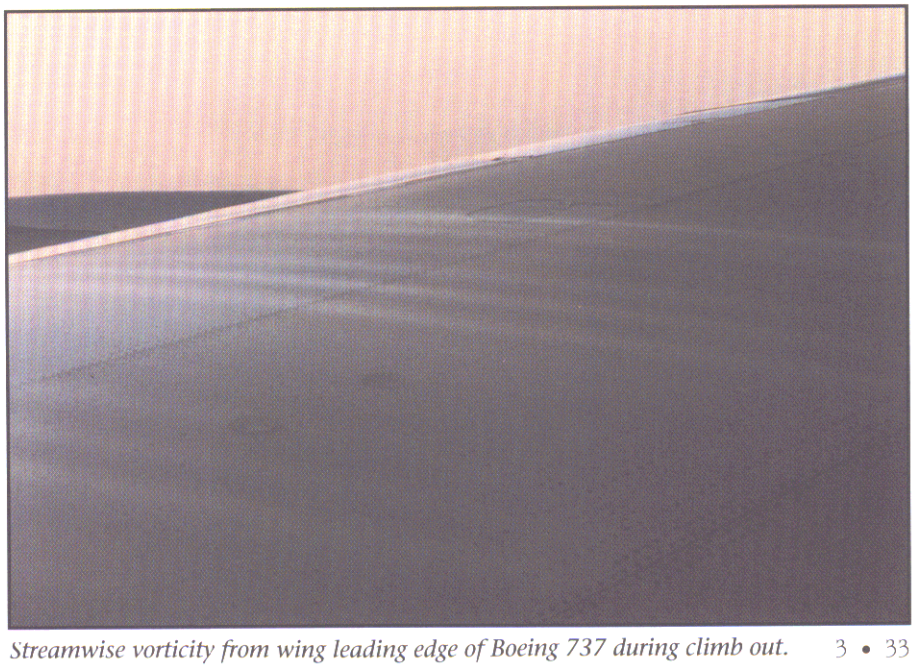

Streamwise vorticity from wing leading edge of Boeing 737 during climb out. 3 • 33

3.3.5 Streamwise Vorticity from Wing Leading Edge

An unusual streamwise condensation pattern that is not normally observed on airplanes was found coming from the wing leading-edge region and occurred on a variety of transport, bomber, and fighter wings during flights at and above cruise lifts. Two transports—a Boeing 737 and an Airbus A300—are shown in figures 3.33 and 3.34 during climb out with

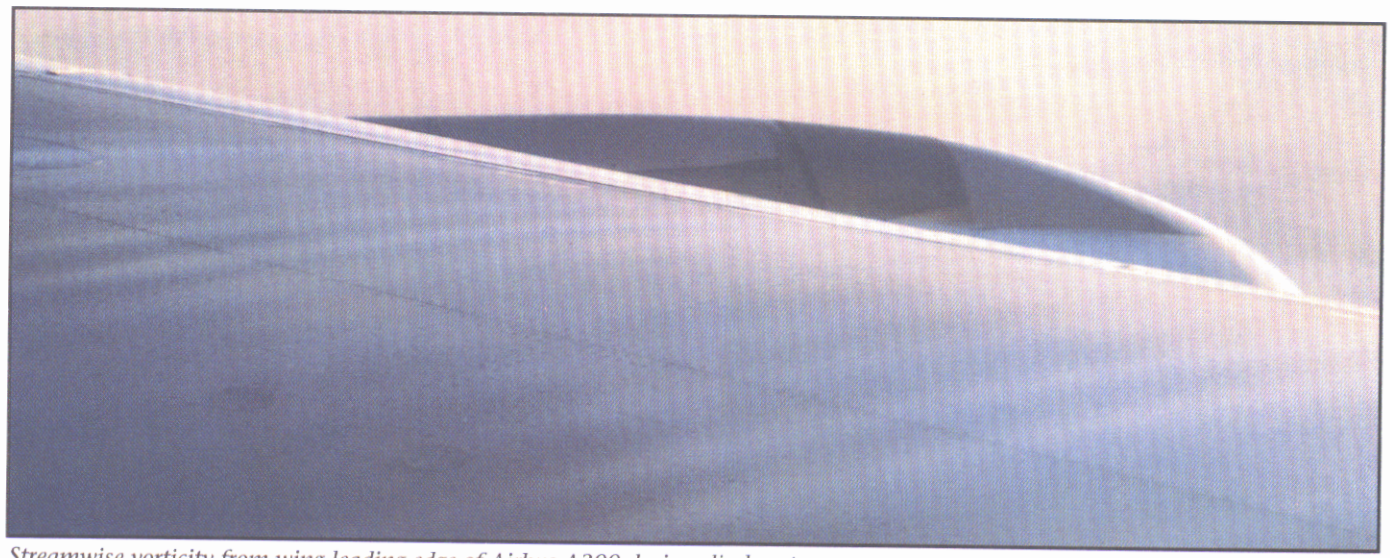

Streamwise vorticity from wing leading edge of Airbus A300 during climb out.

3 • 34

Streamwise vorticity from F-16 wing leading edge during maneuver.

3 • 35

Streamwise vorticity from F/A-18 wing leading edge during maneuver. 3 • 36

their leading-edge devices retracted; these figures show equally spaced streams of condensed flow on the inboard portion of the wings. In figure 3.33, the right wing upper surface leading edge is to the left, and in figure 3.34, the left wing upper surface leading edge is to the right. The same pattern occurred on the inboard wing surface for an Airbus A300 at cruise (figs. 3.51(b) and 3.51(d)). Because this flow pattern was found on a variety of airplanes over a range of lift conditions, it is postulated that these are parallel vortices that originate from the wing leading-edge region and that the occurrence is natural and not artificially created by bumps on the surface of the airplane or by vortex generators.

One reason why small vortical flows can occur in an upper surface flow on a wing is because the three-dimensional boundary-layer flow around a swept round leading edge can develop instabilities in its velocity profile which can result in small cross-flow vortices. These vortices are corotating and streamwise and are usually studied for their implications on the transition process of three-dimensional laminar boundary layers at cruise lift. In the photographs (figs. 3.33 and 3.34), the vortices are much larger and spaced farther apart than those for the classical laminar cross-flow vortices. This difference is probably because the boundary layer is turbulent for this flight condition, because of the higher lifts and because boundary-layer separation, rather than transition, appears to be the principal flow mechanism.

Similar condensation patterns were obtained for a number of fighters and bombers, such as the A-6E (fig. 4.2), F-16 (fig. 4.50), F/A-18 (fig. 4.59), and B-1A (figs. 3.27 and 4.10). Examples of the F-16 and F/A-18 are shown in figures 3.35 and 3.36, respectively, for conditions where the strake vortices are condensed and the wing leading-edge and trailing-edge flaps are deflected during a maneuver. For both airplanes, the vorticity is shed streamwise from the leading-edge region and spanwise over the whole wing, although the size and spacing appear to be larger than observed on the transport (e.g., fig. 3.33). In addition, the pattern on the wing appears to stop at the mid chord. This effect is interpreted to be the result of the compressing of the upper surface flow approaching the trailing edge, which

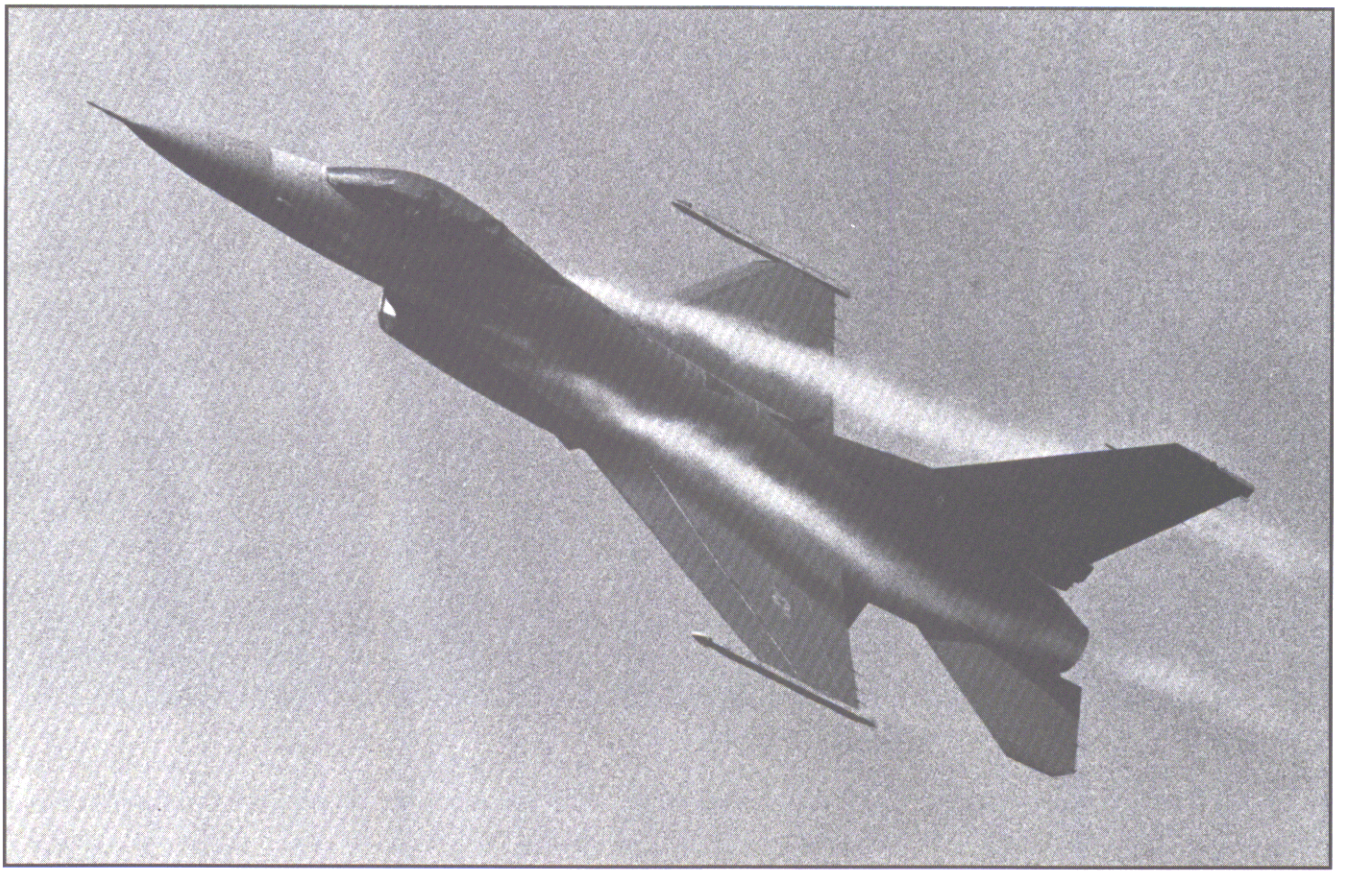

(a) Moderate lift.

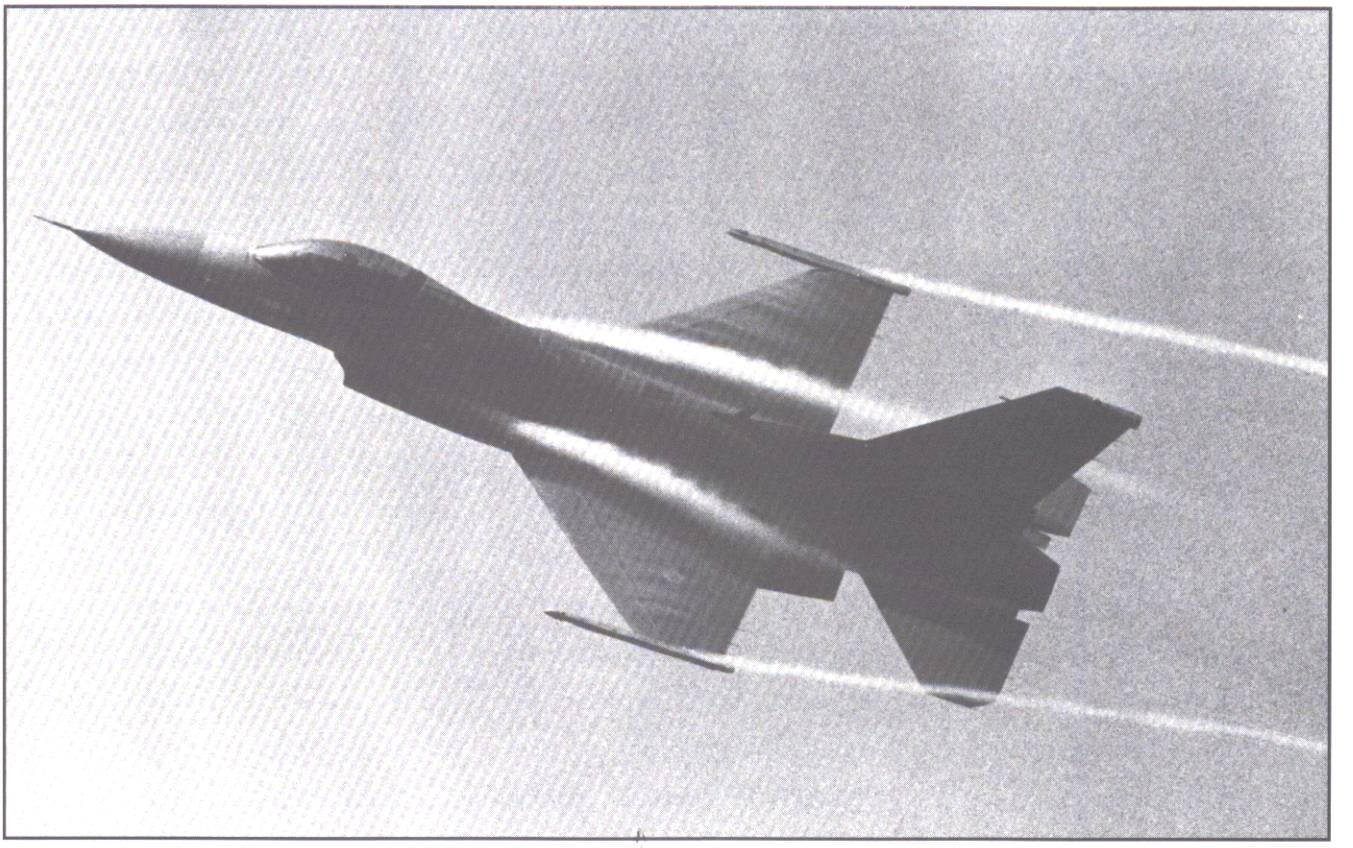

(b) Higher lift.

Streamwise condensed vortices over leading-edge area of F-16C wing as lift increases during maneuvers.

Streamwise vortices on 68° swept wings of F-14A. 3 • 38

increases temperature and pressure and could cause evaporation. The streamwise vortices would be expected to continue over the wing and into the wing wake.

The F-16C photographs in figure 3.37 were taken during a maneuver sequence. Figure 3.37(a) shows the condensed strake vortex but no condensation on the wing. In figure 3.37(b), the lift should be higher because the wingtip vortices are visible, streamwise condensation has started on the wing, and the condensed flow in the strake vortex is evaporating farther forward.

The 68° swept wings of an F-14A (fig. 3.38) provided the highest wing sweep this phenomenon was observed for. From this perspective, it is particularly noticeable on the outer portion of both wing panels. The streamwise vortices are shown (figs. 4.23(f) and 4.24) for the F-14A with the wing at low sweep.

3.3.6 Vortex Generators

Vortex generators are flow control devices that are located at various places on an airplane to help control flow separation and improve airplane performance and controllability. The airplane designer decides where they need to be placed to work best in the vehicle flight envelope of lift, speed, and variable geometries. One type of generator that is frequently used consists of small surfaces that are perpendicular to the upper surface of a wing. They are approximately the height of the boundary-layer thickness and generate discrete streamwise vortices to help energize the boundary-layer flow and delay separation to a higher angle of attack. This type of vortex generator is shown in figure 3.39 for a Buccaneer airplane during a flight near an ocean surface. The vortex generators are in a line approximately parallel to the leading edge of the wing on the forward part

Vortices created by generators located across wing upper surface of Buccaneer flying near ocean surface. 3 • 39

Vortices created by generators on outboard portion of right wing of Airbus A300 during cruise. 3 • 40

of the upper surfaces which cause the condensation to occur. It is especially notable on the left wing of the airplane (i.e., to the viewer's right) where the individual vortices show up as discrete bumps in the pattern. An additional condensation pattern is on the underside of the horizontal tail which has the appearance of small streamwise vortices; however, the airplane does not have vortex generators located on the horizontal tail. These vortices are probably generated from the leading-edge area as described in section 3.3.5 from wing leading edges. To trim a stable airplane at cruise flight, the aft tail has to produce negative lift to trim the wing nose-down pitching moment. This means that the tail lower surface becomes the suction surface which is why the condensation occurs only on the lower surface.

A number of transport airplanes use this type of vortex generator on the wing upper surface, such as the Airbus A300 shown in figure 3.40. This photograph was taken looking forward at the right wing and shows the generators located in a row along the upper surface of the outboard portion of the wing. (See section 3.3.9.)

A more unusual type of vortex generator has been developed during the past decade to help control the adverse interactions that occur between nacelle separated flow and wing flow for a number of transport airplanes during high-lift operation. As shown in figure 3.41, small strakes or chines are positioned on the inboard side of the engine fan cowl of a Boeing 707 to generate strong vortices that pass over the wing upper surface. The favorable interference improves wing flow at the high-lift conditions, during which the leading-edge devices are deflected down. The chine vortices help control separated flow from the nacelles at high lift; this reduces both the required approach speed of the airplane and landing field length. The vortex cores are clear of

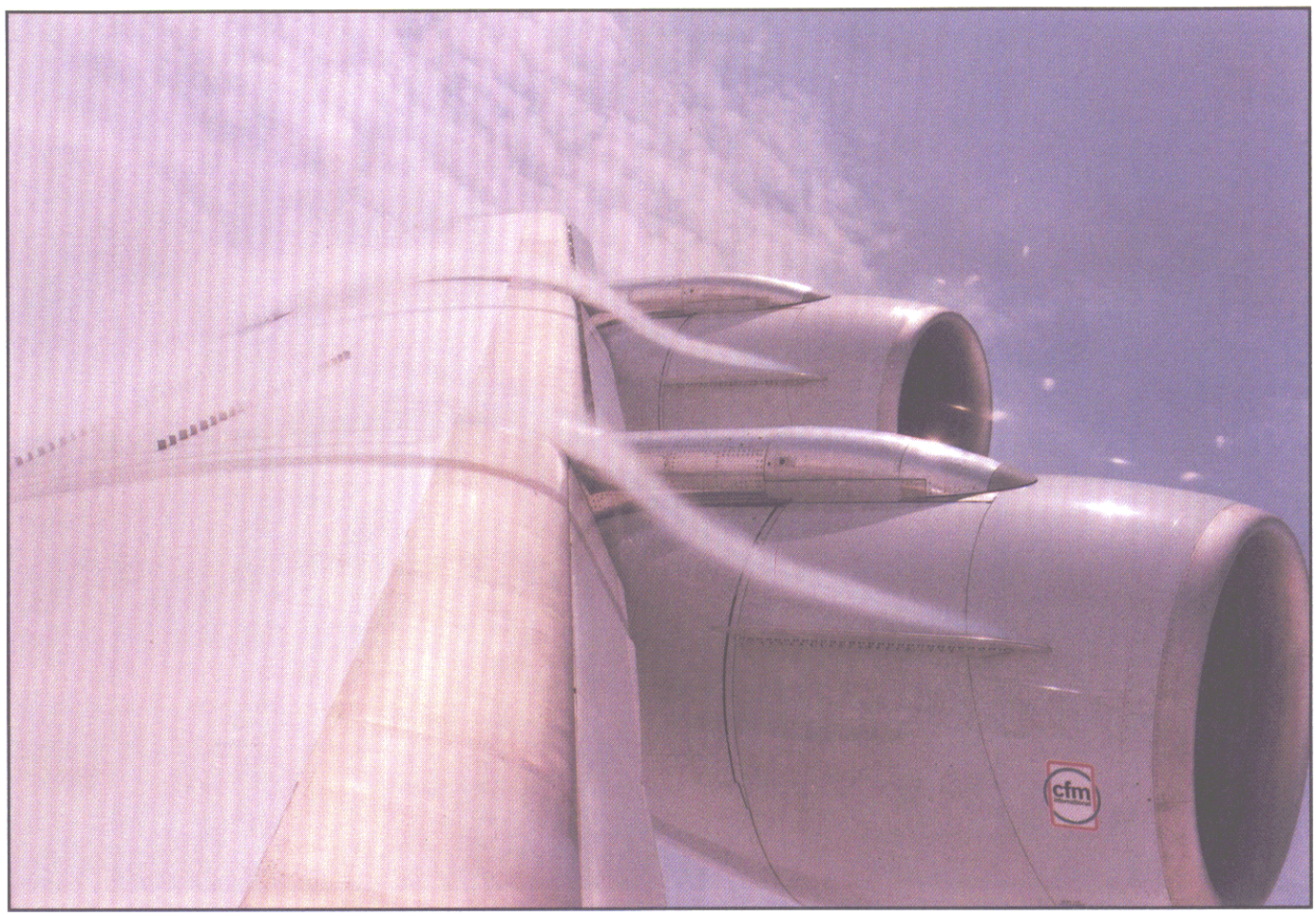

Vortices generated by nacelle strakes on Boeing 707 during high-lift test. 3 • 41

condensed flow, appearing like hollow tubes, which may be caused by two effects discussed in section 3.3.1: the lower humidity level in the core leads to vaporization and centrifugal effects move condensed and uncondensed particles out of the core. Many transport airplanes have incorporated chines in their designs, such as on the inboard side of the nacelles on the Boeing 767 and the McDonnell Douglas DC-10 and on both sides of the nacelles on the Boeing 737-300 and the McDonnell Douglas MD-11.

3.3.7 Ground Vortices

Interaction of the airflow from propulsion units and the ground causes a vortex that starts at the ground and bends around into the inlet.

This unusual type of vortical flow can occur with all classes of military and commercial airplanes. It is a potential safety hazard when these small vortices create suction forces strong enough to pick up foreign objects from the runway and ingest them into the internal machinery of the engine. In addition, the vortex can cause nonuniform flow ahead of the compressor blades which can result in compressor stall. The vortex is strongest when the airplane is stationary or taxiing and fortunately disappears at higher runway speeds.

This phenomenon is dramatically illustrated for the YC-14 prototype military transport (figs. 3.42 and 3.43) and for the Asuka STOL research aircraft (fig. 3.44), where ground vortices are being drawn into the engine inlets. Both these aircraft have engines that exhaust over the wing upper surfaces; therefore, the inlets are positioned very far above the

Propulsion-induced vortex flows drawn into inlet of YC-14 during high thrust. 3 • 42

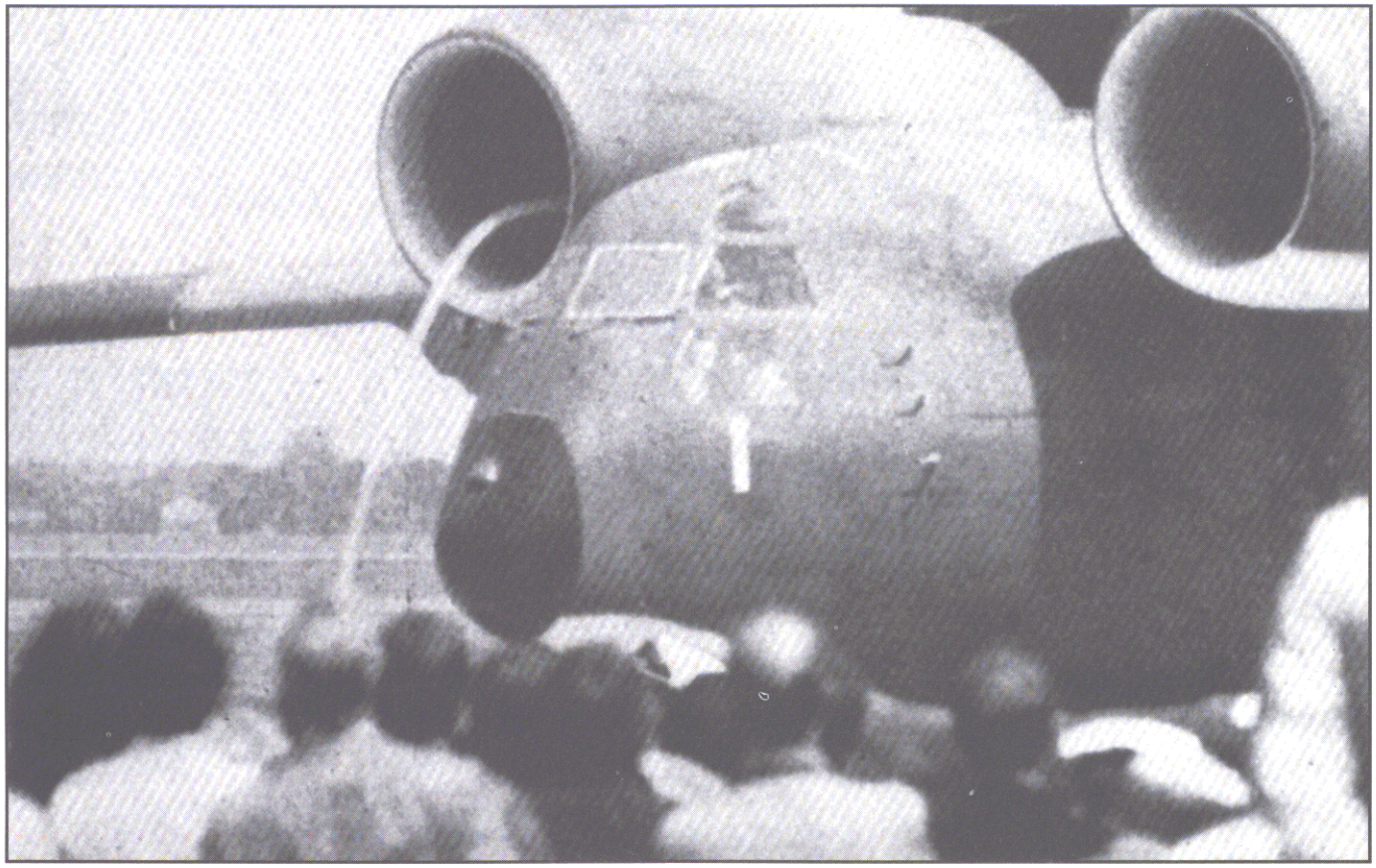

Ground vortex drawn into inlet of YC-14 at high thrust levels. 3 • 43

Ground vortices between engine intake and ground and between adjacent engines for Asuka STOL research aircraft during static tests. 3 • 44

Ground vortices generated by outboard propeller for C-130 transport. 3 • 45

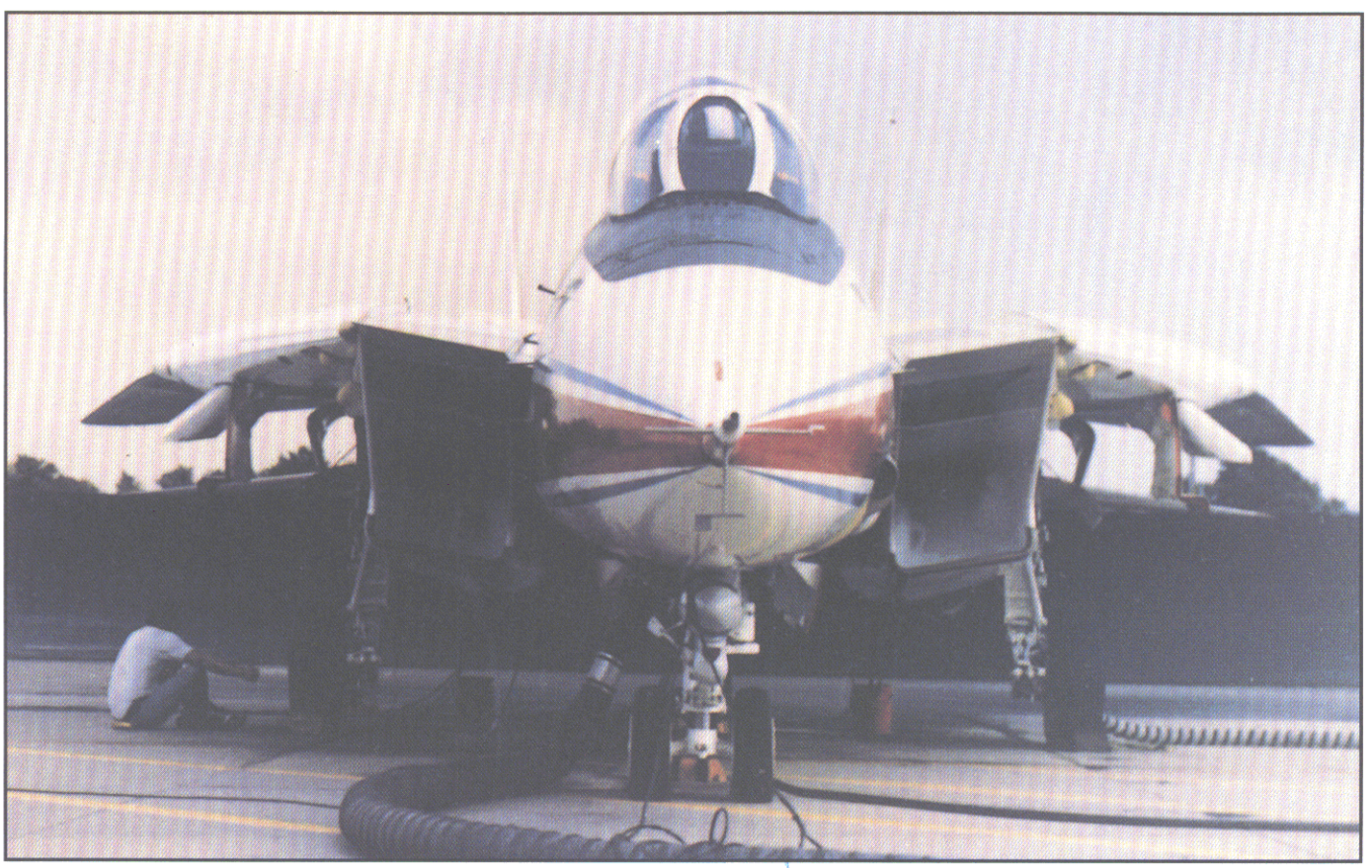

Ground vortex drawn into inlets of F-14A during static tests. 3 • 46

Separation-induced vortices generated by boundary-layer splitter plate on inlet of RAF F-4 during high-speed pull-up. 3 • 47

ground. The propulsion system on the Asuka also generates a vortex between adjacent engines. Ground vortices can also occur for propeller airplanes as observed in figure 3.45 for a C-130 transport.

Fighters are especially susceptible to ground vortices since their jet engines are in close proximity to the runway or carrier deck. This is illustrated in figure 3.46 for the F-14A during a static engine test. The F-15 airplane with its F100 engines can affect an area up to 25 ft in front of the inlet and has even picked up missile firing pins from the ground 4 ft behind the inlet with the engines at idle. At operational air bases, ground crews use a variety of maintenance techniques to minimize accidently ingesting foreign objects, including regularly walking up to 10 abreast to clear runways and taxiways. The ingestion problem is especially hazardous for Navy aircraft because of the high thrust levels required during carrier takeoffs.

3.3.8 Engine Inlet Related

During maneuvers, some fighters attain angles of attack where flow separation occurs around or near their engine inlets. These separation-induced vortex flows may affect inlet and engine performance as well as interact with aft surfaces. The first example is for an RAF F-4 airplane during a high-speed pull-up (fig. 3.47), where the flow appears to separate along the upper surface side edge of the boundary-layer splitter plate on

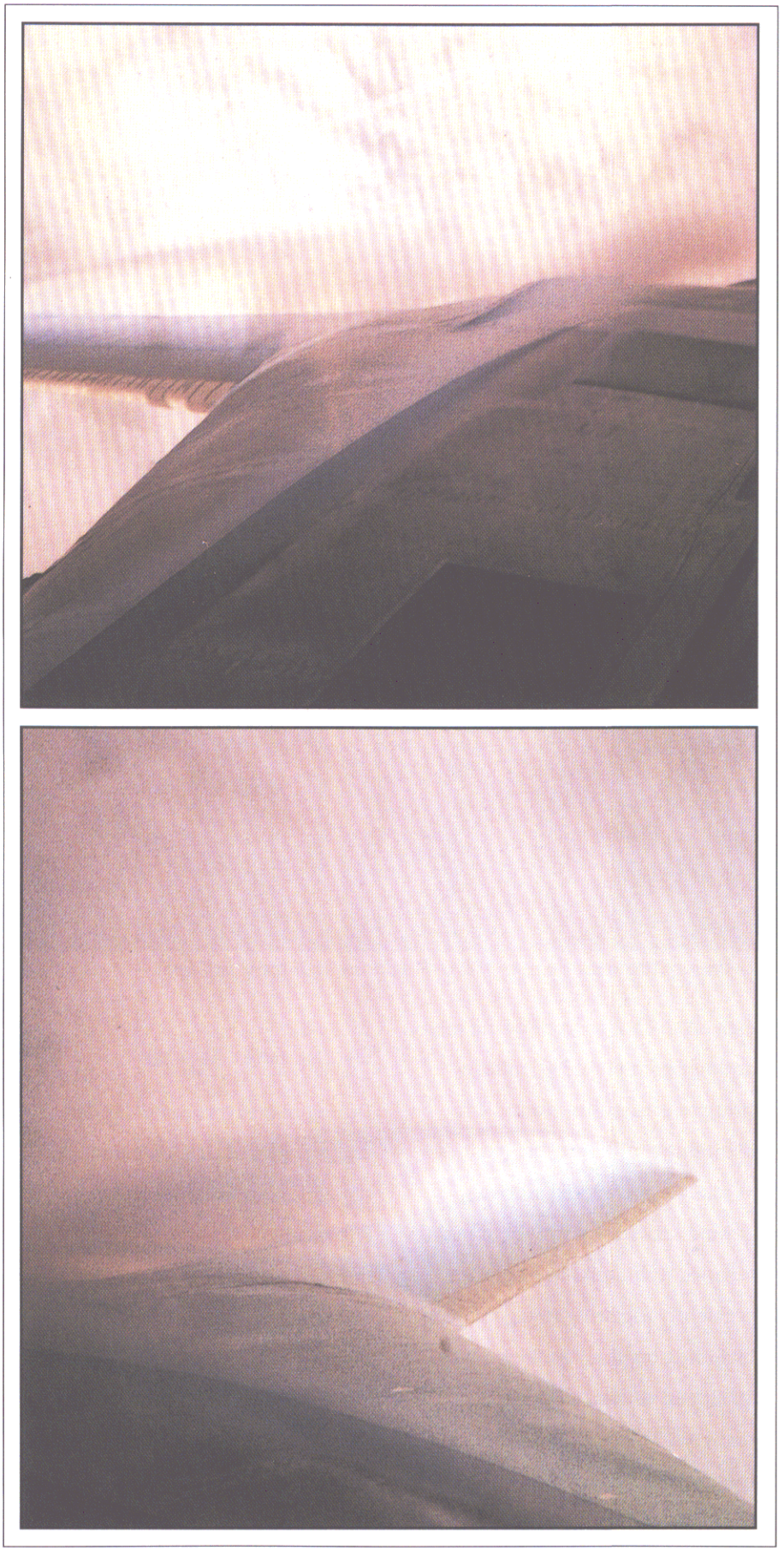

Vortices created along outside edges of inlet upper surfaces of F-14A during maneuvers. 3 • 48

the inlet. The resulting vortex streams aft between the engine and the rear canopy before vaporizing.

Another example of this class of flow was found for an F-14A in figure 3.48, which shows two photographs taken from an F-14A cockpit during a maneuver sequence. (See section 4.7.) Large condensed streamwise patterns are evident along the inboard part of the gloves on both sides of the airplane. The flow originates from points forward of the photographic fields of view and appears to be vortices that are created at the junction of the glove with the side-mounted inlet. The inlet upper surface extends forward of this juncture (sketch A) so that the outer surface has a thin side edge which generates a separation-induced vortex. The vortex passes just outboard of the inlet bleed air doors, between the carapace stiffeners, and outboard of the vertical tails. The maneuver condition is such that condensation occurs over the wing and in the wingtip vortices, but no condensation occurs on the glove to suggest that a strong glove vortex is present. Other airplanes that have similar rectangular shaped side-mounted inlets, such as the F-15 and Tornado, also generate separation-induced vortices at high-g maneuver conditions.

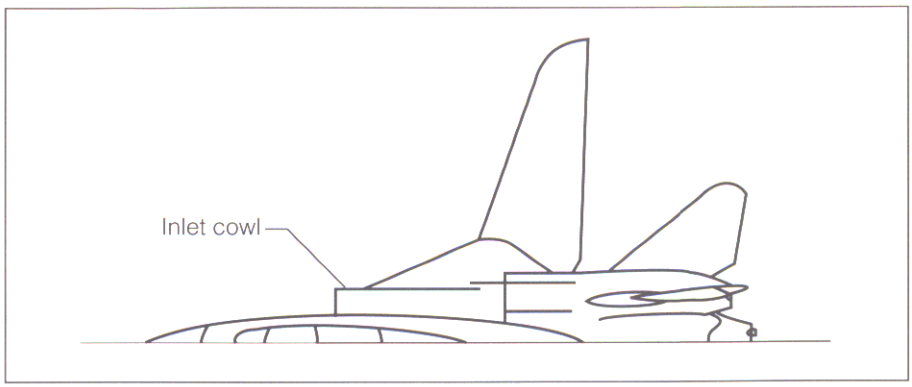

Sketch A

3.3.9
TYPICAL TRANSPORT SCENES

People who fly on civil transports under favorable atmospheric conditions have ample opportunities to observe a variety of condensation patterns during takeoff, landing, climb out, descent, and cruise. A number of these patterns are caused by vortex flows that occur on transports during normal operations. Previously, some vortex flows were discussed that exist during takeoff and landing such as the engine-nacelle strake vortices on the Boeing 707 (fig. 3.41) and the leading-edge vortices on the Concorde supersonic transport (fig. 3.12).

Another example of vortical flows on transports is shown for a Boeing 737 (fig. 3.49) and a McDonnell Douglas DC-9 (fig. 3.50) with their trailing-edge flaps deflected down for high-lift operation during landing. The flow separates around the outside side edge of the flap and forms a vortex which follows the flap contour. Near the flap trailing edge, the vortex combines with the exterior streamwise flow to give a corkscrew appearance in the wake.

A variety of condensed vortex patterns (fig. 3.51) occurred on an Airbus A300 during the cruise portion of a flight. The photographs in figures 3.51(b) and (d) show the streamwise patterns near the surface of the wing. The outer wing panel is equipped with vortex generators located at the front of the airfoil section,

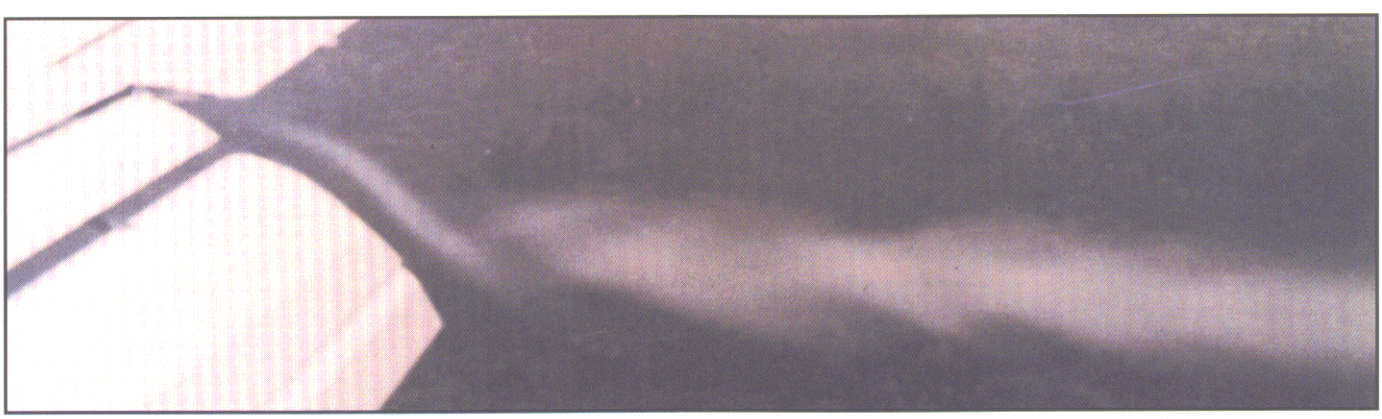

Separation-induced vortex generated along side edge of trailing-edge flap deflected for landing on Boeing 737. 3 • 49

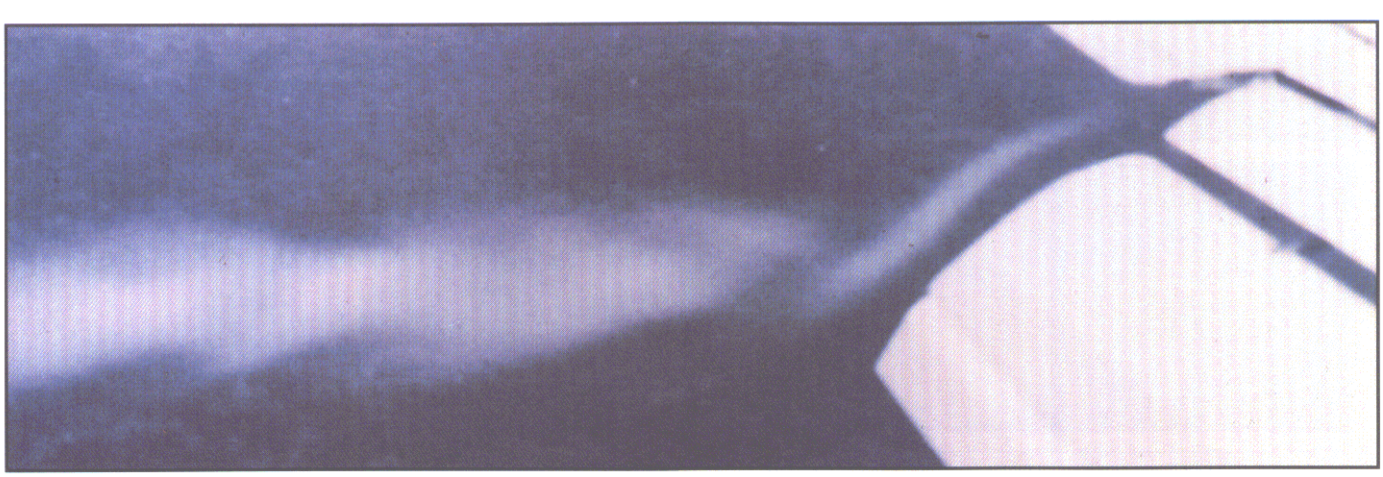

Separation-induced vortex generated along side edge of trailing-edge flap deflected for landing on McDonnell Douglas DC-9. 3 • 50

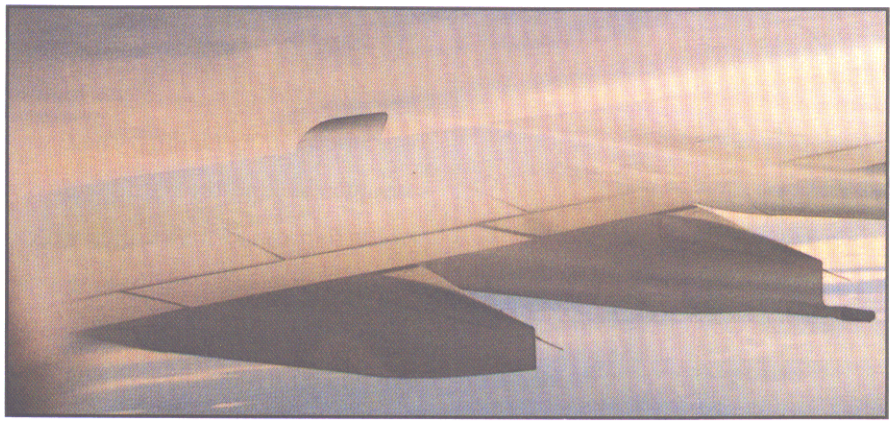

(a) Vortex from leading-edge fence.

(b) Streamwise vortices from wing leading edge inboard and from generators outboard.

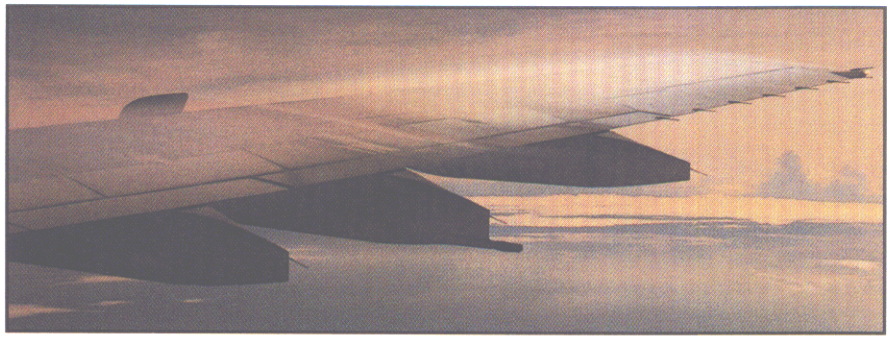

(c) Vortex from leading-edge fence at later time.

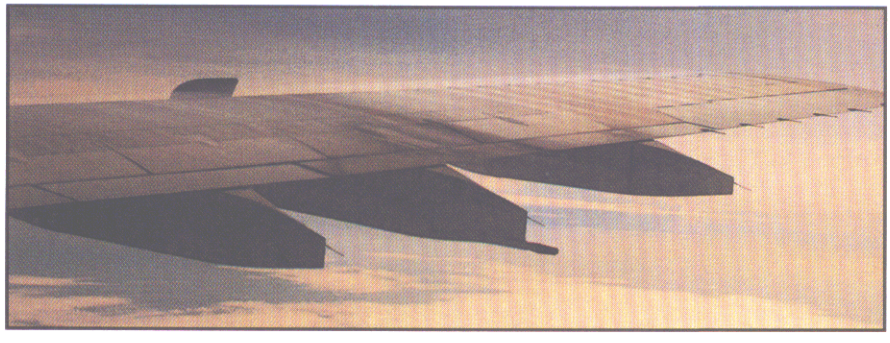

(d) Streamwise vortices from wing leading edge inboard and from generators outboard at later time.

(e) Trailing vortex from wingtip.

Flow fields occurring for Airbus A300 during cruise flight.

which create streamwise vortices from the generators. The inboard part of the wing panel does not have vortex generators but does have a distinct streamwise condensation pattern which is similar to that described previously for an Airbus A300 and a Boeing 737 (figs. 3.33 and 3.34). An additional vortex appears to be generated from the upper part of the leading-edge fence (figs. 3.51(a) and (c)) and streams aft over the upper surface of the wing. This vortex rotates in a direction that restricts the outward spanwise flow of the boundary layer. The wingtip vortex, which is shown in figure 3.51(e), flows aft of the airplane to start the trailing-vortex system.

3.3.10 Trailing Vortices: Breakdown, Vortex Rings, and Aerial Application

Whenever wings create lift, a pair of counterrotating vortices forms near the wingtips and trails rearward into the wake of the airplane. This section shows examples of how these trailing vortices first develop in the near wake

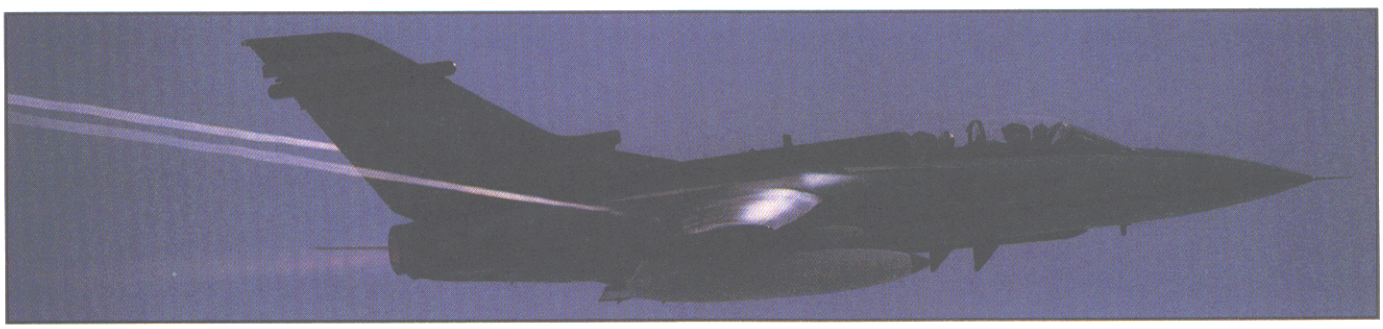

Wingtip vortices on Tornado. 3 • 52

Wingtip vortices on Active Control Jaguar Demonstrator with Tornado. 3 • 53

Wingtip vortices on X-29 forward-swept wing research airplane during maneuver flight. 3 • 54

Wingtip vortices on F-15 during pull-up. 3 • 55

of the airplane and then how they eventually can break down and form vortex rings in the far wake. These vortices have been studied extensively for transports because they represent a hazard around airports. Condensation patterns caused by wingtip vortices are seen more frequently than any other, partly because they are the strongest vortex at low and moderate angles of attack and because they are present on all configurations that produce lift.

The Tornado (fig. 3.52) is a good example of the type of condensation pattern that can occur as a fighter begins to increase its angle of attack during a maneuver. The tip vortex is usually the first part of the flow field to condense and is the only condensed flow in this photograph. This type of condensation pattern is also seen for some other fighters

Wingtip vortices on F-15 during turn.

3 • 56

during pull-ups or maneuvers, such as the Jaguar Active Control Demonstrator (fig. 3.53), the X-29 (fig. 3.54), and the F-15 airplanes (figs. 3.55 and 3.56). Some additional examples are included for an F-4 during landing (fig. 3.57), an F-105B during takeoff (fig. 3.58), and an F/A-18 during launch from a carrier (fig. 3.59). The wavy appearance of the tip vortices on the F-4 (fig. 3.57) is caused by spiraling around the core and not because the core undulates. The same type of wavy pattern is observed for the F-16 strake vortices in figure 3.18 and figure 4.42. In addition to wingtip vortices, fighters can also have vortices that form at the side edges of trailing-edge flaps similar to the civil transports shown previously. These two vortex flows are

Wingtip vortices on F-4 during landing.

3 • 57

Wingtip vortices on F-105B during takeoff.

3 • 58

corotating as illustrated in figure 3.60 by a British Aerospace airplane and begin rotating around each other as they pass into the wake.

In the Jaguar photograph in figure 3.53, the tip vortices appear to develop a cellular pattern as they get farther downstream. Similar cellular patterns are observed in the tip vortices for the F-15 (fig. 3.56) and for the Mission Adaptive Wing (figs. 4.67 and 4.68). The patterns are circles around the outer edge of the vortex core, and they begin just aft of the wingtip when the vortex is first forming. In fact if you look carefully,

Wingtip vortices on F/A-18 during launch from carrier. 3 • 59

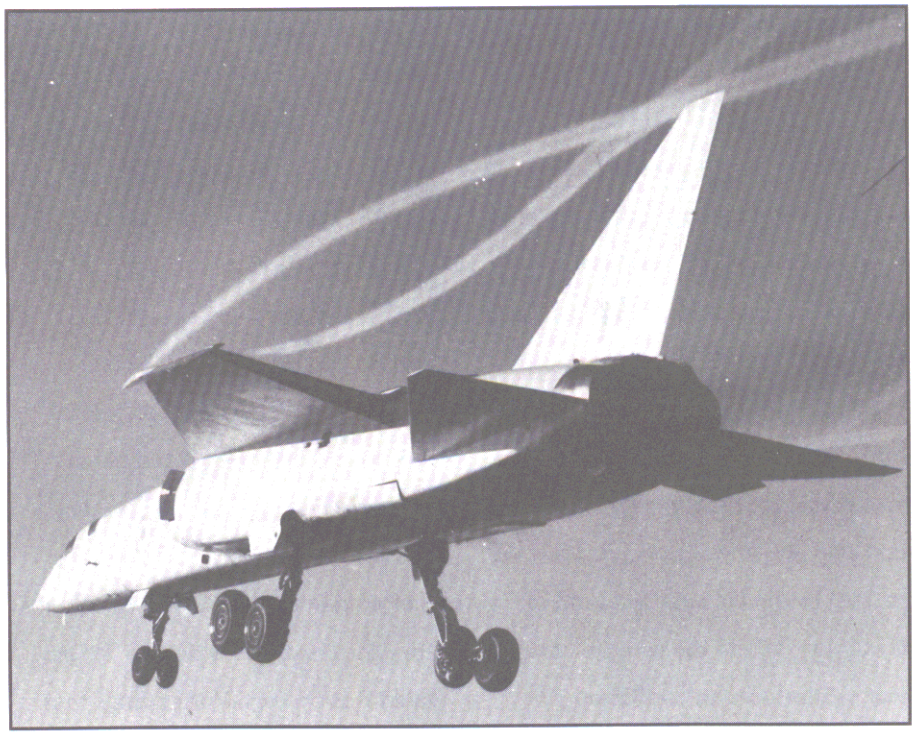

Vortices formed at wingtips and side edges of trailing-edge flaps for British Aerospace airplane during landing. 3 • 60

you will find the pattern in most of the trailing-vortex flows. When the vortex begins to form at and just behind the wingtips, the shear layer spawns small vortices that follow a helical path and collect around the outer edge of the vortex core. This flow is the same mechanism that was previously described for the formation of small streamwise vortices in the shear layer of leading-edge vortex flows (figs. 3.22 to 3.26). Evidence to substantiate this is found for the SR-71 (fig. 4.97) where the vortex filaments that formed in the chine leading-edge vortex have proceeded

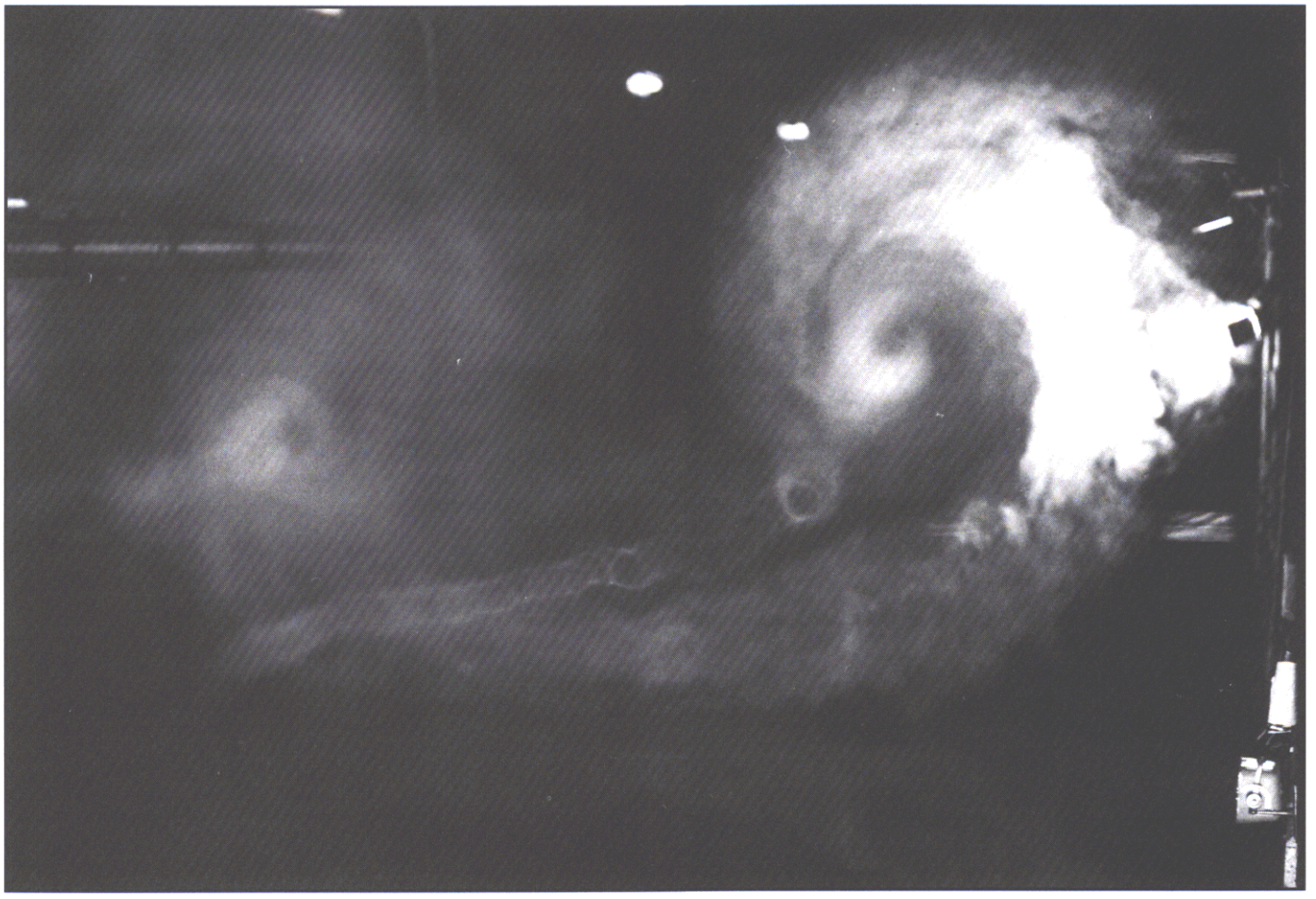

Small vortices wind around core of trailing vortex during low-speed tests with smoke in Langley Vortex Research Facility. 3 • 61

to the wake and have a similar appearance as patterns formed by the F-15 and the Jaguar wingtip vortices. An example is shown in figure 3.61, where researchers recorded filaments around the tip vortex core during a 1971 test in the Langley Vortex Research Facility. A monorail catapult carried a model through the test area at about 50 ft/sec, where smoke was used to visualize the trailing vortex. In the photograph, the model has passed out of view to the left.

A recent flight experiment was performed by NASA as part of continuing concerns about the safety problems created by wake vortices from transports around airports. A Boeing 747 was used to examine the interactions of wing trailing-edge flaps and tip vortices by using smokers to visualize the flow. The photographs (fig. 3.62), in sequence beginning with the approach and ending with completed flyover, show wingtip and trailing-edge flap vortex flows rotating around each other into the far wake. Recall that figures 3.49 and 3.50 showed the formation of the trailing-edge flap vortices in the near wake for two transport airplanes. The wavy sinusoidal pattern in the far wake is a form of instability, where the wingtip vortex pair self-induces an oscillation motion. Similar trailing-vortex phenomena are illustrated in two photographic sequences where smokers were installed on a Sea Fury airplane (figs. 3.63(a) to (d)) and on an MB339 MACHI airplane (figs. 3.63(e) and (f)). Initially (figs. 3.63(a) and (b)), the wingtip vortices form a definitive pair close to the airplane. Farther behind the airplane, the vortex cores began to make an oscillating pattern (fig. 3.63(c)) until they touch (fig. 3.63(d)) and pinch off into separate ring vortices (figs. 3.63(e) and (f)). This linking phenomenon is often named the "Crow" instability after the researcher who first investigated this process. Vortex rings that evolve into small circles of vorticity

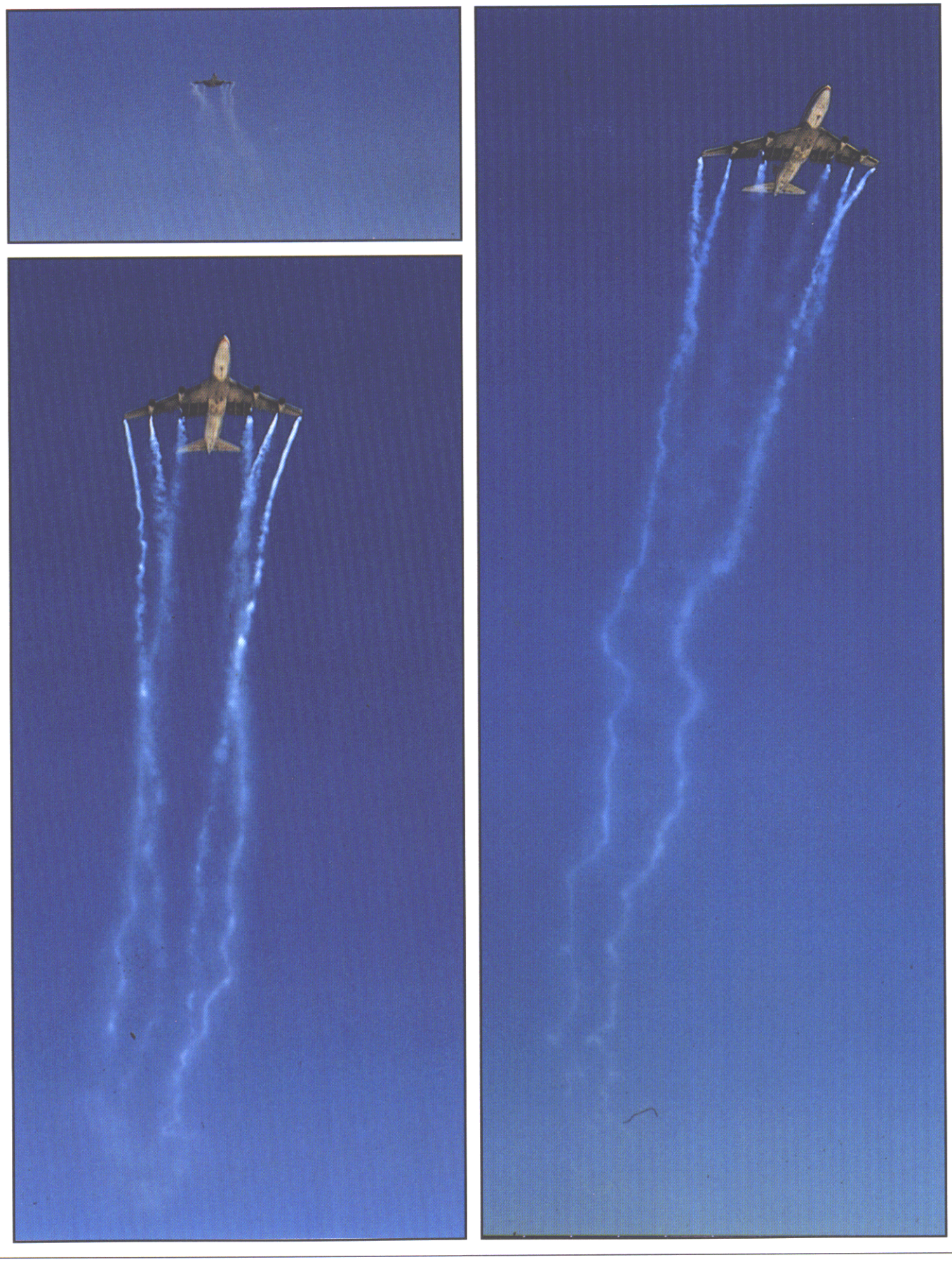

Smokers used to visualize trailing vortices behind Boeing 747 during research flight by NASA.

3 • 62

Smokers used to visualize trailing vortices behind Boeing 747 during research flight by NASA–concluded. 3 • 62

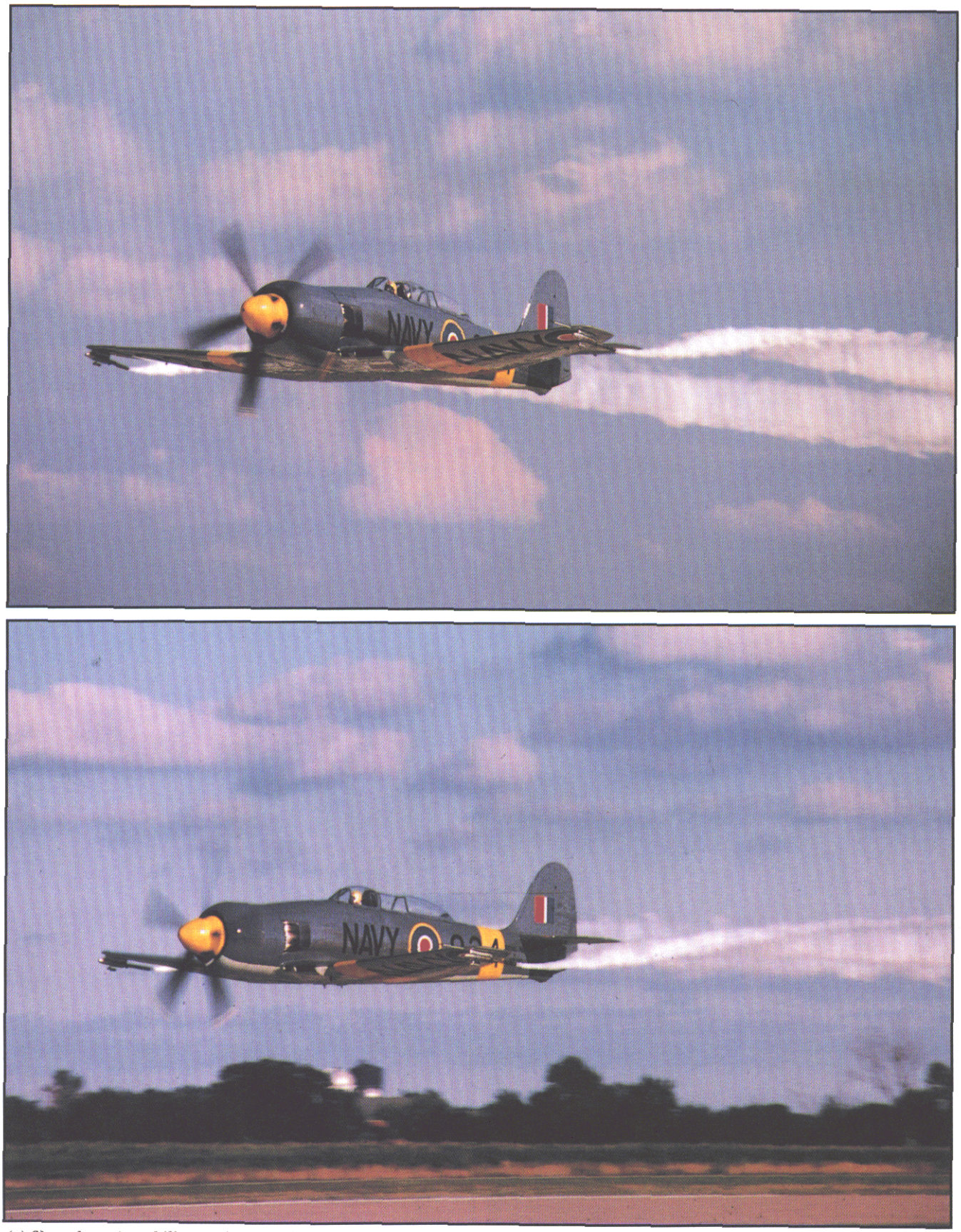

(a) Shear-layer instability vortices rotating around outer edge of tip vortex cores.

Trailing vortex properties visualized by smokers evolve with increasing time and distance behind airplane. 3 • 63

(b) Wingtip vortex pair maturing.

(c) Vortex pair inducing oscillatory instability.

Trailing vortex properties visualized by smokers evolve with increasing time and distance behind airplane–continued. 3 • 63

(d) Instability continuing to grow until vortices touch.

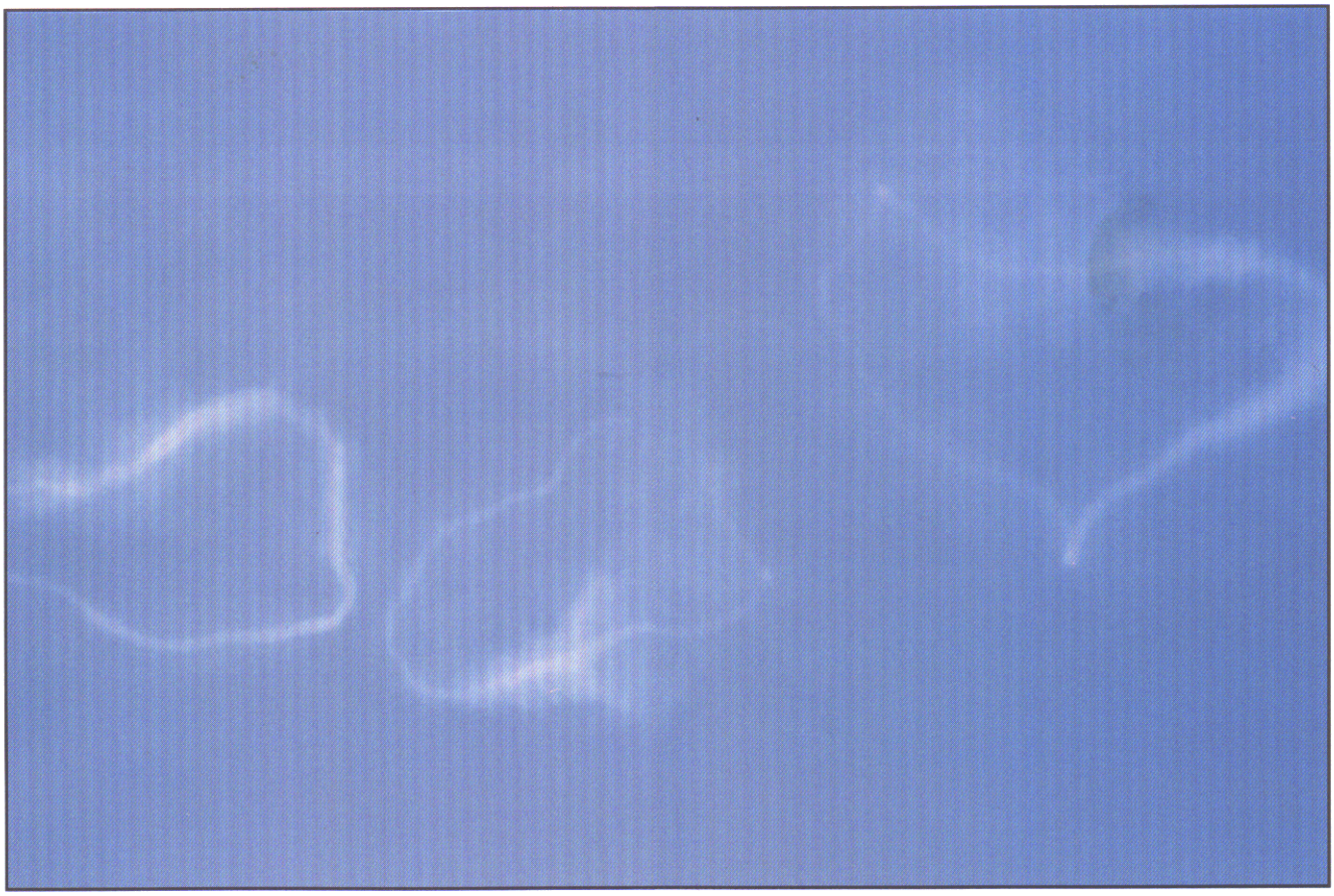

(e) Separate ring vortices forming after being pinched off.

Trailing vortex properties visualized by smokers evolve with increasing time and distance behind airplane–continued. 3 • 63

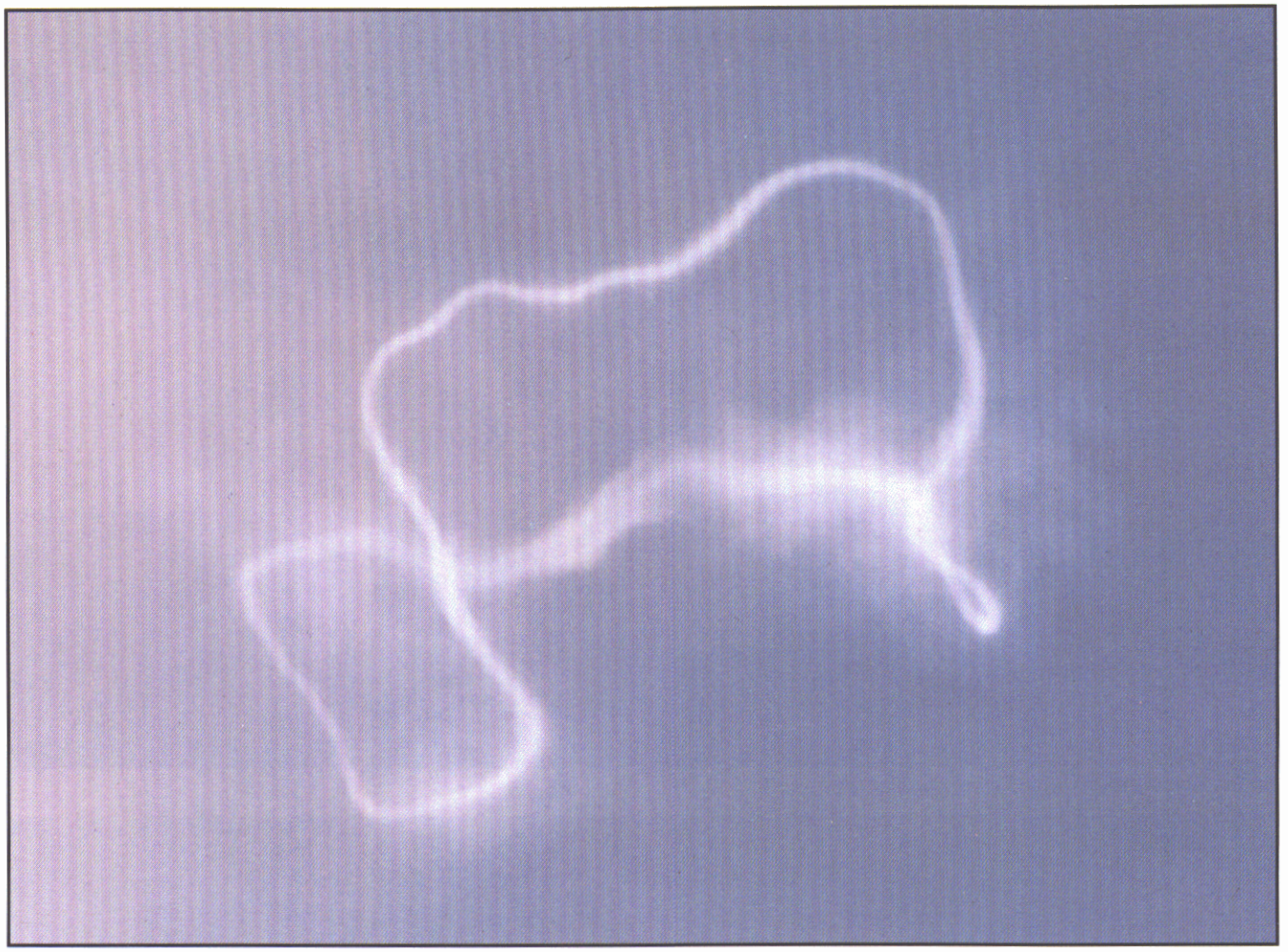

(f) Ring of vorticity forming smaller vortex rings.

(g) Small ring vortices decaying slowly into turbulence.

Trailing vortex properties visualized by smokers evolve with increasing time and distance behind airplane–concluded. 3 • 63

Crop duster spray becoming entrained in wingtip vortices during spraying operation. 3 • 64

Thrus crop duster flying over red smoker and giving unusual perspective of right wingtip vortex. 3 • 65

are shown in figure 3.63(g). These patterns can often be seen when airplanes are at high altitudes, where jet engine exhaust mixes with the cooler air to condense and form the condensation trails.

Two final examples of wingtip vorticity are shown in figures 3.64 and 3.65.

Figure 3.64 presents the front view of a crop duster, where the spray is emitted along the wing underside and wraps up into the tip vortices in the wake. In figure 3.65, a Thrus duster makes a close flyby over a red smoke generator to give this unusual perspective of the right wingtip vortex.

3.3.11 Propeller/Rotor Tip Vortices

Airplane propellers and helicopter rotors have blades which are airfoils that rotate at high speeds to provide the propelling thrust for the airplane and the lift force for the helicopter. As the blades rotate, they create tip vortices similar to those that occur

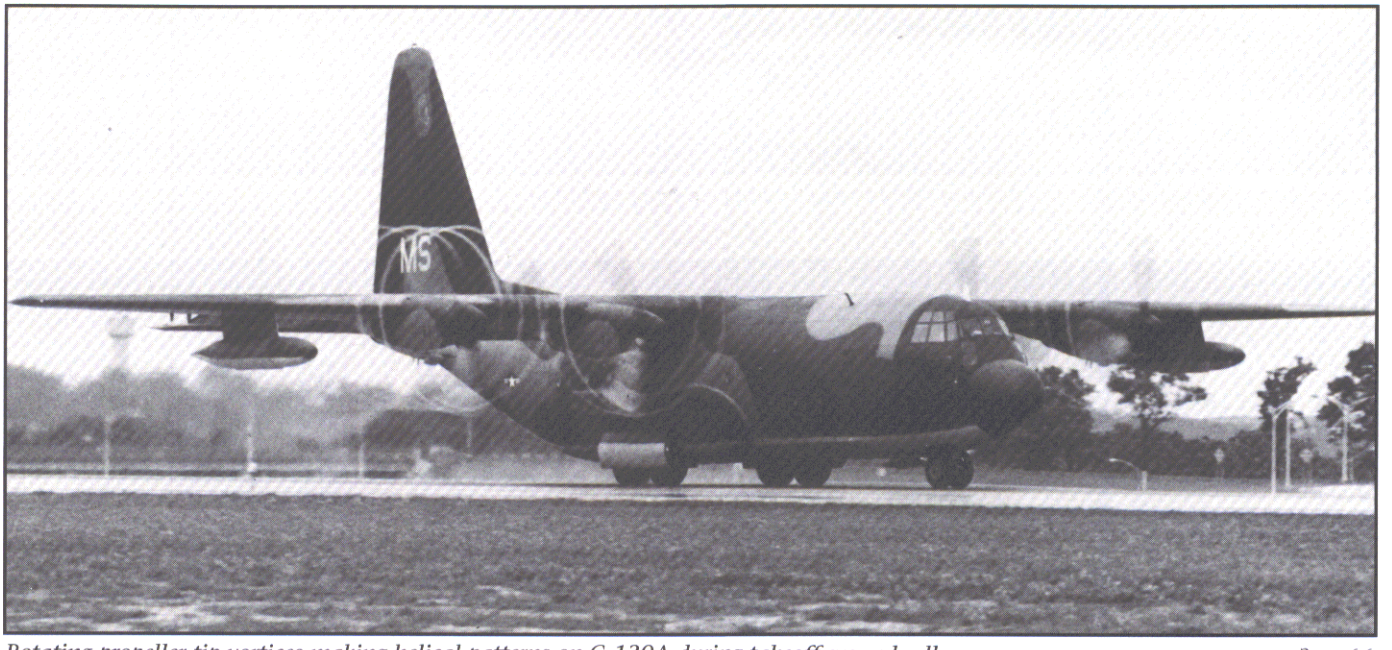

Rotating propeller tip vortices making helical patterns on C-130A during takeoff ground roll. 3 • 66

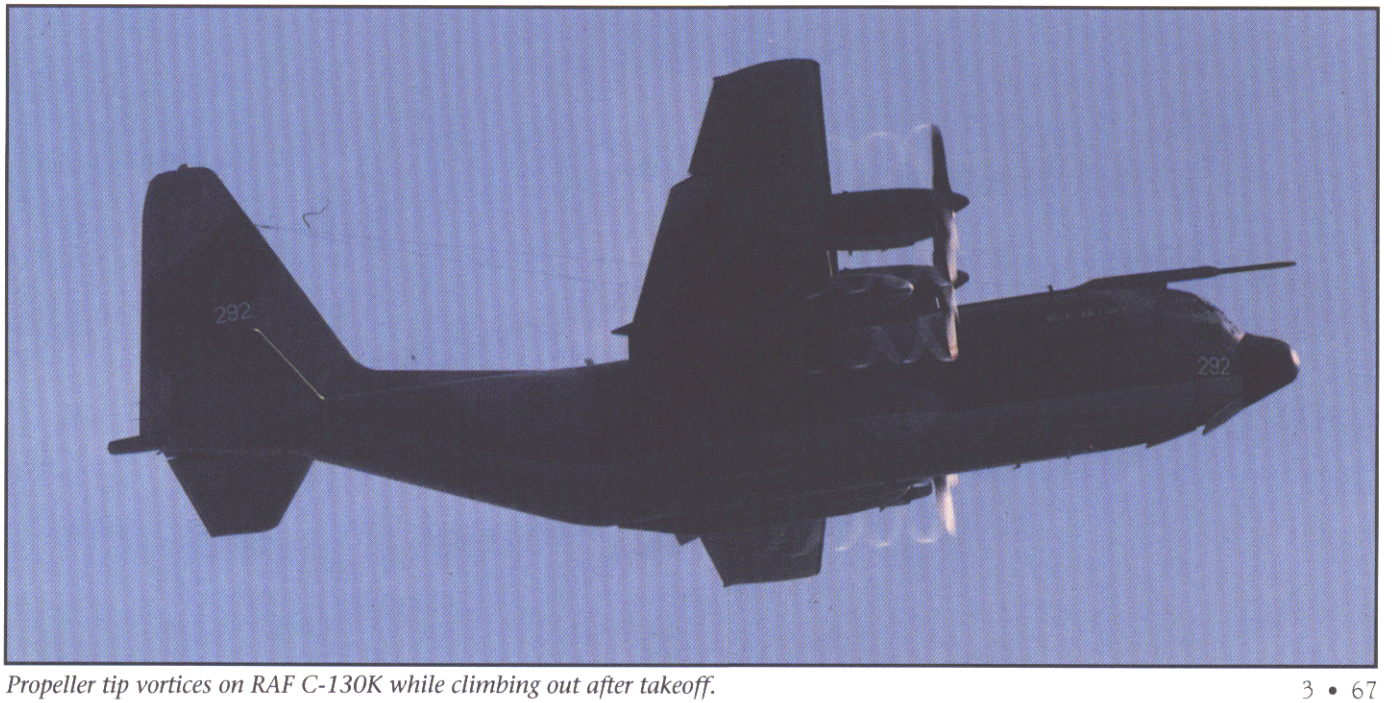

Propeller tip vortices on RAF C-130K while climbing out after takeoff. 3 • 67

View from behind and below with propeller tip vortices interacting with C-130A upper surface flow field. 3 • 68

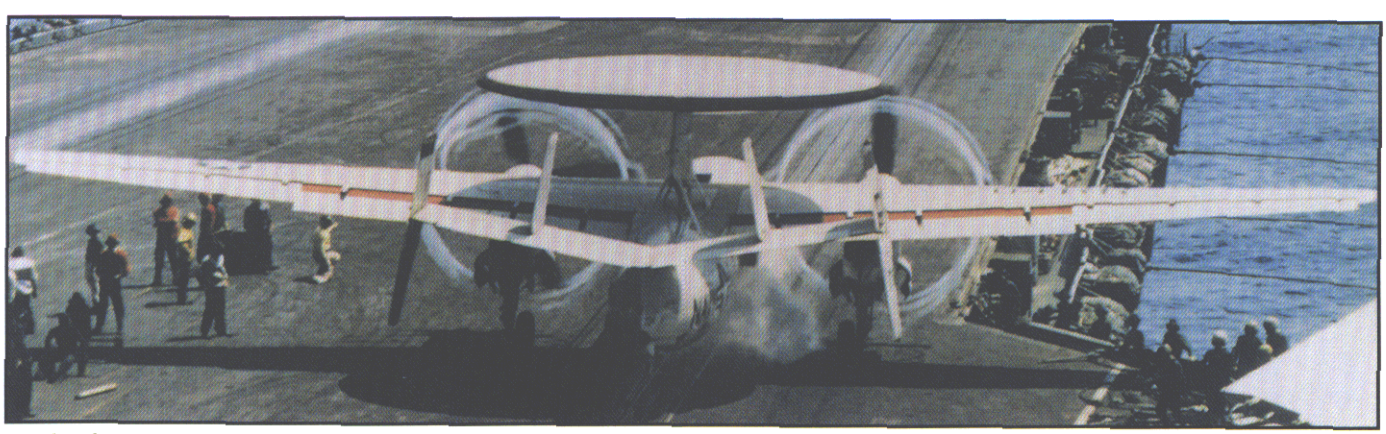

Circle of vorticity appearing at propeller tips of E-2A Hawkeye ready for carrier launch. 3 • 69

on lifting wings and can show up in condensation patterns. This is illustrated in figure 3.66 by a C-130A during a takeoff ground roll where the nose wheel is just beginning to lift off the runway. A condensed vortex traces the path of each of the four propeller tips as they rotate clockwise around the propeller axis and move forward at the speed of the airplane. The combination of rotating and forward velocities causes the tip vortices to make a helical path rearward from the blades, at approximately the blade diameter, until passing above and below the wing. The curved pattern in front of and below the inboard engine on the right side of the airplane may be a ground vortex that was described previously. The repeating curved pattern of the propeller tip vortices is more obvious viewed from the side and below (fig. 3.67) for an RAF C-130K during climb out after

Propeller tip vortices creating helical pattern on E-2A Hawkeye after launch. 3 • 70

Tip vortices form from rotating blades of Bell 204 helicopter during lumbering operation. 3 • 71

takeoff. After they are split in half at the wing leading edge, the propeller vortices are distorted by the wing flow fields; this is illustrated for a C-130A in figure 3.68, where the condensed vortices evaporate when exposed to the lower surface flow field but remain condensed above. The initially circular vortex pattern distorts when it interacts with the wing upper surface flow. The inboard vortex, observed best on the left side, reaches a point where the inboard part interacts with the side of the fuselage and the outboard side interacts with the second vortex.

Another example of propeller tip vortices is shown in figure 3.69 for an E-2A Hawkeye sitting on the deck of a carrier where the airplane is ready for the catapult launch. Even though the airplane is not flying, the tip vortices might move slightly because of carrier speed, prevailing winds, and propeller backwash. At launch (fig. 3.70), the distinctive helical pattern of the vortices has crossed over and under the wing.

The Bell 204 helicopter (fig. 3.71) provides the final example for condensed tip vortices formed by rotating blades. The tip vortices follow a helical path downward because the blades generate a strong downwash flow field.

4

Condensation Patterns by Airplane Type

4 • 1

A-4 Airplane

The A-4 Skyhawk is a light attack jet used for close air support by the U.S. Marine Corps. It features a modified delta wing and is built by McDonnell Aircraft Company. The photograph of figure 4.1 was taken of an A-4M during a high-speed pass. The condensed pattern over the wing is probably caused by supersonic flow as discussed previously in section 3.2.

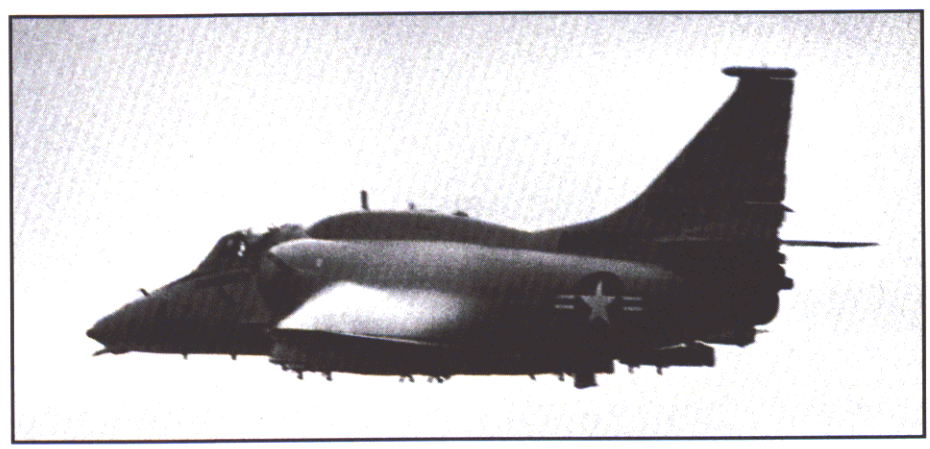

Condensed transonic pattern over wing of A-4M making high-speed pass. 4 • 1

4 • 2

A-6E Airplane

The A-6E is the current operational version of the Intruder used by the U.S. Navy and the U.S. Marine Corps. It is built by Grumman Aerospace as an all-weather carrier-borne airplane that can fly deep strike missions

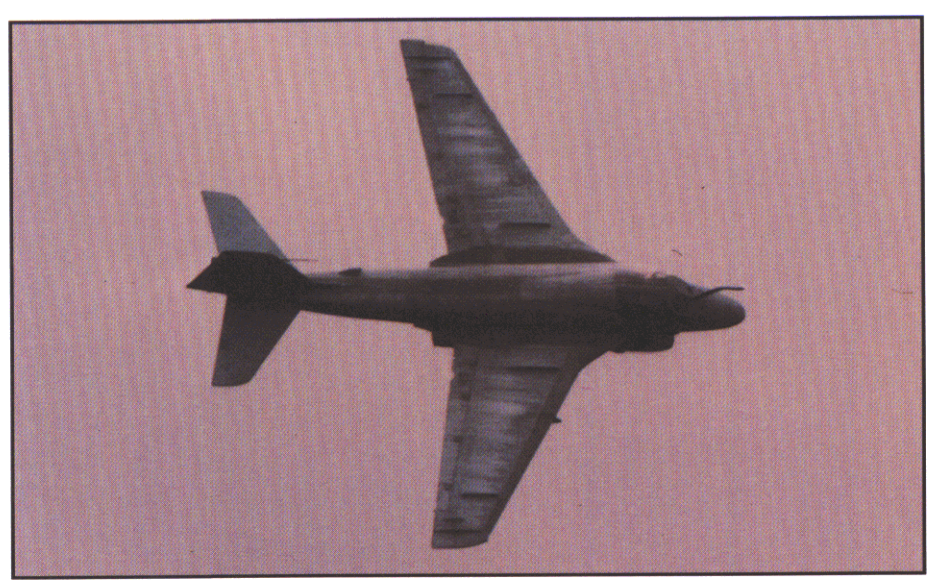

Streamwise condensation pattern appearing on wing upper surface during maneuver of A-6E. 4 • 2

Canopy and wing flow during high-speed pull-up of A-6E. 4 • 3

or perform close air support. A variety of flow patterns is shown for the A-6E. During a maneuver, a top view (fig. 4.2) shows streamwise streaks in the condensation pattern on the wing upper surface. Because this airplane does not have vortex generators on the wing, this streamwise pattern should be the vorticity from the wing leading edge that was described in section 3.3.5.

Wingtip vortex and streamwise flow from crest of canopy during high-speed pull-up of A-6E. 4 • 4

Condensed flow over all of upper surface of A-6E breaking into landing pattern. 4 • 5

During high-speed pull-ups (figs. 4.3 and 4.4), condensation occurs from the canopy area and proceeds back in a straight line. The flow probably separates near the intersection of the front part of the canopy and the top. Both figures show flow condensing at the junction between the surfaces. The flight refueling probe visible in the photograph is mounted just forward of the canopy along the centerline.

A view from below (fig. 4.5) shows an A-6E breaking into the landing pattern with condensation spanwise

Vortices from wingtips and gap at outside edge of leading-edge slat on right side of A-10 during roll maneuver. 4 • 6

over the whole airplane upper surface. This view shows the small flap surfaces at the wingtips which split into upper and lower halves for use as speed brakes.

4 • 3

A-10 Airplane

The A-10 Thunderbolt is a tactical attack airplane used by the U.S. Air Force and has many distinctive features for performing its close air support mission. Some of these are engines mounted on pylons above and aft along the fuselage to minimize damage from ground fire, outboard twin vertical tails, and an unswept wing planform with multiple weapons racks. The wing has a slat along the innermost portion of the leading edge which automatically adjusts with a change in flight condition. Roll control is provided by ailerons located outboard along the wing trailing edges. The wingtip curves down to become almost vertical.

In figure 4.6, the ailerons are deflected for a roll to the left so that the trailing edge up deflection of the left aileron distorts the condensation pattern along the wing. From this perspective, you can see through the gap made by the leading-edge slat on the left side. In addition, the outside surface of the slat is a fixed vertical surface, which extends above and forward of the wing leading edge. During maneuvers like the one for this figure, a vortex is created by the outer edge of the leading-edge slat and the gap between it and the wheel fairing. This causes the streamwise condensation pattern seen on the right side which appears to go into the right

Vortices streamwise over wing generated by gap at outside edge of leading-edge slats of A-10 during roll maneuver. 4 • 7

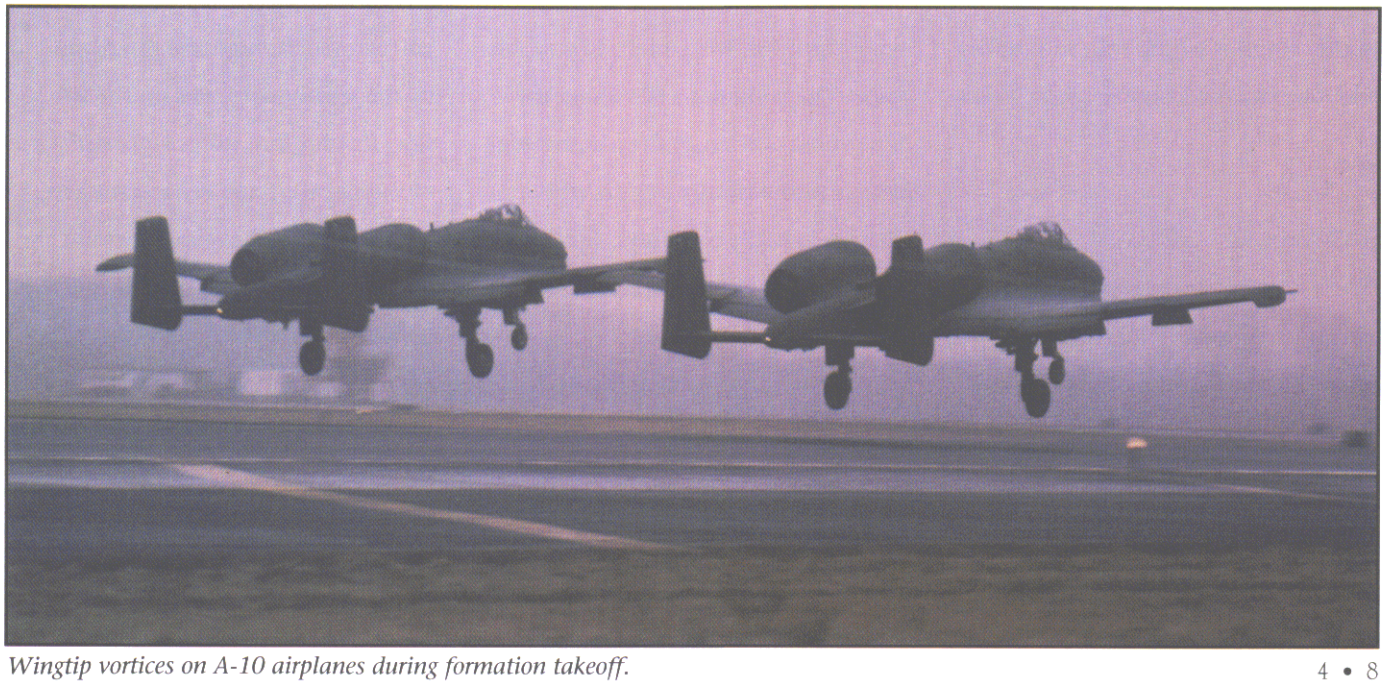

Wingtip vortices on A-10 airplanes during formation takeoff. 4 • 8

inlet. Tip vortices create the other condensation pattern which occurs at the cambered wingtips and streams past the outboard vertical tails.

A similar roll maneuver is shown in figure 4.7 for an A-10 carrying missiles under the wings. Vortices are generated by outer edges of the slats, which are evident in the wing condensation pattern, where the vortex on the right wing appears to be stronger than the one on the left. The left wingtip vortex has a change in curvature just aft of the wingtip which is probably caused by the roll maneuver, in which the left wingtip has lower lift and is rotating downward, rather than the wing camber that curves downward at the tip. A similar path for the left tip vortex can be seen in figure 4.6. Figure 4.8 shows the wingtip vortices created by two A-10 airplanes during takeoff.

4 • 4

B-1 Airplane

The B-1 bomber is built by Rockwell International and uses variable-sweep wings, sophisticated avionics, and air-to-ground missiles or bombs mounted in internal weapons bays to provide a multirole strategic capability. The airplane was initially produced in the 1980's as the B-1A and is now being produced as the B-1B for operation by the U.S. Air Force. Because of the variable-sweep feature, the airplane experiences a variety of flow fields as evidenced by the various condensation patterns.

The photograph in figure 4.9 was taken from below with the wings of

Condensation streams from wing upper surfaces during pull-up of B-1A. 4 • 9

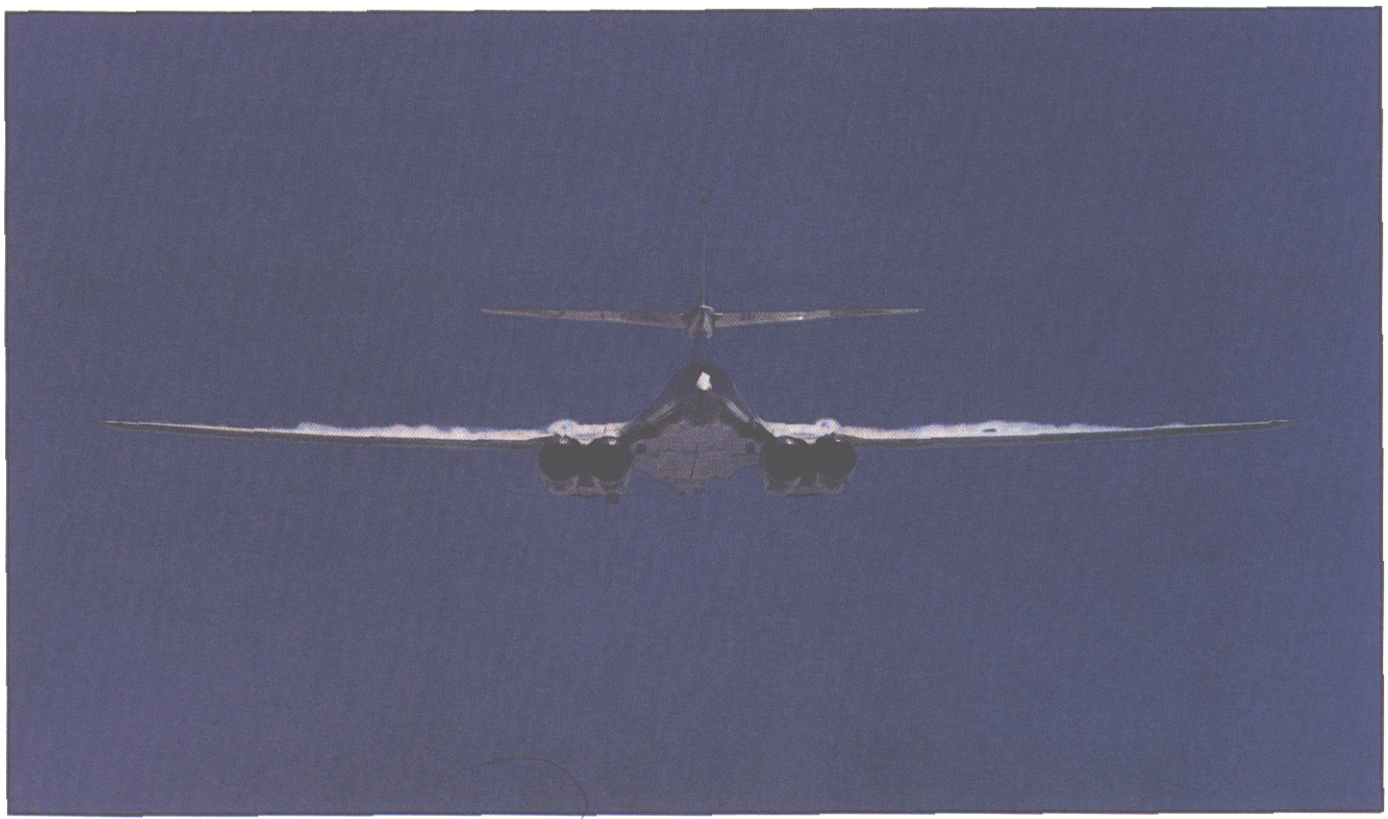

Glove and streamwise wing vortices on B-1A with wing sweep of 25° at Mach number of 0.7. 4 • 10

the B-1A bomber in a low sweep position. The remarkable thing about this picture is that a considerable amount of condensed flow is streaming into the wake from the upper surfaces of the wings. The flow passes below the horizontal tails as noted by the shadow of the horizontal tail on the condensation from the left wing. Recall that many condensation patterns have been presented for fighters, bombers, and transports with wings of moderate sweep at subsonic speeds. In most of these photographs, the wing flow conditions were such that the condensate evaporated near the wing trailing edges, and very little or no condensation was observed in the wake. In figure 4.9, the wing may have lift just high enough to have the flow condense over the wing but low enough so that the condensed flow does not evaporate when it passes through the trailing-edge flow gradients into the wake or it may be caused by flow separation. There appears to be a spanwise repeating pattern in the condensed flow at or just behind the wing trailing edge, which may be caused by streamwise vorticity from wing leading edges that was discussed earlier for the 737 and A300 transports and the F-16 and F/A-18 fighters.

This observation is reinforced in figure 4.10, which was taken for the same airplane during a different flight, where the wing sweep was 25° and the flight Mach number was about 0.7. This rear view shows that rounded condensation patterns have developed on the inboard part of the upper surface of the wing, which are indicative of streamwise vortices originating from the wing leading-edge region. The circular pattern above the outboard engines is caused by the vortex flow from the gloves. Figure 3.27 was taken during the same time frame and shows the same flow patterns.

Flight tests have been conducted to help expand the flight envelope of the B-1B. The sequence of three photographs shown as figure 4.11 was taken during part of the high-angle-of-attack testing over the Pacific Ocean. With the wings swept to 67°, the B-1B airplane is performing a 3*g* turn to a maximum angle of attack.

Leading-edge vortices forming over highly swept (67°) wings during B-1B flight test.

4 • 11

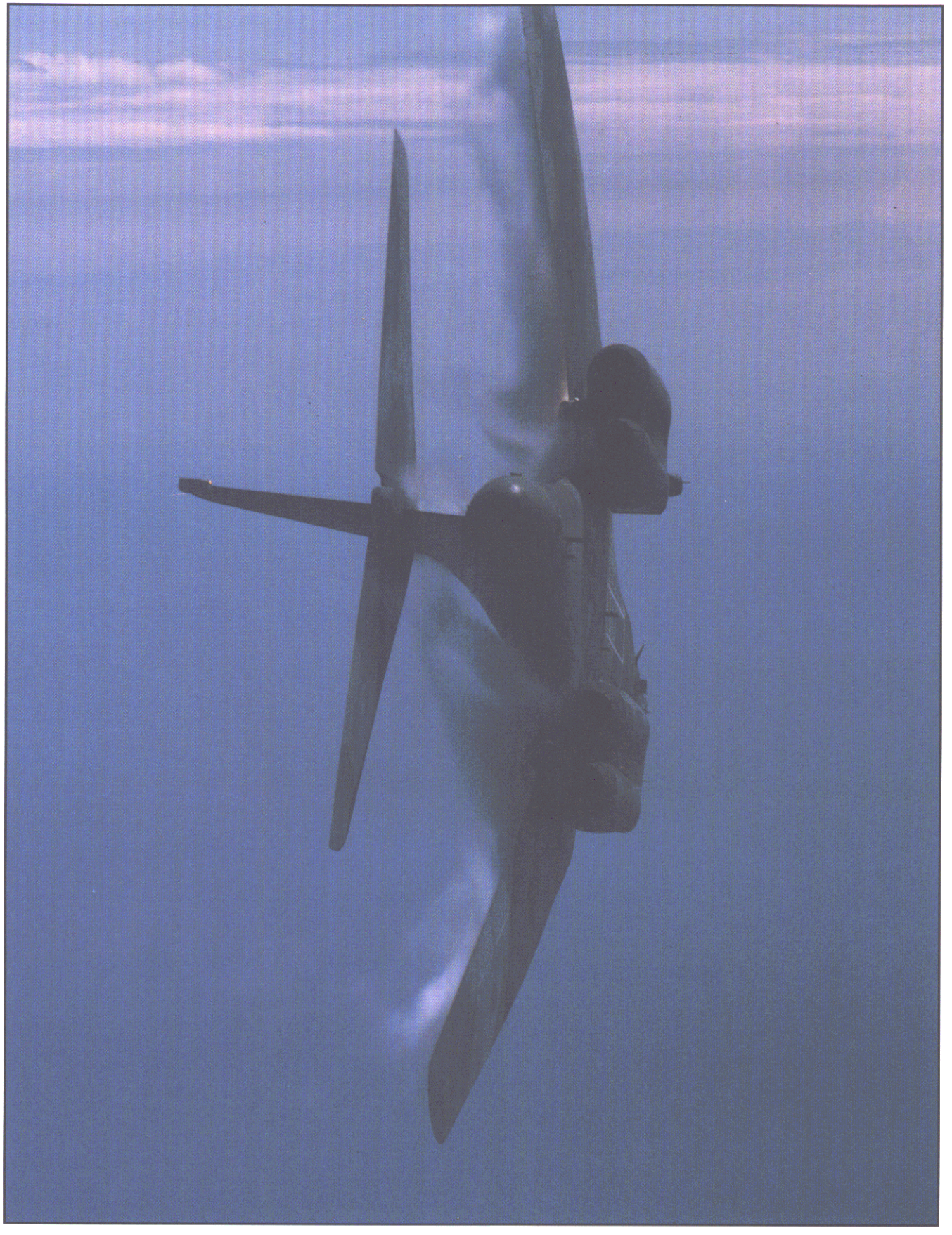

Leading-edge vortices forming over highly swept (67°) wings during B-1B flight test–concluded. 4 • 11

(a) Over water.

(b) Over land.

Transonic flows over wing upper surface of B-1A.

4 • 12

Transonic flow pattern on B-1A making high-speed flight over desert. 4 • 13

Condensation occurring above and below engine exits and vortex created by antenna blade of B-1B during high-speed cruise flight. 4 • 14

During the maneuver, the airplane descends in altitude from 10 000 to 4000 ft while maintaining a constant Mach number of 0.9. The highly swept wing panels have leading-edge vortices which cause the condensation noted in the photographs. The condensed flow pattern above the engines, more noticeable on the right side, may be the vortex generated by the gloves.

The photographs in figures 4.12(a) and (b) were taken during a flight of the B-1A while executing a high-speed run over water and then inland. The wings are in a high sweep position and condensation is occurring above and below the airplane. A similar condensation pattern (figure 4.13) is created for a B-1A making a high-speed flight over the desert. The condensation is in contrast to the dark camouflage coloring of the airplane.

A B-1B was photographed during a high-speed cruise flight which resulted in the unusual pattern shown in figure 4.14. The flow condenses above and below the jet engine exit and in the flow near the trailing edges of the horizontal tails. An additional pattern, which is a vortex generated by the tip of an antenna blade that protrudes out into the flow, can be seen along the upper part of the fuselage. The blade is located on the side of the fuselage and aft of the canopy. The condensed vortex casts a shadow onto the fuselage surface as it follows a path rearward, eventually curving downward as it approaches the engine exhaust area. This antenna was not on the B-1A but was added to the B-1B as part of the defensive avionics system.

4 • 5

F-4 Airplane

The design of the F-4 Phantom II fighter built by McDonnell Douglas Corporation has proved to be useful for a variety of roles, including fighter and attack capabilities. Over the years, a number of variants have been developed for domestic use by the U.S. Navy, U.S. Marines, and U.S. Air Force and for overseas use in a number of countries. Some features include leading-edge slats located inboard and outboard on the wing to improve maneuver performance. The outer wing panel has an upward slope, called dihedral, and a distinctive leading-edge snag, sometimes referred to as dogtooth or sawtooth. The horizontal tails have a downward slope, called anhedral. Pylons and missile launchers are mounted on the underside to accommodate bombs, missiles, and fuel tanks.

Condensation patterns were obtained for the F-4 airplane during cruise and maneuver. In this first group of photographs, the condensation patterns occur because of supersonic flow around the airplane during high-speed subsonic flights. Figure 4.15

Mach diamond pattern occurring on F-4J during high-speed subsonic cruise. 4 • 15

shows a condensation pattern for a Navy F-4J during a high-speed cruise flight. The large supersonic region of the wing extends above and below the airplane in a diamond pattern, whereas a much smaller condensed flow occurs aft of the canopy. The diamond pattern is widest in the plane of the wing and reduces with increased vertical distance away from the wing. In addition, the condensation pattern due to the wing extends

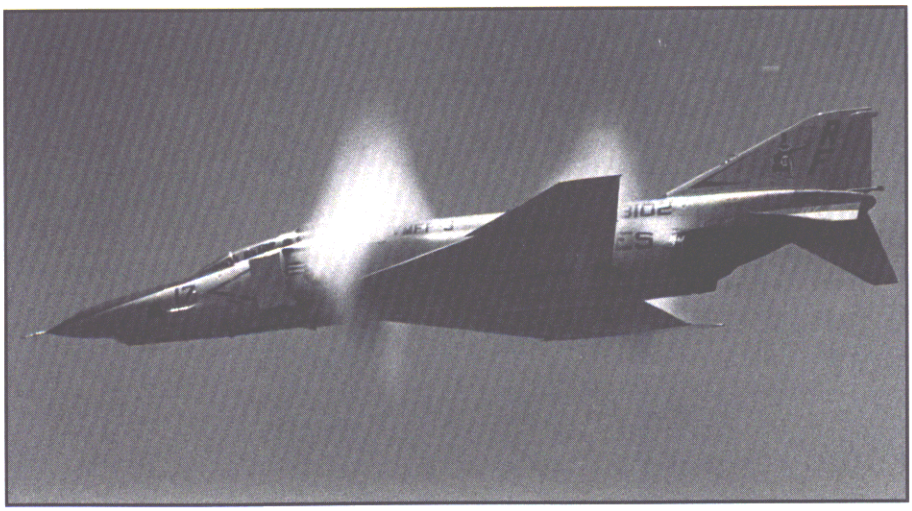

Condensation pockets of supersonic flow occurring on RF-4B during high-speed subsonic flight. 4 • 16

Pockets of supersonic flow occurring on RAF F-4 during high-speed subsonic flight. 4 • 17

to a much larger vertical distance than the pattern at the fuselage station just aft of the canopy. The pattern is very similar to the flyby of another Navy F-4J presented previously as figure 3.8.

The photographs in figures 4.16 and 4.17 are for an RF-4B and an RAF F-4, respectively, during high-speed level flight and show that the condensed pattern aft of the canopy is much larger and appears to be as large or larger than the wing pattern. Expanded flow over the canopy is not the only cause for this pattern, otherwise the condensation would only show up locally at the top of the fuselage behind the canopy. The pattern occurs outboard of the engines and underneath the fuselage; this suggests that this is a region of supercritical flow similar to the one at the back of the airplane that was previously described. One further point is that the cross-sectional area of the fuselage, including the engines, becomes a maximum in the proximity of where the wing joins the engine.

The last high-speed photograph (fig. 4.18) shows an RAF FG.Mk1.F-4 making a high-speed pull-up. Condensation occurs at or near the vortices from the wingtips and from the engine inlet splitter plate described earlier in section 3.3.8. Also, the condensation pattern that is streaming aft from the canopy top is separated flow from a rearview mirror. Condensation occurs around the engine housing and the flow over the wing is condensing to form the transonic pocket. This is different from figure 3.9, which had a condensed triangle of supercritical flow on top and no condensation underneath. Finally, the vertical tail appears to have a streamwise condensation pattern along the surface and from the leading edge. Because the airplane does not have vortex generators on the vertical tail, it may have enough sideslip angle to result in streamwise vortices along the side surface of the tail like we showed earlier for the upper surfaces of lifting wings in section 3.3.5.

The last three photographs (fig. 4.19) show the RAF F-4 during maneuvers

Vortices from wingtips and engine-inlet splitter plate, transonic flow over wing, and streamwise pattern on vertical tail occurring on RAF F-4 during high-speed turn. 4 • 18

Wing chord extensions inducing leading-edge vortices along outer panels and separation-induced vortices from inlet splitter plate during maneuvers of two RAF F-4's. 4 • 19

and depict condensation patterns on the wing and from the boundary-layer splitter plate near the inlets. An additional example of the vortex from the splitter plate was presented as figure 3.47. The wing design included a chord extension (sawtooth) about two thirds of the way out along the leading edges. This location promotes attached flow on the inboard panel and generates a vortex on the outboard panel to improve maneuver aerodynamics. The outer-panel vortices begin at the chord extensions as shown in the photographs.

4 • 6

F-5 and F-20 Airplanes

The F-5 and F-20 fighter airplanes were built by Northrop and feature a strake or leading-edge extension forward of the wing root. This surface generates vortices to provide vortex lift and to energize the wing-root region which improves the takeoff, landing, and maneuvering characteristics for the airplane.

A landing sequence is shown in figure 4.20 for an F-5E. The Sun angle is just right in the front views (figs. 4.20(a) and (b)) to make the strake vortices look like the airplane has jets blowing out of the fuselage sides. The bright spot at the left wingtip is the tip vortex. At touchdown (fig. 4.20(c)), the airplane has passed the camera position to provide a rear view, which shows the vortex originating at the junction of the strake leading edge and the side of the inlet and proceeding inboard of the strake side edge. The vortex has this trajectory because the inboard portion of the strake planform has a low leading-edge sweep angle, a result of the design to maximize the vortex effect on the area while being restricted in length by the presence of the inlet. The F-16 and F/A-18 did not have this length restriction; therefore, they could have slender planform shapes with the initial strake sweep angle very high. The vortices cast shadows on the upper surface as they flow over the wing and then pass over the trailing-edge flaps, which are deflected down.

The F-20, designed with a similar strake shape as the F-5E, is shown in figure 4.21 during maneuvering conditions. The strake vortices can be seen in figure 4.21(a) looking from the rear and above where they pass over the deflected trailing-edge flaps. It is not obvious where the right-side vortex originates, but it appears to be forward on the strake and inboard of the side edge. In figure 4.21(b), the strake vortex is not apparent until aft of the wing-strake

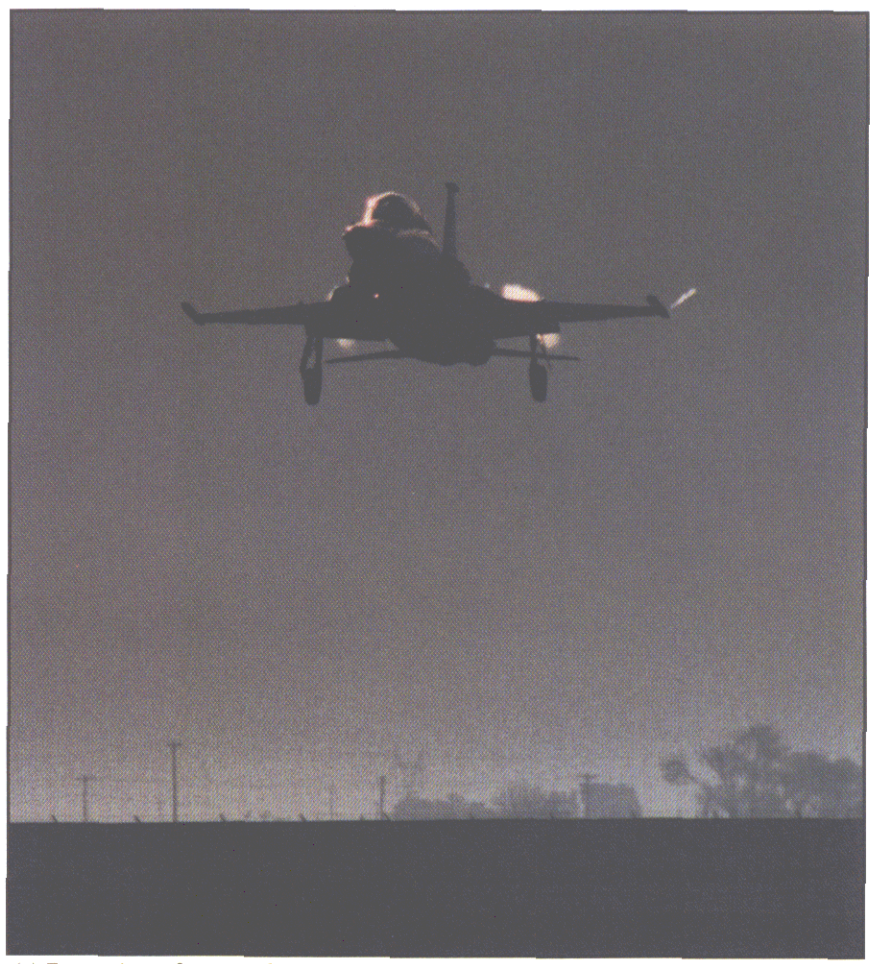

(a) Front view of approach.

F-5E generating strake vortices during landing sequence. 4 • 20

(b) Front view just prior to touchdown.

(c) Rear view of touchdown.

F-5E generating strake vortices during landing sequence–concluded. 4 • 20

(a) Passing over deflected trailing-edge flap.

Strake vortex flows occurring on F-20 during variety of maneuver conditions.

(b) Becoming visible after wing-strake juncture.

(c) Vortex bursting at higher lift.

Strake vortex flows occurring on F-20 during variety of maneuver conditions–concluded. 4 • 21

juncture; in figure 4.21(c), the airplane is at a higher incidence because the strake vortex appears to burst over the wing. The vortex appears larger than those at lower lift observed in figures 4.21(a) and (b) and evaporates just aft of the junction with the wing leading edge.

Small strake surfaces are located on the inboard side of the missile launch rails and forward of the wing leading edges to generate counterrotating vortices to clean up the wingtip flow. The condensation illuminated vortices can be observed in figure 4.21(b).

4 • 7

F-14 Airplane

The F-14A Tomcat built by Grumman is a supersonic combat airplane which operates from U.S. Navy aircraft carriers to provide long-range air defense to the Navy fleet. It has a two-man crew seated in tandem, a clear canopy which provides good visibility, and variable-sweep outer wings which can pivot from 20° at the lowest sweep angle to 68° in the full-aft position. The inboard glove has a vane which is usually deployed with the wings at the highest sweep. The airplane also has all-movable horizontal tail surfaces, full-span leading-edge slats, and trailing-edge flaps. The Phoenix, Sparrow, and Sidewinder missiles can be carried from pylons located on the underside of the glove, wing, and fuselage.

Because of its variable wing sweep and engine capabilities, the F-14A can operate at high-g levels, angles of attack greater than 50°, and Mach numbers greater than 2. This large performance envelope results in a wide variety of flow fields. The first group of photographs shows condensation patterns for subsonic maneuvers, where the wings have different sweep angles from the full-forward to the full-aft positions. Figures 4.22 to 4.24 are for the wings in the low sweep condition which is useful for generating high lift for takeoffs and landings and for maneuvers to high-g levels. In figure 4.22, the pattern has formed a gull shape over the wing upper surfaces, which was discussed in section 3.1 on wing-body flows. The round holes in the condensed pattern near the wing surfaces are probably caused by vorticity that passes over the wing at these locations.

The photographs in figure 4.23 were taken during one flight by the Radar Intercept Officer from the rear seat of the cockpit of an F-14A flying from an aircraft carrier. The speed of the airplane was about 350 to 400 knots while it maneuvered up to 5g. A number of flow features are observed for both the right and left sides of the

Front view of F-14A during maneuver with wings at low sweep showing wing-body gull pattern. 4 • 22

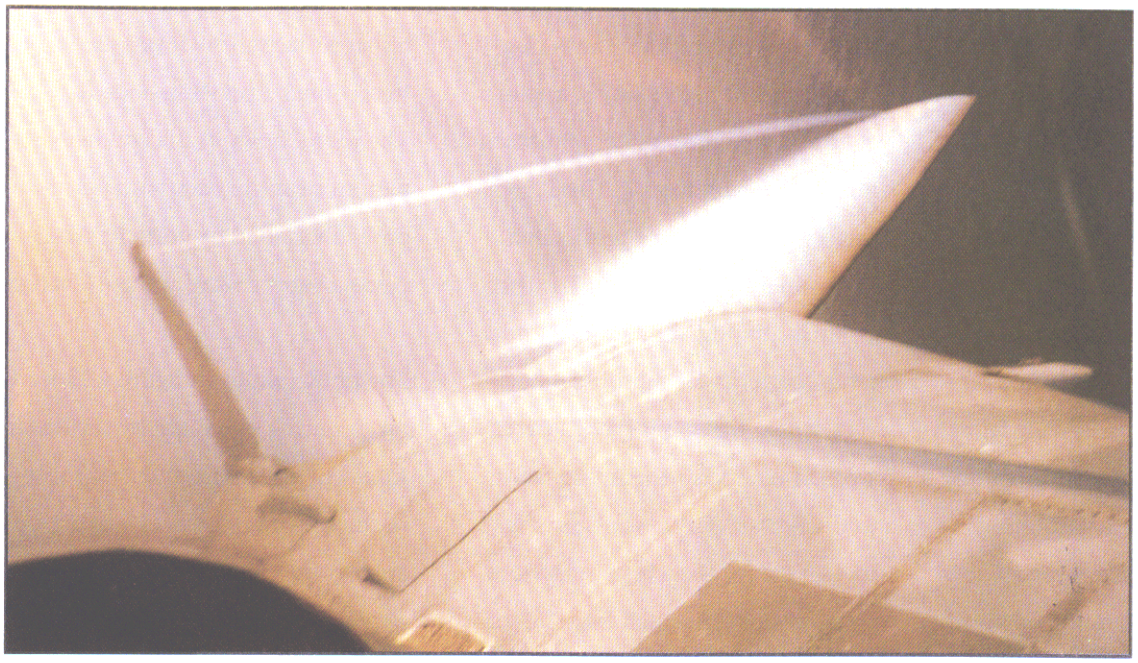

(a) Wing gull pattern, inlet side-edge vortex, and wingtip vortex.

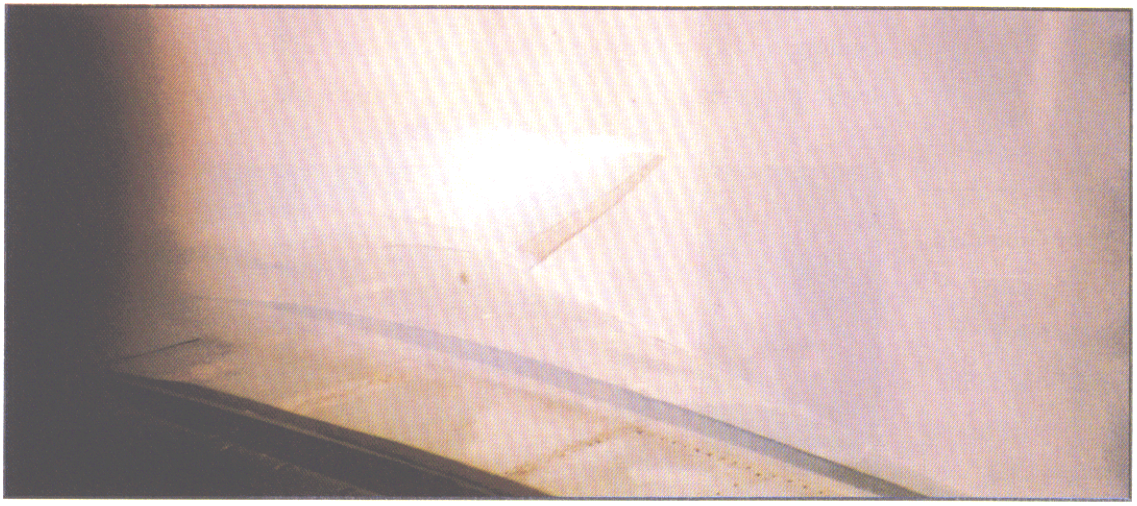

(b) Wing gull pattern and missile pylon vortex.

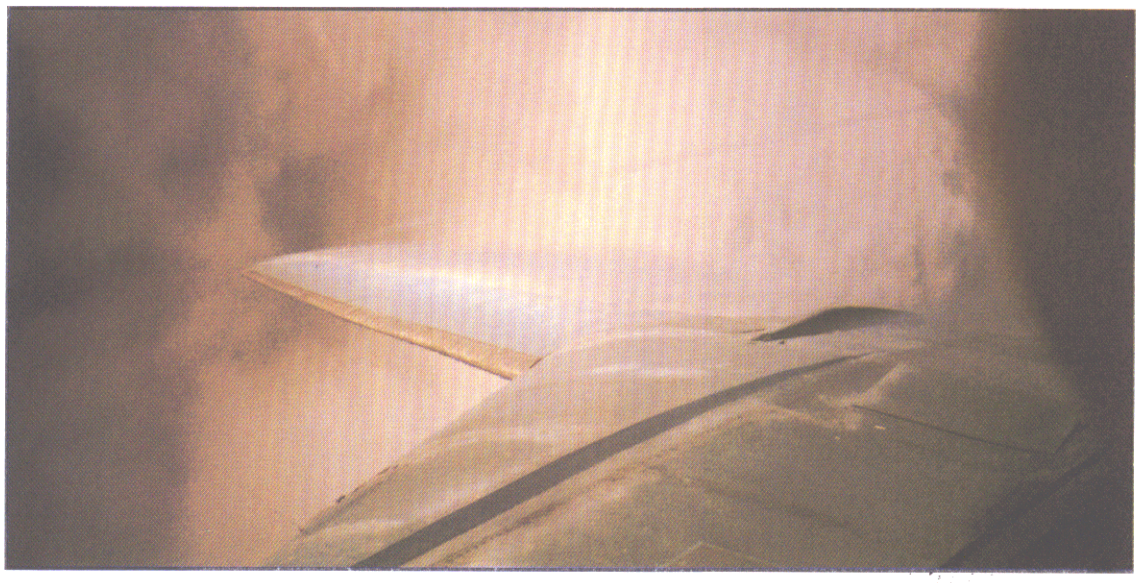

(c) Wing gull pattern and inlet side-edge vortex.

Variety of flow patterns during high-g maneuvers of F-14A with wings at low sweep.

(d) Wing gull pattern, inlet side-edge vortex, and missile pylon vortex.

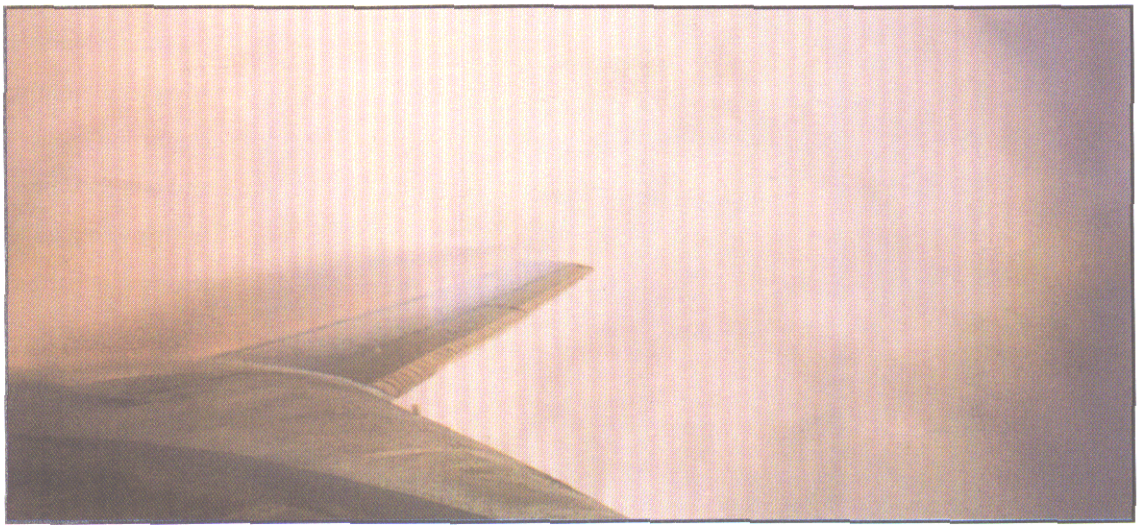

(e) Wing gull pattern, inlet side-edge vortex, missile pylon vortex, and wingtip vortex.

(f) Streamwise vorticity from wing leading edge.

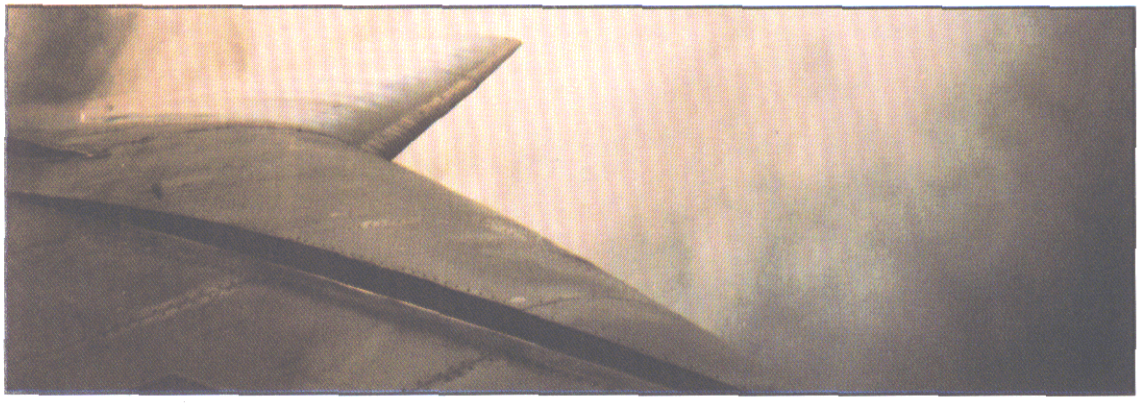

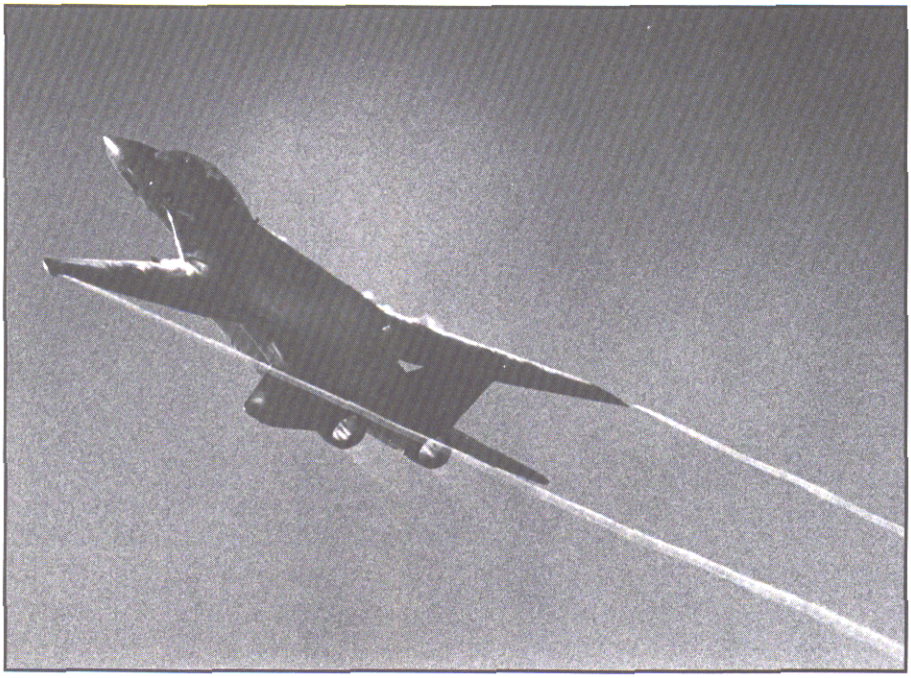

Streamwise pattern occurring along wing leading edge during high-speed pull-up of F-14A. 4 • 24

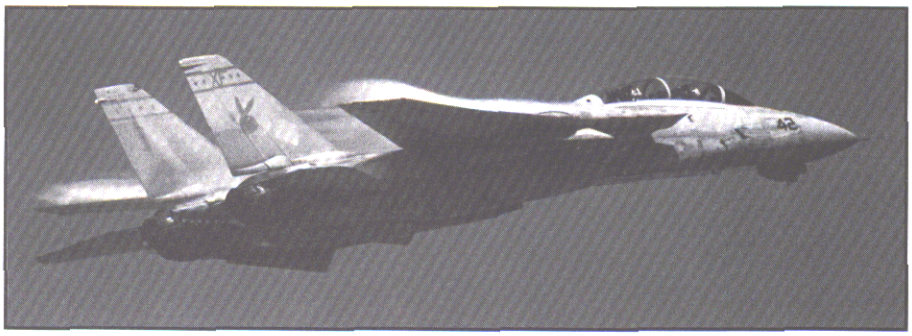

Leading-edge vortices occurring over highly swept wing of F-14A during high-speed pull-up. 4 • 25

F-14A creating leading-edge vortices while breaking into landing pattern with F-5E. 4 • 26

airplane with the wings at a low sweep position. Figures 4.23(a) to (e) show wing condensation patterns that are beginning to take on a gull shape, and wingtip vortices are observed in figures 4.23(a), (c), (d), and (e). The streamwise pattern at the wing-glove juncture (figs. 4.23(b), (d), and (e)) is probably a vortex generated by the missile pylons which are mounted from the lower surfaces of the gloves. The nose of the Sparrow missile can be seen in several views of the left wing of the airplane.

A condensed flow pattern is observed in figures 4.23(a), (c), and (d) along the inboard part of the glove and flows aft over the airplane. This is a vortex generated by the side edges of the upper surface of the inlet and was described in more detail in section 3.3.8. A repeating streamwise pattern along the wing upper surface originating from the wing leading edges is seen in figures 4.23(f) and 4.24. These are the same streamwise vorticities from wing leading edges described earlier in section 3.3.5. Additionally, figure 4.24 shows condensation occurring aft of the inlet cowl, and at the wing-glove juncture; the pattern on the horizontal tail is caused by a leading-edge vortex.

The next photographs were taken at subsonic maneuvering conditions with the wings swept farther aft than the wings with low sweep that were

just presented. With the wing panels at higher sweep, wing leading-edge vortices begin to develop during high-lift conditions as noted in figure 4.25 for this high-speed pull-up and in figure 4.26 where the airplane is breaking into the landing pattern. In a sequence made during a high-speed pull-up, the side view (fig. 4.27(a)) shows a large condensation region over the wing, whereas there is a pattern flowing streamwise from the canopy crest. In the rear view (fig. 4.27(b)), the airplane probably has massive separation over the upper surfaces to cause the condensation from wingtip to wingtip, which appears like half of a sphere, that is, a hemisphere.

At a 6.5*g* maneuver (fig. 4.28), separation-induced leading-edge vortex flows are generated by the glove, glove vane, and the wing.

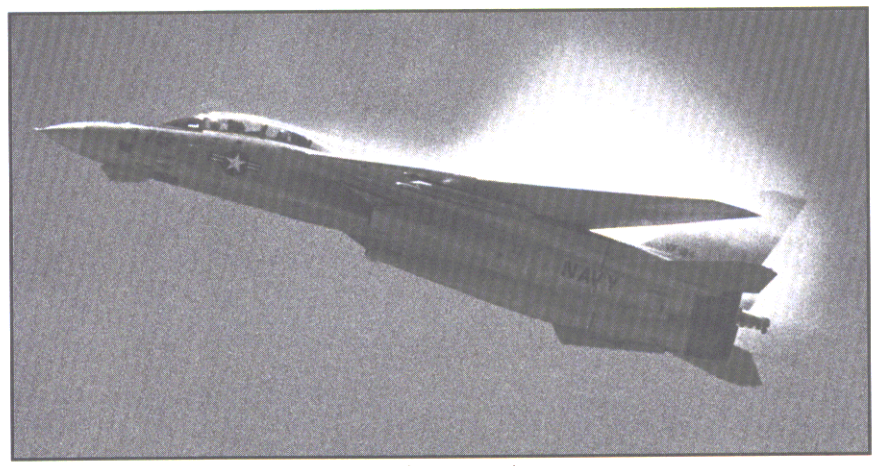

(a) Side view of large condensation region over wing.

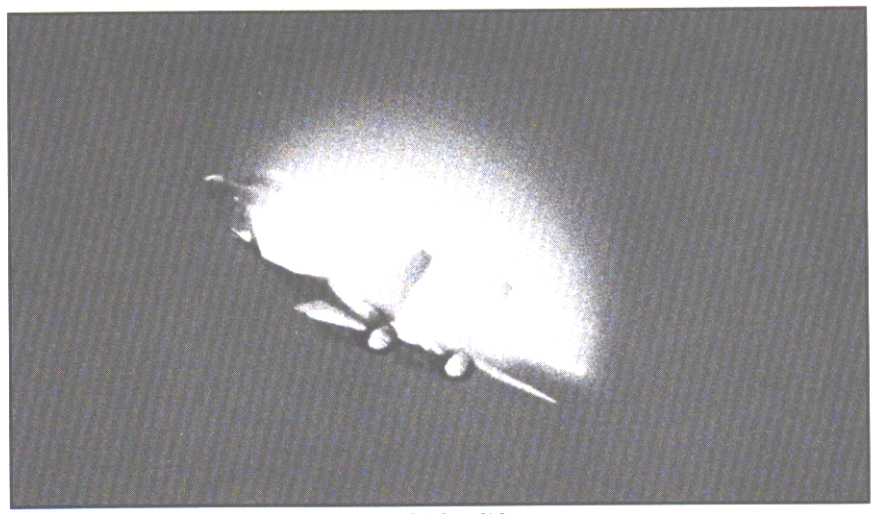

(b) Rear view of massive separation at higher lift.

Condensation patterns occurring during high-speed pull-up of F-14A with wings at high sweep. 4 • 27

Leading-edge vortex flows generated by wing, glove, and horizontal tail surfaces for F-14A at 6.5g and about 480 knots during maneuvers. 4 • 28

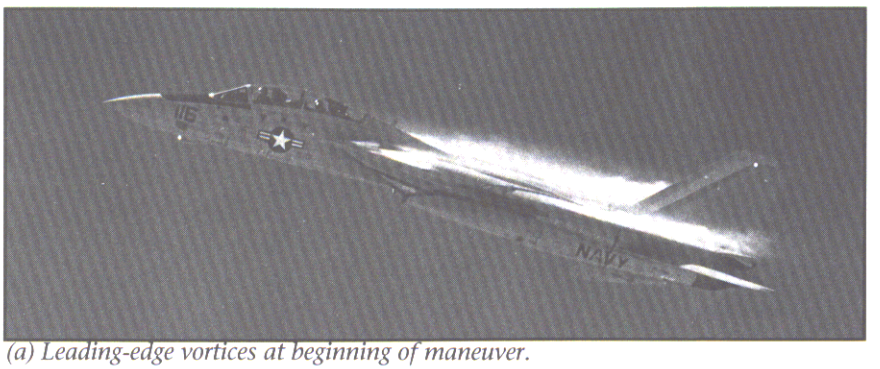

(a) Leading-edge vortices at beginning of maneuver.

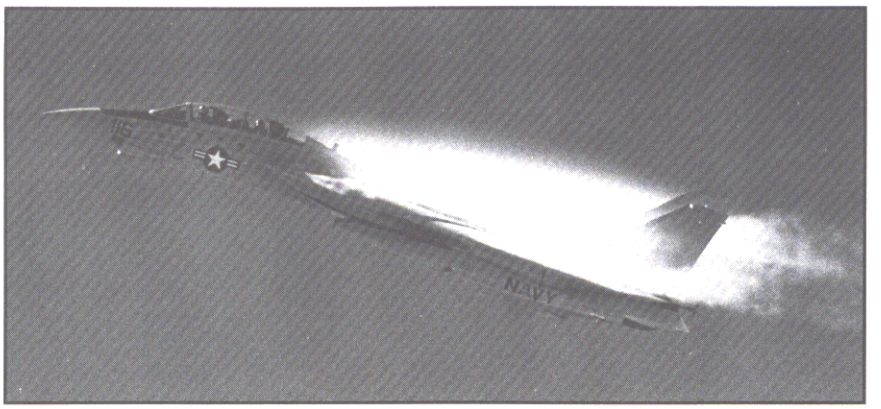

(b) More condensation at moderate angle of attack.

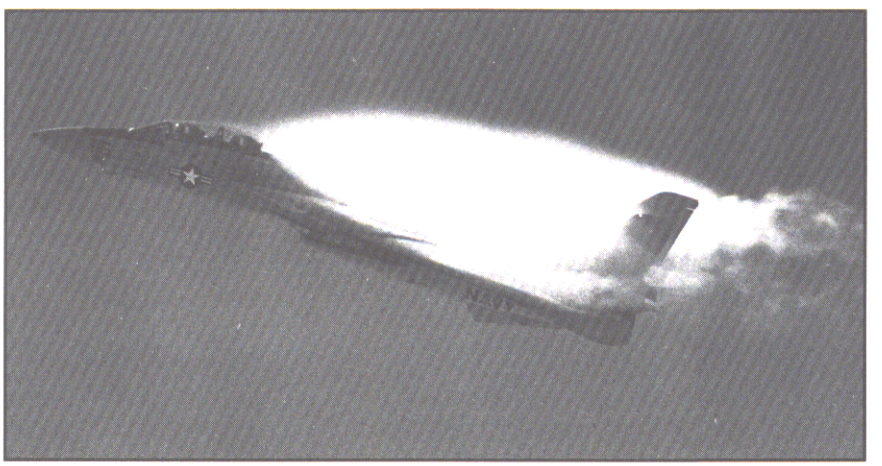

(c) Largest condensation at highest angle of attack.

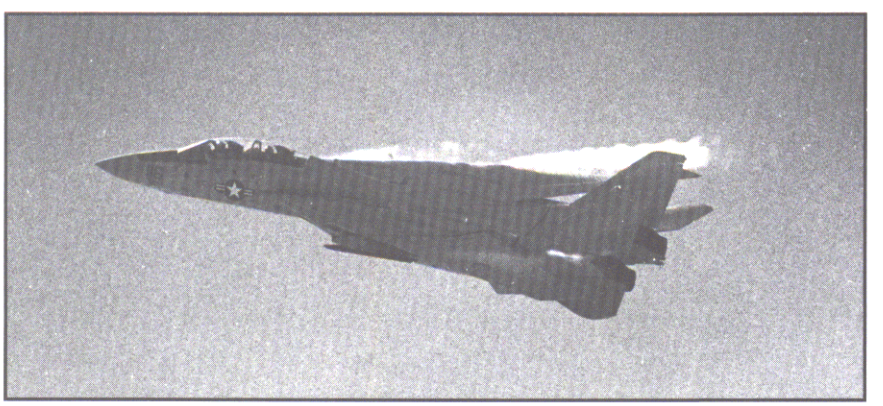

(d) Leading-edge vortices at end of maneuver.

Sequence capturing changing leading-edge vortex flow patterns occurring over highly swept wings during F-14A breaking into landing pattern. 4 • 29

In addition, the lift and humidity are high enough to see a pronounced vortex generated by the horizontal tail leading edge. The vortex generated by the side edge of the fairing to the top of the engine inlet is readily apparent in this side view. The junction of the trailing edge of the glove-vane and the leading edge of the glove produces a counterrotating vortex similar to that for a notch or chord extension. The vortex flows over the wing leading edge and back over the wing to provide the demarcation noted in the condensed patterns between the vane and glove leading-edge vortex systems. The missile pylon creates a vortex which comes over the wing leading edge and is also observed in figures 4.23(d) and (e). The wing leading-edge vortex develops a large swirling motion in its outer edge as it nears the wing trailing edge. As it proceeds farther downstream, the vortex core appears to turn downward toward the horizontal tails and evaporates.

The sequence in figure 4.29 was taken while breaking into a landing pattern. In figure 4.29(a), the condensation over the wings and the glove-vane is caused by the leading-edge vortex flows that are generated because of high sweep. In figures 4.29(b) and (c), additional condensation over the airplane is due to pitch-up to higher angles of attack, which generates more lift and drag for decelerating. The

wing leading-edge vortices appear to be larger because of this maneuver. The airplane pitches down to a lower attitude in figure 4.29(d), and the condensation patterns again are similar to figure 4.29(a). An additional sequence with the wings at high sweep (fig. 4.30) shows the glove and wing vortices that occur during a pitch-up maneuver. At higher lifts, the condensation covers the airplane aft of the canopy and back to the vertical tails and hides the vortex systems. Figure 4.31 was taken from behind and below the airplane and shows the wing leading-edge vortices that form during a high-*g* turn.

The second group of the F-14A photographs was taken during high-speed flights where some very dramatic condensation patterns are seen. The sequence of two (fig. 4.32) was made during a high-speed pass. Although the airplane speed is subsonic, the airflow expands to supersonic flow above and below the airplane. This type of condensation was discussed earlier in section 3.2. The front view looks bigger, but as the airplane passes, the side view shows that the pattern is limited to a narrower region.

Although the picture quality of figure 4.33 is not good, it still shows the large condensed region extending vertically away from the airplane with the shock wave at the back almost perpendicular to the flight path.

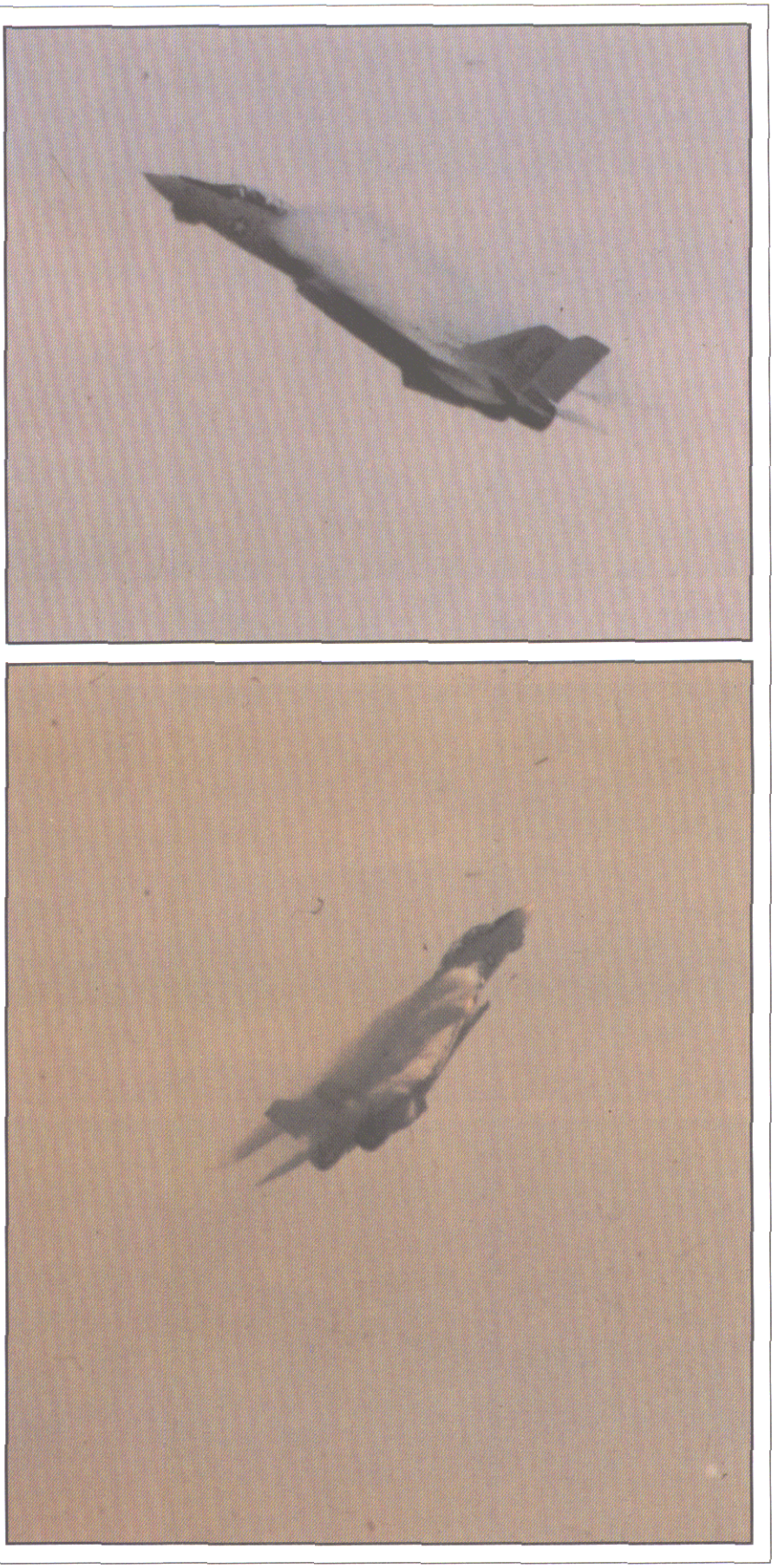

Sequence showing wing and glove leading-edge vortices on F-14A with wings at high sweep during pitch-up maneuver. 4 • 30

C-2

Rear view of wing leading-edge vortices forming on F-14A with highly swept wings. 4 • 31

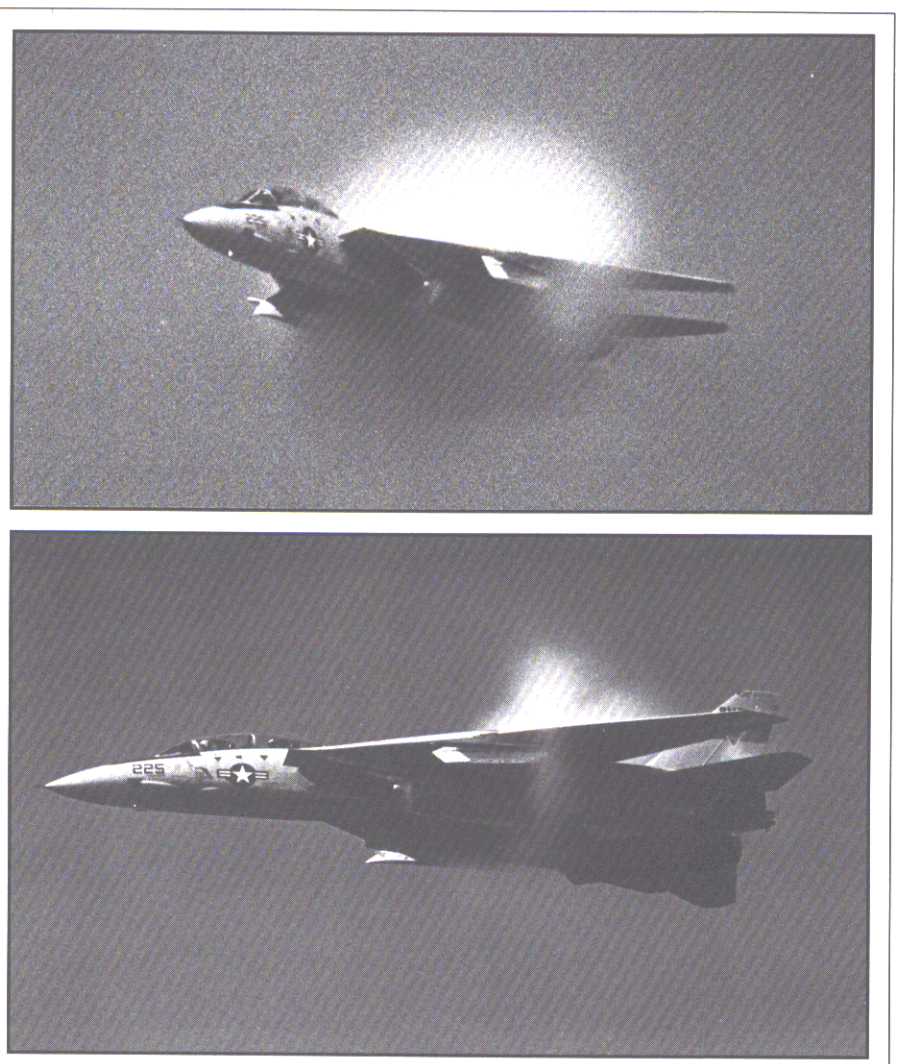

Sequence showing supersonic flow occurring on F-14A with wings at high sweep during high-speed pass. 4 • 32

The flow expands and condenses over the canopy and over the housing that covers the sensor unit on the lower surface of the nose. Figure 4.34 is of marginal quality but is a spectacular picture that shows the large vertical extent of the supersonic region and the condensation over the canopy.

The F-14A often makes low-altitude supersonic passes close to aircraft carriers, where the speed of the airplane is slightly higher than the speed of sound with a Mach number usually about 1.05. This was true for the F-14A shown in the photograph in the Preface, where the shock wave reached the water surface to cause the spray. The pressure differential across the shock wave causes the so-called sonic boom. In figure 4.35, the pass resulted in a doughnut shape, whereas other patterns are shown in figures 4.36 and 4.37.

Thus far, condensation patterns have been shown which change during a flight sequence because of changes in the airplane flow field due to the maneuver. The last sequence of seven photographs (fig. 4.38) was taken during an air show, the eighth in the flight sequence was presented as figure 3.6. An F-14A was making a low-altitude high-speed pass, flying at a Mach number of about 0.9. The photographs were taken with a motor-driven camera to record this special sequence. Starting with figure 4.38(a),

Large condensed region of supersonic flow occurring on F-14A at high subsonic speeds. 4 • 33

the patterns begin with little apparent organization above and below the airplane. At this speed and cruise angle of attack, the airplane is not in a maneuver and the condensed supersonic flow region should be reasonably symmetric from above and below. As the airplane approaches, the patterns change continuously from above and below. Going from figure 4.38(e) to figure 4.38(f), the supersonic condensed flow below the airplane looks reasonable, whereas it almost disappears entirely above the airplane. Figure 4.38(g) shows the fully developed condensation pattern. If the lift and speed of the airplane were constant during this flyby, the actual flow field would not change. Therefore, the reason for these apparent changes in the condensation patterns may be that the humidity the airplane is flying through is not uniform, and this

Condensed pattern of supersonic flow extending to large vertical distances above F-14A. 4 • 34

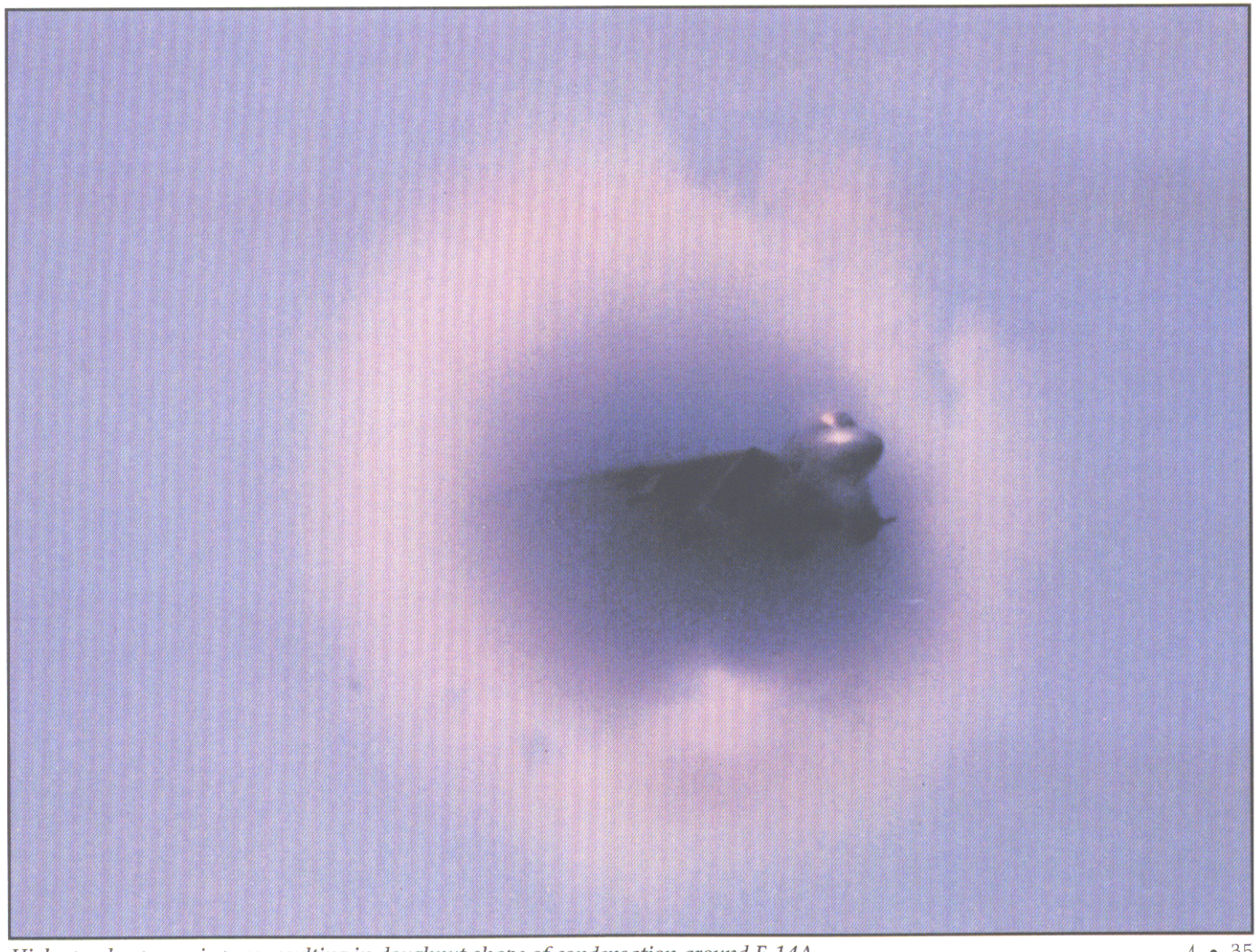

High-speed supersonic pass resulting in doughnut shape of condensation around F-14A. 4 • 35

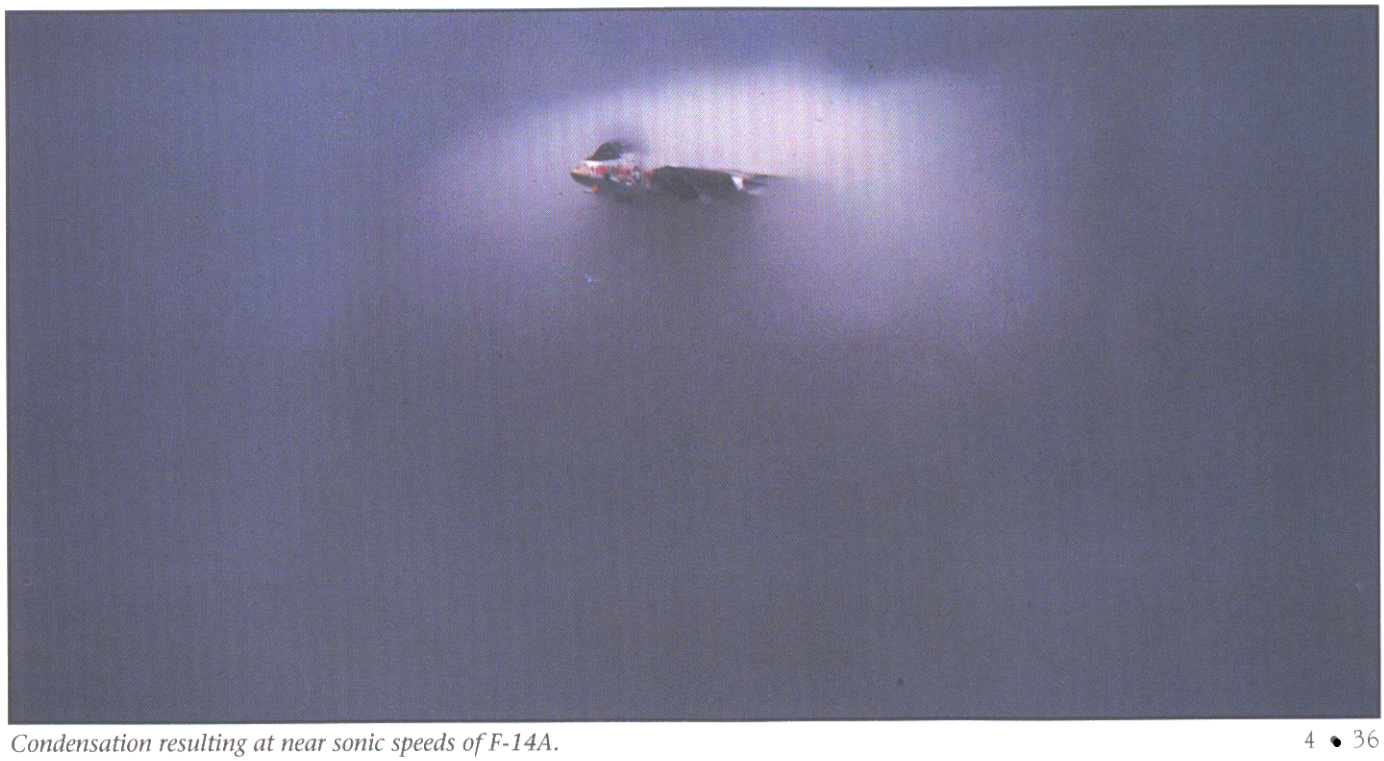

Condensation resulting at near sonic speeds of F-14A. 4 • 36

Supersonic condensation region occurring on F-14A during high subsonic speeds.

4 • 37

Amount of condened supersonic flow changes around F-14A during 15-sec photographic sequence with Mach number (0.9) and lift constant. 4 • 38

would cause the visual changes seen above and below the airplane.

4 • 8

F-16 Airplane

The F-16 Fighting Falcon is a single-seat tactical fighter built by General Dynamics for the U.S. Air Force and some European countries, such as Belgium, Denmark, The Netherlands, and Norway. It was initially designed as a small, lightweight fighter to perform highly maneuverable air-to-air combat. It features a moderate-sweep trapezoidal wing with highly swept strake surfaces that extend forward from the wing leading edges and along the fuselage nose. The leading edges of the strakes are sharp, which generate separation-induced vortex flows that increase maneuver lift. The wing has movable leading- and trailing-edge flaps that are deflected together to provide the optimum lift and drag for takeoffs and landings, subsonic and supersonic cruise, and transonic maneuver. The airplane has permanent missile launch rails mounted at the wingtips.

The condensation pattern on the F-16 usually consists of the strake vortex flows that were discussed previously in section 3.3.2. Figure 4.39 shows a perspective from above an F-16B, which is a two-seat version, where the leading-edge flaps are deflected down for this maneuver condition. The strake vortex sheds rearward at the wing-strake juncture and passes over the wing upper surface. As condensed flow passes over the wing trailing edge, it appears to thin out somewhat and eventually vaporizes and disappears aft of the tail surfaces. In figure 4.40, the strake and wingtip vortices are asymmetric during the maneuver, whereas the strake vortex on the right side of the airplane has condensed flow farther aft than that

Wing-body strake vortices generated during maneuver of F-16B.

Wing-body strake vortices generated during maneuver of F-16A. 4 • 40

Asymmetric strake vortices occurring for F-16A during formation flying. 4 • 41

Condensed flow spirals around vortex core causing wavy appearance of strake vortices for F-16A. 4 • 42

on the left side. Having a nonzero sideslip angle causes differences in the flow between the right and left sides.

In figure 4.41, four Falcons are flying in formation. The lead airplane has just initiated a bank and a turn toward the viewer and has generated enough lift to result in condensed strake vortices. The airplane flow field is asymmetric as suggested by the strake vortex evaporating over the wing on the left side and over the horizontal tail on the right side.

In figure 4.42, an F-16A is in a maneuver with wing leading-edge flaps deflected and Sidewinder missiles at the wingtips. The strake vortices have a wavy appearance caused by the spiraling around the vortex core. Similar flow features occurred for an F-16B presented as figure 3.18. Strake vortices are observed from a rear view for an F-16A during a pull-up maneuver (fig. 4.43). Figure 4.44 is from a U.S. Air Force squadron and shows strake and wingtip vortices during a maneuver. The strake vortices have the repeating patterns in their flow, which are a result of the small shear-layer instability vortices described earlier in figures 3.22 to 3.26.

In the front view in figure 4.45, condensation in the strake vortices persists far into the airplane wake. On the right wing, the strake vortex

Rear view of strake vortex occurring on F-16A during pull-up.

4 • 43

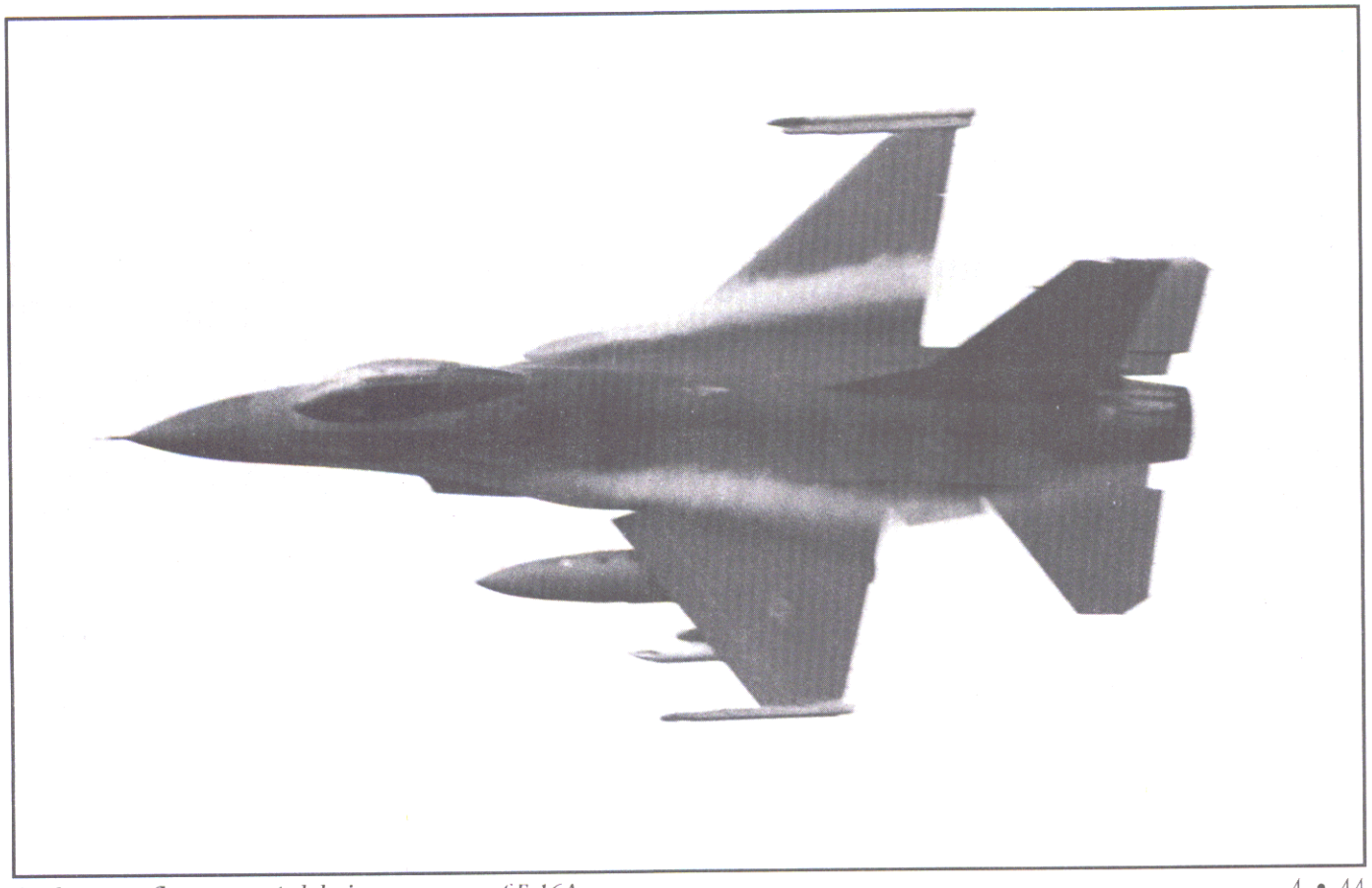

Strake vortex flows generated during maneuver of F-16A.

4 • 44

Front view of strake vortices during maneuver of F-16A.

4 • 45

Strake vortex occurring during flight evaluation of F-16C.

4 • 46

Strake vortex and wing condensations occurring during flight evaluation of F-16C at high lift. 4 • 47

interacts with the wing flow at the wing-strake juncture, where a gap is created by the deflected leading-edge flaps. Outboard on the wings, there is a condensation pattern that flows rearward over the wingtips. This is a separation-induced vortex flow that may be generated at the junction between the inboard edge of the missile launch rail and the wing leading edge. More of a gap is exposed when the wing leading-edge flaps are deflected to large angles during maneuver. It is also possible that the vortices are generated by the nose or fins of the Sidewinder missiles.

Condensation patterns are shown in figures 4.46 and 4.47 during maneuvers of the F-16C. A third photograph made during the same flight is presented as figure 3.24 during the discussion of shear-layer instability vortices. In the side view for figure 4.46, the condensation begins in the core close to the strake apex and experiences much more condensed flow as it passes over the wing. In this region, the outer edge of the flow pattern shows evidence of

Strake vortices occurring during maneuver of F-16. 4 • 48

the spiraling effect of the small vortex filaments in the shear layer. As the vortex passes over the horizontal tail, the outer portion of the condensed vortex flow evaporates and leaves some condensation around the outer edge of the core. The other view from the aft and to the side for a high-lift condition (fig. 4.47) shows that the strake vortex condensation grows rapidly in size at about halfway along the strake, then joins the rest of the wing condensation over much of the airplane.

The maneuver in figure 4.48 results in condensation in the strake vortices. The strake vortex on the right side has a circular pattern in the lower portion of the strake vortex just aft of the wing trailing edge. These are the small vortices that start in the vortex sheet.

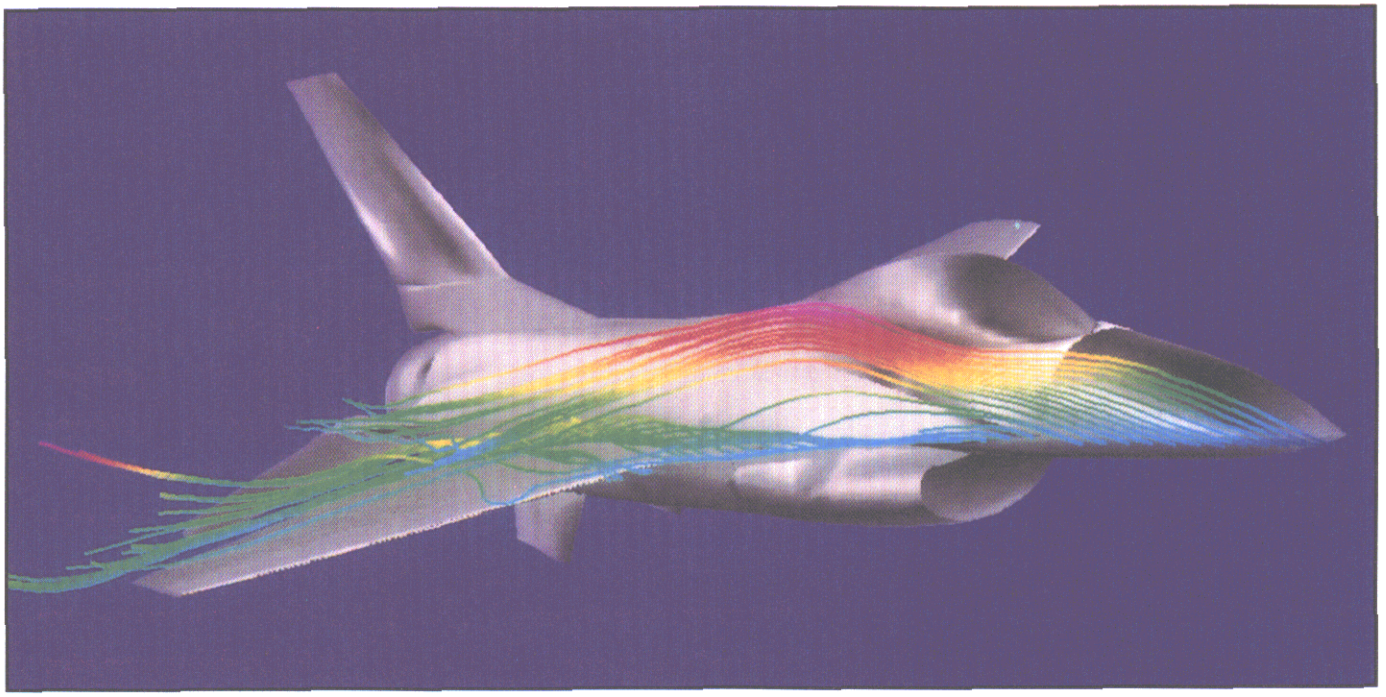

Flow traced in computation of F-16 flow field at M = 0.6 and α = 10° showing interaction of strake vortex with wing leading-edge vortex. 4 • 49

Similar vortices are seen as the vortex passes the horizontal tail showing a skeletal flow around the core as evaporation occurs. This gives an idea of the size of the strake vortex because the rings should be at or close to the outer edge of the vortex flow. An additional condensed flow pattern is noted at the inboard portion of the wing upper surfaces and is due to streamwise vorticity from the leading edges.

Researchers have conducted studies to calculate the flow field for the F-16. An early attempt is shown in figure 4.49 for a Mach number of 0.6 and an angle of attack of 10°. Particle traces in the flow field show the strake vortex interacting with the vortex generated by the wing leading edge.

A further illustration is presented in the flight sequence of figure 4.50 to show the development of streamwise vorticity near the wing leading edges of an F-16A. The maneuver starts in figure 4.50(a), where the strake vortex is present but there is no wing condensation. In figure 4.50(b), the wing is showing some streamwise condensation, and it is even more developed in figure 4.50(c), where the appearance of wingtip vortices is a clue that the airplane is at a higher lift.

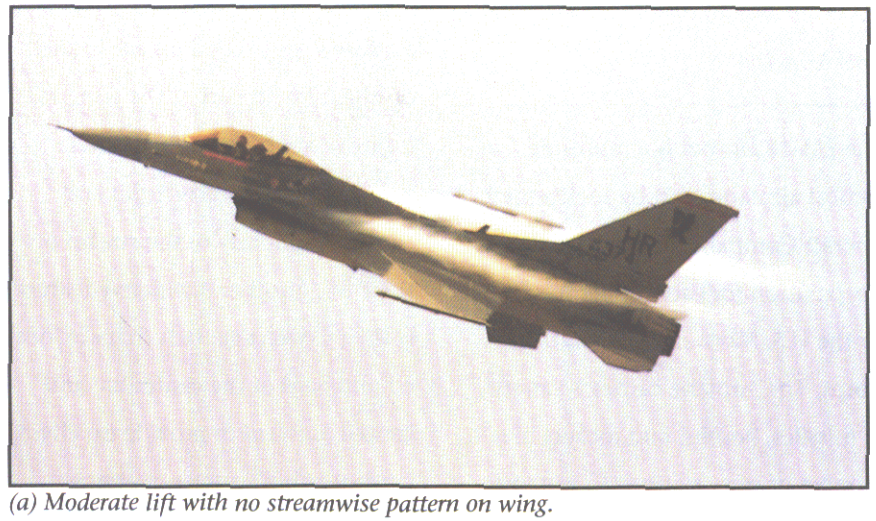

(a) Moderate lift with no streamwise pattern on wing.

(b) Higher lift.

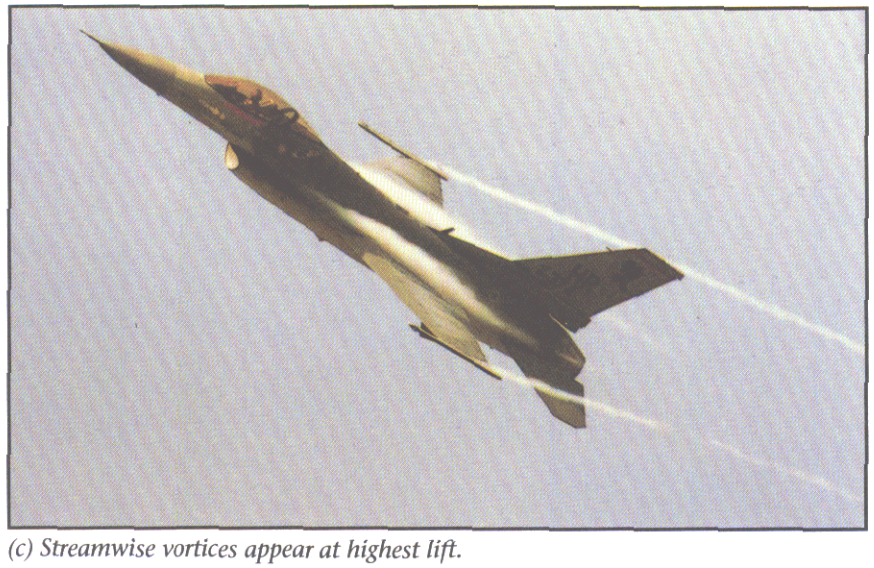

(c) Streamwise vortices appear at highest lift.

Strake vortex and streamwise vorticity appearing on upper surface of wing leading edges during F-16A maneuver as lift increases. 4 • 50

4 • 9

F-18 Airplane

The F/A-18 Hornet is a multirole tactical airplane built by McDonnell Aircraft Company and the Northrop Corporation for carrier operation by the U.S. Navy and U.S. Marine Corps. The airplane carries a variety of missiles, bombs, and rockets in a number of store stations to support air-to-air and air-to-ground missions, including Sidewinder missiles mounted on missile launch rails at the wingtips. The moderately swept wings have leading-edge and trailing-edge flaps which deflect automatically to optimize the performance during cruise and maneuvering flight. Highly swept leading-edge extensions are located on the inboard part of the wing to improve the high-angle-of-attack aerodynamic characteristics and function similarly to the strakes on the F-16. Another distinctive feature is the twin vertical tails that are located outboard of the centerline and canted outward to provide excellent control at high angles of attack.

Some of the most dramatic condensation patterns occur during high-angle-of-attack maneuvers, as exemplified in figures 4.51 and 4.52, where LEX and wingtip vortices are visible on the airplane. As described earlier in section 3.3.2, small vortices are generated by the instability of the LEX vortex sheet and rotate around the outer edge of the core as the vortex develops. Evidence of this flow mechanism can be seen in the LEX vortex flows. The LEX vortices evaporate as they reach the rear of the airplane near the vertical tail because of pressure recovery in the wake or an indication of vortex burst. Figure 4.53 shows a rear view of the airplane during a similar high-angle-of-attack maneuver. The LEX vortices grow in size and evaporate at the vertical tail leading edges because of the bursting of the vortices, which was described in figures 3.20 and

Instability vortices in LEX vortex shear layer causing undulations around outer edge of vortex core during maneuver of F/A-18. 4 • 51

Shear-layer instability vortices forming in LEX and wingtip vortex flows for F/A-18 at high angles of attack. 4 • 52

3.21 in section 3.3.2 and is shown for a wind tunnel model later in this section in figure 4.58.

Although the LEX vortices allow an airplane to fly successfully at high angles of attack, they have special aerodynamic characteristics that require attention. During a maneuver, the LEX vortical flow fields pass close to the vertical tail surfaces, induce positive or adverse flow on the tail, and thus affect airplane stability and controllability. A complication can occur at higher angles of attack and high dynamic pressures when the LEX vortices burst at or upstream of the tails. The resulting turbulent, high-energy air can result in structural buffet and fatigue.

NASA is currently conducting a High Alpha Technology Program (HAPT), which coordinates research efforts from the wind tunnel, flight tests, and computational fluid dynamics to help understand separated and

LEX vortices bursting and evaporating at vertical tail leading edges during high-angle-of-attack maneuver of F/A-18. 4 • 53

Smoke used to visualize LEX vortex of NASA F/A-18 research airplane at Mach number of about 0.3, $\alpha = 20°$, and sideslip angle near zero. 4 • 54

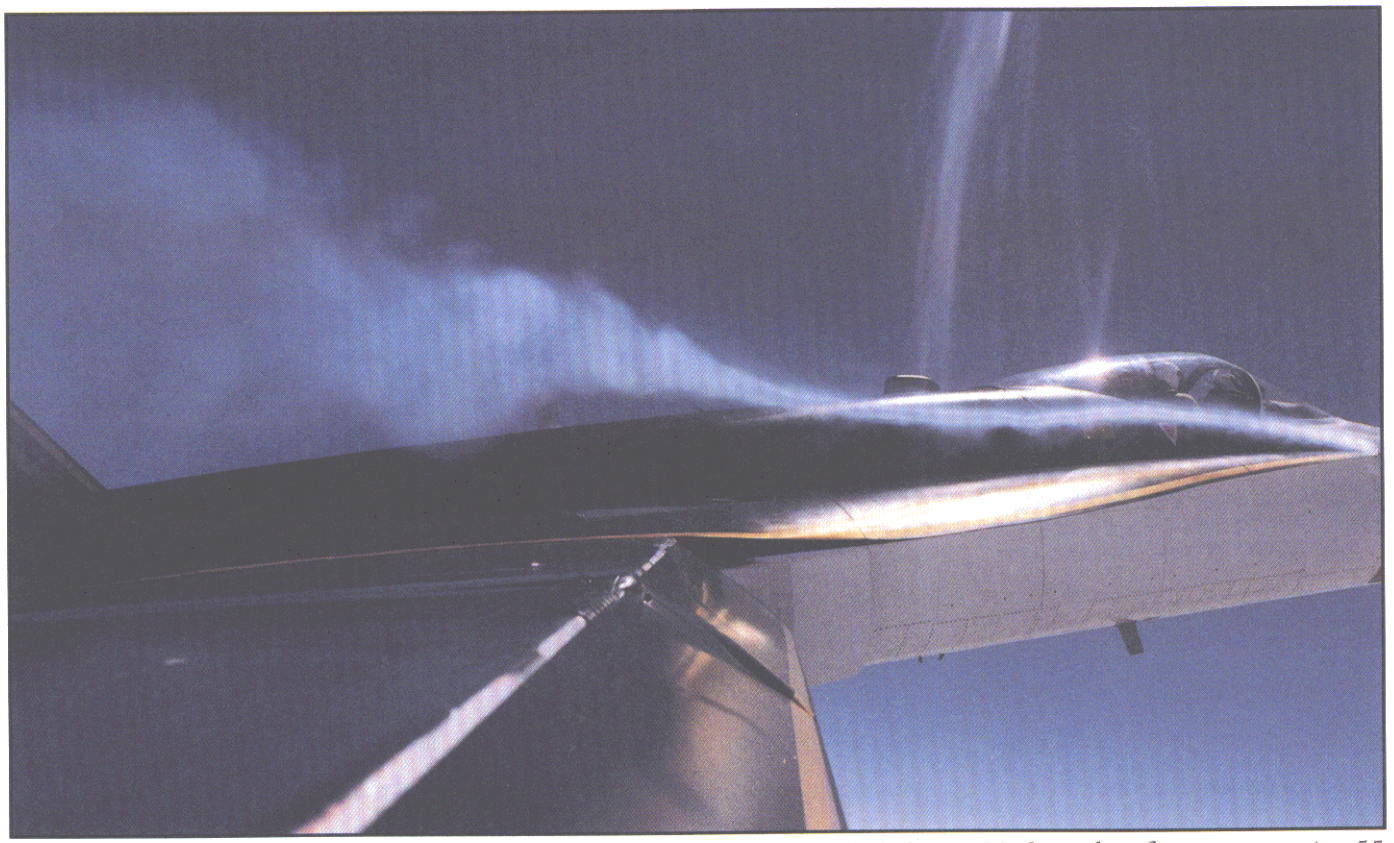

Smoke-visualized LEX vortex using right wingtip camera on NASA F/A-18 research airplane at Mach number of about 0.3, α = 25°, and sideslip angle near zero. 4 • 55

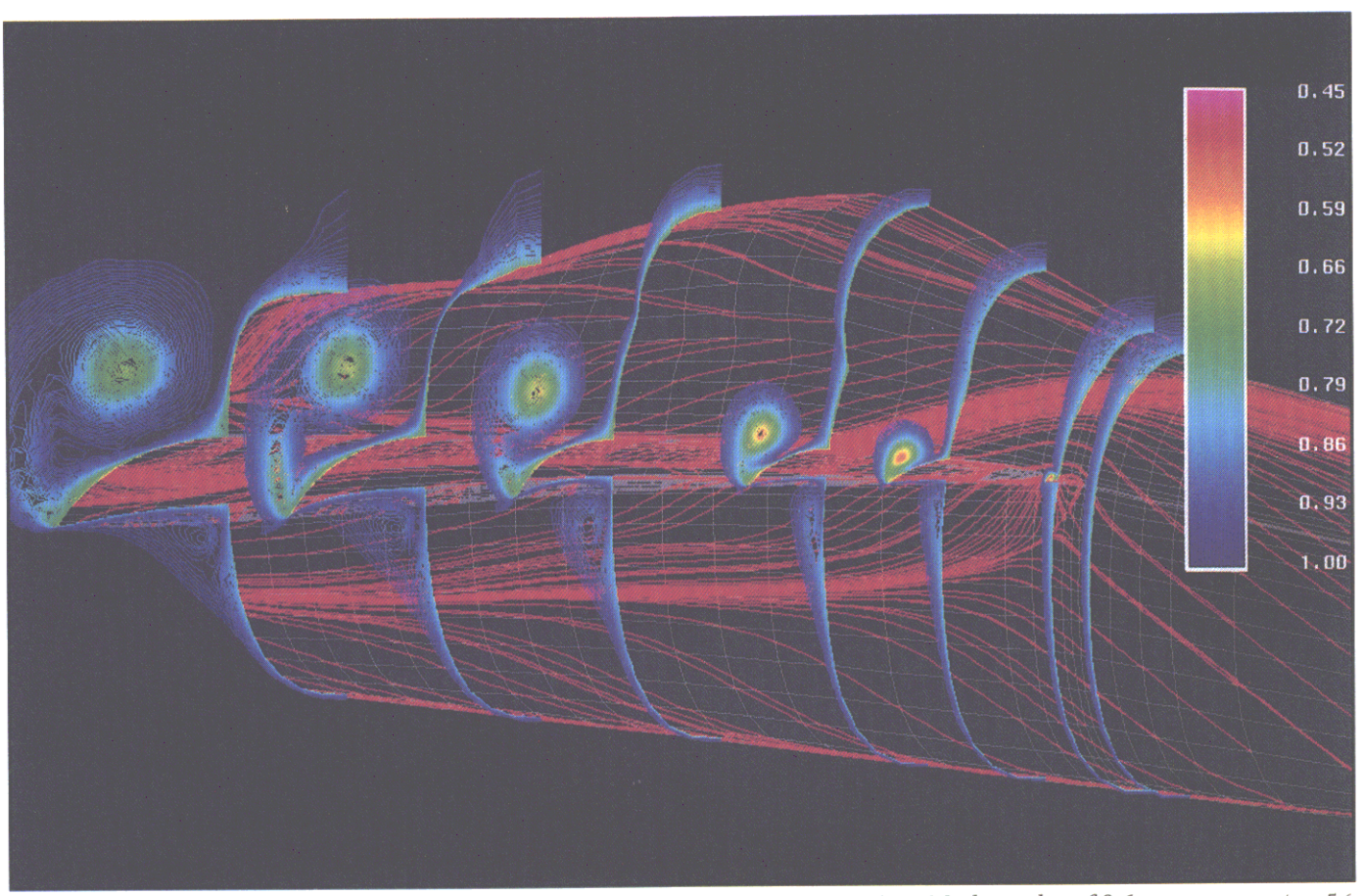

Computed total pressure contours and surface flow pattern for F/A-18 LEX and forebody at Mach number of 0.6 and α = 20°. 4 • 56

vortical flow problems associated with high-angle-of-attack flight. An F/A-18 was chosen for this research effort because it could be trimmed at angles of attack greater than 55°, and thus can provide an excellent platform to acquire data. The NASA F/A-18 research airplane is shown in figures 4.54 and 4.55, where smoke has been injected at the LEX apex to visualize the vortex flows. The upper surface was painted black to provide contrast with yarn tufts on the surface and the smoke above. A chase plane provided the air-to-air photograph in figure 4.54, whereas a 35-mm camera mounted on the right wingtip took the photograph shown in figure 4.55. Vortex burst is indicated by the swirling and sudden growth in size of the core. As angle of attack increases, the vortex bursts upstream of the vertical tail leading edge. Evidence of shear-layer instability vortices is noted in the rotation of the smoke around the outer edge of the vortex core in both figures.

Several examples are shown from wind tunnel and computational studies that were conducted to support the High Alpha Technology Program. A calculation was made for the F/A-18 forebody and LEX combination and is presented in figure 4.56. The results were obtained with the same computational theory that provided the leading-edge vortex flows on a delta wing in section 3.3.1. The total pressures are color coded to illustrate the LEX vortex which is superimposed over the surface streamlines. Experiments were conducted to measure pitot pressure profiles over an F/A-18 model at low speeds (fig. 4.57) for $\alpha = 23°$. The results are plotted with the pressures color scaled; black represents minimal pressure loss and white represents a maximum pressure loss. A flow visualization study conducted at subsonic and transonic speeds used the laser

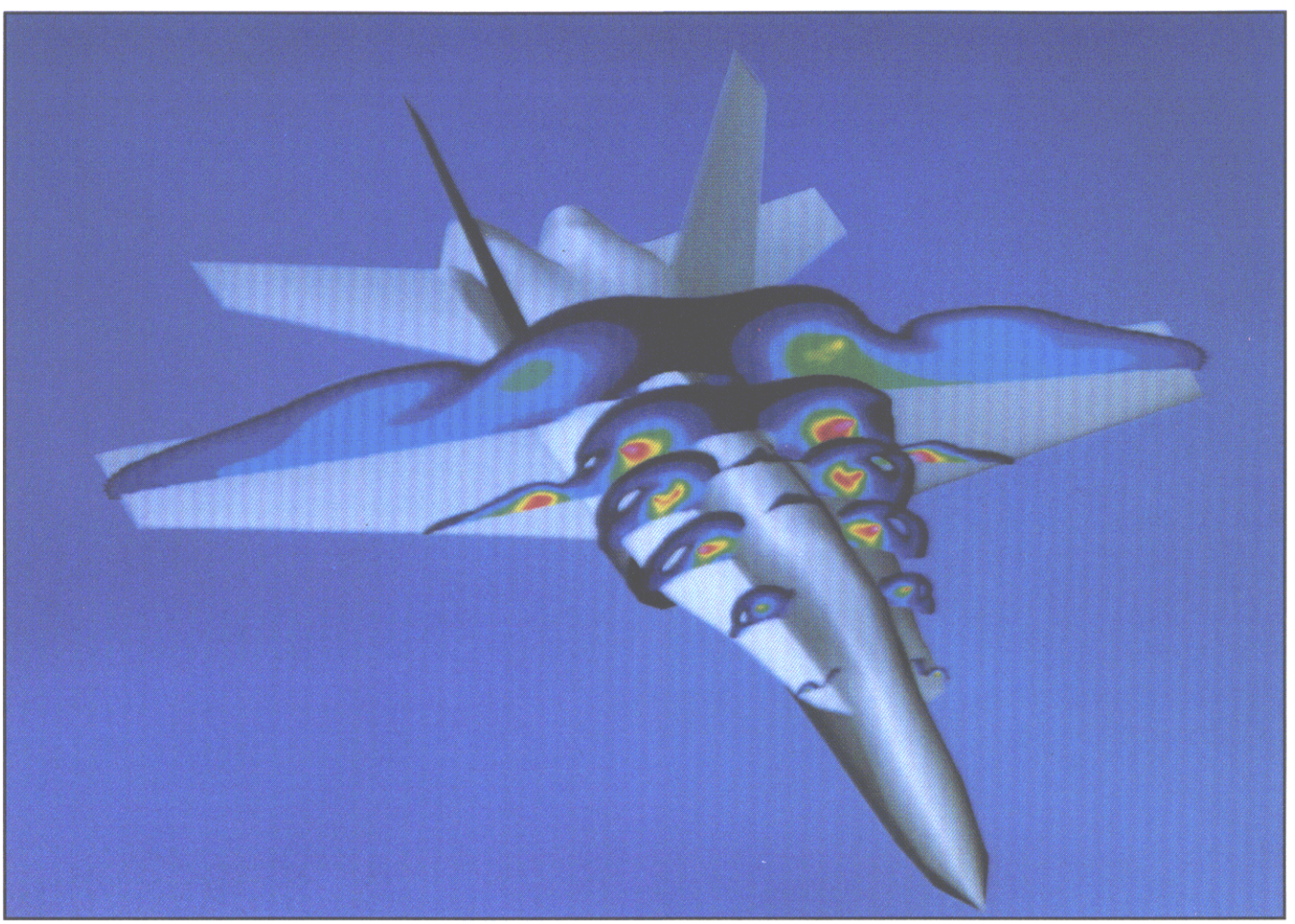

Pitot pressure survey of F/A-18 model at low speeds and $\alpha = 23°$ in Langley Basic Aerodynamics Research Tunnel. 4 • 57

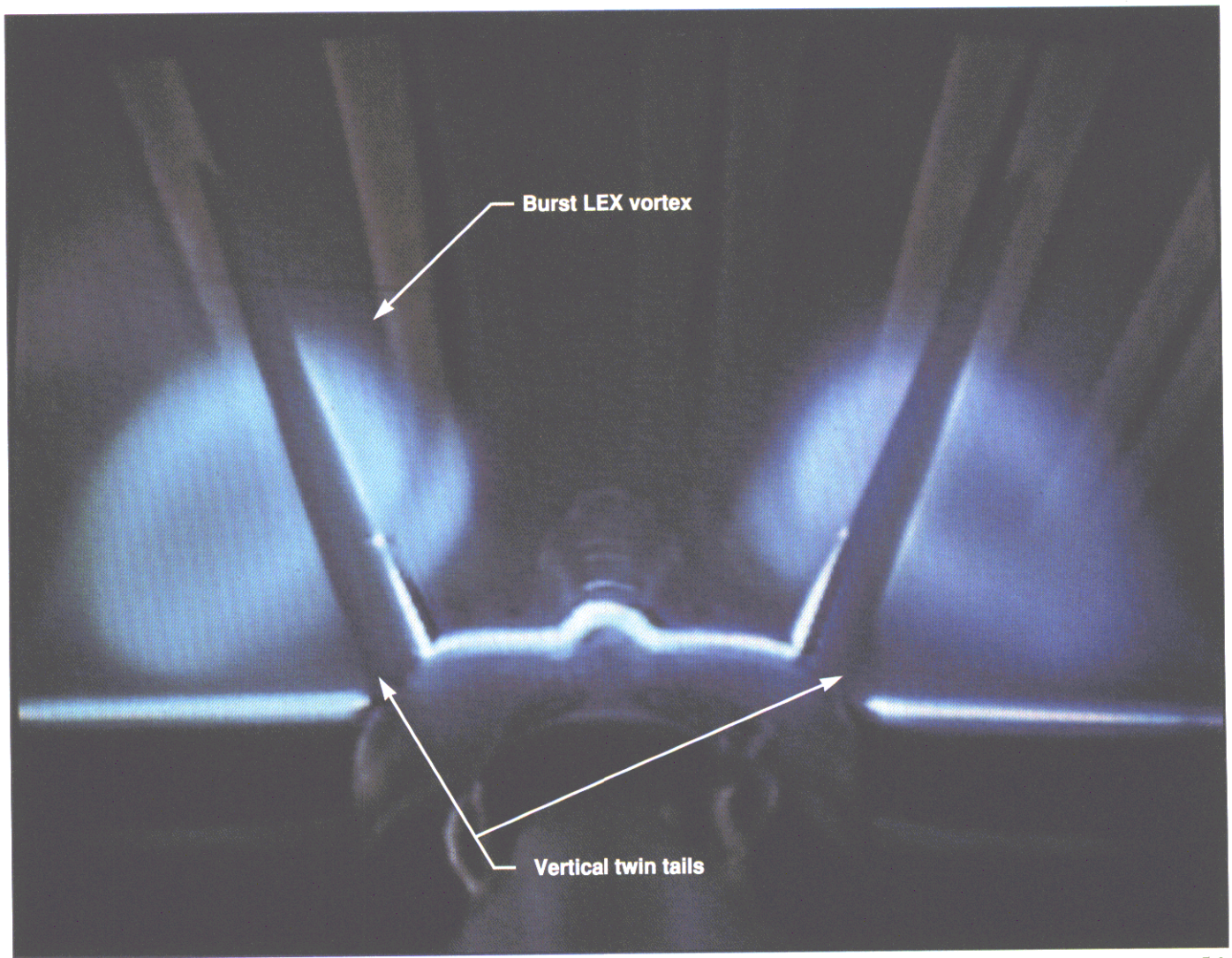

Laser vapor screen study of F/A-18 model at M = 0.6 and α = 20° in 7- by 10-Foot Transonic Tunnel at David Taylor Research Center. 4 • 58

LEX and wing condensation patterns occurring on F/A-18 during Blue Angels maneuver. 4 • 59

Wing condensation patterns occurring during maneuvers of F/A-18.

4 • 60

Supersonic flows on F/A-18 making high-speed pass. 4 • 61

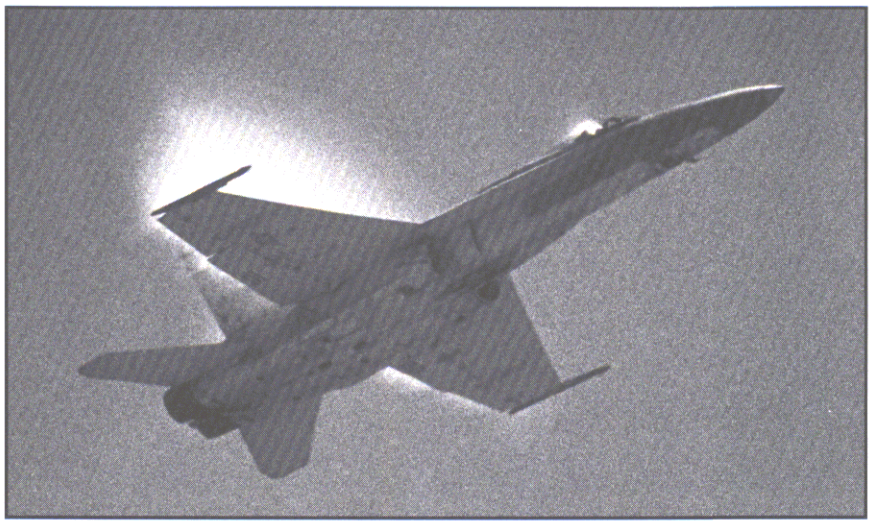

Supersonic flow on F/A-18 making high-speed pull-up. 4 • 62

vapor screen technique shown in figure 4.58. A camera mounted behind the model recorded the cross-flow image which shows the LEX vortices bursting upstream of the twin vertical tails.

The blue paint scheme of the Blue Angels (fig. 4.59) is very effective in showing the white condensed LEX and wing flows. At this maneuver condition, streamwise vorticity can be seen from the wing leading edges. The three photographs in figure 4.60 were taken of the same airplane while it was performing maneuvers and show some unusual wing condensation patterns. Condensation patterns above the wing and across the span appear similar to those discussed earlier in section 3.1. The condensed flow on the outer part of the right wing shows evidence of streamwise features.

The condensed pattern presented in figure 4.61 is for an F/A-18 at high subsonic speeds during a flyover at cruise lift. The flow condenses in two supersonic regions, a small one over the canopy and a large one above and below the wing. The two photographs in figure 4.62 are part of a sequence made during a pull-up maneuver, with figure 3.9 taken between these two.

4 • 10
F-104 Airplane

The F-104 Starfighter was one of the Century-Series Fighters designed and built originally by Lockheed to be a

Supersonic flow occurring over upper surface and wingtip vortices forming during high-speed pull-up of Japanese Air Force F-104. 4 • 63

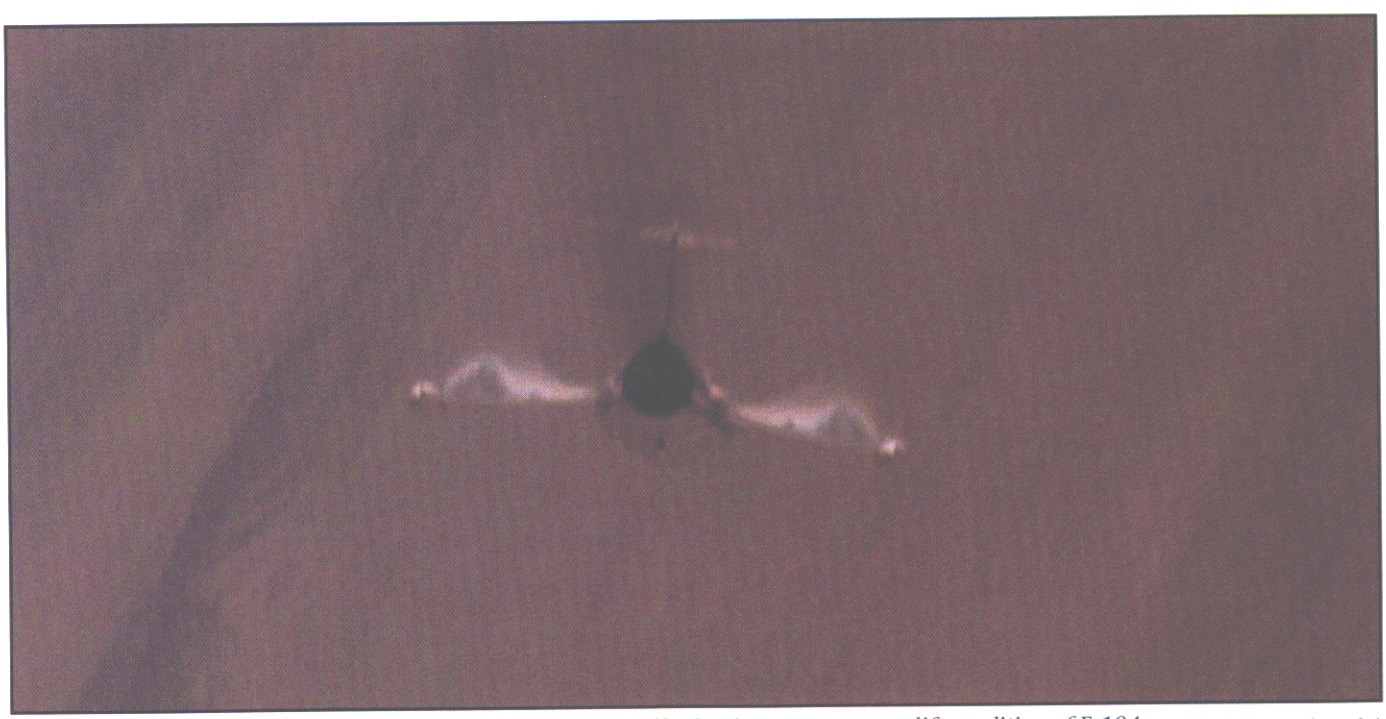

Gull-type condensation pattern occurring over upper surfaces of both wings at maneuver lift condition of F-104. 4 • 64

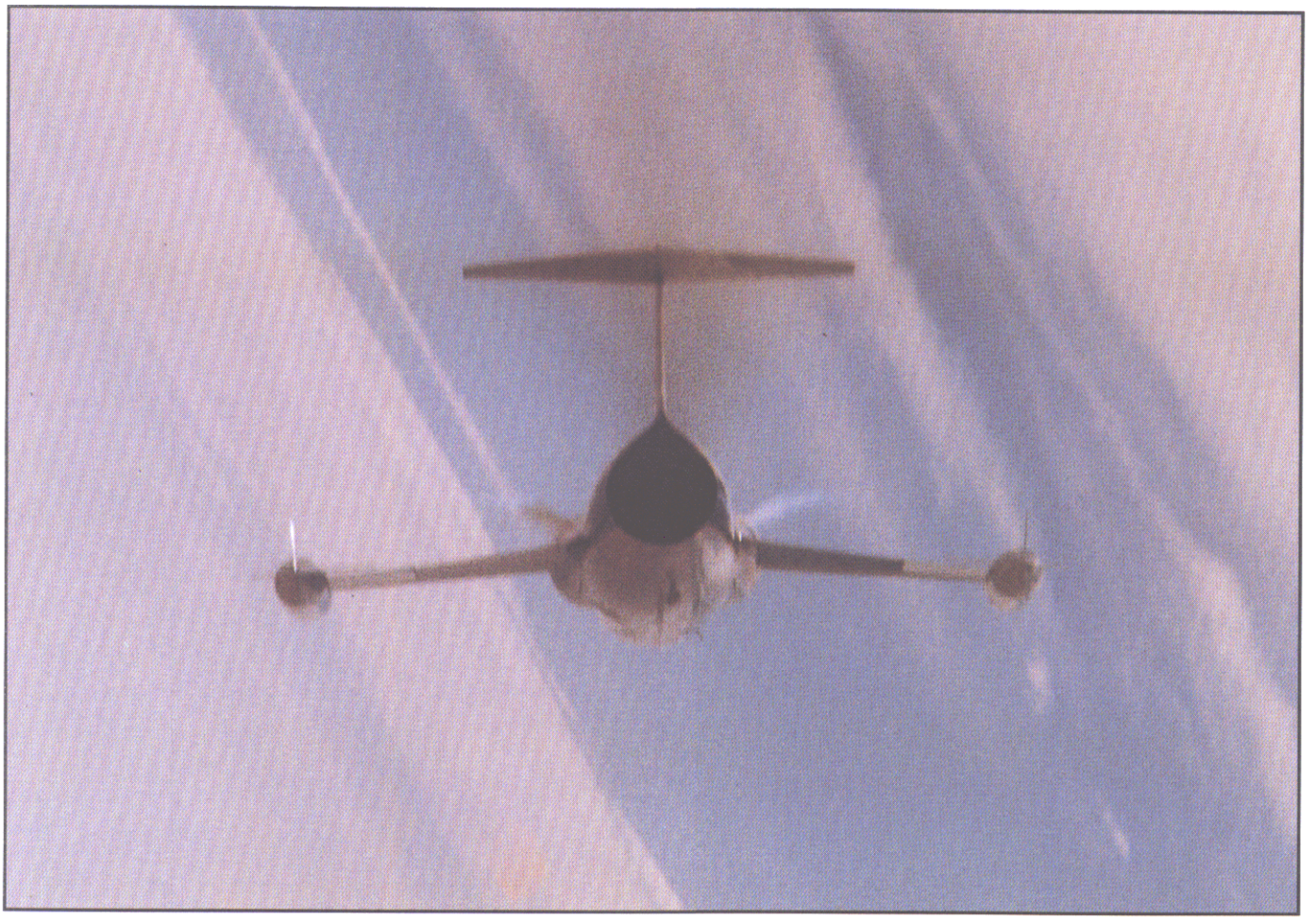

Condensed flow occurring near wing root and in tip vortices generated by horizontal tail of F-104. 4 • 65

supersonic fighter. The wings, which have a trapezoidal planform, are very thin with sharp leading edges to permit supersonic cruise at about a Mach number of 2.2. The T-tail was added to help avoid pitch-up. The F-104A was initially used as an interceptor by the USAF Air Defense. The F-104C was assigned to the USAF Tactical Air Command for fighter duty. A number of NATO countries and Japan produced follow-on models, especially the F-104G.

During a high-speed pull-up (fig. 4.63), the flow condenses as it expands to supersonic speeds over the upper surface of the wing, then evaporates as it goes through a shock wave at the rear of the pattern. Another expansion to a shock wave is suggested by the condensation seen around the fuselage aft of the engine inlet. Wingtip vortices are seen aft of the shock wave, where small vortex filaments are visible in the flow around the outer edge of the vortex core. The wingtip vortices form easily because the wing side edge is very thin and separates quickly with increased lift. They appear to form inboard of the wingtip; this may be because of the trapezoidal shape or long tip chord of the planform. During maneuvers, a gull-type condensation pattern occurs over the wings in figure 4.64. In figure 4.65, flow condenses near the wing root, and the horizontal tails form tip vortices while lifting to control the airplane pitching moments.

4 • 11

F/B-111 TACT/MAW Airplane

The F/B-111 was developed as a fighter-bomber airplane in the 1960's and used variable-swept wings to achieve good supersonic performance with the wings swept fully back and to obtain efficient subsonic cruise and good takeoff and landing characteristics with the wing at minimum sweep.

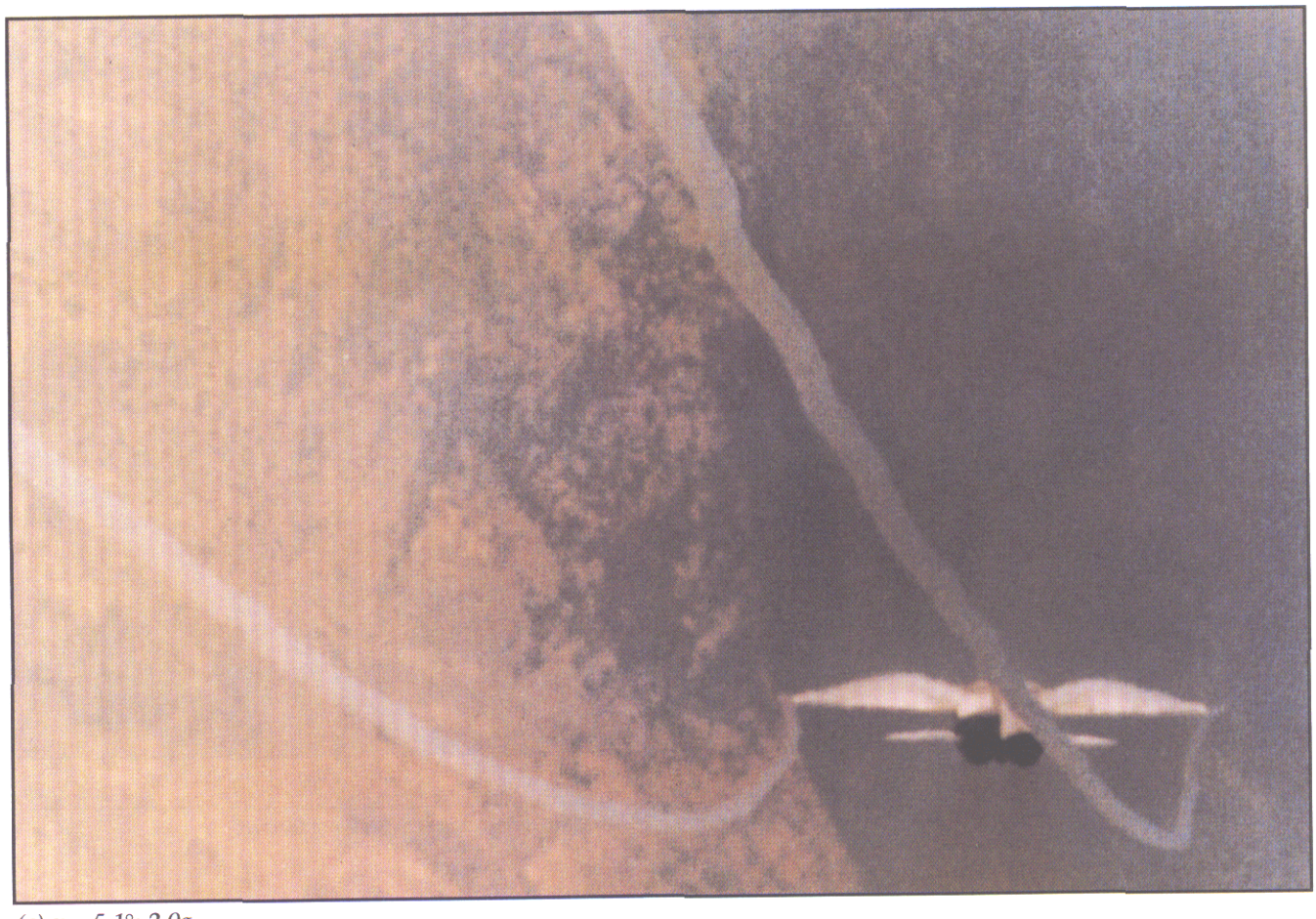

(a) α = 5.1°; 2.0g.

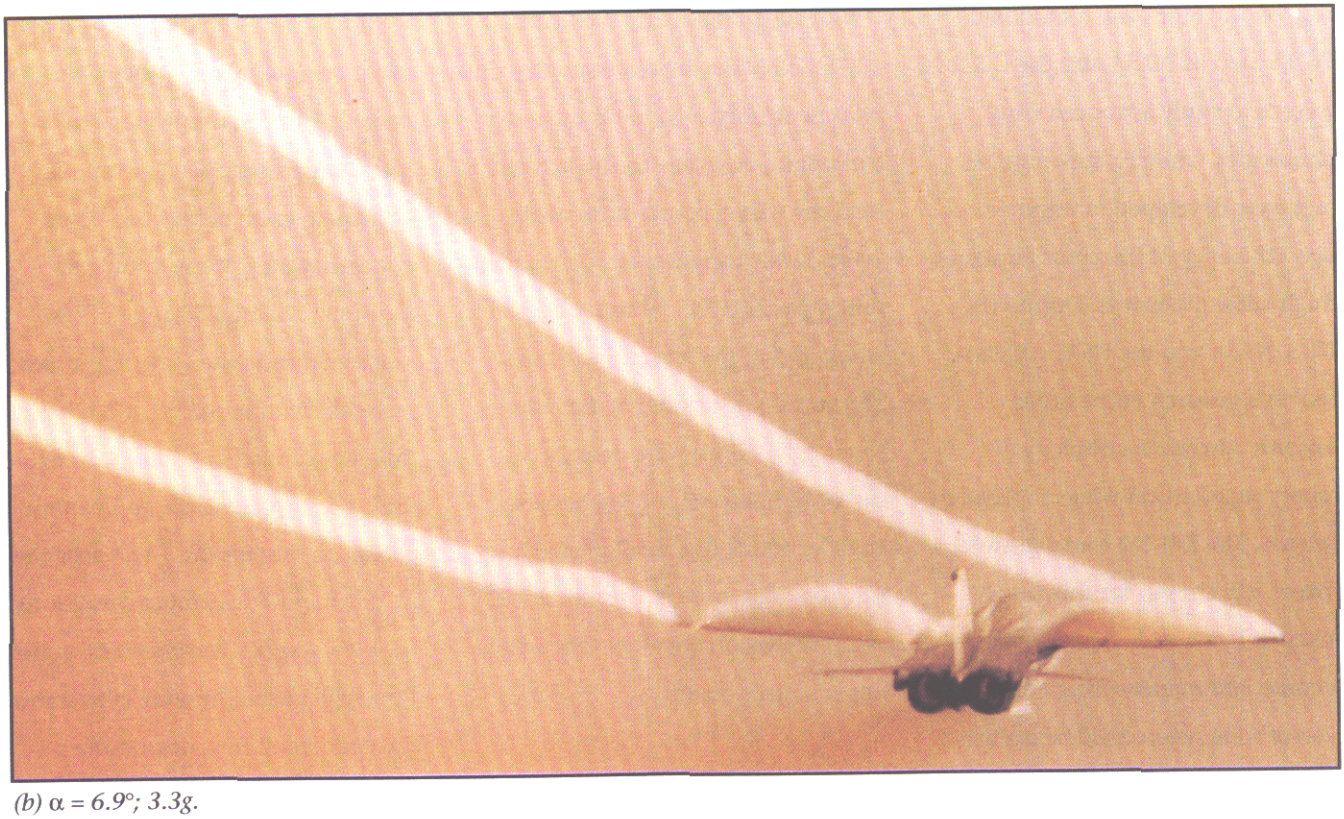

(b) α = 6.9°; 3.3g.

TACT airplane creating wing-body gull patterns and wingtip vortices during maneuver sequence with wing leading-edge sweep of 26° and Mach number of 0.82.

4 • 66

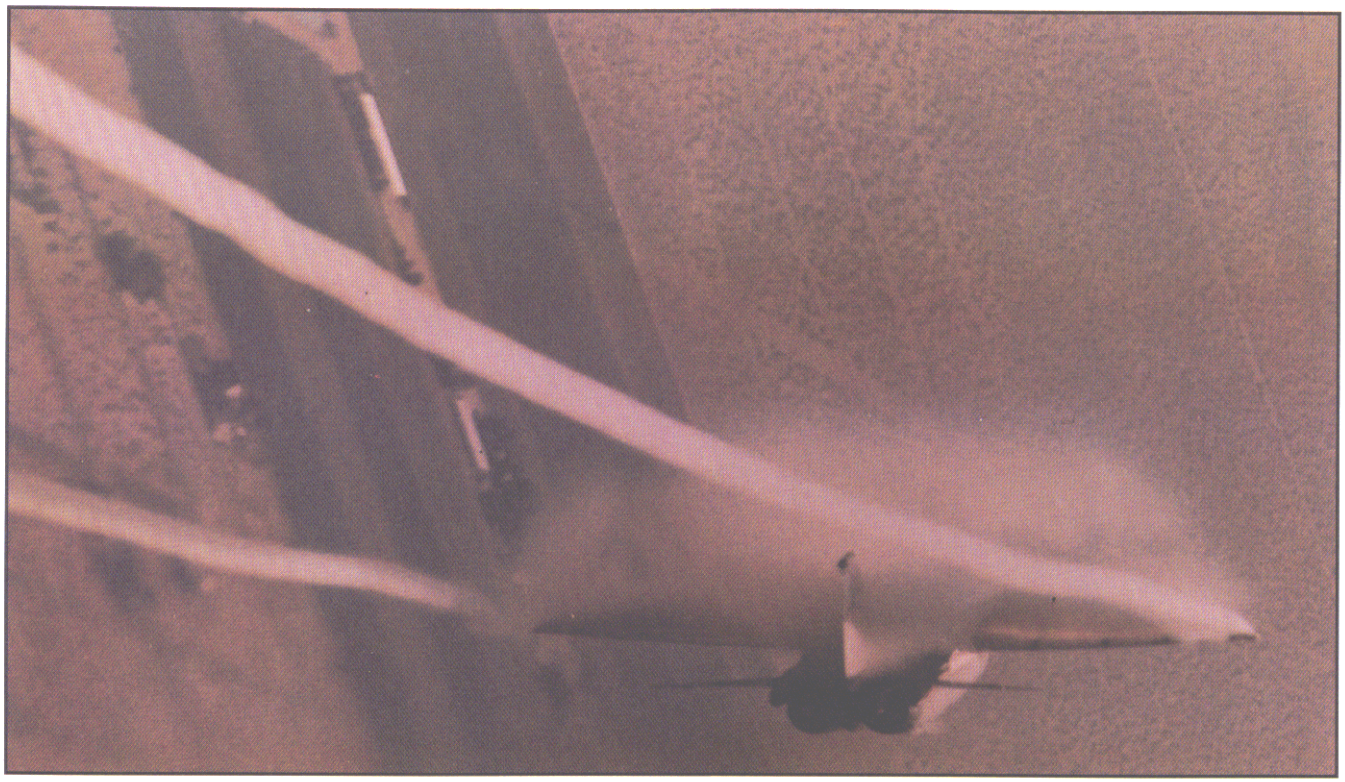

(c) α = 8.1°; 4.1g.

TACT airplane creating wing-body gull patterns and wingtip vortices during maneuver sequence with wing leading-edge sweep of 26° and Mach number of 0.82–concluded. 4 • 66

The airplane shown in the accompanying photographs was a modified F/B-111 used by NASA and the U.S. Air Force to study advanced wing technologies. Initially, supercritical wings were developed to improve the cruise efficiency of transport airplanes at high subsonic speeds. During the 1970's, NASA and the USAF collaborated on a research effort called Transonic Aircraft Technology (TACT) to apply supercritical wings to fighter airplanes. The F/B-111 variable-sweep airplane was chosen for this study because it had a wide flight envelope for cruise and maneuvering and the effects of wing sweep could be evaluated.

The condensation patterns in figure 4.66 were obtained during a research flight of the TACT airplane at NASA Dryden Flight Research Facility in 1979. To obtain the photographs, the pilot performed a wind-up turn to banking the airplane to the left and held the *g* level constant for about 10 sec at each angle of attack. Condensation patterns can be seen over the wings and in the wingtip vortices. The gull shape results for the 3.3*g* level (fig. 4.66(b)) were described earlier in figure 3.1. At the highest angle of attack (fig. 4.66(c)), the fuselage provides more of the airplane lift as condensation envelopes the whole upper surface region.

After the TACT program was completed, the USAF and NASA modified the airplane to evaluate the mission adaptive wing (MAW) concept. The leading-edge and trailing-edge regions of the wing distort to provide a variable-camber airfoil shape to increase transonic lift-drag ratio (*L/D*) at maneuver lift conditions. The condensation patterns shown in figures 4.67 and 4.68 were photographed during the same flight (last research flight of MAW) and have different camber conditions. In figure 4.67, the airplane has a gull pattern similar to that for the TACT airplane. At this flight and camber conditions ($\alpha = 9°$), a shock wave present in the flow field above the wing evaporates the condensed flow nearest the surface which enables the wing upper surface and trailing edge to be seen from this rear view. Condensation

Shock wave evaporating condensed flow at wing trailing edge during maneuver of Mission Adaptive Wing airplane. 4 • 67

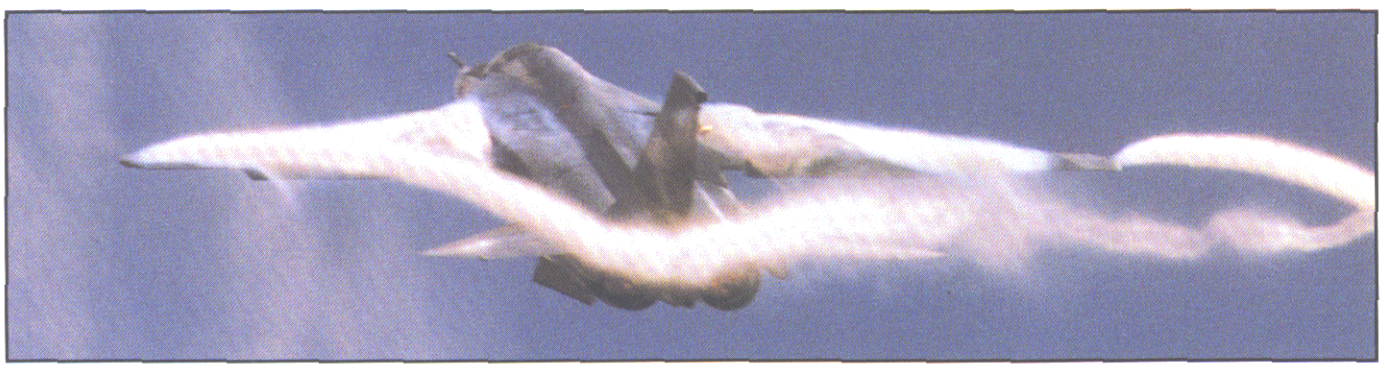

Small vortices occurring in glove and wingtip vortices with wing sweep of 26° and Mach number of approximately 0.7 during maneuver of Mission Adaptive Wing airplane. 4 • 68

occurs in the vicinity of the cores of the trailing vortices in figures 4.67 and 4.68, both of which show the appearance of circular patterns created by small vortices rotating around the outer edge of the cores. They can be seen better in the right wingtip vortex in figure 4.67 and in the left wingtip vortex in figure 4.68. These are the same flow features shown previously for the Jaguar (fig. 3.53). The gloves on this airplane are highly swept (70°) so that at some angle of attack, the flow separates at the leading edges to form vortices that pass over the wing. The condensation pattern in figure 4.68 obtained for $\alpha = 10°$ shows these glove vortices. Instability vortices in the glove vortex shear layer cause the circular patterns seen in their outer edges. The flow mechanism was discussed previously (figs. 3.24, 3.25, and 3.26) for the F-16 and F/A-18 airplanes.

4 • 12

Buccaneer Airplane

The Buccaneer was built in the 1950's by Hawker Siddeley Aviation, now a

Vortices from wingtips and wing-mounted vortex generators on Buccaneer during maneuvers.

British Aerospace company, as a transonic low-level strike airplane to operate from aircraft carriers. It has twin engines and an all-movable horizontal tail located at the top of the vertical tail, commonly called a T-tail. The wing has trailing-edge flaps, and the horizontal tail has trim tabs at its trailing edge. Upgrades in the propulsion and avionics systems have kept the airplane an active part of the British Royal Navy and Air Force. Figure 4.69 shows vortices developed by the wingtips and from vortex generators located along the wing upper surface near the leading edge. Recall that the vortices created by the generators are shown in a front view as figure 3.39.

4 • 13

Harrier Airplane

The Harrier is a multirole fighter which diverts all the engine airflow through movable nozzles to achieve vertical or short takeoffs and landings and to turn and decelerate rapidly. A number of versions were built by British Aerospace for the British Royal Navy and Air Force and the U.S. Marine Corps. The Harrier has the ability to takeoff and land without using conventional runways, which enables it to remain close to the ground troops it supports and to be used from aircraft carriers. It has reaction jets in the wingtips, nose, and tail to control the airplane during hovers and transition.

The wing has fences to control the airflow at two locations along the

Vortex generators provide flow control over upper surface of Harrier during rocket test firing.

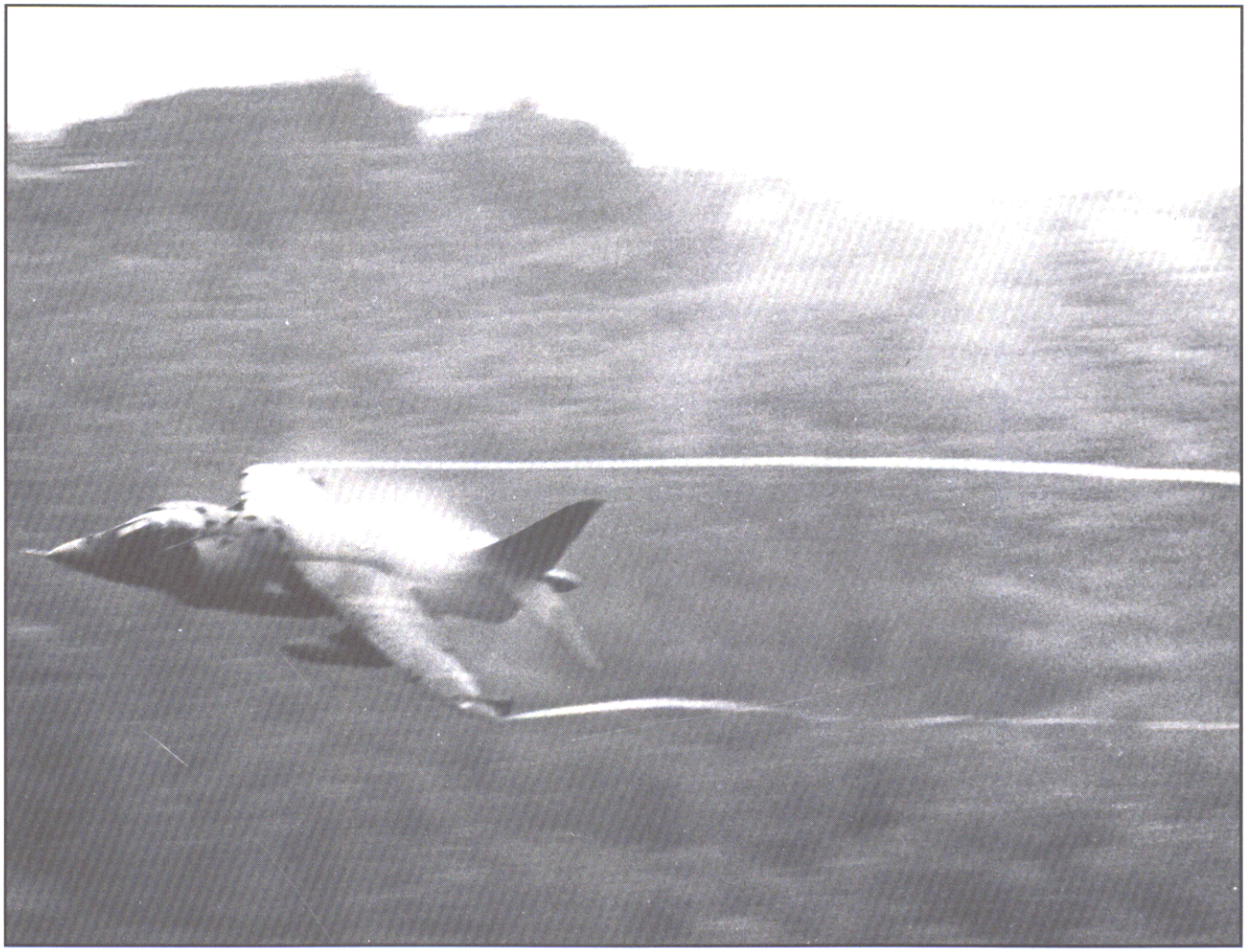

(a) During level flight.

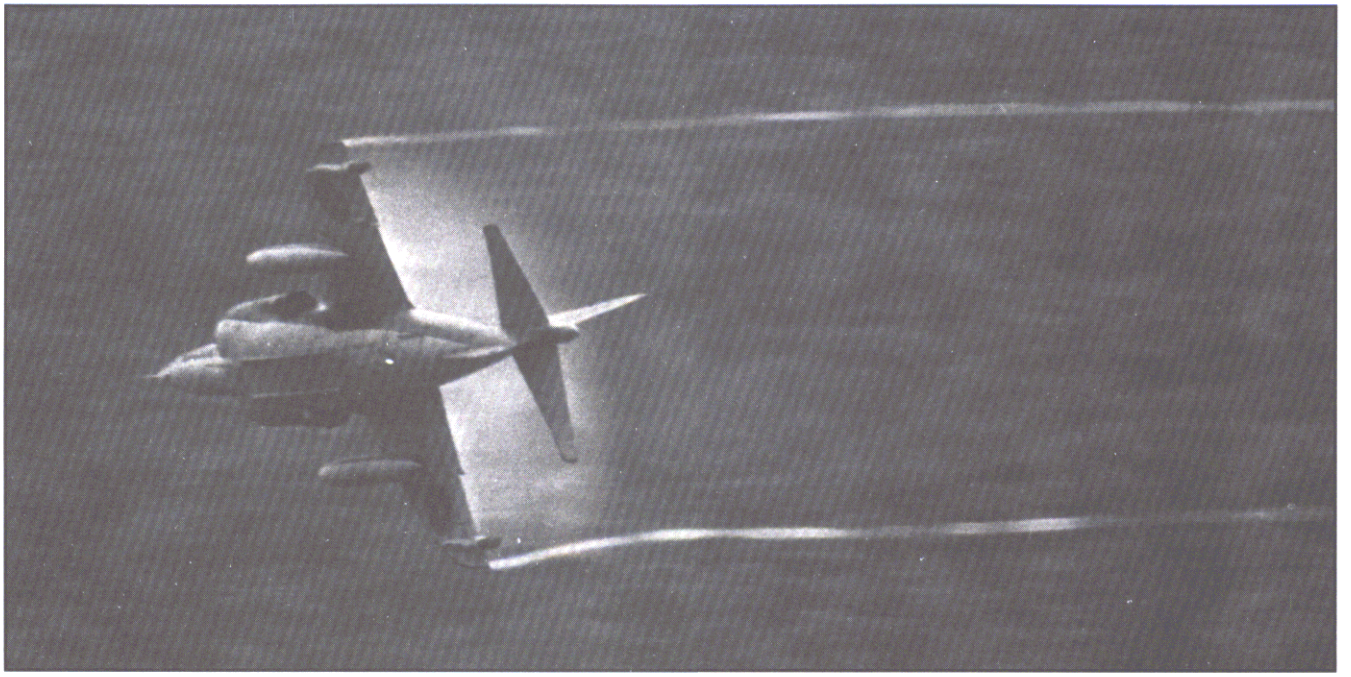

(b) During bank.

Condensation occurring over wing and in tip vortices during maneuver of Harrier. 4 • 71

Condensation patterns on AV-8B during high-speed turning pass to right. 4 • 72

leading edge. The dramatic photograph of a Harrier during a rocket firing test (figure 4.70) provides an excellent example of flow condensation caused by vortex generators located in a row along the forward portion of the upper surface of the wing. These vortices remain parallel to each other as they follow the wing contour back to the wing trailing edge. As described in section 3.3.6, these vortices help the wing boundary layer remain attached to a higher level of lift.

During maneuvers at low levels and high speeds (fig. 4.71), condensation occurs over the wing and in the wingtip vortices. In figure 4.71(a), streamwise vortices due to the vortex generators can be seen along the upper surface of the wing, and in figure 4.71(b), they are seen to go beyond the wing trailing edge. In figure 4.71(b), condensation occurs over the airplane from wingtip to wingtip. Similar condensation patterns are seen in figure 4.72 for an AV-8B, which is an advanced version of the Harrier developed by McDonnell Douglas and British Aerospace for use by the U.S. Marine Corps.

4 • 14

Lightning Airplane

The Lightning airplane, constructed by British Aerospace, was designed as an all-weather supersonic interceptor

Leading-edge vortices forming along inboard and outboard of wing during maneuvers of RAF Lightning F.6. 4 • 73

(a) At moderate lift.

(b) During landing.

(c) At higher lift.

Leading-edge vortices occurring at various lift conditions for RAF Lightning F.3. 4 • 74

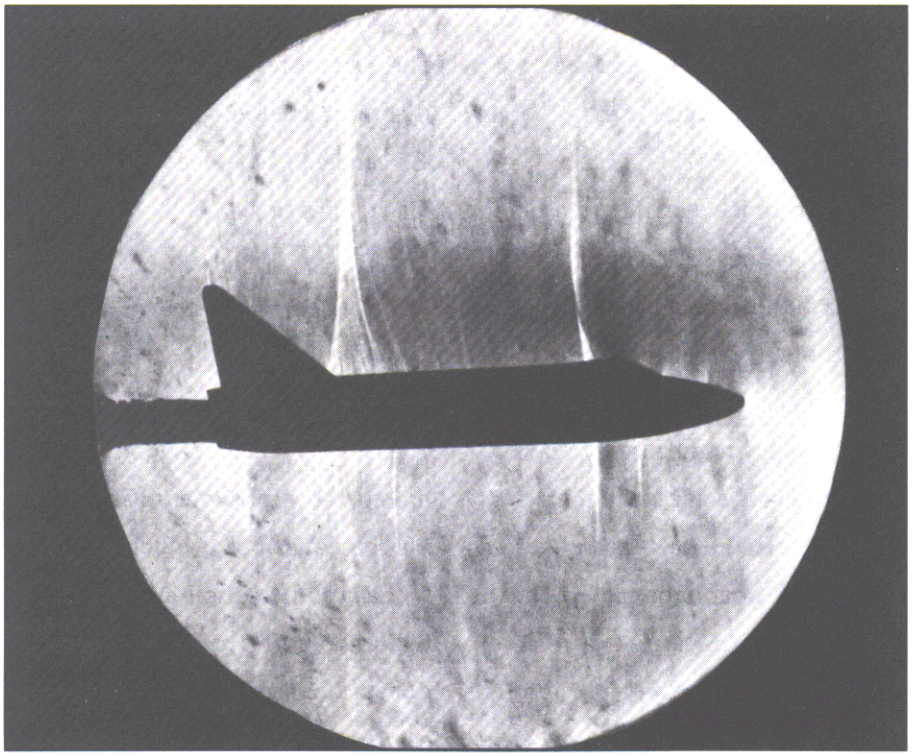

Schlieren showing shock-wave pattern produced by Lightning F.1 model in British high-speed wind tunnel and Mach number of 0.98. 4 • 75

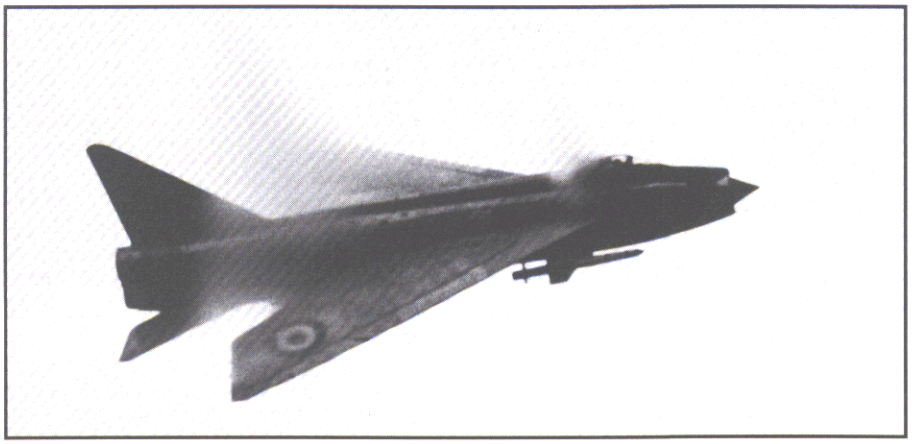

Condensation patterns of Lightning F.1 airplane at Mach number of 0.98 corresponding to wind tunnel results. 4 • 76

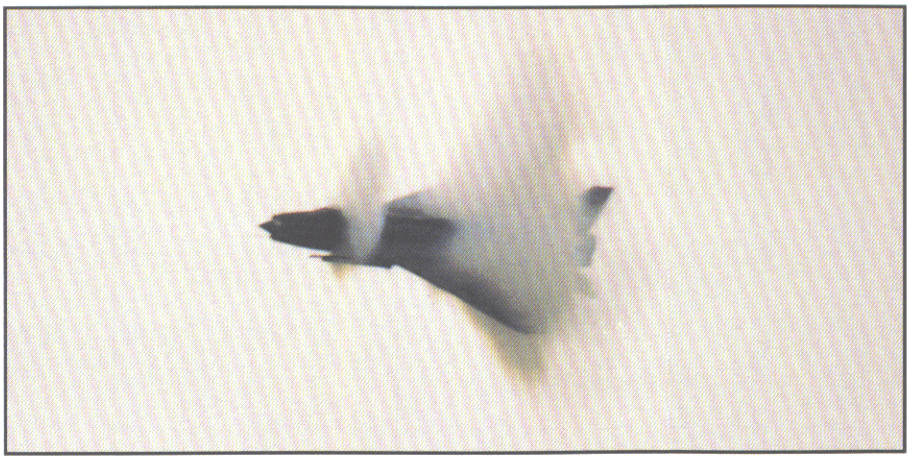

Condensation patterns at Mach number of about 0.98 for Lighning F.6 during heavy rain. 4 • 77

and entered service with the Royal Air Force in 1960. The wing is highly swept to achieve efficient supersonic cruise performance and has a cambered leading edge to reduce drag at subsonic speeds. The wing leading-edge sweep is 60° on the inboard portion and changes to about 53° at 66 percent along the edge, where a small notch is located. The high wing sweep angle results in leading-edge vortices as shown in figure 4.73. This photograph was presented earlier as figure 3.14 in section 3.3.1 as an example of leading-edge vortex flow. The vortex appears to start outboard of the wing-body juncture and grows in size until it becomes affected by the outer panel and the leading-edge notch. At maneuver conditions, the notch becomes a flow control device which forces a division between the low-energy inboard wing panel flow and a reenergized outboard flow. The notch creates a small streamwise vortex near the wing upper surface, although the notch flow is not condensed in the picture. The notch works in conjunction with the change in the outer-panel sweep to cause the inboard-panel vortex to separate from the leading edge and proceed over the wing, where it evaporates. Then, a new leading-edge vortex begins on the outer panel. The inboard-panel vortex on the left side appears to have a puffiness in the outer edge of the condensed pattern, which is probably caused by the instability vortices in the vortex shear layer.

Figure 4.74 shows additional examples of the inboard and outboard leading-edge vortex flows at different lift conditions. In the rear view of figure 4.74(a), the vortices are more apparent on the left side of the airplane. Similar to figure 4.73, both inboard and outboard leading-edge vortex flows form and then evaporate over the wing. During landing (fig. 4.74(b)), the outer-panel vortex on the left side of the airplane is more condensed than the inboard vortex. In figure 4.74(c), the Lightning appears to be at a higher lift condition where the outer-panel leading-edge vortex is evident on the right side of the airplane and the condensed halo occurs over the wings.

When the airplane reaches transonic speeds, it creates supercritical flows similar to those described in section 3.2. In high-speed wind tunnels, schlierens are used to visualize shock waves, as shown in figure 4.75 by a Lightning model at a Mach number of 0.98. It shows the flow expansion to a shock wave around the canopy and then a second and larger expansion region over the wing and fuselage to a shock near the wing trailing edge. These compare qualitatively to the flight condensation patterns in figures 4.76 and 4.77 obtained at comparable Mach numbers.

4 • 15

Tornado Airplanes

The Panavia Tornado is jointly produced by British Aerospace, Messerschmitt-Bolkow-Blöhm, and Aeritalia as a multirole all-weather fighter/bomber. The airplane was designed to perform close air support,

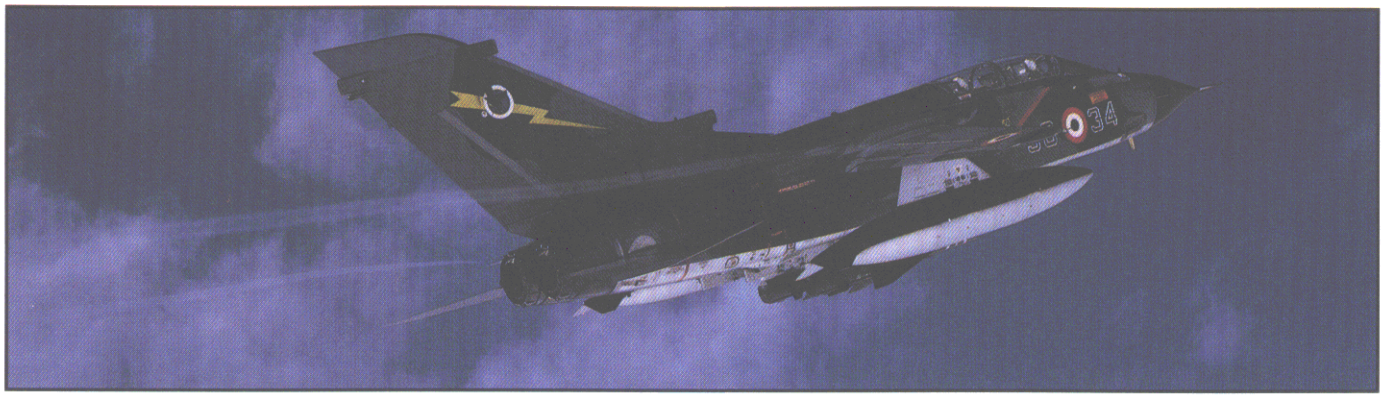

Wingtip vortices created during pull-up of Italian Air Force Tornado IDS with long range fuel tanks on underwing pylons. 4 • 78

Gull pattern occurring over wing during maneuver of RAF Tornado ADV. 4 • 79

interdiction and air strike, air superiority, interceptor, naval strike, and reconnaissance. The airplane has twin engines, two seats, and uses variable swept wings to achieve operational flexibility. At low sweep, the wings have higher span, which provides higher lift for takeoffs and landings and for efficient cruise for long distances. Highly swept wings provide the best gust response when flying close to the ground at high subsonic speeds and allow supersonic cruise at higher altitudes. The lowest sweep is 25° and the highest 68°. The fixed inboard glove is swept 60°. The Tornado IDS (interdictor/strike) is in service with the British, West German, Italian, and Saudi Air Forces and the German Navy. The Tornado ADV is the Air Defense Variant developed by the British and is in service with the British and Saudi Air Forces.

The Tornado is shown in figures 4.78 to 4.81 making a variety of maneuvers

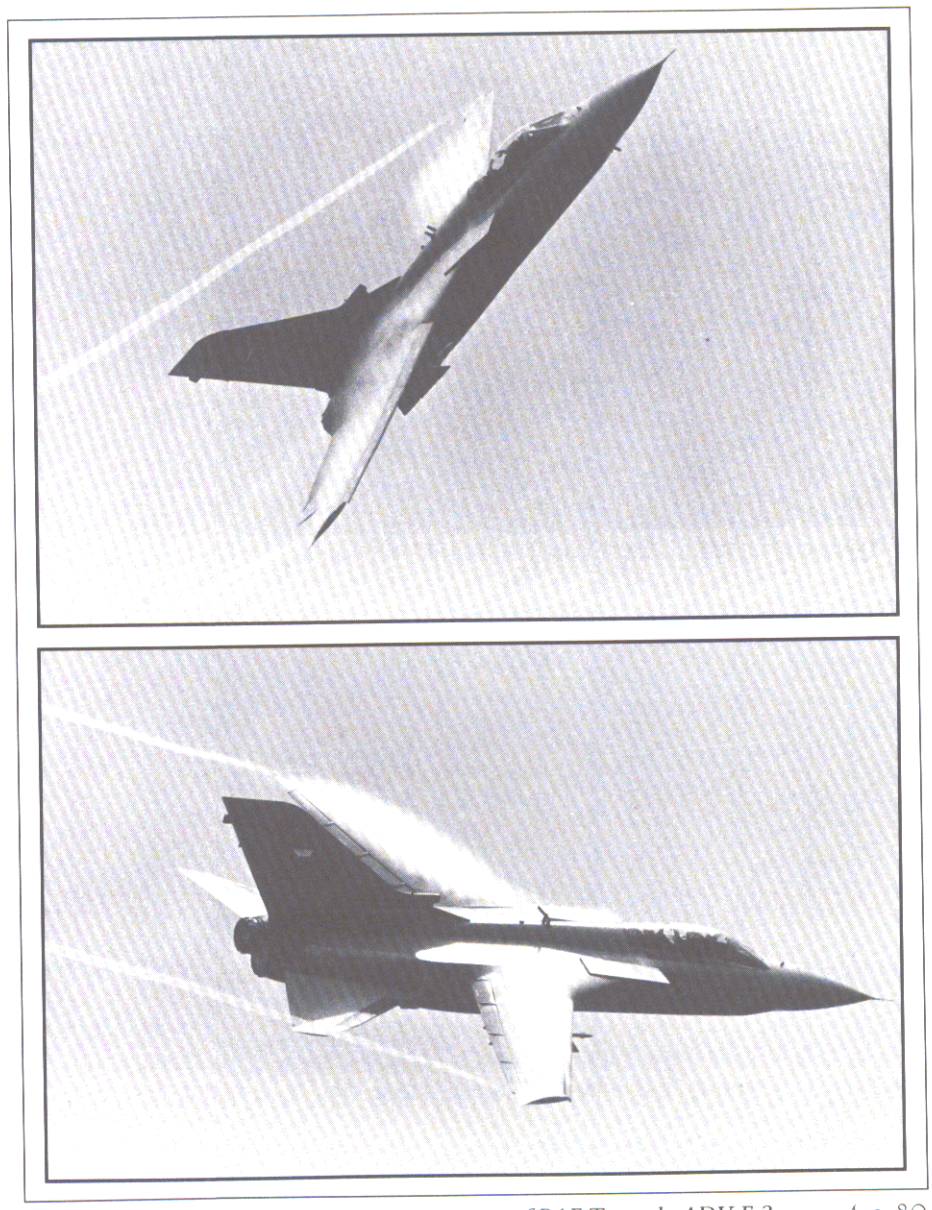

Wing condensation occurring during maneuver of RAF Tornado ADV F.3. 4 • 80

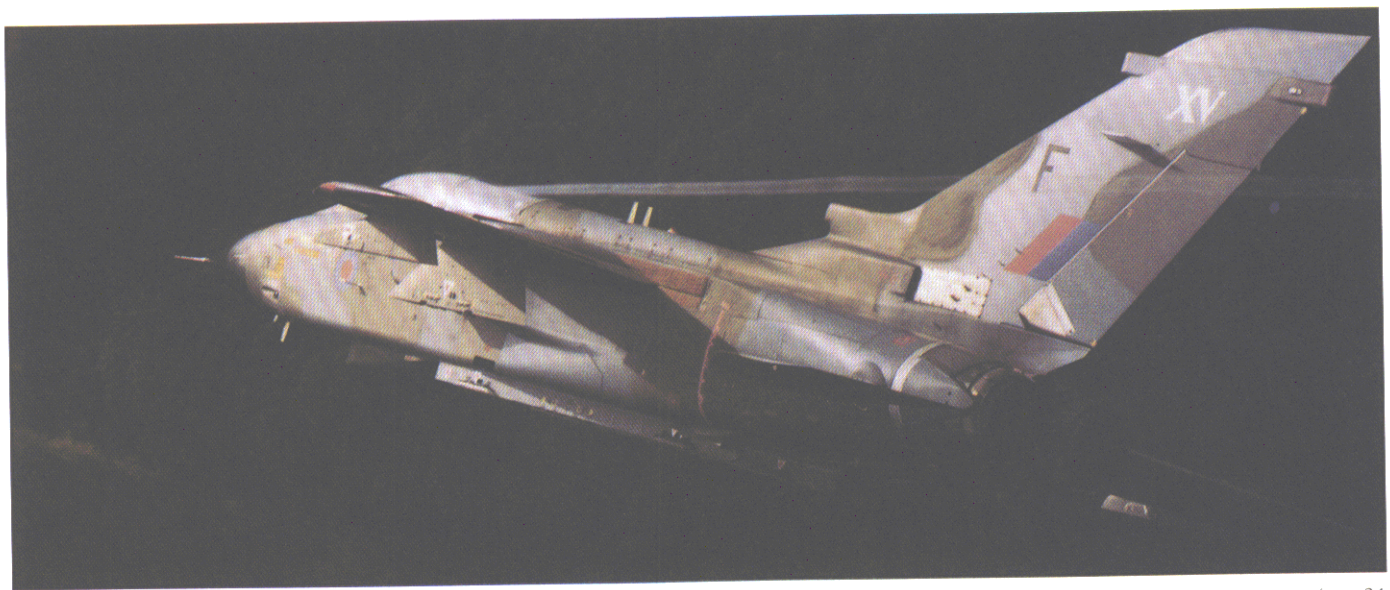

Wingtip vortices created during hard turn at low altitudes of RAF Tornado IDS. 4 • 81

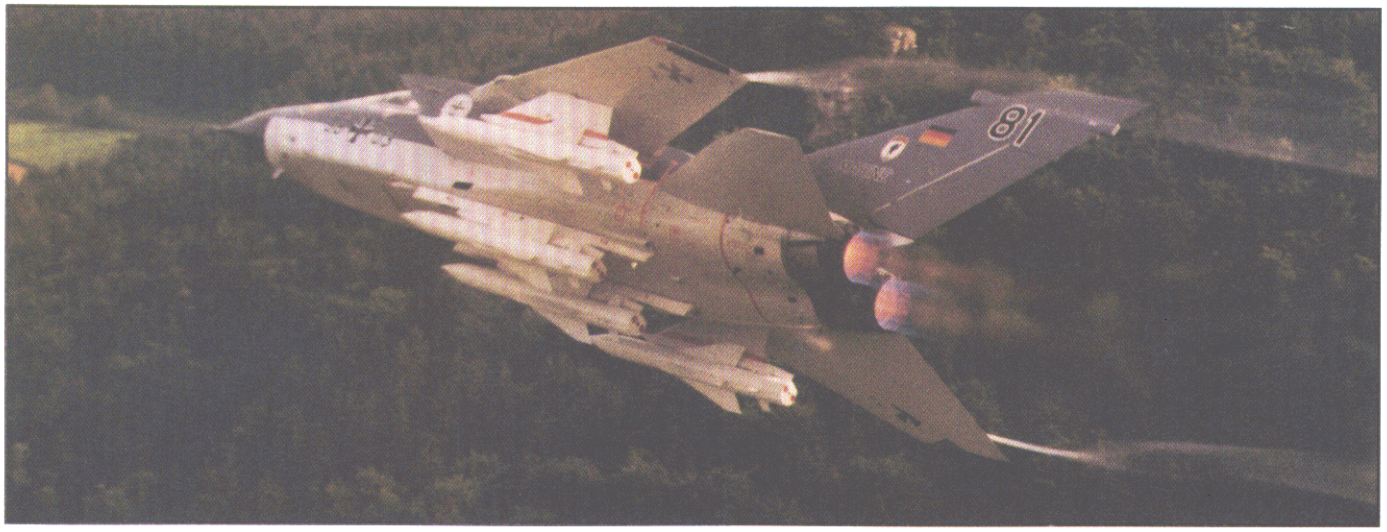

Wingtip vortices created during hard turn at low levels of German Navy Tornado IDS carrying four Kormoran missiles. 4 • 82

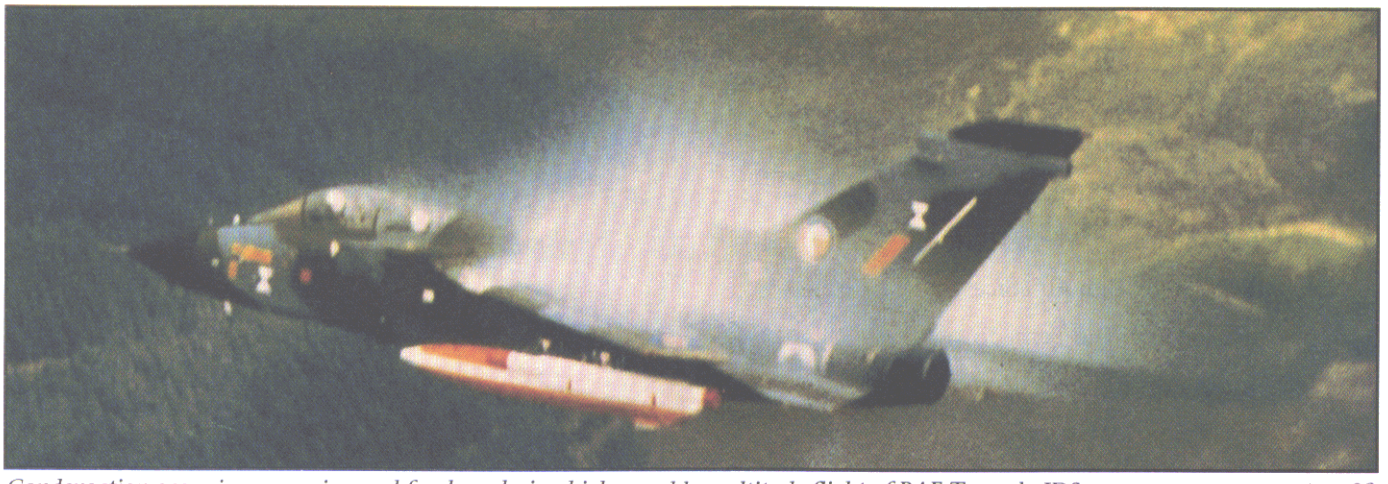

Condensation occurring over wing and fuselage during high-speed low-altitude flight of RAF Tornado IDS. 4 • 83

Wings at high sweep creating leading-edge vortices on Italian Air Force Tornado IDS during low-level maneuvers. 4 • 84

with the wings at a low sweep position, which usually generates wingtip vortices. In figure 4.79, lightly condensed gull patterns occur over the wing. For this air defense version, the airplane carries four Sky Flash medium-range air-to-air missiles mounted on the underfuselage and two Sidewinder short-range air-to-air missiles on the inside of the wing pylons. Condensation results over the wing upper surfaces (fig. 4.80) with the leading-edge slats deflected. A variety of flow patterns is obtained with the wings at a high sweep position as shown in the remaining

photographs. Wingtip vortices become visible during a hard turn (fig. 4.82), whereas condensation occurs over the wing and fuselage during a high-speed low-altitude flight (fig. 4.83). Wing leading-edge vortices form during pitch-up maneuvers (fig. 4.84).

4 • 16

French Airplanes

The Rafale demonstrator airplane had its initial flight in 1986 and is built by Avions Marcel Dassault-Breguet Aviation. It features a close-coupled wing-canard arrangement, as shown in figure 4.85, and was designed as a multirole fighter for the French Air Force and Navy. During the maneuver condition in figure 4.85(a), leading-edge vortices form along the higher swept inboard portion of the wings. The outer wing panel is at lower sweep than the inboard portion, which is separated by a notch in the leading edge. The notch, which is seen in figure 4.85(b), and change in the leading-edge sweep stop the leading-edge vortex from continuing spanwise, and it begins to pass over the wing. In figure 4.85(a), the vortex may be bursting over the wing, which causes the flow to evaporate. New leading-edge vortices appear to have started on the wing outer panels. The flow field from the close-coupled canards helps stabilize the wing leading-edge vortices at maneuver conditions; this improves the lift and drag characteristics of the airplane.

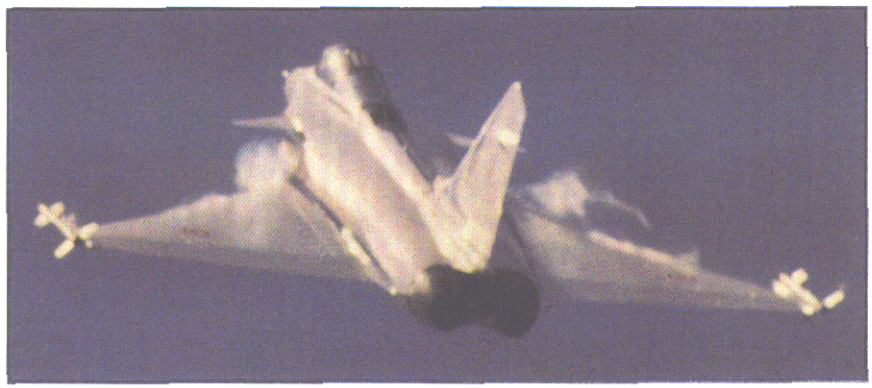

(a) View from rear and above.

(b) View from below.

Wing leading-edge vortices created during maneuvering flight of Rafale airplane. 4 • 85

The Mirage F1 was designed by Avions Marcel Dassault-Breguet Aviation to perform a number of missions, including all-weather interceptor and ground attack fighter. A large number were built for the French Air Force and for export to many countries. During a pull-up in figure 4.86, condensation occurs over the wing with moderate sweep and in the wingtip vortices. The Mirage 2000, shown in figure 4.87, was also built by Dassault-Breguet as an interceptor and air-superiority fighter with a secondary ground attack capability. It first flew in 1978 and has a delta wing planform with a leading-edge sweep of 58°. It has full-span leading-edge flaps which operate with the elevons at the wing trailing edge during takeoff, landing, and maneuvering. For the interceptor duties, it carries air-to-air missiles which include

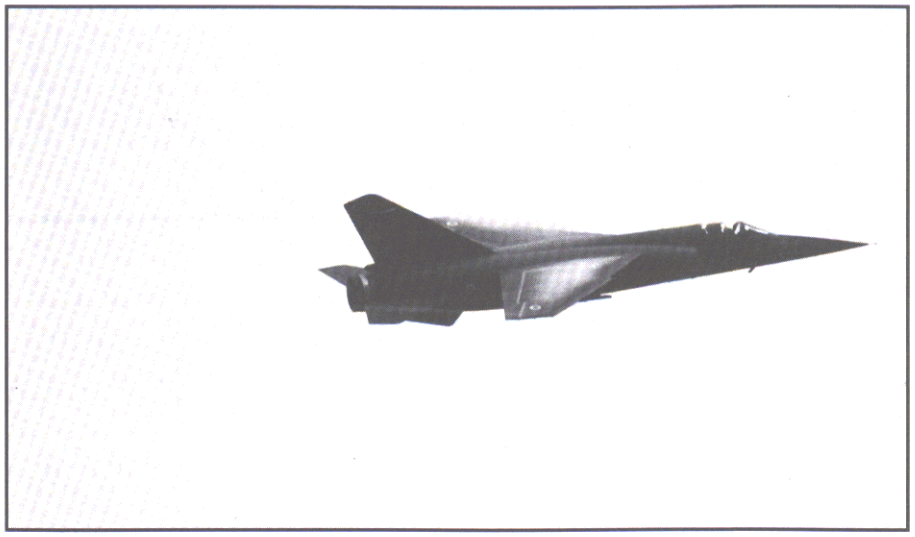

Wing condensation pattern and tip vortices resulting during pull-up of Mirage F1. 4 • 86

Fuselage-strake vortex on Mirage 2000 during maneuvers. 4 • 87

two Matra Super 530F missiles inboard and two Matra Magic missiles outboard. Small fixed strakes are located on the sides of the engine inlets to improve the directional stability of the airplane and cause the strake vortex that streams aft at this maneuver condition.

The Super Etendard is a naval strike fighter introduced in 1978 by Avions Marcel Dassault-Breguet Aviation as an updated version of the Etendard. The wings have a sweep of about 45° and a leading-edge extension or snag. In figure 4.88, the carrier-based airplane has air-to-air Matra Magic missiles mounted on underwing attachments which create wingtip vortices during takeoff.

4 • 17

Soviet Airplanes

The airplanes for which photographs were received were all constructed by the Mikoyan-Gurevich design bureau, the MiG-21, MiG-23, and MiG-29.

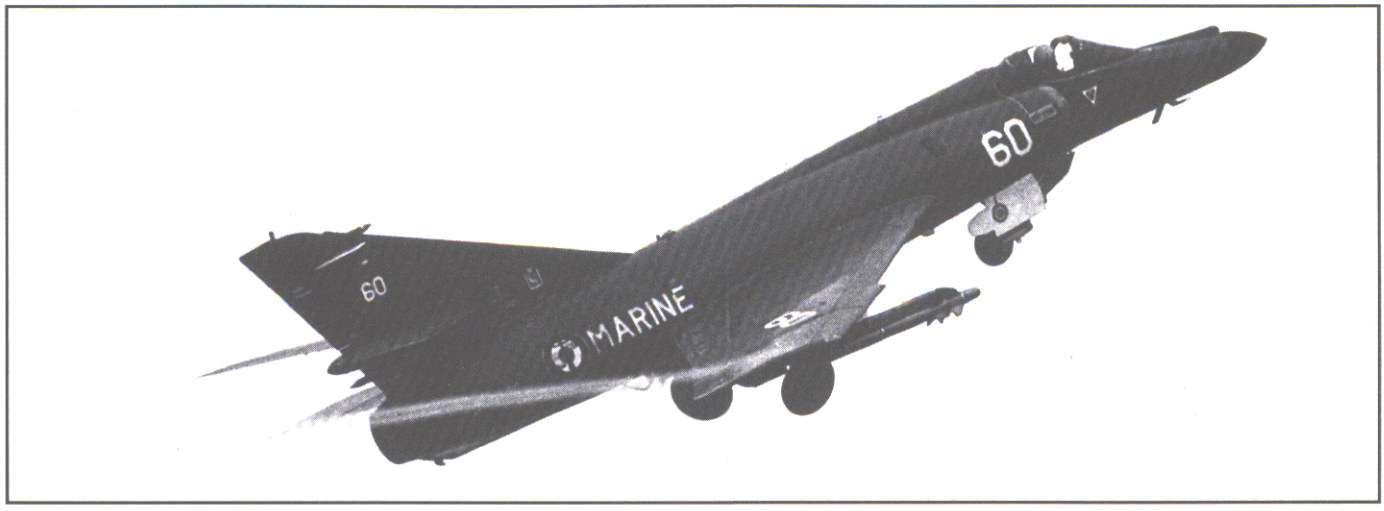

Wingtip vortices on Super Etendard with wheels retracting after carrier takeoff. 4 • 88

(a) View from above.

(b) View from below.

Leading-edge vortices forming from glove and highly swept wing during high-lift maneuvers of Hungarian Air Force MiG-23MF.

Condensed flow over MiG-21 wings probably caused by leading-edge vortices. 4 • 90

The MiG-23 entered service in the 1960's as a fighter airplane that utilized variable wing sweep. The arrangement was similar to other variable-sweep airplanes like the F/B-111, with a highly swept glove inboard, and a variable-sweep wing panel that sweeps from 16° to 72°. A large number have been produced, including a number of modifications, as well as the MiG-27 derivative. The wing has leading-edge flaps as well as a wing chord extension at the wing-glove juncture that creates a notch that changes size with wing sweep. At low sweep, the notch is closed and as the sweep increases, the notch gets progressively larger. The horizontal tail is all movable and the vertical tail has a large dorsal fin.

The condensation patterns in figure 4.89 were taken during the same flight of the MiG-23MF during maneuvers at an air show. The wing sweep is at the full-aft position, 72°. A vortex formed from the glove leading edge is interrupted by the notch, then passes rearward over the wing. Just outboard of the notch, an additional vortex begins at the wing leading edge and is observed in both views, figure 4.89(a) from above and figure 4.89(b) from below. The notch is designed to split the vortices from inboard to outboard. Both these vortices are visible over the wing and evaporate as they approach the wing trailing edge. In figure 4.89(a), a condensation pattern is apparent just downstream of the wing trailing edge on the right side of the airplane that appears to be a different vortex flow from the glove and wing. As noticed previously for leading-edge vortex examples, wing leading-edge vortices usually do not remain condensed beyond the trailing edge, and once they evaporate there is no mechanism to cause them to recondense. It is possible that a vortex is generated from the underside of the wing, maybe the missile rack, and that the airplane has some sideslip angle. A curved pattern of condensation is seen above and behind the inlet on the right side (fig. 4.89(a)). This is a separation-induced vortex originating at the boundary-layer splitter plate and is similar to that discussed in section 3.3.8 for an F-4.

The MiG-21 is an air-superiority fighter which initially entered the service in 1959. The basic design features a clipped delta wing with a wing sweep of 57°. Missile launch pylons are seen on the underside as seen in figure 4.90. The condensation pattern over the wings may be due to wing leading-edge vortices, although the flight condition is not known. On both right and left sides, the condensation begins inboard and diminishes before it reaches the wingtips. The sudden drop in condensation at that location may be caused by a large streamwise fence located on the upper surface at about 90 percent of the semispan, although the fence cannot be seen from this perspective. Fences are intended to stop the flow from the inboard part of the wing from getting farther outboard, then begin a new flow on the outboard side, which disrupts the condensation pattern and causes the small condensed patterns over the outer wingtip.

(a) Strake vortex burst.

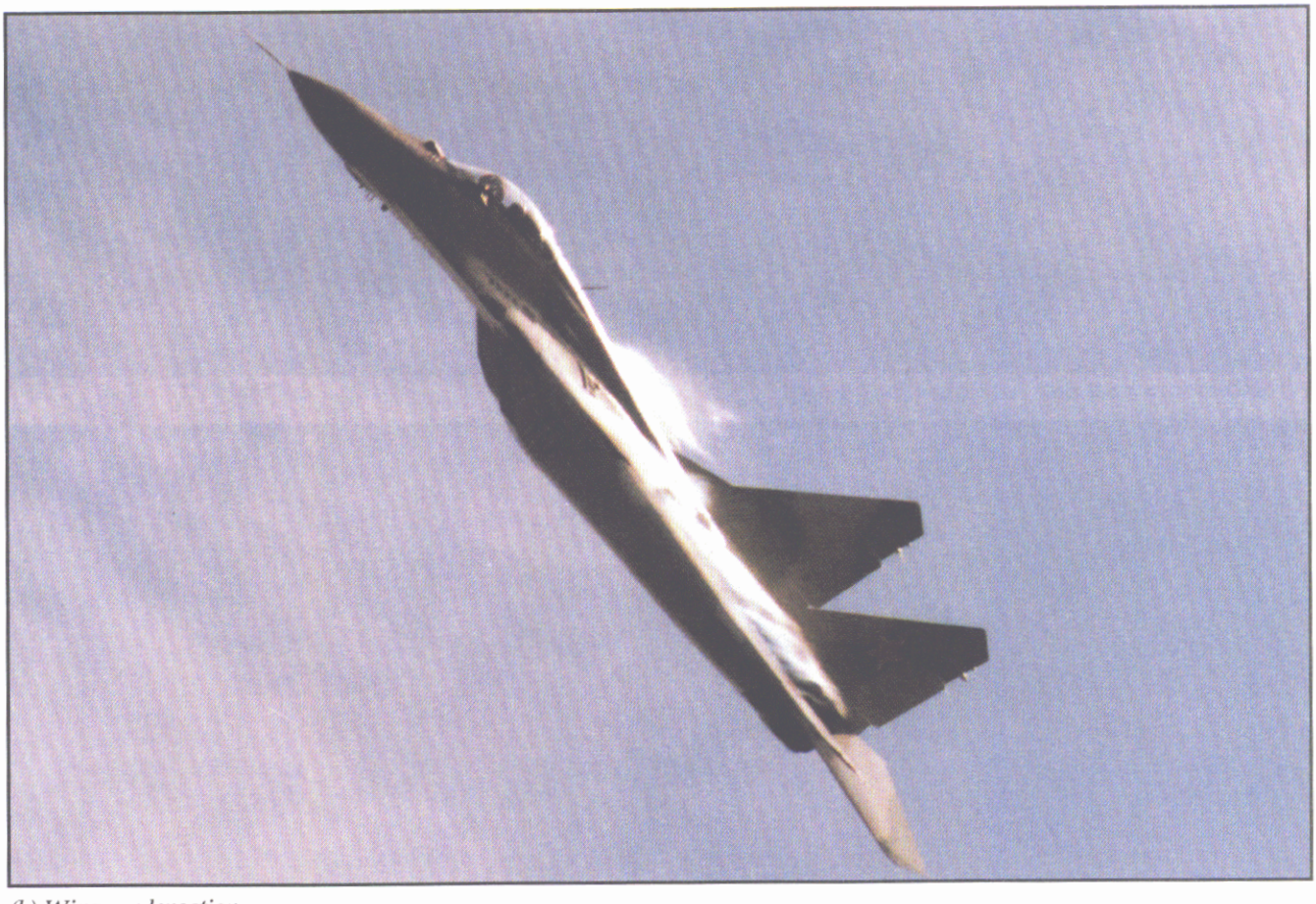

(b) Wing condensation.

Condensation patterns occurring for Soviet MiG-29 during maneuvers.

(c) Vortex from underwing.

(d) Strake vortex burst near vertical tail leading edge.

(e) Strake vortex burst.

Condensation patterns occurring for Soviet MiG-29 during maneuvers–concluded.

The MiG-29, one of the newer Soviet fighter airplanes, became operational in 1984. It has a number of similarities with the F/A-18, such as size and weight and it also features wing-body strakes and twin vertical tails. The performance of the MiG-29 is comparable to the F-16A. The wing has a sweep of about 40° and leading-edge and trailing-edge flaps that deflect to optimize maneuver performance. As can be seen in figure 4.91(a), the vertical tails have dorsal fins, which are the highly swept surfaces added in front of tail surfaces in a fashion similar to strakes or chines added in front of wings. Fences extend forward of the intersection of the dorsal fins with the wing upper surface. The photographs were taken during maneuvers at an air show. Figure 4.91(a)shows the condensed strake vortices evaporating due to vortex burst. In figure 4.91(b), a strake vortex flow evaporates, perhaps because of vortex burst, and condensed flow occurs on the wing panel. Figure 4.19(c) has strake vortex flow and what appears to be a vortex from under the wing which turns toward the red star on the vertical tail. If the airplane is at a sideslip angle, the missile pylons underneath the wing could generate a vortex. Figures 4.91(d) and 4.91(e) show strake vortices; vortex burst occurs far forward over the wing in figure 4.91(e).

4 • 18

XB-70 Airplane

The XB-70 Valkyrie was designed by North American (Rockwell) to be a supersonic bomber for the U.S. Air Force. Although the program was canceled after two prototypes were constructed, the preliminary flight tests provided some insight into the airplane design logic. The airplane had a slender shape to minimize supersonic wave drag which permitted the bomber to cruise at a supersonic Mach number of 2.5. A highly swept delta wing was used along with canards on the forward fuselage and twin vertical tails at the rear. One of the unique aerodynamic features is the variable outer wing panel, which is undeflected at subsonic speeds to take advantage of the full wingspan and wing area to increase subsonic cruise *L/D* and improve takeoff and landing performance. At supersonic speeds, adequate cruise *L/D* can be developed with less wingspan so that the outer portion of the wing deflects down to (1) interact with the inlet shock wave in the lower surface flow field to reduce drag, (2) reduce area aft of the airplane center of gravity as the

Condensation appearing in vortex flows generated by canard tips, from folding wingtips, and in expansion over the down deflected elevons for XB-70 during cruise at supersonic speeds. 4 • 92

center of pressure moves rearward with increasing Mach number to reduce trim drag, and (3) provide more vertical surface to improve directional stability.

The condensed flow patterns shown in figure 4.92 occurred during the same supersonic flight presented previously in figure 3.10. As before, the airplane is at cruise with the outer wing panel deflected down about 25°. The reader is referred to section 3.2 for a description of this photograph. Condensation occurs in the canard tip vortices during subsonic cruise flight,

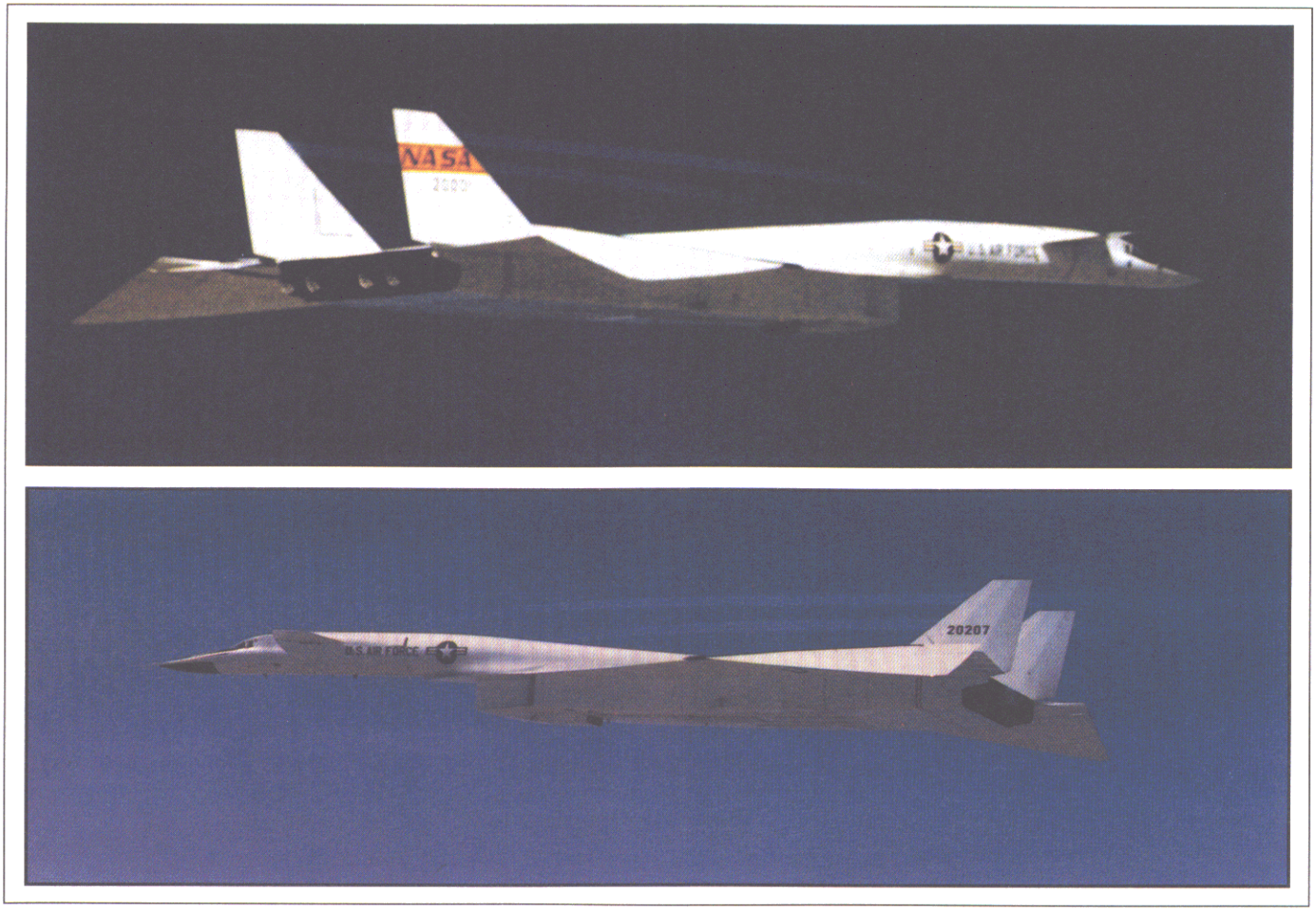

Canard tip vortices streaming aft past twin vertical tails during subsonic flight of XB-70 with wingtips deflected down. 4 • 93

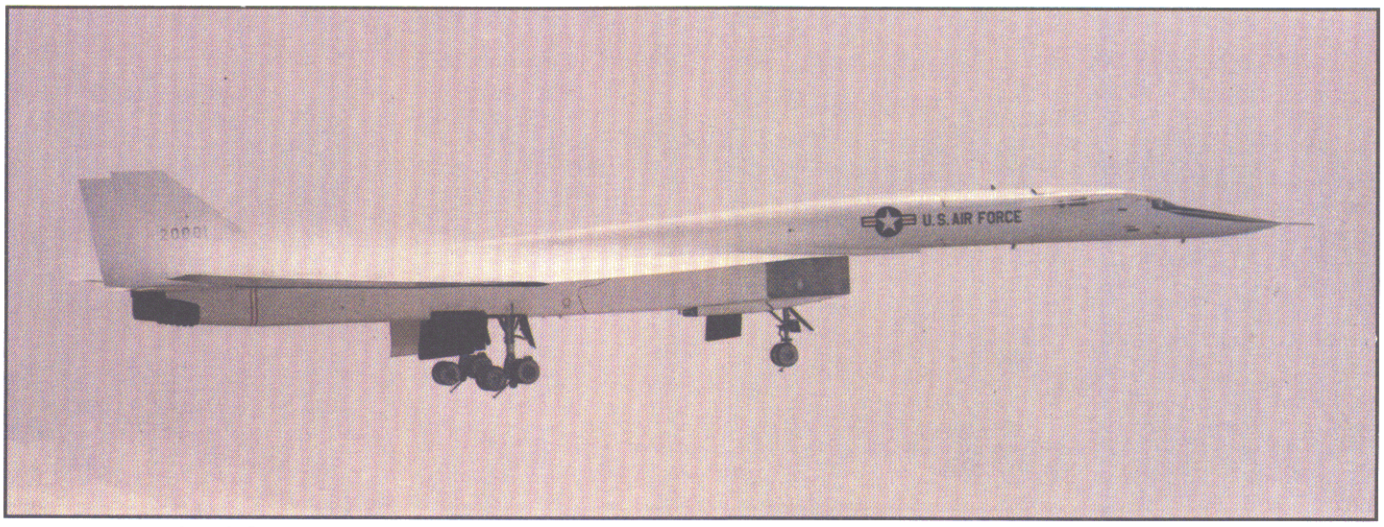

Wing outer panel undeflected on XB-70 for takeoff and landing to provide maximum lifting effects of leading-edge vortex. 4 • 94

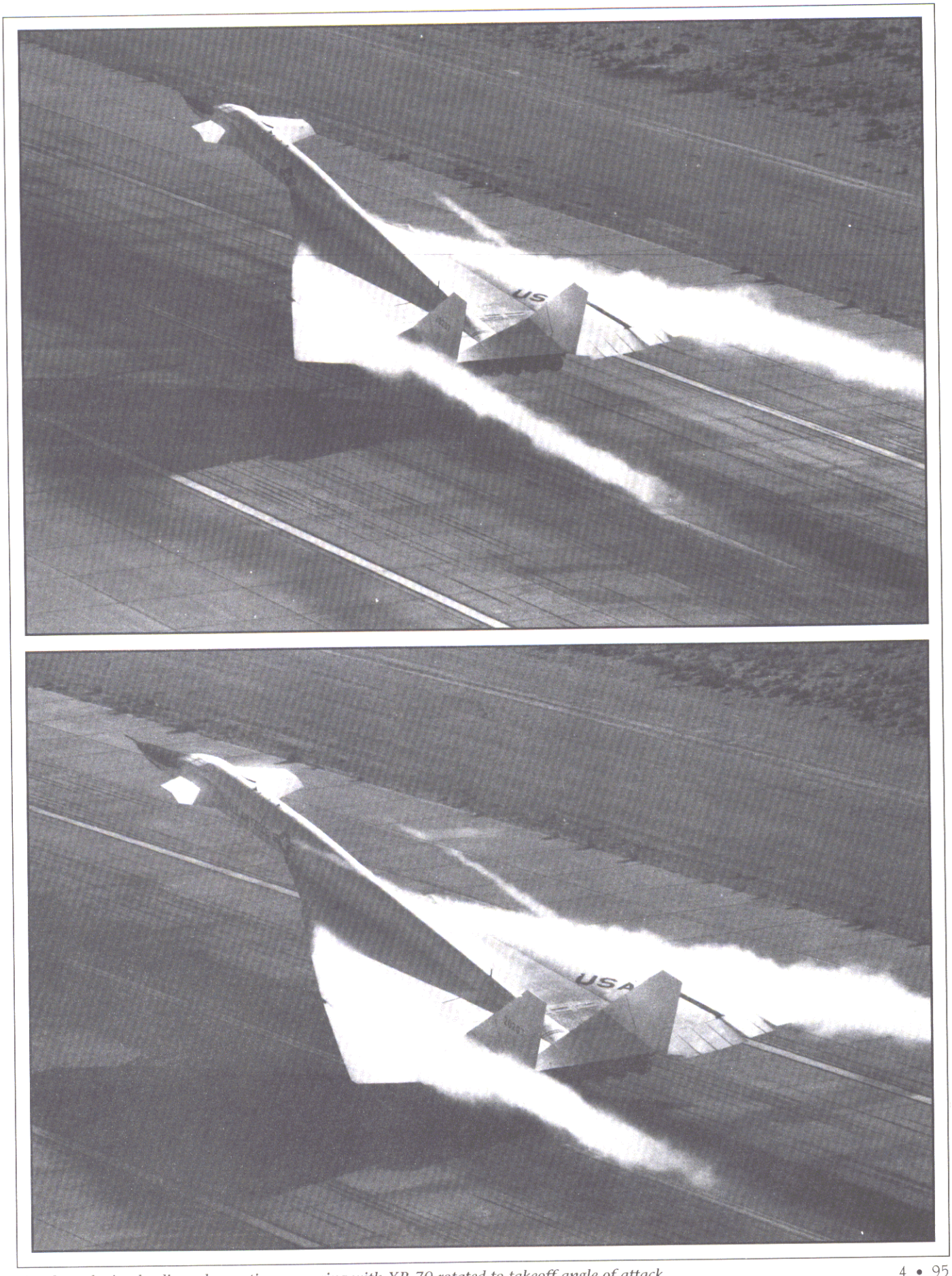

Condensed wing leading-edge vortices occurring with XB-70 rotated to takeoff angle of attack.

as shown in figure 4.93, where the canard is deflected up and the wing trailing-edge flaps and outer panel are deflected down. The vortices appear to pass outboard of the vertical tails.

Recalling the previous discussion in section 3.3.1, the XB-70 and the Concorde supersonic transport were designed to use wing leading-edge vortex flow to provide lift during takeoff and landing. The next four photographs illustrate the leading-edge vortex condensation patterns that result during low-speed operation of the XB-70 where the outer panel is undeflected. The leading-edge vortex forms over the wing during landing with the gear down as shown in the side view in figure 4.94. Figure 4.95 is a sequence of photographs taken by a chase airplane passing by the XB-70 during takeoff and gives an excellent perspective of the condensed leading-edge vortex flows. The vortex on the right side of the wing shows interesting developments in the condensation pattern. There appears to be a swirling into, or around, the core where it is initially condensing toward the forward part of the wing. In addition, the outer portion of the vortex pattern has irregularities. These developments in the pattern may be the result of the shear-layer instability vortices in the leading-edge vortex similar to those described previously for the F-16 and F/A-18 strake vortices in section 3.3.2. Also note the right-side canard-tip vortex flowing over the wing.

4 • 19

SR-71 Airplane

The SR-71 Blackbird built by Lockheed-California is a strategic reconnaissance airplane designed to sustain supersonic cruising speeds in excess of a Mach number of 3. The design features thin delta wings swept to 53° and blended

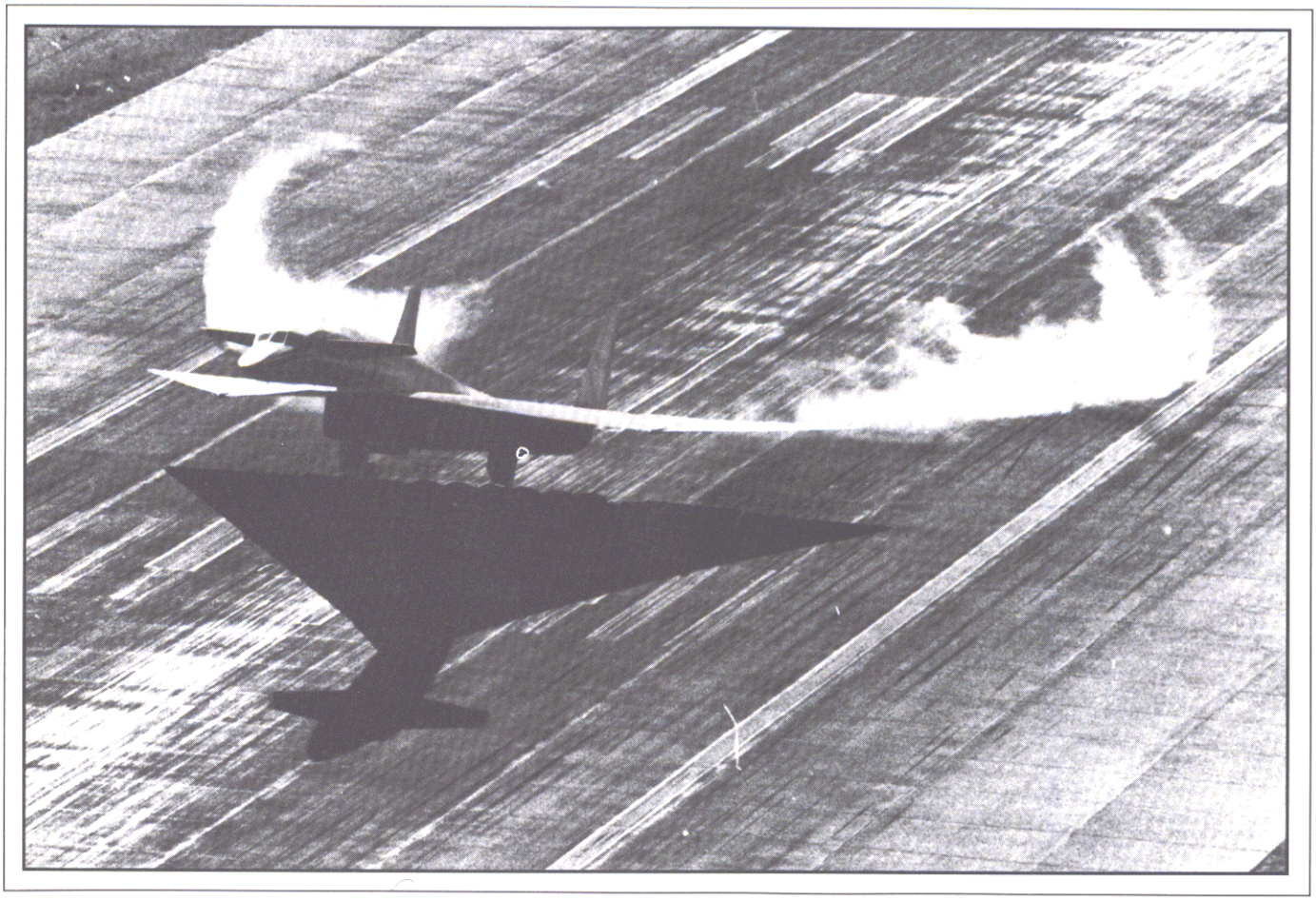

Condensed wing leading-edge vortices occurring with XB-70 rotated to takeoff angle of attack–concluded. 4 • 95

Wing and chine leading-edge vortex flows created by SR-71A during knife-edge turn. 4 • 96

with the fuselage. The fuselage cross-section shape results in the distinctive chines at the sides from the nose rearward to the wing juncture. Additional smaller chine surfaces are located along the outboard side of each of the wing-mounted engine nacelles. The chine surfaces were added to reduce trim drag at supersonic speeds and to generate vortex-induced lift to lower takeoff and landing speeds and to improve directional stability.

During takeoffs and landings and subsonic maneuvers, the flow separates along the leading edges of all the lifting surfaces, that is, the wing and chines, and forms a vortex flow over the upper surfaces. This is dramatically illustrated in figure 4.96 taken during a knife-edge turn which allows all the upper surface vortices to be seen. (The flames emanating from the right-hand engine were caused by "squawk" developed on afterburner selection; the airplane was in no danger.) This was taken during the same flight event as the photograph presented previously in the Foreword. The airplane is at a high-lift condition, where condensation occurs in vortex flows from the leading edges of the fuselage-chines, from the inboard wing panels, and from the nacelle-chines and outer wing panels. The fuselage-chine vortices proceed over the inboard wing panel curving outboard (or down) until they evaporate just ahead and inside of the outboard-mounted vertical tails. A condensed vortex forms along the leading edge of the inboard wing panel, stops and turns streamwise when it reaches the nacelle side, then probably bursts. The leading-edge vortices for the nacelle-chine and the wing outer panel appear to be merged over the wing at this high-lift condition. Recall that at lower lifts (fig. 3.31), these vortices were separate and rotated around each other. A helical flow pattern appears in the wing outer-panel vortex that is particularly clear on the left side of the airplane near the chine-wing juncture. This pattern is caused by small shear-layer instability vortices shown in figures 3.22 to 3.26.

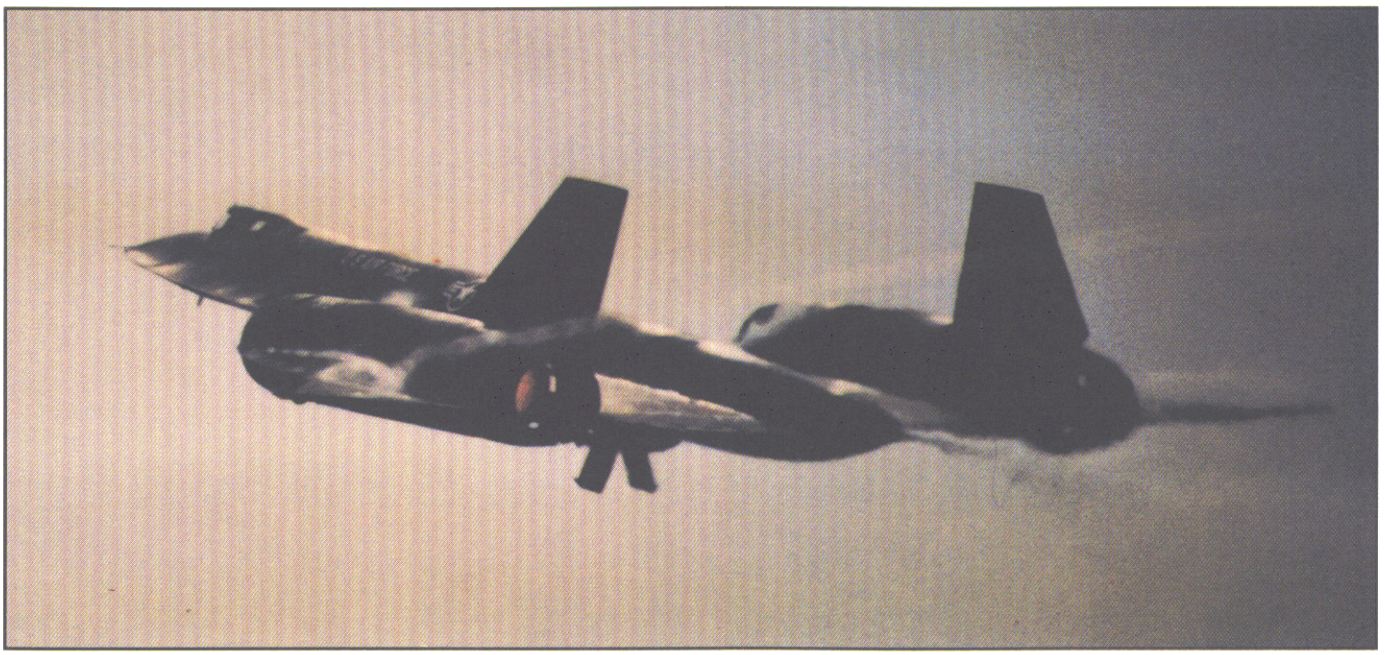

Nacelle-chine vortex generated during climb-out after takeoff of SR-71A. 4 • 97

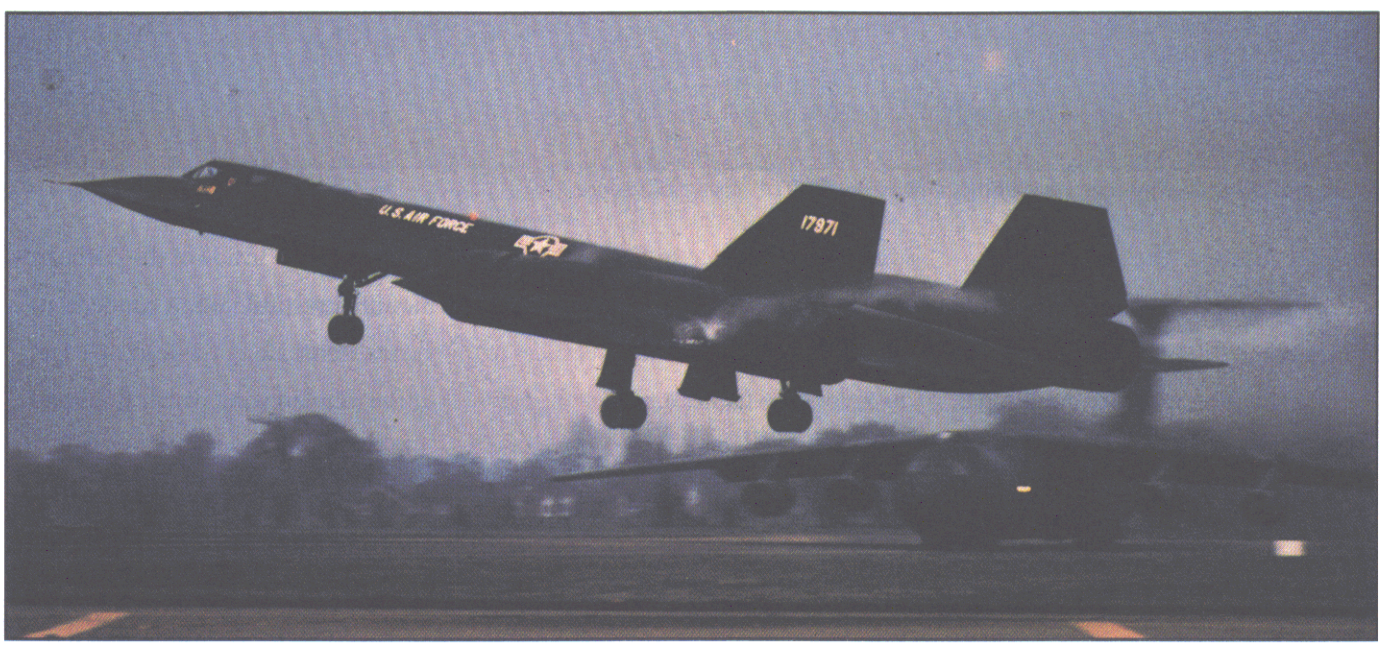

Nacelle-chine and wing outer-panel vortices interacting with each other during SR-71A landing. 4 • 98

The SR-71 climbing out after takeoff (fig. 4.97) has condensation near the core of the nacelle-chine vortex on the left side of the airplane. When the chine vortex reaches the wing, it rapidly changes direction to begin rotating around the wing vortex, which is present in the flow field but not condensed at this lift condition.

Interactions between inboard and outboard wing panel vortex flows were discussed for the SR-71 in figure 3.31. As the chine vortex proceeds into the wing wake, a discernible pattern can be seen around the outer edge of the core, which gives the flow a cellular appearance. These are small shear-layer instability vortices that were created when the chine vortex sheet first formed, then proceeded to work their way to the outer edge of the vortex core, and stayed with the core on into wake. The leading-edge vortex along the wing inboard panel has to change directions when it reaches the side of the nacelle, where the vortices are turned streamwise, rise to the

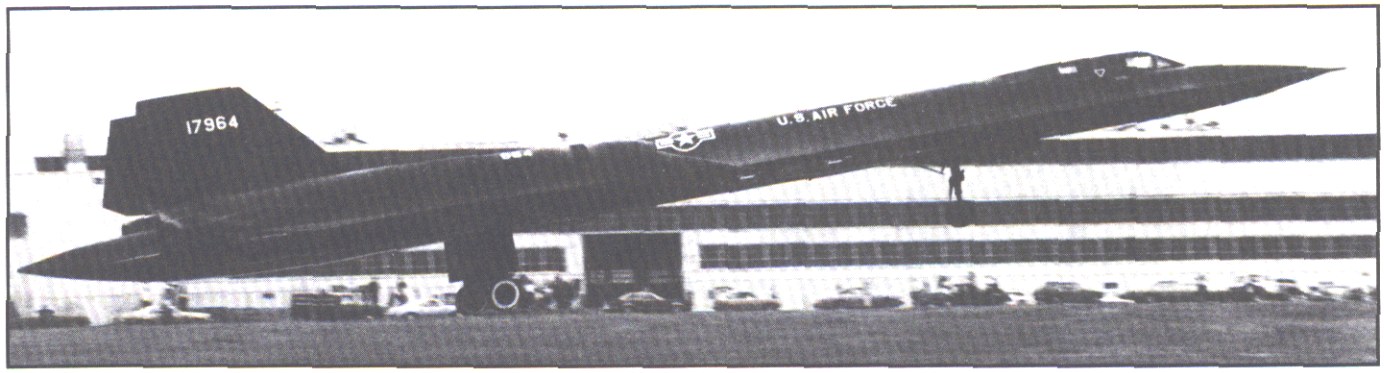

Nacelle-chine and wing outer-panel vortices rotating around each other during SR-71A landing. 4 • 99

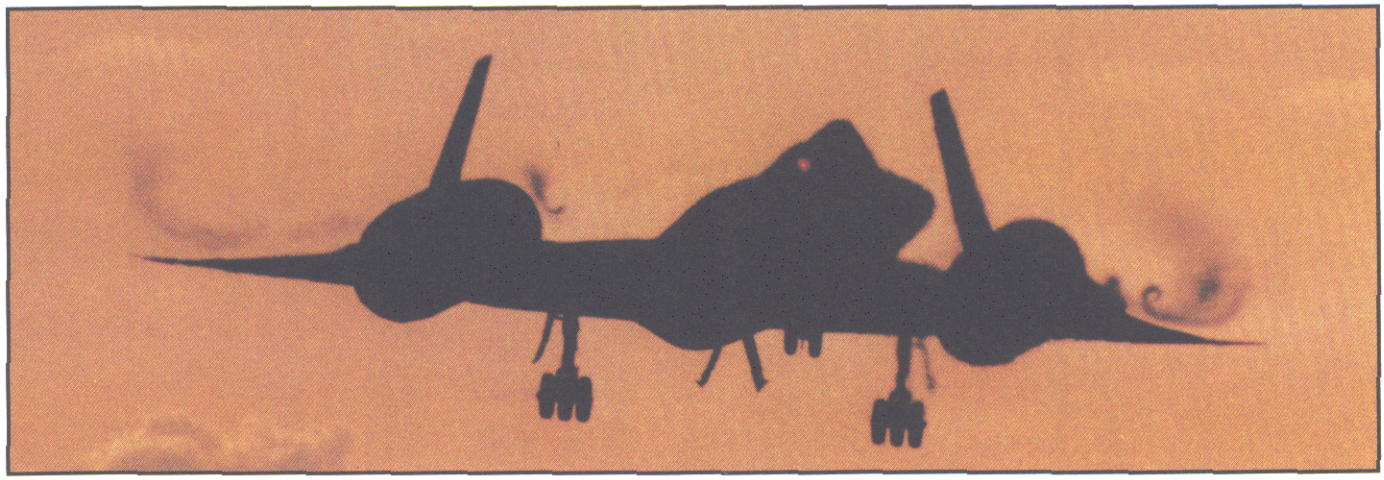

Nacelle-chine vortices rotating around uncondensed wing outer-panel vortices on SR-71A landing. 4 • 100

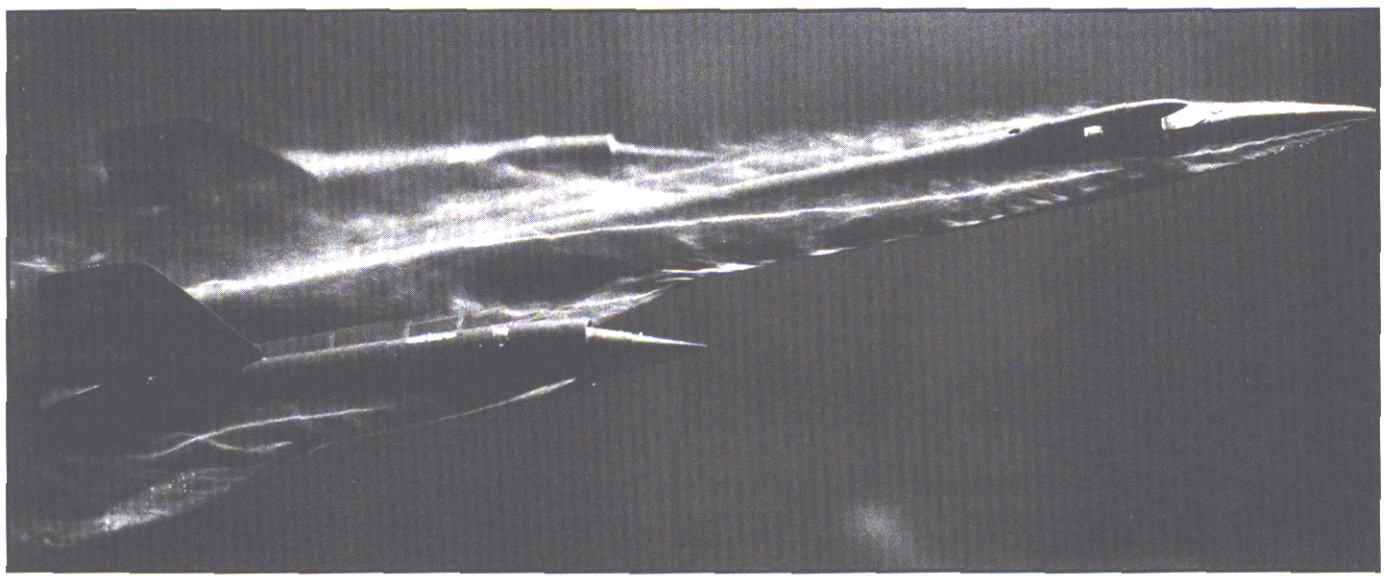

Similar vortex features obtained for small-scale water tunnel model at α = 10°. 4 • 101

height of the nacelles, then burst. (The visible flow stream behind the airplane is fuel jettisoned from a vent valve at the aft end of the fuselage.) Figures 4.98, 4.99, and 4.100 contain further examples of the rotation of the nacelle-chine and the outboard wing panel vortices around each other. These are often observed during takeoffs and landings.

An experiment performed in a water tunnel for a small model of the SR-71 is shown in figure 4.101 at an angle of attack of about 10°. Dyes are injected along the wing and chine leading

Nacelle-chine vortices condensing and streaming rearward on SR-71 after refueling. 4 • 102

edges and yield this amazing detail of the same vortex flow features that were shown in the condensation patterns in flight. The chine vortex begins at the fuselage nose and passes over the wing inboard of the vertical tail. A vortex begins along the leading edge of the inboard wing panel and shortly turns downstream before the nacelle and may be bursting. Outboard of the nacelle, the chine vortex and panel vortex have formed and are rotating around each other.

One interesting design feature of the airplane is that the fuel tanks have holes in them to allow for expansion due to the large heating differences between subsonic and supersonic speeds. This is especially notable after refueling, as seen in figure 4.102, where the fuel leaks occur from the internal tanks located in the fuselage and portions of the inboard wing panels. During the refueling operation at subsonic speeds, the angle of attack has to increase to offset the large increase in weight, usually about 70 000 lb. The higher lift that is necessary is evidenced by the existence of nacelle-chine vortex flows that condense and stream aft of the airplane.

4 • 20

Space Shuttle

The Space Shuttle orbiter is manufactured by Rockwell International as part of the NASA Space Shuttle Transportation System. The Shuttle system lifts off vertically from Earth like a rocket, carries a crew and

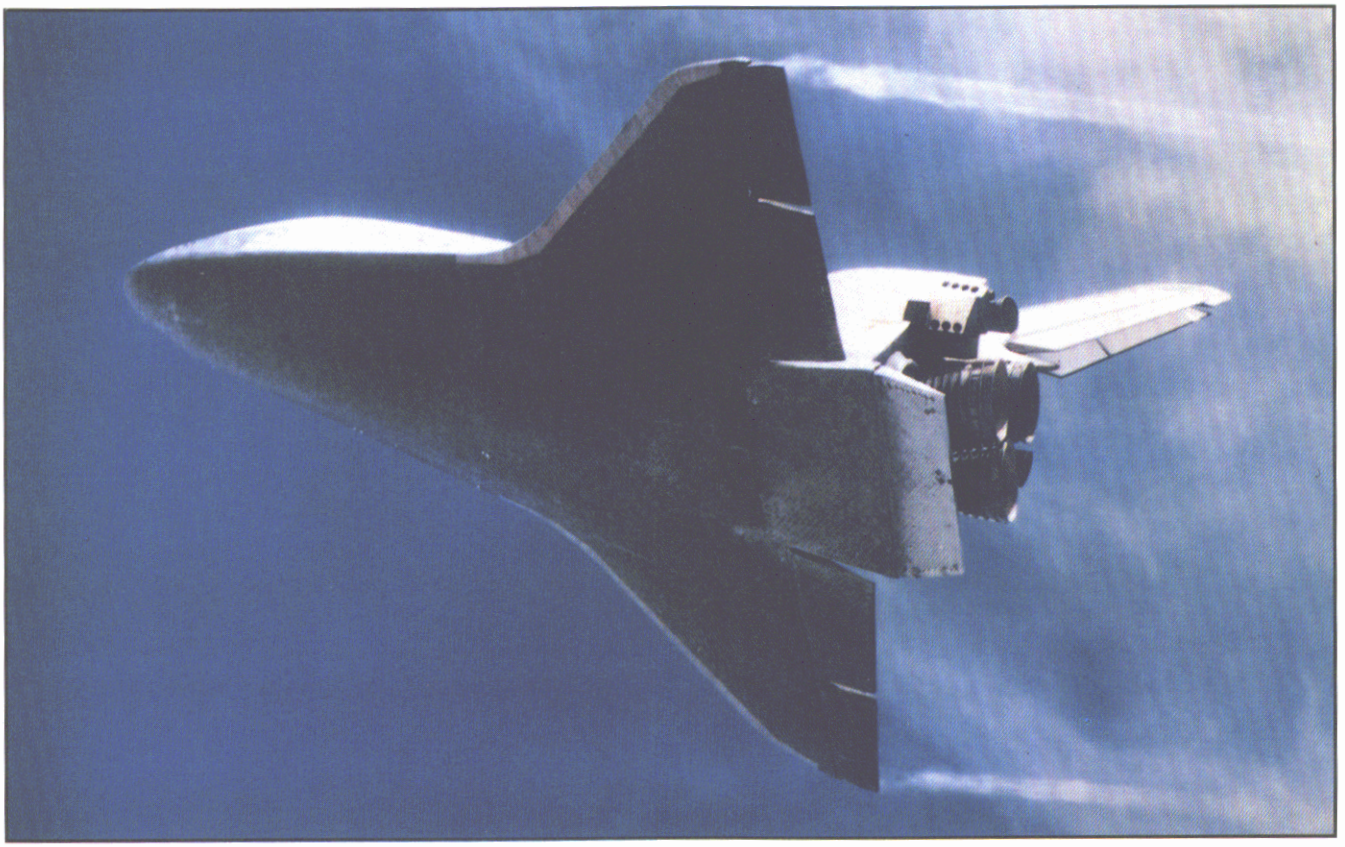

(a) On approach viewed from below.

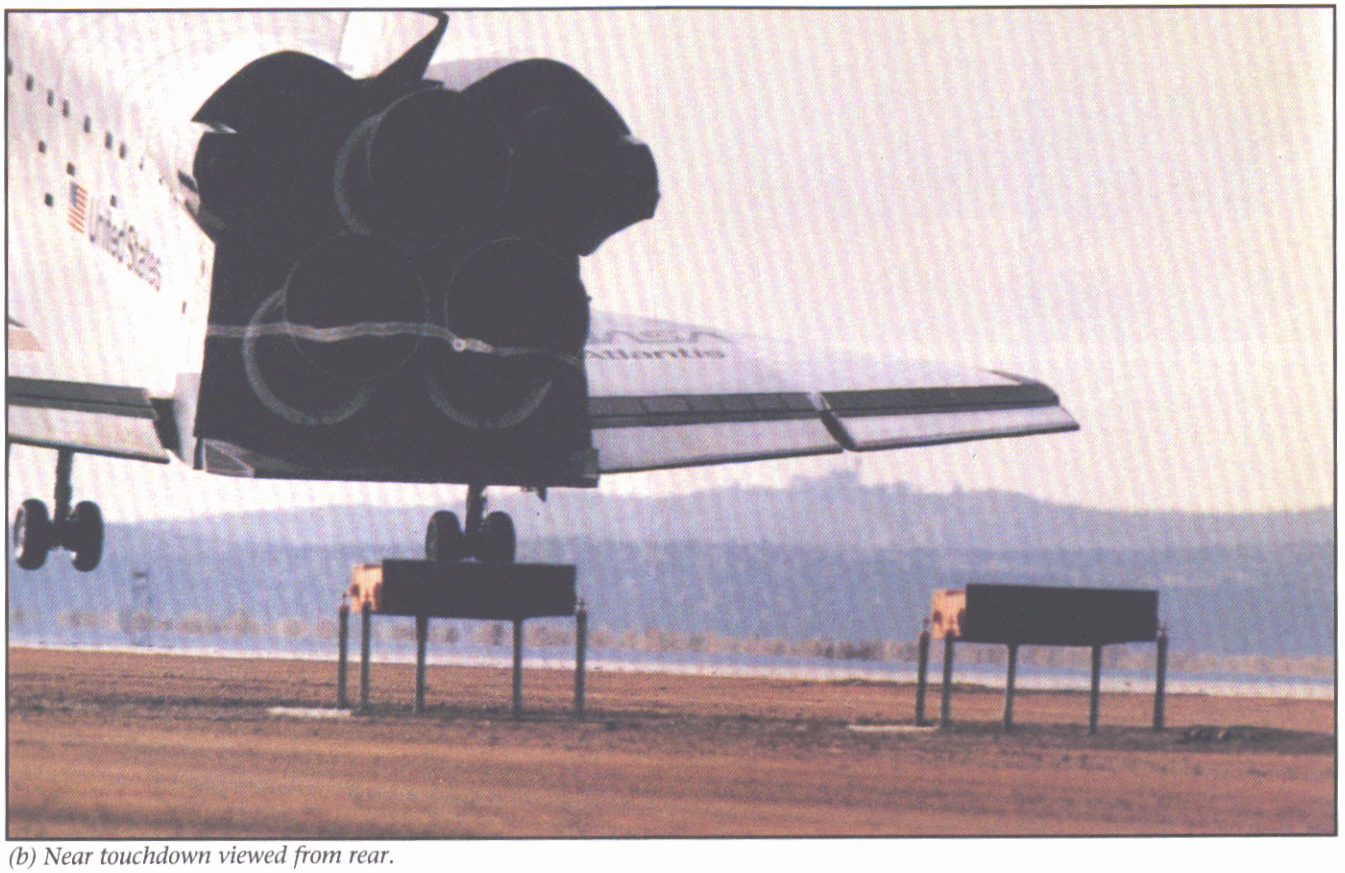

(b) Near touchdown viewed from rear.

Shuttle creating wingtip vortices while landing at Edwards Air Force Base. 4 • 103

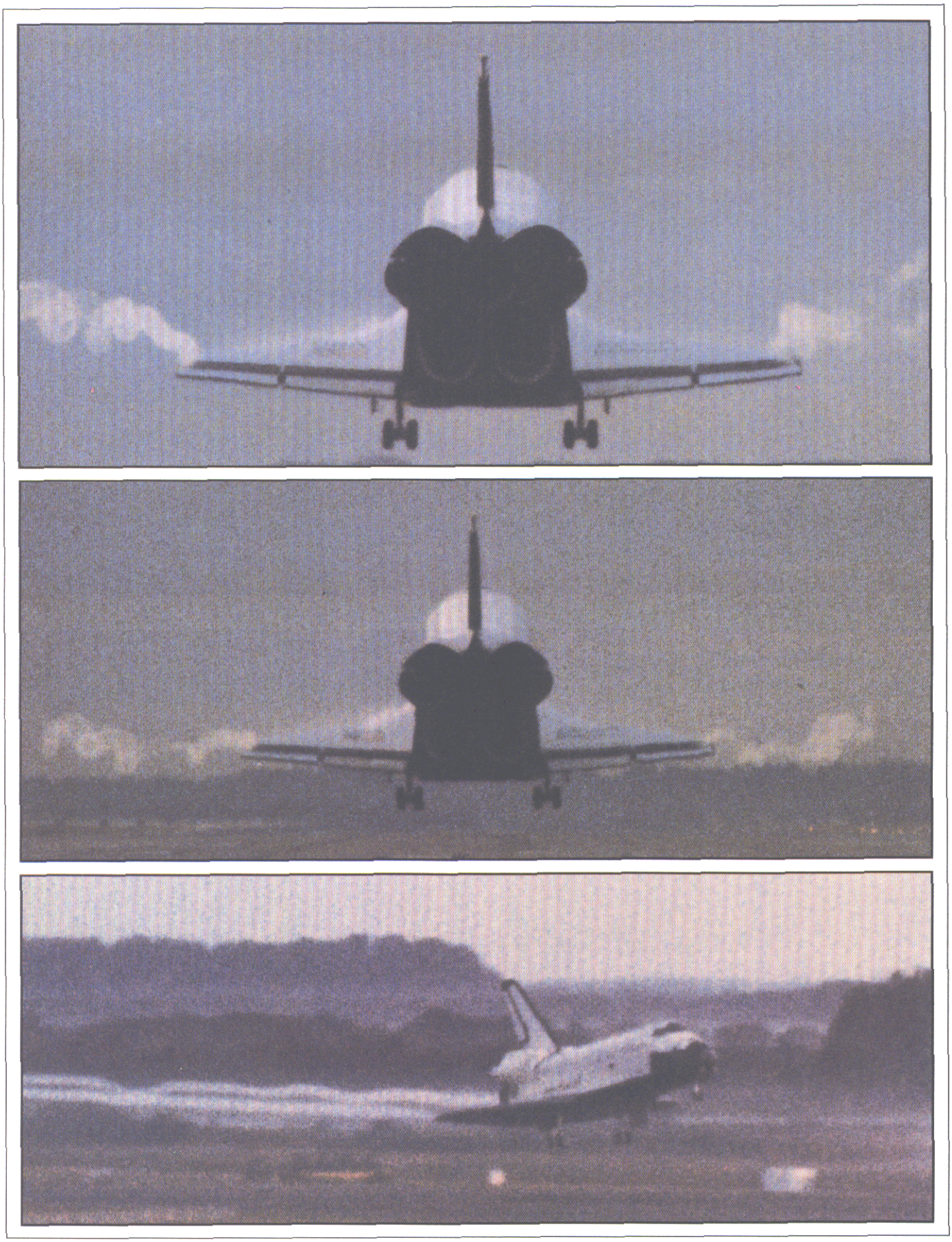

Condensed wingtip vortices streaming aft of STS-51A during landing at NASA Kennedy Space Center. 4 • 104

payload to orbit, then returns to land horizontally like an airplane. Its first flight was in 1981. The wing has a double-delta planform with a sweep of 81° on the inner panel, 45° on the outer panel, and a very blunt leading edge. Elevons are located on the wing trailing edge to provide pitch and roll control. The vertical tail has both a rudder and speed brake. The Shuttle lands at an angle of attack of about 12° so that the wings provide enough lift to offset the weight of the vehicle. This lift creates vortices that trail from the wingtips which are seen during favorable atmospheric conditions at the landing sites, such as those shown in figures 4.103 and 4.104.

5

Concluding Remarks

Several years ago, NASA Langley Research Center began to evaluate natural condensation as a way to visualize portions of an aircraft flow field and solicited visual material from professional aircraft photographers, military squadrons, industry peers, and aviation enthusiasts. The results of this study showed that many flight condensation patterns were obtained for a variety of airplane flow fields, which represent a unique source of in-flight flow visualization not previously utilized. Moist flows can condense because of the rapid expansions in leading-edge and separation-induced vortex flows and at high subsonic speeds, where the flow accelerates locally to supersonic speeds. In addition, condensed flows can evaporate because of compressions from shock waves, wing trailing-edge pressure recovery, and vortex burst. Water vapor relationships were postprocessed with solution fields of standard computational codes to calculate relative humidity. The results provided a qualitative indicator of flight condensation patterns for three common flow types: (1) the wing-body gull, (2) high-speed transonic, and (3) leading-edge vortex flows. The calculations showed that relative humidity is a more sensitive indicator to temperature changes than to the changes in pressure for expanding and compressing flows. In addition, low relative humidity levels were found in wing boundary layers and in the cores of leading-edge vortex flows, which help explain the lack of condensation adjacent to the wing upper surface and in the vortex pattern, respectively.

Flow condensation occurred in separation-induced leading-edge vortex flows for highly swept wings for a variety of airplanes with swept, delta, and variable-sweep planforms. In addition, leading-edge vortices were also visible from highly swept wing-body chines, strakes, leading-edge extensions (LEX's), and gloves and showed the interaction between two vortices for double-delta type of wing planforms. Condensation appeared in separation-induced vortices that occurred from engine boundary-layer splitter plates, from the outside edge of the upper surface of an inlet cowl, and from the side edge of a deflected trailing-edge flap. Separation and separation-induced vortices were observed in many flow fields from pylons, stores, weapons, sensors, antennae, and mirrors which were added to make the military airplane more combat effective. In addition, condensation appeared in flows of vortex generators on wing upper surfaces; from chines on the sides of transport engine fan cowls; wingtip and trailing vortices; in wingtip vortices from rotating propeller and helicopter blades; and in propulsion-induced ground vortices.

Some flow features were found that had not been seen in flight before, or were not known to exist, such as the streamwise vorticity from wing leading edges, which occurred for transports (Boeing 737 and Airbus A300), bombers (B-1), and fighters (A-6, F-14, F-16, and F-18) at different lift conditions. An additional flow phenomenon identified was the shear-layer instability vortices that occurred in leading-edge vortex flows generated by highly swept chines (SR-71), strakes/LEX's (F-16 and F-18), gloves (F-111), and wings and in wingtip and trailing vortex flows. Three types of vortex flows were found in flight condensation patterns that also exist in research performed in wind and water tunnels: (1) strake/LEX vortex flows and burst, (2) leading-edge and multiple interacting vortices, and (3) shear-layer instability vortices in wing and strake leading-edge vortex flows, and in wingtip and trailing vortex flows. This is useful information for engineers who perform experiments in low Reynolds number facilities. Results are shown for more recognizable flow visualization techniques, such as dyes in water tunnels and smoke in wind tunnels and flight, as well as for a few examples of computational flow, to help intelligently speculate on what the condensed flow patterns are, as well as provide results that researchers are more familiar with. While flight condensation shows only part of the flow field, the flows that were visible are the same as those in wind tunnels. The document was written for the aerodynamicist, although it is of interest to and readable by a wide range of individuals including other aviation specialists, airplane manufacturers, pilots, and university students.

6 ACKNOWLEDGEMENTS

We appreciate the photographs that many individuals and organizations contributed to this publication and regret that we cannot print all the photographs we received. Contributors are listed here by aviation industry and university, defense and government, and private individuals, photographers, and magazines. (Even though some organization names have changed since we received the photographs, we did not find it feasible to make them current.) In the list, the sources from the USA do not have the country showing. Individual photographs are credited in section 7 "Photograph Credit."

Aviation Industry/University:

Air France, North and Central American Division, New York

Avions Marcel Dassault-Breguet Aviation, Paris, France

James Blackwell, James Titus, and Jay Cahill, Lockheed Corporation, Marietta, Georgia

Charles Boppe, Brian Salisbury, and Gary Cote, Grumman Aircraft Systems, Grumman Corporation, Bethpage, New York

Terry Clawson, Aircraft Division, Northrop Corporation, Hawthorne, California

Richard Cooke, Geoffrey Hill, and Trevor Saunders, Military Aircraft Division, British Aerospace, PLC, Preston, England

Harry Gann, Douglas Aircraft Company, McDonnell Aircraft, Long Beach, California

General Dynamics Corporation

Dr. Robert Nelson and Jeffery Baker, University of Notre Dame, Notre Dame, Indiana

Northrop Corporation

Panavia Aircraft, GmBH, Munich, Germany

Dr. Frank Payne, Boeing Commercial Airplane Company, Seattle, Washington

Leo Schefer, British Aerospace, Inc., Washington Dulles International Airport

Albert Schoenheit and Christopher Wamsley, North American Aircraft Operations, Rockwell International, Los Angeles, California

Charles Smith and William Wolf, Fort Worth Division, General Dynamics Corporation, Fort Worth, Texas

Robert Williams, McDonnell Aircraft Company, Saint Louis, Missouri

Hideo Yoshihara, Boeing Military Airplane Company, Seattle, Washington

Defense/Government:

British Embassy, Washington, DC

Owe Bjorneland, Swedish Air Force

Jahn Charleville, Swedish Air Force (FlygrapenNytt), Stockholm, Sweden

Capt. Margaret Durrett, USAF 36th Tactical Fighter Wing, Bitburg Air Base, West Germany

John Del Frate, NASA Dryden Flight Research Facility, Edwards, California

Gary Erickson and Todd Hodges, NASA Langley Research Center, Hampton, Virginia

Donald Haley, Air Force Flight Test Center, Edwards Air Force Base, California

Commander C. J. Heatley, U.S. Navy VF-21, San Diego, California

Italian Air Force (via Embassy, Washington, DC)

Petty Officer Dennis Mattingly, U.S. Naval Air Station, Norfolk, Virginia

James McCue and William McNamara, Naval Air Test Center, Patuxent River, Maryland

Ministry of Defence, London, England

NASA Ames Research Center, Moffett Field, California

NASA Dryden Flight Research Facility, Edwards, California

NASA Kennedy Space Center, Florida

NASA Langley Research Center, Hampton, Virginia

Derek Peckham, Royal Aerospace Establishment, Farnborough, England

Joseph Piesco, USAF Tactical Air Command Public Affairs Officer, Langley Air Force Base, Virginia

William Price, NASA Kennedy Space Center, Florida

Joy Samuelson, U.S. Navy Hospital, Camp Pendleton, California

Makoto Sasaki, National Aerospace Laboratory, Tokyo, Japan

Swedish Embassy, Washington, DC

David Thompson, Aeronautical Research Laboratories, Melbourne, Australia

Larry Wilson, USAF Foreign Technnology Division, Wright-Patterson Air Force Base, Ohio

Dr. Stephen Wolf, MCAT Institute, NASA Ames Research Center, Moffett Field, California

Lt. Steven Zini, U.S. Navy, Fighter Squadron 41, Nimitz Aircraft Carrier

Private Individuals/Photographers/Magazines:

Air International, Bromley, England

Aviation Week & Space Technology, Washington, DC

Dennis Baldry, Osprey Publishing Limited, London, England

Paul Crickmore, Woodley, England

Duncan Cubitt, Stamford, England

Victor Flintham, Bushey, England

Peter Gunti, Solothurn, Switzerland

Mike Jerram, Spalding, England

Paul Ludwig, Seattle, Washington

Elizabeth Luman, Belleville, Michigan

Charles Mayer, Minneapolis, Minnesota

Eddie Mets, Toronto, Canada

Larry Milberry, Toronto, Canada

Frank Mormillo, Covina, California

Lindsey Peacock, England

Photo Press International, Ltd., Alexandria, Virginia

Mi Seitelman, International Defense Images, Alexandria, Virginia

Ray Sumner, Reading, England

Katsuhiko Tokunaga, DACT, Tokyo, Japan

7

PHOTOGRAPH CREDITS

Figure	*Aircraft*	*Source*
Cover	*USN F/A-18*	*Katsuhiko Tokunaga, Japan*
Foreword	*USAF SR-71A*	*Duncan Cubitt, Flypast Magazine, Stamford, England*
Preface	*USN F-14A*	*Lt. Todd Brophy, Public Affairs Officer, VF-143, Naval Air Station, Virginia Beach, Virginia*
2.1	*Wind tunnel*	*Pope, Alan; and Goin, Kennith L.: High-Speed Wind Tunnel Testing. John Wiley & Sons, Inc., c.1965*
2.4	*RAE 2822 Airfoil Computation*	*Christopher Rumsey, NASA Langley*
3.1	*NASA USAF F-111/TACT*	*NASA Dryden, via Elliott Schoonover, NASA Langley*
3.2	*Boeing 747 Calculation*	*Kyle Anderson, NASA Langley*
3.3	*USN F-14A*	*Katsuhiko Tokunaga, Japan*
3.4	*USN F-14A*	*Gary Cote, Grumman*
3.5	*USMC A-4M*	*Frank Mormillo, California*
3.6	*USN F-14A*	*Paul Ludwig, Washington*
3.7	*NACA 0012 Airfoil computation*	*Chris Rumsey, NASA Langley*
3.8	*USN F-4J*	*Harry Gann, Douglas Aircraft*
3.9	*USN F/A-18*	*Frank Mormillo, California*
3.10	*USAF/NASA XB-70*	*NASA Dryden*
3.11	*USAF/NASA XB-70*	*Albert Schoenheit, Rockwell*
3.12	*Concorde*	*Air France*
3.13	*76° delta wing computation*	*James Thomas, NASA Langley*

Figure	Aircraft	Source
3.14	RAF Lightning F.6	Katsuhiko Tokunaga, Japan
3.15	FAF Rafale	Henri Suisse, Dassault-Breguet Aviation, France
3.16	USN F-14A	Gary Cote, Grumman
3.17	HAF MiG-23MF	Peter Gunti, Switzerland
3.18	USAF F-16B	General Dynamics
3.19	USN F/A-18	Robert Elliott
3.20	USN F/A-18	Katsuhiko Tokunaga, Japan
3.21	F/A-18 water tunnel model	Gary Erickson, NASA Langley
3.23	85° delta wing wind tunnel model	Frank Payne, Boeing
3.24	USAF F-16C	Bill Wolf, General Dynamics
3.25	CAF CF/A-18	Mike Jerram, England
3.26	CAF CF/A-18	Eddy Mets, Toronto, Canada
3.27	USAF B-1A	Albert Schoenheit, Rockwell
3.28	Russian MiG-23bis	Owe Bjorneland, Swedish Air Force, via FlygrapenNytt
3.29	USN F-14A	Frank Mormillo, California
3.30	RAF SEPECAT Jaguar GR.1	Stephen Wolf, MCAT Institute
3.31	USAF SR-71A	Charles Mayer, Minnesota
3.32	Double-delta wing calculation	Peter Hartwich, ViGYAN, Inc.
3.33	Boeing 737	Stephen Wolf, MCAT Institute
3.34	Airbus A300	Todd Hodges, NASA Langley
3.35	USAF F-16	General Dynamics
3.36	USN F/A-18	Bob Williams, McDonnell Aircraft
3.37	USAF F-16C	Mike Jerram, England
3.38	USN F-14A	Katsuhiko Tokunaga, Japan
3.39	RN Buccaneer	British Aerospace
3.40	Airbus A300	Todd Hodges, NASA Langley
3.41	Boeing 707	Hideo Yoshihara, Boeing
3.42	USAF YC-14	USAF via Charles Boppe, Grumman
3.43	USAF YC-14	Via James Blackwell, Lockheed
3.44	Asuka STOL Research Airplane	S. Sekine, via Makoto Sasaki, National Aerospace Laboratory, Japan
3.45	USAF C-130	Jay Cahill, Lockheed
3.46	USN F-14A	Via Charles Boppe, Grumman

Figure	Aircraft	Source
3.47	RAF F-4	Stephen Wolf, MCAT Institute
3.48	USN F-14A	Lt. Steven E. Zini, U.S. Navy
3.49	Boeing 737	Via Charles Boppe, Grumman
3.50	DC-9	James Blackwell, Lockheed
3.51	Airbus A300	Todd Hodges, NASA Langley
3.52	IAF Tornado IDS	Katsuhiko Tokunaga, Japan
3.53	ACT Jaguar Demonstrator	Geoffrey Hill, British Aerospace
3.54	NASA/USAF X-29	NASA Dryden, via Charles Boppe, Grumman
3.55	USAF F-15	Don Haley, AFFTC
3.56	USAF F-15	Stephen Wolf, MCAT Institute
3.57	USAF F-4	Photo Press International
3.58	USANG F-105B	Frank Mormillo, California
3.59	USN F/A-18	Bob Williams, McDonnell Aircraft
3.60		British Aerospace
3.61	Wind tunnel test	Claude Patterson, NASA Langley (ret)
3.62	Boeing 747	NASA Dryden
3.63(a)–(d)	Sea Fury	Mike Jerram via Dennis Baldry, Osprey Publishing, England
3.63(e) and (f)	MB339 MACHI	Stephen Wolf, MCAT Institute
3.63(g)		Via Claude Patterson, NASA Langley
3.64	Crop duster	James Blackwell, Lockheed
3.65	Thrus crop duster	NASA Wallops Flight Facility
3.66	USAF C-130A	Charles Mayer, Minnesota
3.67	RAF C-130K	Stephen Wolf, MCAT Institute
3.68	USAF C-130A	Elizabeth Luman, Michigan
3.69, 3.70	USN E-2A	Via Charles Boppe, Grumman
3.71	Bell 204	Via Larry Jenkins, Bell
4.1	USMC A-4M	Frank Mormillo, California
4.2	USN A-6E	Stephen Wolf, MCAT Institute
4.3	USN A-6E	Harry Gann, Douglas Aircraft Company
4.4	USN A-6E	Stephen Wolf, MCAT Institute
4.5	USMC A-6E	Frank Mormillo, California
4.6	USAF A-10	Katsuhiko Tokunaga, Japan
4.7	USAF A-10	USAF, Joe Piesco, TAC P.A.O.

Figure	Aircraft	Source
4.8	USAF A-10	Larry Milberry, Toronto, Canada, via New York Air National Guard, 174th TFW
4.9	USAF B-1A	Chris Wamsley, Rockwell
4.10	USAF B-1A	Albert Schoenheit, Rockwell
4.11, 4.12, 4.13	USAF B-1A	Chris Wamsley, Rockwell
4.14	USAF B-1B	Don Haily, Air Force FTC
4.15	USN F-4J	Rusty Lowry, via Naval Air Test Center, Patuxent River, MD
4.16	USN RF-4B	Frank Mormillo, California
4.17	RAF F-4	Derek Peckham, RAE
4.18, 4.19(a), 4.19(b)	RAF FG.Mk1.F-4	Stephen Wolf, MCAT Institute
4.19(c)	RAF FGR.Mk2.F-4	Stephen Wolf, MCAT Institute
4.20	USAF F-5E/F	Mi Seitelman, International Defense Images, Alexandria, VA
4.21	USAF F-20	Northrop Corporation
4.22	USN F-14A	Katsuhiko Tokunaga, Japan
4.23	USN F-14A	Lt. Steven Zini, U.S. Navy
4.24, 4.25, 4.26, 4.27	USN F-14A	Frank Mormillo, California
4.28	USN F-14A	CDR C. J. Heatley, U.S. Navy
4.29	USN F-14A	Frank Mormillo, California
4.30	USN F-14A	Gary Cote, Grumman
4.31	USN F-14A	Photo Press International
4.32	USN F-14A	Frank Mormillo, California
4.33	USN F-14A	Dennis Mattingly, U.S. Navy
4.34	USN F-14A	Via Charles Boppe, Grumman
4.35	USN F-14A	CDR C. J. Heatley, U.S. Navy
4.36	USN F-14A	John Porter
4.37	USN F-14A	Joy Samuelson, U.S. Navy
4.38	USN F-14A	Paul Ludwig, Washington
4.39	USAF F-16B	Jeff Parker via Robert Nelson, Notre Dame University
4.40	USAF F-16A	Stephen Wolf, MCAT Institute
4.41	USAF F-16A	Bill Wolf, General Dynamics
4.42	USAF F-16A	Charles Smith, General Dynamics
4.43	USAF F-16A	Bill Wolf, General Dynamics

Figure	Aircraft	Source
4.44	USAF F-16A	Capt. Margaret Durrett, USAF 36th TFW, Germany
4.45	USAF F-16A	Bill Wolf, General Dynamics
4.46, 4.47	USAF F-16C	Bill Wolf, General Dynamics
4.48	USAF F-16A	Charles Smith, General Dynamics
4.49	F-16 Calculation	Jolen Flores, NASA Ames
4.50	USAF F-16A	Ray Sumner, England
4.51	USN F/A-18	Katsuhiko Tokunaga, Japan
4.52	USN F/A-18	Bill Sellers, NASA Langley
4.53	USN F/A-18	Katsuhiko Tokunaga, Japan
4.54, 4.55	NASA F/A-18 HARV	John Del Frate, NASA Dryden
4.56	F/A-18 Computation	Farhad Ghaffari, NASA Langley
4.57	F/A-18 Pressure survey	Scott Kjelgaard, NASA Langley
4.58	F/A-18 Vapor screen	Gary Erickson, NASA Langley
4.59	USN F/A-18	James Elliott
4.60	USN F/A-18	Bob Williams, McDonnell Aircraft
4.61, 4.62	USN F/A-18	Frank Mormillo, California
4.63	JAF F-104	Katsuhiko Tokunaga, Japan
4.64, 4.65	USAF F-104	NASA Dryden
4.66	NASA/USAF F-111/TACT	NASA Dryden, via Elliott Schoonover
4.67, 4.68	NASA/USAF F-111/MAW	Lew Steers, NASA Dryden
4.69	RAF S2 Buccaneer	Stephen Wolf, MCAT Institute
4.70	RAF Harrier	Richard Cooke, British Aerospace
4.71	RAF Harrier	Leo Schefer, British Aerospace
4.72	USMC AV-8B	Frank Mormillo, California
4.73	RAF Lightning F.6	Katsuhiko Tokunaga, Japan
4.74	RAF Lightning F.3	Stephen Wolf, MCAT Institute
4.75	Lightning F.1 wind tunnel model	British Aerospace, England
4.76	RAF Lightning F.1	British Aerospace, England
4.77	RAF Lightning F.6	Victor Flintham, England
4.78	IAF Tornado IDS	Katsuhiko Tokunaga, Japan
4.79	RAF Tornado ADV	Geoffrey Hill, British Aerospace
4.80	RAF Tornado ADV F.3	Mike Jerram, England
4.81	RAF Tornado IDS	British Ministry of Defence, England
4.82	GN Tornado IDS	Panavia Aircraft, GmbH, Germany

Figure	Aircraft	Source
4.83	RAF Tornado IDS	Panavia Aircraft
4.84	IAF Tornado IDS	Italian Air Force, via Italian Embassy, Washington, DC
4.85	FAF Rafale	Henri Suisse, Avions Marcel Dassault-Breguet Aviation, France
4.86	FAF Mirage F1	Peter Gunti, Switzerland
4.87	FAF Mirage 2000	Henri Suisse, Avions Marcel Dassault-Breguet Aviation, France
4.88	FN Super Etendard	Col. Robert Walsh, USAF, WPAFB
4.89	HAF MiG-23MF	Peter Gunti, Switzerland
4.90	Soviet MiG-21	Peter Gunti, Switzerland
4.91	Soviet MiG-29	Via Derek Peckham, R.A.E., England
4.92, 4.93, 4.94	USAF XB-70	NASA Dryden
4.95	USAF XB-70	Albert Schoenheit, Rockwell
4.96	USAF SR-71A	Ray Sumner, via Paul Crickmore, England
4.97	USAF SR-71A	James Goodall, via Charles Mayer
4.98	USAF SR-71A	Lindsey Peacock, via Paul Crickmore, England
4.99	USAF SR-71A	Chris Mayer, Minnesota
4.100	USAF SR-71A	Sgt. Gary Jones
4.101	SR-71A water tunnel model	David Thompson, Aeronautical Research Laboratories, Australia
4.102	USAF SR-71A	Aviation Week & Space Technology
4.103	NASA Shuttle	NASA Dryden, via John Del Frate, NASA Dryden
4.104	NASA Shuttle STS-51A	William Price, NASA Kennedy

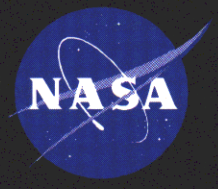

Langley Research Center
Hampton, Virginia 23681-0001